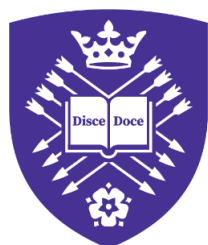


INVESTIGATION OF CHEMICAL REACTION NETWORKS FOR SIGNAL DETECTION AND AMPLIFICATION IN ENZYME-PARTICLE BIOSENSORS

Ludovica Luongo
Prof. Annette F. Taylor



University of
Sheffield

Submitted in accordance with the requirements for the Ph.D. degree



October, 2023

Acknowledgements

First and foremost, I would like to thank my supervisor, Professor Annette F. Taylor. She gave me the opportunity of a lifetime, choosing me for the role of ESR 1.3, four years ago, for this astonishing PhD project. She has been a fierce teacher, a kind guide and an outstanding example of intelligence and education. I would not be able to put into words my appreciation for her, but she has formed me as a student, a researcher and a human being. I will never forget the way she has guided me during these years and her total sympathy for any circumstances. I will never be able to express gratitude to her enough.

Thanks to her, I have had the chance to meet one of my dearest friends, I dare to say the sister I never had, my working companion and trusted go-to person, Maheen. She has been there since day 1, through thick and thin, not only academically but also in my everyday life. She has been by my side as a supportive and passionate cheerer, always rooting for me, giving me the best bits of advice and the huge support anyone needs during a PhD. We have been together during the good days and the pandemic days, and I am not able to imagine how could have I coped with all of that without her. She is part of me now, and I cannot envision a world without her in it.

Following and with my heart full of joy, I would like to thank my beautiful girls, Federica, Vittoria and Anna. We have shared so many lovely memories. They have made this PhD journey less lonely and a lot more wonderful. Our time together is stuck in my mind as one of the happiest I have experienced.

One mention goes also to all of my fellows who have accompanied me during this stage. These amazing human beings I have had the chance to meet in Sheffield have made this experience so much more special. They gave me a taste of internationality and gifted me with so many cultural experiences, thanks to them I feel I am a better person now.

Subsequently, I need to mention my family. They have been there all the time, coming to visit me when I needed it the most and always being ready to be by my side even from far away. They really have proved and embodied the meaning of “love knows no distance”.

Least but not last, my hometown friends, the true ones. We have a bond that not even space and time can destroy. Every time I return to them, it feels like time never passed and I never left. They have given me the comfort that only “home” can provide.

Finally, I would like to thank all the people who have contributed to this amazing project making it real. Besides the academic purpose of shaping us as future scientists and competent people, they have gifted me with the best experiences ever. The amount of places I have visited, people I have met and incredible events I have undergone ... is just breath-taking. Every single person has contributed to build a little piece of memory that I will cherish forever.

One last special thanks to F. who has always been there by my side. *Finally.*

Leaving three years abroad, having a life of my own for the first time and just diving into all the cultural differences this world is full of, had made me who I am today. There would never be enough appreciation for what this life has given me today, I can just feel blessed to have had the opportunity to live through all of it and I am very excited to see where the next chapter of my life will take me.

I would also like to thank Anthony Mai and Professor John Pojman for the precious instructions on the use of watermelon seeds.

This project has received funding from the European Union’s Horizon 2020 research and innovation programme under the Marie Skłodowska-Curie grant agreement no. 812868

Abstract

Living organisms depend on precisely calibrated biological mechanisms that are governed by enzymes. Scientists have always been captivated by the complexity of these systems and have endeavoured to replicate them by constructing cascade reactions and chemical reaction networks catalysed by enzymes. Enzymes play a crucial role in numerous applications as they possess the ability to function as sensors. Biosensors utilize the reaction's end product to generate a signal applicable in various fields, including biomedicine, the food and pharmaceutical industry, environmental pollution, and forensic science. Enzyme biosensors also have the potential for signal amplification, enhancing their sensitivity towards analytes present in low concentrations by augmenting the concentration of output molecules in response to input signals.

Our focus in this study is the utilization of enzymes in particle biosensors and reactions that display amplification, such as the urease reaction which is autocatalytic in pH. We also examine the role of transport phenomena, including diffusion, in sensing processes for enzyme-loaded micro and nanoparticles. The urease reaction has already been utilized in sensing applications, but its feedback and ultrasensitivity capabilities have not yet been fully exploited. When dealing with an autocatalytic reaction, positive feedback can be utilized to fine-tune sensor properties. In this particular study, we focused on optimizing parameters in enzyme particle biosensors to reduce response time, using experiments and computer simulations of the urea-urease reaction. We discovered that entrapment of the enzyme in thiol-acrylate polymer particles resulted in an optimum particle size for minimum response time, taking into account the diffusion of both substrate and product. These findings will aid in the design of enzyme-particle biosensors with autocatalysis.

Immobilized enzymes offer reusability, which makes them ideal for applications such as biosensors, industrial monitoring and transformations, and water quality

examination. However, creating a suitable combination of enzyme and supportive material can be challenging as it may lack stability, especially due to enzyme denaturation over time or storage conditions. To address this issue, researchers have suggested a sustainable, process-free, and robust enzyme source such as the enzymes present in watermelon seeds (WMS) as an alternative to standard commercial enzymes. These enzymes are shielded from the external environment by a lipid layer known as 'protein microbodies', making them reusable and reproducible. We designed a system with WMS in various hydrogel particles that detected urea down to 0.4 mM in just one hour and were stored at room temperature for over a month.

Our research investigated the utilization of enzyme combinations in constructing chemical reaction networks to facilitate more complex sensing and chemo-mechanical processes. Enzyme networks that can modify pH can serve various purposes, such as pulsatile drug delivery. Nonetheless, acquiring enzymes from different sources can prove costly and result in incompatible or unstable enzymes. Our objective was to combine diverse enzyme types like urease, catalase, glucose oxidase, and beta-glucosidase to program pH shifts. We found that watermelon seeds yielded numerous enzymes that were not only easy to use, without requiring extensive processing, but also affordable. By combining these enzymes and building reaction networks, we were able to enhance the reaction rate of certain processes and accomplish significant amplitude pH changes that would have been otherwise difficult to achieve.

The integration of chemical stimuli with a mechanical response is an innovative concept that scientists find particularly intriguing. Smart hydrogels, which can transform by shrinking and swelling in response to changes in external conditions, are becoming increasingly popular in applications such as drug delivery, active sensors, and artificial tissues. This work has produced a pH-responsive gel equipped with multiple enzymes and a colourimetric indicator capable of producing a chemo-

mechanical response when exposed to analytes, such as urea and glucose, that generate a basic or acidic environment. We investigated the reusability of particles with different enzyme sources and also obtained an enhanced mechanical response as a result of combining the effects of enzymes in watermelon seed, including catalase. This type of device has the potential to be used as a sensor that can regulate the release of a substance in time, such as drugs or chemicals for neutralising toxins.

Overall, these findings will aid in the enhancement of enzyme-particle biosensors, benefitting a wide range of industries from biomedicine to environmental pollution monitoring.

Table of Contents

Acknowledgements.....	2
Abstract.....	4
Table of Contents.....	7
List of abbreviations.....	11
List of Figures.....	13
List of Tables.....	18
Declaration.....	20
1. Introduction and Background.....	21
1.1. Enzymes.....	23
1.2. Sensors and Enzyme biosensors.....	26
1.2.1. What is a sensor: type of sensors.....	26
1.2.2. Amplification.....	29
1.2.3. Types of enzyme biosensors.....	30
1.2.4. Properties of enzyme biosensors.....	42
1.2.5. Applications.....	46
1.3. New directions in Enzyme biosensors.....	48
1.3.1. Boolean logic gates.....	48
1.3.2. Ultrasensitivity.....	50
1.3.3. Feedback.....	52
1.3.4. Other Amplification mechanisms.....	57
1.3.5. Mass transport and enzyme biosensors.....	61
1.3.6. State of the art and new directions in urease-based biosensors.....	66
1.4 Aims and objectives.....	68
2. Materials and Methods.....	71
2.1. Materials.....	71
2.2. Methods for production and monitoring of urease particle biosensor.....	73
2.2.1. Particle formation in hexane.....	73
2.2.2. Particle formation in mineral oil.....	75
2.2.3. Urea-urease clock reaction.....	75

2.3. Methods for immobilisation of protein microbodies and urease powder in hydrogel particles	76
2.3.1 Enzyme-loaded particles	76
2.3.2 Experimental setup	80
2.4 Methods for characterisation of activity of enzyme networks in watermelon seeds powder	82
2.4.1 Production of catalase- and urease-containing powder	82
2.4.2 Bubble counter.....	83
2.4.3 Oxygen and pH meter	84
2.4.4 Foam front propagation	85
2.5 Methods for production and monitoring of enzyme-loaded chemomechanical gels.....	86
2.5.1 pH-responsive filaments production	86
2.5.2 Experimental setup	87
2.5.3 Analysis	91
3 Particle biosensors: the influence of particle size on response times in enzyme reactions with feedback.....	93
3.1 Overview	93
3.2 Introduction.....	93
3.3 Methods.....	95
3.4 Results and Discussion	101
3.4.1 Experimental results	101
3.4.2 Simulations	108
3.5 Conclusions.....	115
4 Immobilisation of protein microbodies in hydrogel particles for improving stability of enzyme-particle biosensors	117
4.1. Overview	117
4.2. Introduction.....	117
4.3. Methods.....	119
4.4. Results and Discussion	119
4.4.1. pH profile and reaction time.....	120
4.4.2. Reusability and reproducibility tests.....	122

4.5.	Threshold sensing with WMS- thiol-acrylate particles	125
4.6.	Conclusions.....	127
5.	Towards building chemical reaction networks for programming pH changes using watermelon seeds.....	130
5.1.	Overview	130
5.2.	Introduction.....	131
5.3.	Methods.....	134
5.4.	Results and Discussion	134
5.4.1.	Catalase.....	134
5.4.2.	Glucose oxidase.....	142
5.4.3.	B-glucosidase.....	147
5.4.4.	Catalase, glucose oxidase and urease coupling.....	150
5.4.5.	Additional enzymes contained in watermelon seeds	154
5.5.	Conclusions.....	156
6.	Employing multiple enzymes in chemo-mechanical devices: towards smart biosensing and drug delivery systems	159
6.1.	Overview	159
6.2.	Introduction.....	160
6.3.	Methods.....	163
6.4.	Results and Discussion	163
6.4.1.	pH profile, reaction time and reusability	164
6.4.2.	Glucose	167
6.4.3.	Hydrogen peroxide	170
6.4.4.	Glucose and hydrogen peroxide	172
6.5.	Conclusions.....	176
7.	Conclusion of the thesis and future work.....	180
8.	Appendices.....	188
8.1.	Appendix 1. Modelling of enzyme-based sensors	188
8.1.1.	Models, reactions and kinetics.....	188
8.1.2.	Reaction-diffusion processes.....	189
8.2.	Appendix 2. XPP-ODE code for urea-urease reaction chapter 3	193
8.2.1.	Hexane particle sensor	193

8.2.2. Mineral oil particle sensor.....	195
8.3. Appendix 3. Image Analysis in Chapter 4.....	197
8.4. Appendix 4. Analysis and Simulations Chapter 5.....	199
8.4.1. Image Analysis.....	199
8.4.2. Code for analysis of foam fronts.....	200
9. Bibliography.....	205

List of abbreviations

APS	Ammonium persulfate
ATRP	Atom transfer radical polymerization
BGL	β -glucosidase
BIS	N,N'-Methylenebisacrylamide
BRN	Biocatalytic Reaction Network
BTB	Bromothymol Blue
CRN	Chemical Reaction network
DIW	Deionised Water
E	Enzyme
EC	Enzyme Commission (number)
EEO	Electroendosmosis
ETTMP	Ethoxylated trimethyl propane tri (3-mercaptopropionate)
GOX	Glucose-oxidase
H	Acid
HRP	Horseradish Peroxidase
K_{ES1}	Enzyme-substrate complex inactive protonated form
K_{ES2}	Enzyme-substrate complex active protonated form
K_M	Micaelis-Menten constant
K_P	Equilibrium constants respectively for product inhibition
K_S	Equilibrium constants for uncompetitive substrate
LC	Liquid Crystals
MM	Micaelis-Menten

NIPA	N-Isopropylacrylamide
ODE	Ordinary differential equations
PEGDA	Polyethylene glycol diacrylate
pH	pH in the particle
pH _o	pH in the surrounding solution
PVA	Polyvinyl alcohol
TEMED	N,N,N',N'-tetramethylethylenediamine
U	Urea
UP	Urease powder
VIM	1-vinylimidazole
WM	Watermelon
WMS	Watermelon seeds

List of Figures

Figure 1. Enzymes energy plot showing the reduction in terms of activation energy in order to achieve products faster ¹⁴	24
Figure 2. General biosensors' structure	27
Figure 3. Detailed Biosensors' structure ²⁷	28
Figure 4. Mesoporous Silica particle scheme ⁴⁰	33
Figure 5. Sandwich ELISA sensor scheme: (A) Solid-phase adsorbed antibody on microwell plate. (B) Formation of antigen-antibody complex. (C) Detecting enzyme-labelled second antibody combining with "solid-phase" antigen "sandwich." (D) Addition of substrate ⁴²	33
Figure 6. Comparison between A. Eliza sensor and B. Eliza+ sensor ⁴¹ where HRP = Horseradish Peroxidase	34
Figure 7. ZnO based biosensor. The S region represents the biosensor whereas the M1 and M2 regions are the electrodes. The biosensor has been functionalised with three different enzymes in order to detect simultaneously alcohol glucose and lactate ⁴⁶	37
Figure 8. "Glucose and protein detection assays by using varying concentrations of glucose and BSA" ⁵⁰	38
Figure 9. Hydrogel possible applications and use scheme ⁵²	39
Figure 10. Different properties of hydrogels ⁵²	40
Figure 11. Responsive gel stimuli classification ⁵⁶	41
Figure 12. Schematic example of a responsive urease gel shrinking as a pH change consequence ⁶³	42
Figure 13. Schematic functioning of an AND gate. (B) equivalent electronic circuit. (C) Results table ⁷⁸	49
Figure 14. Schematic functioning of an OR gate. (B) equivalent electronic circuit. (C) Results table ⁷⁸	49
Figure 15. Example of sensor used in the forensic field. when it shows the red light, it means the sample belongs to a Caucasian group; when it is blue the sample belongs to an African American group ⁷⁷	50
Figure 16. Example of sigmoidal/switch behaviour ⁷⁹	51
Figure 17. Different mechanisms of feedback loops. (A) regulation of "a" production by "b", symbolized by an arrow with a flat head and the corresponding reaction profile. (B) Representation and reaction rate profile of delayed negative feedback, where the delay induced is represented by an arrow with an empty head. (C) Autocatalytic positive feedback for the formation of "a", symbolized by an arrow with a filled head and the corresponding reaction profile ⁸²	53
Figure 18. Examples of different feedback functions. (A) the negative feedback can stabilize, limit and create an adaptive response. (B) The positive feedback can amplify	

a signal, create a bistable switch, and alter the kinetics. (C) the combination can create pulses or oscillations⁸³54

Figure 19. "Biocatalytic temporal control of a self-regulating transient pH-state by kinetic balancing of two antagonistic feedback-controlled enzymatic pH reactions"⁸⁶56

Figure 20. (a) Positive feedback loop amplification and pH vs urea in the Urea-Urease reaction with different enzyme concentrations Showing (B) ultrasensitivity (C) oscillations (min/max shown) (D) Bistable Switch⁷⁴57

Figure 21. Addition of external noise scheme to amplify a signal ⁸⁷57

Figure 22. Enzymatic mechanism scheme referred to the equations written below (9-10). It can be easily noticed that the addition of noise generated a further term in the equation which affects the concentrations of the species present in the system.....58

Figure 23. Product at the steady-state vs Enzyme using equations [1], [3] and the deterministic curve, in the function of p ⁸⁸59

Figure 24. Enzyme amplification obtained with a secondary enzyme coupled in: a substrate cycle (f), and an enzyme cascade (g) ⁸⁹60

Figure 25. Colorimetric DNA detection coupled with normal ATRP ⁹⁰.....61

Figure 26. "Reported limit of detection (M) and amplification time (s) of polymerization-based bio-detection methods in the literature. Coloured dots represent different types of polymerization methods. The red dotted line indicates the lower bound, under which the amplification time and limit of detection of biosensors are not achieved yet, but potentially more practical."⁹⁰61

Figure 27. Optical biosensor equipped with mass transport control nanofilm ⁹²62

Figure 28. Schematic representation of micromotors producing a chemical signal ⁹³.64

Figure 29. Microgel size changing with pH decreasing ⁹⁵65

Figure 30. "Breathing" pH sensitive microgel which is able to shrink and swell cyclically according to pH changes ⁹⁵65

Figure 31. "Breathing polymersome" reaction scheme ⁹⁶66

Figure 32. Thiol-acrylate polymer formation via ETTMP and PEGDA polymers. A) schematic representation and B) molecules structure.71

Figure 33. Molecular structure of: A) NIPA, B) TEMED, C) Vim, D) APS, E) Bis F) BTB G) Full structure¹⁰²73

Figure 34. WM powder SEM picture showing protein microbodies78

Figure 35. Polymerisation through the autocatalytic increase in pH of the urea-urease reaction.....79

Figure 36. Reactivity limit tests experimental setup¹⁰⁶81

Figure 37. pH measurement for reusability and reproducibility setup82

Figure 38. Representation of the bubble counter measurement set-up.....84

Figure 39. Oxygen measurement configuration scheme85

Figure 40. Foam front propagation configuration.....	86
Figure 41. Schematic representation of the urea urease test 1 setup: gel filaments with enzymes in a solution of urea and acid.....	88
Figure 42. Schematic setup for Reusability test 2: gel filaments were placed alternately in urea/acid solution and glucose solution.....	89
Figure 43. Glucose GOX test 3 representation setup: gel filaments were placed in glucose solution or glucose with hydrogen peroxide	90
Figure 44. Hydrogen peroxide - catalase reaction test schematic representation to assess the filament as oxygen-responsive	90
Figure 45. Experimental setup of all tests	91
Figure 46. System Model representation	96
Figure 47. Distribution of particles sizes obtained through the emulsion polymerisation with hexane expressed via density vs radius and count of particles vs radius.....	102
Figure 48. Thiol-acrylate a) small and b) large urease-particles in which urease powder and pyranine are encapsulated and placed in 0.3 mM urea solution at pH 4. The first image shows the particles in a bright field. The following pictures show the output response in time in terms of increasing fluorescence as a consequence of pH increase due to the urea hydrolysis reaction; scale bar 0.5 mm.....	103
Figure 49. Intensity profile along the diameter of the urease-particles in 0.3 mM urea solution at pH 4. The sizes of the particles considered were $r = 0.22, 0.80, 1.4$ mm. For the first two, the intensity changes uniformly, whereas for the bigger particle, the effect of the reaction-diffusion waves starts showing and the reaction propagates from the edges towards the centre of the particle.....	104
Figure 50. Intensity vs time for increasing urease-particle size in 0.3 mM urea solution at pH 4, and reaction time vs relative intensity for each particle size. Scale bar 0.5 mm	105
Figure 51. Average reaction time vs. particle radius for urease-particles showing the standard deviation for the average reaction time and radii respectively. Particles were placed in 0.3 mM urea solution at pH 4. Particles with a radius below the cut-off point do not display an increase in fluorescence.....	106
Figure 52. Relative intensity comparison between urease-particles made in hexane (no shell) and in mineral oil (shell) for particle radii of 0.35 and 0.4 mm.....	107
Figure 53. Simulated pH, urea and ammonia concentrations in the particle fabricated via hexane vs time for different particle radii (0.07 – 0.85 mm). The initial concentrations are: $[U]_0 = 0.3$ mM, $pH_0 = 4$ in the surrounding solution and $pH = 4$, $E = 80$ u/ml in the particle.	110
Figure 54. Simulated pH, urea, and ammonia profiles vs time in the urease-particle fabricated with hexane with radius $r = 0.35$ mm with varying urea concentration ($1e-5$	

– 5e-3 M). The initial concentrations are: pH=4 in the surrounding solution and pH = 4, E = 80 u/ml in the particle.....	110
Figure 55. pH vs urea plot showing the ultrasensitivity obtained with the hexane particles system (left). Reaction time vs radius for simulations of particles made via hexane with initial concentrations: $[U]_0 = 0.3 \text{ mM}$, pHo = 4 in the surrounding solution and pH = 4, E = 80 u/ml in the particle (right).....	111
Figure 56. Simulated pH, urea and ammonia profiles in the particle fabricated via mineral oil vs time for different particle radii (0.07 – 0.85 mm). The initial concentrations are: $[U]_0 = 0.3 \text{ mM}$, pHo = 4 in the surrounding solution and pH = 4, E = 80 u/ml in the particle.....	113
Figure 57. Simulated pH, urea, and ammonia profiles vs time in the urease-particle fabricated with hexane with radius $r = 0.35 \text{ mm}$ with varying urea concentration (1E-5 – 5E-3 M). The initial concentrations are: pHo = 4 in the surrounding solution and pH = 4, E = 80 u/ml.....	113
Figure 58. pH vs urea plot showing the ultrasensitivity obtained with the mineral oil particles system (left). Reaction time vs radius for simulations of particles made via mineral oil with initial concentrations: $[U]_0 = 0.3\text{mM}$, pHo = 4 in the surrounding solution and pH = 4, E = 80 u/ml in the particle (right).....	114
Figure 59. Absorbance vs time, pH vs. urea and response time vs urea of: a) thiol-acrylate particles with UP; b) thiol-acrylate particles with WM.....	121
Figure 60. Summary of reaction times with by WM vs. UP particles for different urea concentrations.....	122
Figure 61. Reproducibility tests performed consecutively of: a) thiol-acrylate - UP, b) Low EEO agarose - UP, c) low EEO agarose - UP and d) low EEO agarose – WM.....	123
Figure 62. Summary of reaction times performed with WM vs. UP particles for consecutive reusability test	123
Figure 63. Reproducibility tests performed weekly over one month of a) thiol-acrylate - UP b) thiol-acrylate - WM, c) low EEO agarose - WM and d) low EEO agarose – WM	124
Figure 64. Representation of the urea-urease clock reaction. When enough pollutant is detected, it generates a switch in the colour of the particles that corresponds to an optical output signal.....	126
Figure 65. Threshold detection limit (pH vs urea) and response time plots vs. urea of thiol-acrylate particles with WM.....	127
Figure 66. Bubble counts vs time (plot on left) and its first derivative (plot on right) in order to show the reaction rate, for 0.1, 0.01 and 0.001 g of watermelon seeds containing catalase.....	137
Figure 67. Bubble count vs WM powder concentrations (amount in 30 ml) for different hydrogen peroxide concentrations. Standard deviations were calculated from 3 runs.....	138

Figure 68. a) Bubble rate vs. WM powder, b) bubble rate vs. hydrogen peroxide for different WM seeds amounts, c) bubble rate vs. hydrogen peroxide for WM=0.05 g. Standard deviations were calculated from 3 runs.....	139
Figure 69. Trends of dissolved oxygen and pH vs time in the hydrogen peroxide-catalase reaction, tracked by oxygen and pH probes. WM was used both powder or dissolved in solution and then added to 1% hydrogen peroxide.....	139
Figure 70. Foam front propagation versus time (inset shows the image of the front) and its first derivative for the hydrogen peroxide-catalase reaction.....	141
Figure 71. Foam front propagation rate versus watermelon seeds powder (WM) and hydrogen peroxide concentration.....	142
Figure 72. Dissolved oxygen percentage and pH vs time for the glucose-GOX-WM reaction, comparing the addition of WM in solution and dry WM to glucose-GOX solution. Glucose= 30 mM, GOX= 0.001 g and WM= 0.001, 0.008, 0.02 g in 30 ml solution.....	145
Figure 73. Dissolved oxygen percentage and pH vs time for the glucose-GOX-WM reaction. Glucose= 30 mM, GOX= 0.001 g, WM= 0.1 g in 30 ml solution. Number 2 corresponds to the addition of WM.....	145
Figure 74. Dissolved oxygen percentage and pH vs time for the glucose-GOX-WM reaction. Glucose= 30 mM ,GOX= 0.001 g, WM= 0.1 g, H ₂ O ₂ = 0.5 and 0.016% in 30 ml solution. The number 2 corresponds to the addition of H ₂ O ₂	146
Figure 75. Dissolved oxygen percentage and pH versus time for the cellobiose-WM-GOX reaction (added where arrow 1 is pointing). Hydrogen peroxide was added where arrow 2 is showing. 0,15 M cellobiose 15 ml, 5 ml of WM and GOX having concentrations 112 and 200 u/ml, respectively.	149
Figure 76. Dissolved oxygen level vs time representing cellobiose- WM and GOX reaction network functioning autonomously	150
Figure 77. a) pH vs time using the reaction network composed of glucose/GOX, hydrogen peroxide/catalase and b) pH vs time using the reaction network composed of glucose/GOX and two different hydrogen peroxide concentrations (0.5 and 1%) with catalase. WM = watermelon seed powder glucose=30 mM, urea=0.5 mM, GOX=200 u/ml, urease=112u/ml; pH ₀ = 7.....	152
Figure 78. pH vs time using the reaction network composed of glucose/GOX, hydrogen peroxide/catalase added at point 1, and urea/urease added at point 2. UP = urease powder, WM = watermelon seed powder glucose=30 mM, urea=0.5 mM, GOX=200 u/ml, urease=112u/ml; pH ₀ = 7.....	153
Figure 79. Urea urease reaction is shown through the absorbance vs. time plot (on the left) and pH vs. time (on the right) for a) UP and b) WM, encapsulated in gel filaments and placed in 5 mM urea at pH 4. The filaments are ~ 1 cm in length.....	165
Figure 80. Reusability and reproducibility tests for urease from watermelon seeds (WM) and standard urease powder (UP) are shown in the absorbance versus time	

plot. on the right, reaction time vs. repetitions for WM and UP. Standard deviations were calculated from 8 measurements.	166
Figure 81. Filament containing GOX previously let react with urea 5 mM to set it at high pH, then placed in glucose solution 30mM, at time t=0 and t=5000 sec	168
Figure 82. Area growth vs. time for UP and WM (on the left) GOX-filaments placed in glucose solution and their first derivative plot in time to show the growth rate.....	169
Figure 83. pH-responsive WM filament in hydrogen peroxide solution before and after bubble formation and consequent expansion.....	170
Figure 84. Area vs. time plot for different hydrogen peroxide concentrations in volume percentages and its derivative plot to show the area growth rate.....	171
Figure 85. Bar plot showing the growth ratio between max/min area for filaments placed in hydrogen peroxide at 0.5, 1 and 3% concentration.....	172
Figure 86. WM filament used with glucose 30mM and hydrogen peroxide 0.5% before and after the reaction occurred. The gel growth is given by the combined effect of gluconic acid and bubbles.	173
Figure 87. Area growth vs. time plot coupled with its first derivative curve to show the area growth rate for the WM seeds-glucose (30 mM) plus hydrogen peroxide (0.5%) reaction	174
Figure 88. a) Area growth vs time for filaments made with UP, WM, and WM plus hydrogen peroxide (0.5%) in glucose solution. b) Bar plot showing the area growth ratio considering the end of the reaction over the initial stage for UP, WM, and WM plus hydrogen peroxide (0.5%), in glucose solution (30 mM).	175

Appendices.

Figure A 1. Diffusion scheme: (A) without reaction and (B) with the reaction ¹⁰⁶	190
Figure A 2. Enzyme-particle scheme ¹⁰⁵	191
Figure A 3. Film theory representation	191
Figure A 4. pH scale representation.....	197
Figure A 5. intensity vs pH.....	198
Figure A 6. Representation of the initial front point (arrow 1) and final front point (arrow 2) positions to determine the foam front propagation length	199

List of Tables

Table 1. Enzymes properties compared to inorganic catalysts	26
Table 2. Nanoparticle-based enzyme biosensors examples in industrial and clinical application	36
Table 3. Biosensors' type of outputs ⁶²	43
Table 4. Examples of optical biosensors for various enzymes ⁶⁶	46
Table 5. Scheme of hydrogels and enzyme sources used in the experiments	76

Table 6. WM average activity and comparison between different varieties ¹⁰⁹	77
Table 7. Relative stability of different urea biosensors (adapted) ¹³⁴	125
Table 8. Explicative table of other enzymes found in watermelon seeds via mass spectrometry.....	155
<i>Appendices.</i>	
Table A 1. intensity/ pH scale association.....	198

Declaration

I, the author, confirm that the Thesis is my own work. I am aware of the University's Guidance on the Use of Unfair Means (www.sheffield.ac.uk/ssid/unfair-means). This work has not been previously been presented for an award at this, or any other, university.

1. Introduction and Background

The IUPAC definition of biosensors is: "A device that uses specific biochemical reactions mediated by isolated enzymes, immunosystems, tissues, organelles or whole cells to detect chemical compounds usually by electrical, thermal or optical signals"¹⁻². In the 1960s, the first biosensor using the enzyme glucose oxidase for glucose detection was studied and built³ and since then, scientists have developed new materials and techniques to improve these devices. Biosensors have had a great impact on many fields during the last few decades, partly because of the desire to convert many technologies to biotechnologies. Opting for something 'Bio' can reduce environmental pollution by using biological elements (cells, enzymes), increase the number of possible applications with respect to the traditional ones (biological processes, physical changes) and reduce the costs^{4,5}.

Biosensors are the 2.0 version of chemical sensors, and this field is continuously evolving. They can be a valid alternative to analytical methods in the laboratory as a result of their small size and portable properties. Also, they have several advantages such as high sensitivity, fast response, immunity from electrical and magnetic disturbances⁶ and real-time detection^{7,8}.

Biosensors can be constructed based on chemical reaction networks (CRNs) and cascade reactions to produce more complex responses such as signal amplification and ultrasensitivity. A cascade reaction is a chemical process in which the product of the previous reaction is the reactant, substrate or fuel for the next reaction^{6,9}. The system conditions do not change and there is no need to add other reactants. Once the cascade reaction starts it is capable of self-regulating. Amplification is an increase in output response with respect to the small input or stimuli the system is subjected to. It could be the amount of substance present in the system that the biosensor has to detect and can be achieved by many different methods. It is employed in many commercial sensors such as ELISA. Ultrasensitivity is observed in living organisms like cells and refers to a huge change in the output level

corresponding to a small change in the input stimulus¹⁰⁻¹¹. For example, one of the parameters (usually substrate concentration) gives a sharp passage from an “off” to an “on” status - a switch-like behaviour. This property has not been widely exploited in biosensor applications as there are drawbacks e.g. very long response times.

Mass transport phenomena play an important role in biosensing. Enzymatic action is facilitated by a series of chemical reactions but molecules cross short distances between enzymes purely by diffusion. Enzyme reactions are sometimes described as either reaction-limited or diffusion-limited. In a reaction-limited process, the rate of reaction depends mainly on the enzyme process. In a diffusion-limited process, the rate of reaction depends on the diffusive transport of the substrate to the enzyme. Reaction-diffusion (RD) systems are capable of amplification, feedback, self-assembly and self-organization¹² therefore they are of great interest for building synthetic bio-sensing systems for complex responses.

Here, new approaches combining simulations with experiments will be explored to achieve more sustainable, economically viable and easy-to-use enzyme biosensors that display signal amplification and ultrasensitivity. Numerical simulations are a valuable tool for predicting the response of a system to different stimuli or conditions. They allow us to explore the behaviour of a system without the need for costly and time-consuming lab experiments. By using numerical simulations, we can gain valuable insights into how a system will perform under different circumstances, and make better decisions about how to optimize its performance¹².

In this first chapter, we examine the background of enzyme biosensors, their history, the different types, and their development and improvement in the literature up to nowadays, giving an idea of the state of the art, together with several definitions and basic concepts critical to the full understanding of the subject. The methods are covered in chapter 2. In chapter 3, a series of experiments was conducted with enzyme-particles to determine the optimal radius size for constructing a sensitive and fast, reactive system. Thiol-acrylate polymer particles were equipped with

indicator and urease enzyme to gain insights into the reaction time in solutions of urea. These experiments led to the development of models that will serve as a reliable foundation for understanding the pH autocatalytic biosensors. In chapter 4, enzymes were encapsulated in diverse hydrogel supports to enhance their stability and explore alternative biocatalyst sources. Watermelon seeds proved to be a sturdy, reusable, and economical source of urease in a urea sensor displaying a threshold response. In chapter 5, multiple enzymes were combined to obtain more complex pH responses. We characterise other enzymes found in watermelon seed, including catalase, and show how the enzymes could be used together to enhance pH changes. Furthermore, in chapter 6, multiple chemical stimuli were combined with mechanical responses to amplify the changes in pH-sensitive polymers. This resulted in the production of gels that can expand or contract depending on the analytes in the external environment, and we demonstrate the reusability of these particles and their enhanced response using enzymes in WMS. These types of gels hold the potential to be used in advanced devices, such as self-regulating chemical or drug delivery systems.

The last chapter covers the conclusions and future work. An overview of the work is made highlighting the major features of the topic, the systems studied, the results obtained and the limitations observed.

1.1. Enzymes

Enzymes are proteins made of a unique chain of amino acids and they are fundamental elements of all living systems. They take part in the necessary series of chemical reactions in metabolic pathways transforming the reagents into products needed by the cell. The function of enzymes is to act as a catalyst which decreases the energy of activation, increasing the rate, of a reaction [**Figure 1**]. Without enzymes, several important transformations inside the human body could not happen at a significant rate e.g. glucose oxidation, sucrose and lipid transformation.

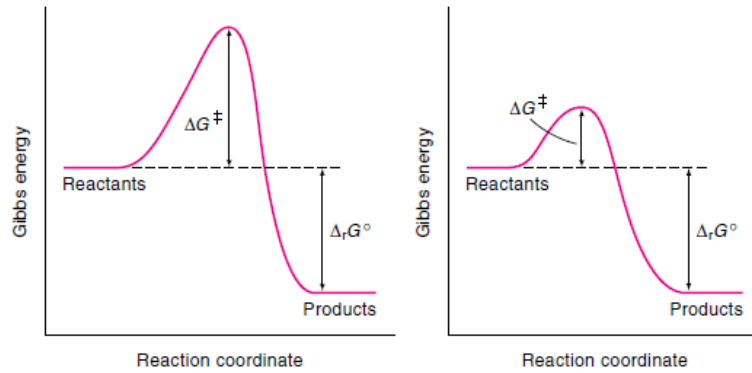


Figure 1. Gibbs energy plot showing the reduction in terms of activation energy in order to achieve products faster with enzymes.

Since the enzyme is a protein macromolecule, the structural organization is important and is divided into four levels:

- The primary structure formed by the amino acid sequence in the peptide chain;
- The secondary structure is obtained by the special conformation of the peptide chain (alpha-helices and beta-sheet)
- The tertiary structure is the three-dimensional configuration
- The quaternary structure is derived from the association of more polypeptide units.

The EC (Enzyme Commission) number classifies enzymes depending on the chemical transformation of substrates into products. At the top level, there are six different classes according to the type of chemistry:

- Oxidoreductases catalyse oxidation/reduction reactions (EC 1),
- Transferases transfer a chemical group (EC 2),
- Hydrolases catalysing hydrolysis reactions (EC 3),
- Lyases also split chemical bonds differently from oxidation or hydrolysis (EC 4),
- Isomerases catalyse structural changes between isomers (EC 5) and
- Ligases join two compounds (EC 6).

These EC classes are then divided into subclasses according to certain criteria such as the chemical bond split or formed, the reaction centre and the transferred chemical group¹³.

The first time the enzyme's biocatalytic properties were discovered was in 1833 with the diastase, which helps the conversion of starch into sugar. During the 1800s - 1900s enzyme research made significant strides, leading to a multitude of innovative breakthroughs. These advancements have revolutionized daily lives and transformed various sectors within the industry. From enhancing food production to boosting energy generation, these remarkable developments have resulted in greater efficiency and sustainability e.g. fermentation (1837 Berzelius), isolation of the enzymes catalysing the transformation of sugar into alcohol (1897 Edward Buchner), extraction of urease (1926 James Sumner), pepsin and trypsin crystallization (1950 John Northrop and his co-workers)¹⁴. With technology improving, progressively more enzymes were discovered, characterized and catalogued by functionality.

Only in the 20th century their importance in medicine and the chemical industry started to be appreciated^{13,15,16}. Nowadays, enzymes are often used in processes¹⁷ e.g. hydrogen peroxide decomposition in living organisms (catalase)¹⁸, hydrolysis of urea (urease)¹⁹, decomposition of complex sugars into more simple ones (β -glucosidase)²⁰, production of lactose-free milk (lactase)²¹, bio-diesel production (lipase)²², paper, food and textile industry (cellulase)²³ etc. This evolution in the use of enzymes is due to their superior properties compared to inorganic catalysts.

Table 1. Enzyme properties compared to inorganic catalysts

PROS	CONS
A small amount generates a big change in the reaction rate	Higher price
High specificity	Less stability
Standard reaction conditions	
Different regulation mechanisms	

Another application of enzymes takes advantage of the properties listed in [Table 1]; in particular, their high specificity for a certain substrate. In complex systems in which several reactions take place at the same time, enzymes can selectively catalyse just one of them resulting in the formation of a particular product before others. In this case, the enzyme is capable of detecting the presence of a specific reactant among others. That is why it was suggested that enzymes could be used as sensors.

1.2. Sensors and Enzyme biosensors

1.2.1. What is a sensor: type of sensors

Sensors are highly advantageous instruments that are capable of detecting diverse substances and altering conditions, subsequently producing a signal that enables comprehension of the situation at hand. These devices are ubiquitous in everyday life, from the smoke detector in one's kitchen to the automated door-opening system at the local supermarket. Additionally, sensors perform a crucial role in scientific applications where exactitude and precision are paramount. For instance, sensors can detect changes in temperature, pressure, sunlight, and other significant parameters²⁴. Examples of sensors in the scientific domain are sensors such as the pH sensor, bromide sensor, and flow sensor are employed to detect changes in pH levels, bromide concentrations, and flow rates, respectively. The utilization of

sensors enables an astonishing amount of knowledge and comprehension concerning the surrounding environment.

The sensors expounded upon in this thesis adhere to Brian R. Eggins' definition of chemical sensors, whereby they exhibit selectivity in reacting to analytes and possess the ability to quantify them either qualitatively or quantitatively. The same author has provided to specify that biosensors are really a sub-set of chemical sensors and are formed by a 'biological sensing element'²⁵. A biosensor is formed by three main parts as can be observed from **[Figure 2]**²⁶:

- A receptor to acquire information about the substance we want to detect
- A converter to transform the chemical signal into an output signal we are able to measure
- A processor to amplify and display the signal.

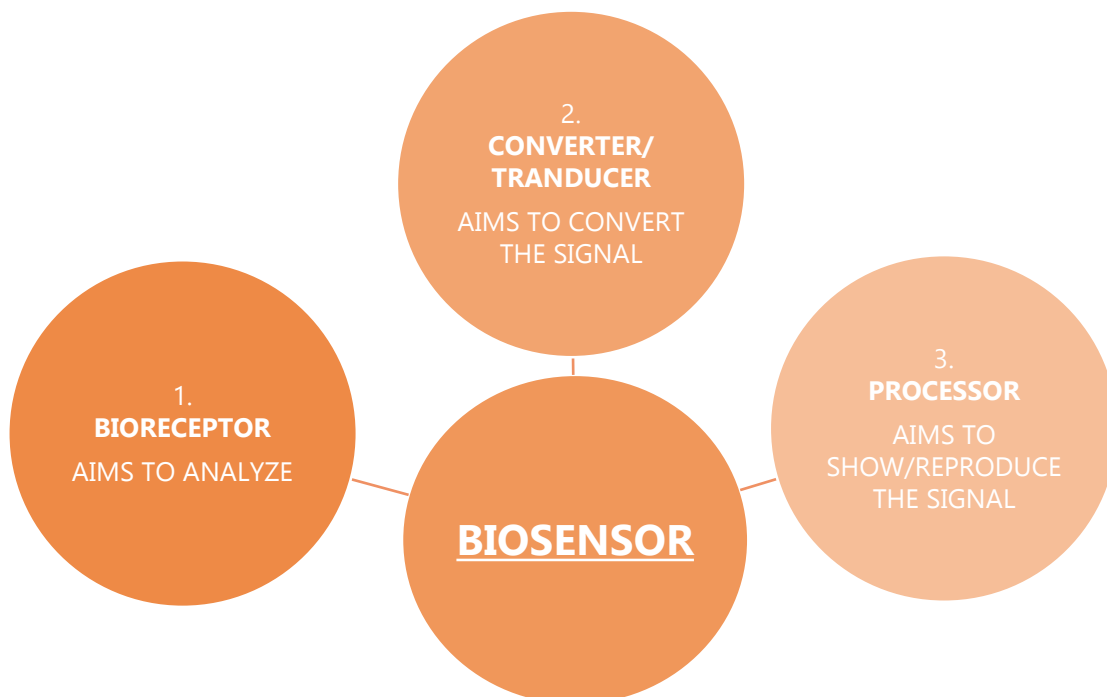


Figure 2. General biosensors' structure.

In particular, the biosensor's components are [Figure 3]:

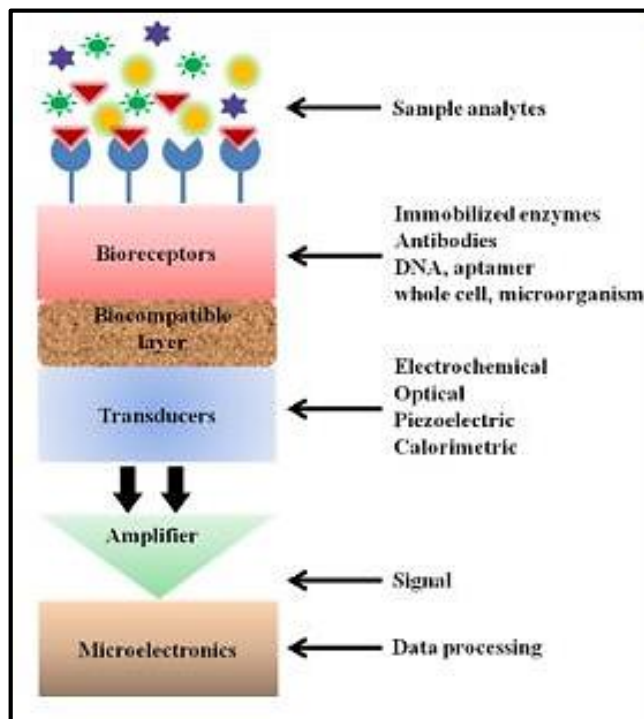


Figure 3. Detailed Biosensors' structure. Reproduced from ref. ²¹ © The Royal Society of Chemistry 2019

Sensors may alternatively be classified according to the detection method. If the detection needs to be accurate, chemical, magnetic, electric or ultrasonic sensors may be employed.

1.1.1.1 Selectivity and Sensitivity

Sensors are characterised according to the performance criteria of sensitivity and selectivity, detection ranges and operational limits, stability and response times. For a sensor, to be 'selective' means to detect just one substance among different reactants. In fact, an enzyme's active site is capable of interacting with substrates only if they are geometrically and functionally complementary. Being 'sensitive' on the other hand indicates the low quantities of reactant necessary for detection. The selectivity is an intrinsic property of an enzyme sensor, contrarily the sensitivity is a property which typically needs to be improved. In this way, the sensor will be

capable of detecting even trace amounts of substances or single molecules in a system. The detection limit or lower limit of detection (LOD) is the lowest quantity of substance that can be identified.

1.2.2. Amplification

Amplification is required to improve the sensitivity of sensors when the analyte is present in low concentrations. This is generally achieved by developing methods to increase the concentration of output molecules in response to the input signal.

According to Goldbeter and Koshland 'sensitivity amplification' is the term used to indicate the increase in the signal strength of the output with respect to the input acquired by the sensor²⁸. If it can be assumed that in the system there is a stimulus (S) that activates the enzyme, the amplification can be defined as the ratio of the final flux (output, Φ) over the initial flux. Analytically, the amplification factor A_s can be defined as:

$$A_s = \frac{\Delta\Phi/\Phi_i}{\Delta S/S_i} = \frac{(\Phi_f - \Phi_i)/\Phi_i}{(S_f - S_i)/S_i} \quad (1)$$

Where the subscripts f and i refer to the final and initial condition, respectively. The amplification factor gives the percentage change in the response relative to the variation in the stimulus. There are a number of basic mechanisms to achieve such sensitivity amplification in enzyme biosensors²⁸ including classical allosteric cooperativity. Allosteric regulation of an enzyme occurs when an effector molecule (or ligand) binds to the enzyme either activating or inhibiting it^{28,29}. Ultrasensitivity is also a type of amplification that results in a sharp "on-off" response.

Numerous studies have attempted to explain how to improve and maximize the amplification process. As an example, Saghatelian et al.³⁰ produced a system with an engineered allosteric enzyme for DNA detection. The allosteric enzyme had the

active site combined with an inhibitor, so it was not active. When a complementary DNA sequence was added to the system, the enzyme was capable of detecting it, activating itself by removing the inhibitor from the active site. Once the enzyme was activated it catalysed a reaction to produce an optical signal. In this way, many output molecules were produced from a small input: 10 fmol of DNA could be detected in less than 3 minutes.

'Magnitude amplification' indicates a process in which the input stimulus is smaller with respect to the number of output molecules which carry the response to the next step of the system²⁸. It can be achieved by a single enzyme or a cascade process. An example is the blood clotting cascade process leading to a magnitude amplification. Basically, magnitude amplification is needed whenever a small amount of signal has to be translated into a readable output response.

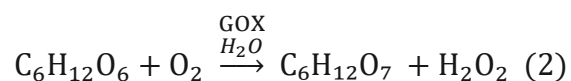
1.2.3. Types of enzyme biosensors

1.2.3.1. Enzyme reactions

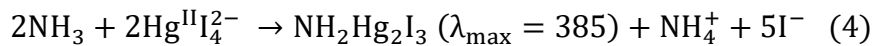
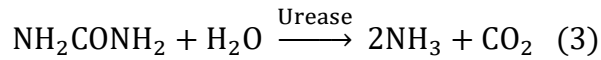
Among all the possible biological elements that might be used to build a biosensor e.g. antibodies, cells, and synthetic molecules, the ones chosen in this work have been enzymes. Although all of them are good candidates for high selectivity, only enzymes have shown to well behave in terms of durability, robustness and range of applications whereas the other biological reagents are often poorly stable on the long term³¹.

It has been observed that an abundance of enzymes is frequently employed in biosensors. Herein, a selection of enzymes shall be presented.

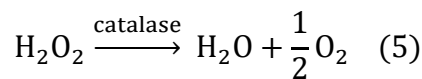
- Glucose oxidase serves as a popular option for detecting glucose levels within the bloodstream³²:



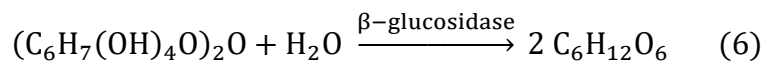
- Ureasases are a group of enzymes, widely used in nature, which catalyse the hydrolysis of urea, producing carbon dioxide and ammonia. The urease reaction is used for the detection of urea³³:



- The enzyme catalase is present in many living organisms and regulates the amount of hydrogen peroxide³⁴:



- B-glucosidase enzyme is widely recognized for its significant capability to catalyse the hydrolysis of complex sugar chains, including cellobiose, into simpler monosaccharides³⁵:



These enzymes represent merely a fraction of the vast variety of enzymes available for use in biosensors, with the ultimate selection being dependent on the specific application at hand.

1.2.3.2. Enzyme supports

Enzyme biosensors typically require immobilization of the enzymes for stable and continuous monitoring. Furthermore, encapsulating enzymes is a brilliant method to improve their stability and enhance their reusability³⁶⁻³⁷. Over the years, researchers' attention has been directed to enzyme immobilization techniques. Specifically, what sustainable processes and materials could be used to develop biosensors. The classic methods can be described as follows^{3,38,39}:

- Entrapment: a gel is formed in the presence of the enzyme. The gel formation does not necessarily need an enzyme, but it impacts on the time scale of the process.
- Adsorption: Enzymes are deposited by dipping the support in an enzyme solution for a certain amount of time followed by a dip-evaporation step. Although the approach is simple, the enzymes are not deposited in an ordered way.
- Sol-Gel Process: A solution in which a gel-like material is created and then put in the oven for solvent evaporation. The sol-gel formation is an easy immobilization method and it is conducted at low temperatures to be compatible with biomolecules.
- Covalent Binding: The nucleophilic groups not involved in the active site, present in the amino acids of the enzyme, are used to form the covalent linkage. The working conditions need to be low temperatures and neutral pH to avoid the loss of functional enzymes.
- Polymeric Films: Enzymes are trapped in polymers as a result of ion-pair interactions and hydrogen bonds. This method also shows excellent biocompatibility, high affinity and low molecule permeability¹³.

Some methods have been improved over time, such as enzyme immobilization on mesoporous silica particles. The first technique consisted of covering an enzyme with a polyelectrolyte multilayer, very easy to make but with leaky encapsulation⁴⁰. A later method used mesoporous silica in which the enzyme was immobilized and the polyelectrolyte layer was deposited layer by layer. Then, the mesoporous silica was dissolved, and the free enzyme was trapped inside the multilayer. When an external condition was altered, like pH, the multilayer permeability changed allowing the enzyme to diffuse outside⁴⁰. The process is shown schematically in **[Figure 4]**.

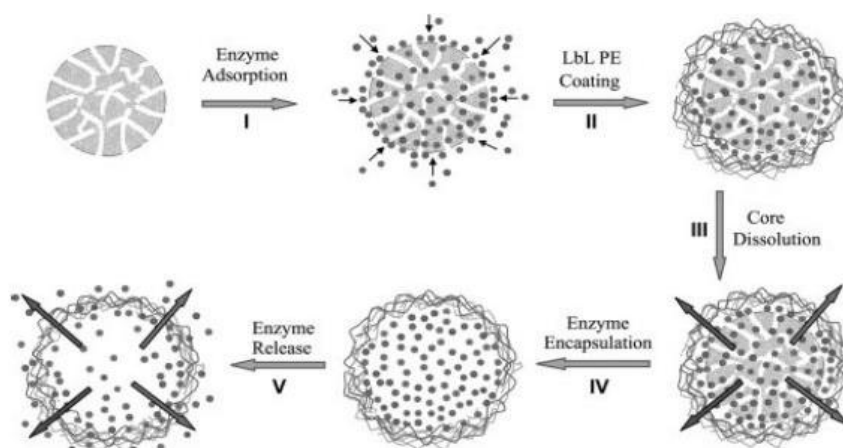


Figure 4. Mesoporous silica particle scheme. Reproduced from ref. ⁴⁰ © 2005 WILEY-VCH

Mesoporous silica has been used in recent research combined with an ELISA (Enzyme-linked immunosorbent assay) sensor introduced by Engvall and Perlmann in 1971 for signal amplification⁴¹. ELISA is a system formed by an antibody and enzymes combined with an antigen (a large biological molecule to be detected). In the presence of an enzyme substrate, ELISA produces an optical output that changes the colour of the solution [Figure 5]. Typical enzymes used include horseradish peroxidase (HRP) with substrate tetramethylbenzidine (TMB).

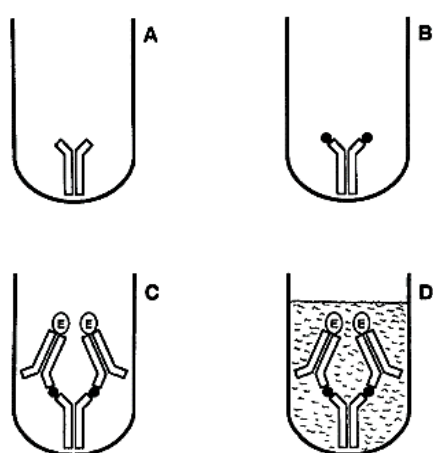


Figure 5. Sandwich ELISA sensor scheme: (A) Solid-phase adsorbed antibody on microwell plate. (B) Formation of antigen-antibody complex. (C) Detecting enzyme-labelled second antibody combining with "solid-phase" antigen "sandwich." (D) Addition of substrate. Reproduced from ref. ⁴² © Humana Press 1994

To advance the signal amplification, a large quantity of enzymes needs to be present requiring biocatalysts immobilization in particles. In contrast to past work in which liposomes and polymers have been used, a new technique with dendritic mesoporous silica nanoparticles has been tried²⁰. This material has a large surface area, high pore volume and large pore size so it is possible to immobilize a high quantity of enzyme with a simple physical absorption. The new improved sensor is called ELISA+ [Figure 6].

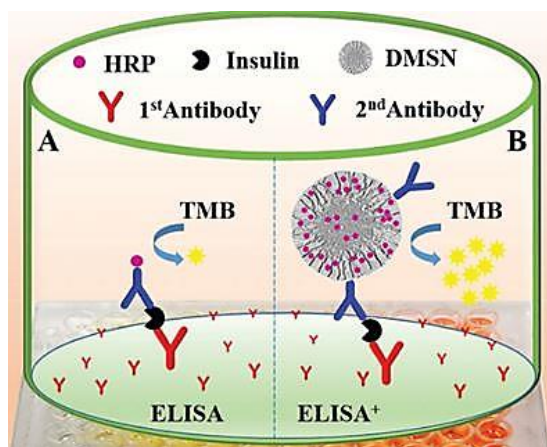


Figure 6. Comparison between A. Eliza sensor and B. Eliza+ sensor where HRP = Horseradish Peroxidase. Reproduced from ref.⁴¹ © The Royal Society of Chemistry

Many new studies and discoveries have taken place in the last twenty years regarding the immobilization of enzymes on nanoparticles. Nanoparticles are defined as nanomaterials with a diameter smaller than 100 nm⁴³ and the main reason to use such a small size is to decrease the diffusion limitation and at the same time increase the surface area⁶. The big advantage of nanoparticles is their versatility in size and shape. Nevertheless, it is possible to combine inorganic core, which gives them properties not achievable with an organic compound, with organic ligands. Then one can decorate the end of the ligands with different functional groups, according to the external stimuli of the system. These can be both chemical e.g. solvents, acid/base, metal ions or redox and physical e.g.

temperature, magnetic field or light. By altering the nanoparticle structure, it is also possible to generate self-assembled nanoparticles using different ligands which respond to different stimuli²⁷. Moreover, enzymes immobilized on nanoparticles are more resistant to a severe range of temperature and pH⁶.

An example of an inorganic core enriched with organic functional groups is the metallic nanoparticles, in particular, gold nanoparticles⁴⁴. They are chemically robust, highly stable and lightly soluble, perfect biosensors for chemical or biological samples [**Table 2**]. Furthermore, there is increasing interest in the gold nanoparticles properties: catalytic, optical, magnetic and electronic⁴⁵, making them very versatile for every substance that needs to be detected⁴³.

Table 2. Nanoparticle-based enzyme biosensors examples in industrial and clinical application. Reproduced from ref. ⁶ © 2011 Elsevier Inc.

Enzyme immobilized	Type of nanoparticle	Application	References
Glucose oxidase	Selenium nanoparticle	H ₂ O ₂ biosensor, determination of free glucose in body fluids, food and agricultural products	Zhang et al., 2004a, b
Uricase	ZnO nanoparticle	Uric acid biosensor, evaluation of serum uric acid	Zhang et al., 2004a, b
Glucose oxidase	Gold nanoparticle	Biosensors, catalytic nanodevice to construct nanoreactors	Yang et al., 2006; Li et al., 2007
Laccase	Zinc-tetra-amino-phthalocyanine-Fe ₃ O ₄ , laccase-modified silica nanoparticles, magnetic core-shell (Fe ₃ O ₄ -SiO ₂) nanoparticles	Fiber optic biosensor, catechol biosensor and in degrading bisphenol A	Huang et al., 2007; Zhang et al., 2007; Galliker et al., 2010
Glucose oxidase	Nickel oxide nanoparticle	Amperometric biosensor and electrochemical investigation of glucose oxidase	Salimi et al., 2007
Glucose oxidase	Platinum nanoparticle, gold nanoparticles	Biosensors, naked eye detection of glucose in urine	Zhao et al., 2007; Radhakumary and Sreenivasan, 2011
Urease	Silver nanoparticle, phosphonate grafted iron oxide nanoparticle	Biosensors, analysis of urea content in blood, urine, alcoholic beverages, natural water and environmental wastewaters	Crespilho et al., 2009, Sahoo et al., 2011
Peroxidase	Gold-chitosan nanoparticle	Rapid deterioration of H ₂ O ₂ , water treatment, pharmaceutical and biomedical applications	Lin et al., 2007
Glucose oxidase	Pt/FGS/chitosan, silica nanoparticle	Glucose biosensor, quantitative estimation of glucose	Wu et al., 2009a, b, Jang et al., 2010
Cyclodextrin glycosyl transferase, alcohol oxidase	Cellulose-silver nanoparticle	Biosensors, determination of methanol and methyl ester content of pectin	Ma and Ding, 2009; Mahmoud et al., 2009; Ling and Heng, 2010

An additional challenge scientists are trying to overcome is the immobilization of several enzymes on the same support for the detection of multiple species. In one of these works, the biosensor was prepared using a ZnO film functionalized with three different enzymes on a flexible membrane for the simultaneous detection of alcohol, glucose and lactate. Detection was possible in a sample of sweat.

In [Figure 7] it is possible to observe a picture of the biosensor; the M1 and M2 regions are the electrodes, whereas the S region is the biosensor⁴⁶.

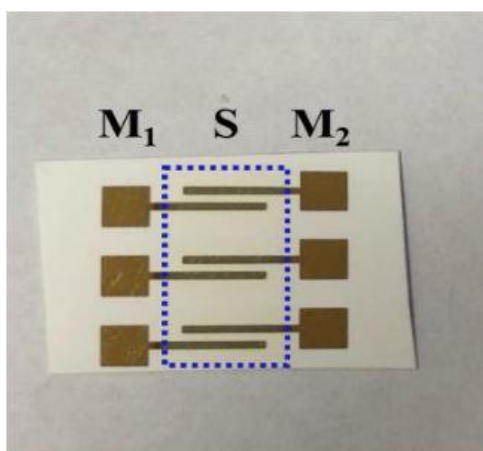


Figure 7. ZnO based biosensor. The S region represents the biosensor whereas the M1 and M2 regions are the electrodes. The biosensor has been functionalised with three different enzymes in order to detect simultaneously alcohol glucose and lactate. Reproduced from ref. ⁴⁶ © MDPI

Recently, biosensors were created and developed using materials such as quantum dots and liquid crystals to take advantage of their different properties and improve the technology. Quantum dots (QDs) are semiconductor nanocrystals characterized by high brightness, good photostability and long fluorescence lifetime. Their integration with various nanomaterials such as noble metal nanoparticles can create new possibilities in nanoscience and nanotechnology for biomedical and environmental applications⁴⁷. In particular, the combination of QDs with molecule detection creates QD-based nanosensors with significant advantages of high signal-to-noise ratio, low sample consumption, and high sensitivity gold nanoparticles (AuNPs) exhibit unique electrical, optical and catalytic properties. The coupling of AuNPs with QDs may lead to the QD–AuNP configuration for biosensing. This method could reach a detection limit of 0.52 μM and a penetration depth of 400 μm without the biological environment interfering^{5,47}.

Liquid crystals (LCs) are materials that can exhibit both the mobility of liquids and the anisotropy of solid crystals. The LC molecules can transform chemical and biomolecular binding events into amplified optical signals that can be easily

observed, even with the naked eye⁴⁸. The LCs are used as sensing elements in the detection of biomolecules because they can localize biomolecules with micrometre resolution. In this way, the LC biosensing technique is used in bioassays for low concentrations or trace amounts of analyte. The procedure can be carried out in natural light without electricity. A protein assay on plain glass substrates coated with an organosilane has been produced for inducing the homeotropic alignment of LCs⁴⁸. The method can conveniently provide a yes/no answer when the protein concentration exceeds a critical value. The LC cells' surface modification plays a key role in the orientation, it has a great influence on the signal-to-noise ratio and the distinction between positive and negative results which can indicate both the identity and/or concentration of the substance.^{48,49}

Another technique to incorporate enzymes is obtained using a patterned paper. It is formed by compartments hydrophilic separated by hydrophobic "walls". This allows to detect and analyse different samples at the same time just taking advantage of the capillary action, using small volumes. These sensors are inexpensive, portable, easy to fabricate, small and disposable. It is based on the use of protein for detection and a colorimetric change to show and amplify the output response. In **[Figure 8]** it is possible to observe an example of how it works⁵⁰.

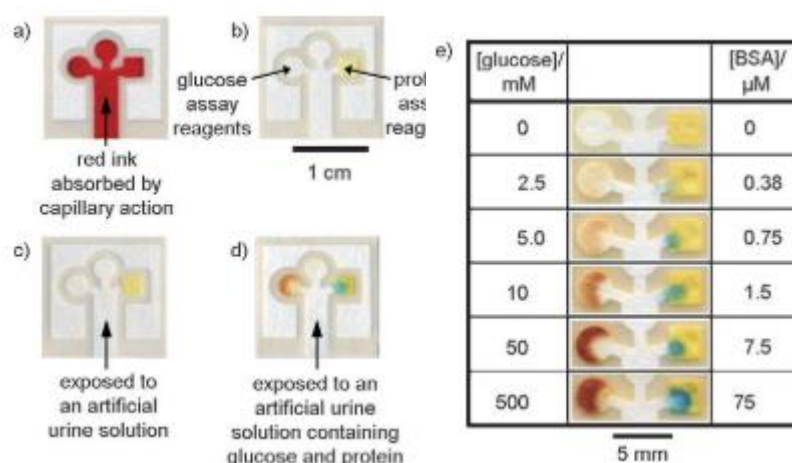


Figure 8. Paper-based detection assay for glucose and protein BSA. Reproduced from ref. ⁵⁰ © 2007 WILEY-VCH

However, due to the necessity of improving biosensors' characteristics, many applications rely on the use of hydrogels⁵¹. Hydrogels are a crucial material in sustainable and biocompatible biosensors, playing a pivotal role in recent studies. Engineered hydrogels offer a vast range of possibilities [Figure 9], including industrial, biomedical, drug delivery, soft robotics, and regenerative medicine applications^{52,53}.

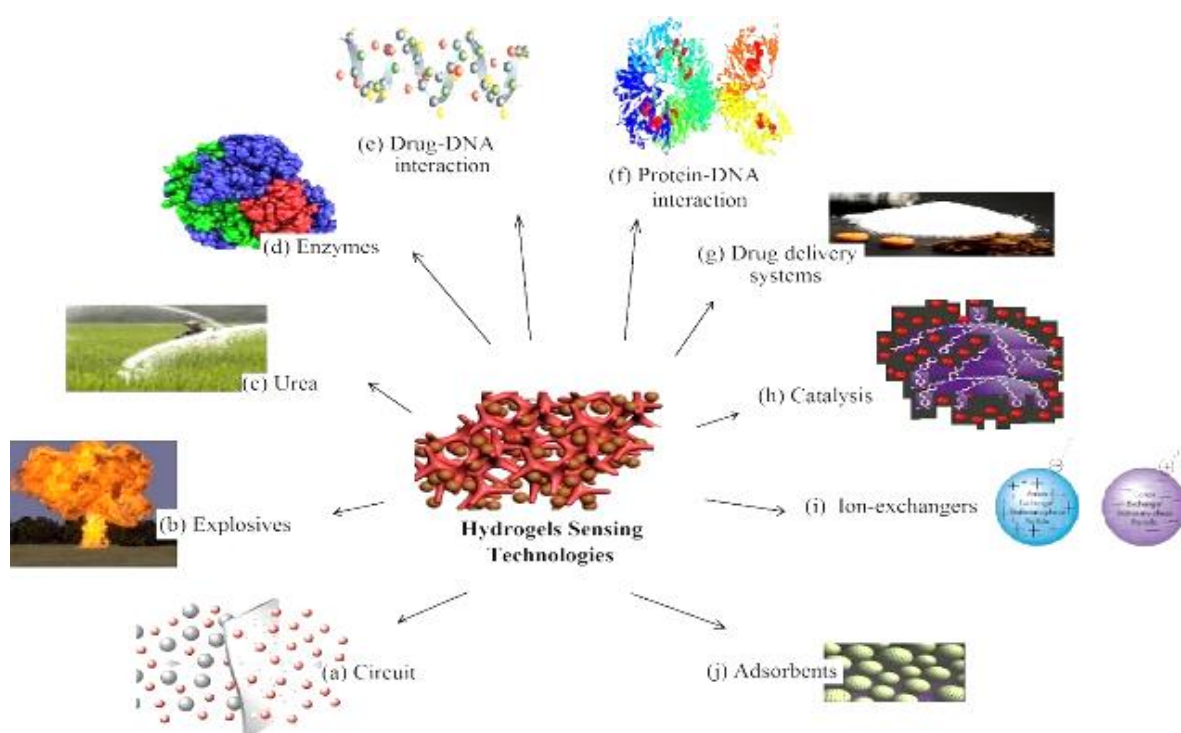


Figure 9. Hydrogel possible applications and use scheme. Reproduced from ref. ⁵² © 2015 Elsevier

Researchers are actively working to understand and replicate the features and materials by combining polymers in hydrogels. When applied to medicine and pharmaceuticals, these materials are referred to as biomaterials and possess the ability to adapt and replace tissues and structures in the human body. Today, the most commonly used materials include natural polymers and combinations of them. Many hydrogels are created through polymer cross-linking in an aquatic environment, and different and enhanced features can be achieved depending on

the polymer combination and technique used. One particularly intriguing aspect of hydrogels is the stimuli-responsive nature of gels that can react to various stimuli, such as light, pH, temperature, and chemical species. With its vast potential, hydrogels continue to be a significant area of interest for researchers and scientists alike [Figure 10].

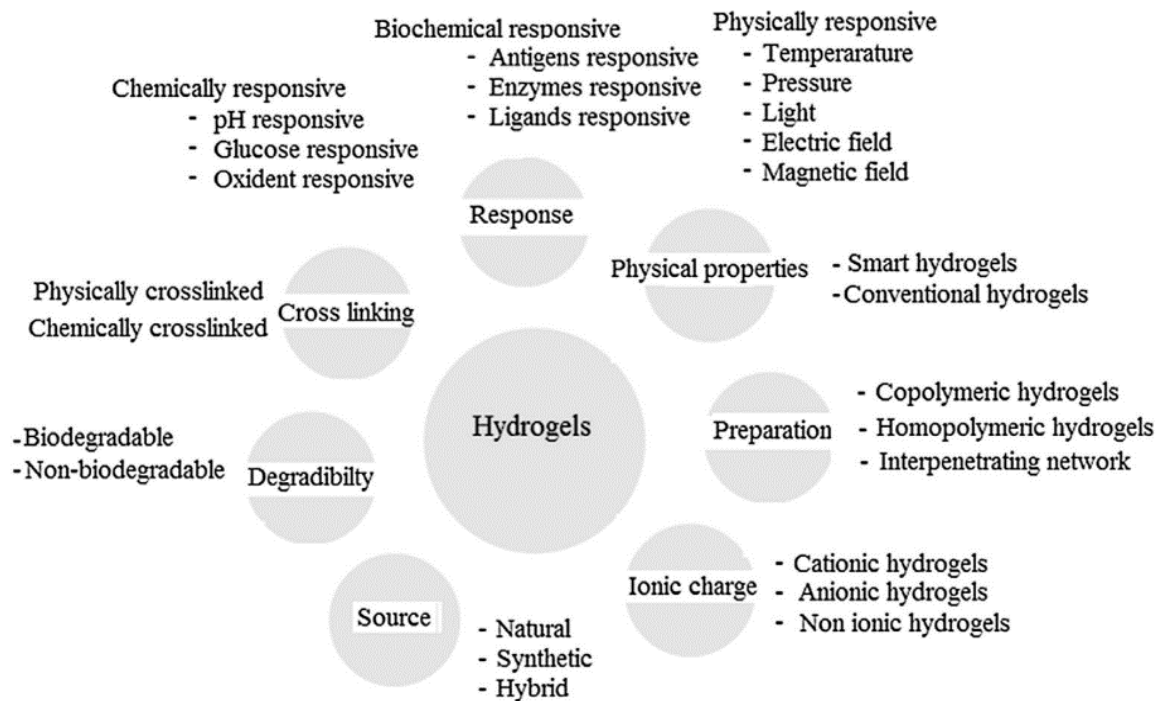


Figure 10. Different properties of hydrogels. Reproduced from ref. ⁵² © 2015 Elsevier

The advancement in material science and enzyme encapsulation technology has paved the way for the development of responsive gels, which have garnered significant interest in the scientific community. These materials are designed to exhibit changes in size and shape in response to external stimuli, with temperature and pH being the most common triggers [Figure 11]. Responsive gels have the unique ability to swell or shrink based on the input stimuli, which enables them to be used in a wide range of applications^{54,55}.

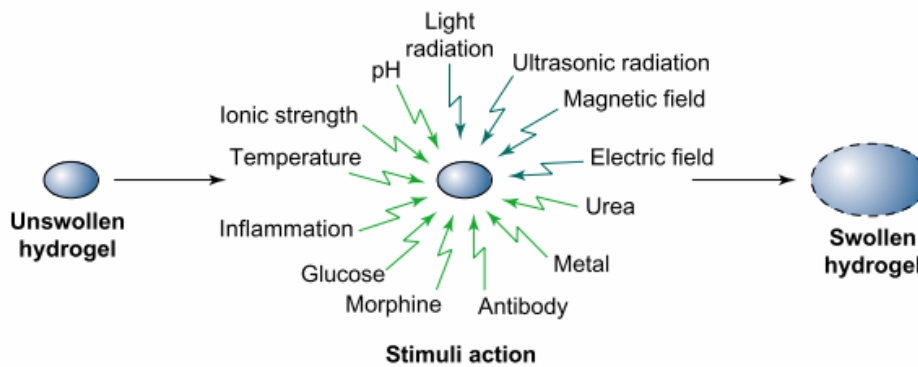


Figure 11. Responsive gel stimuli classification. Reproduced from ref. ⁵⁶ © 2002 Elsevier Science Ltd.

When exposed to chemical stimuli, such as changes in pH, the responsive gels exhibit a chemo-mechanical response mechanism, whereby they react to the external chemical stimulus by altering their physical structure. This unique property enables the creation of smart materials that can self-regulate in response to various stimuli, including different substrates [Figure 12]. The versatility of responsive gels is further enhanced by their ability to be loaded with a diverse range of enzymes. This feature enables the creation of more complex systems, including chemical reaction networks and cascade reactions⁵⁷.

The development of responsive gels is a complex scientific challenge, and their successful application requires intricate adjustments to enable their use in various applications, including sensors⁵⁸⁻⁵⁹ and drug delivery devices^{60,61,56}. One interesting example of application is given by Isakova and Novakovic⁶² who were able to couple oscillatory systems and smart materials in order to generate a drug delivery device based on the chitosan-palladium combination.

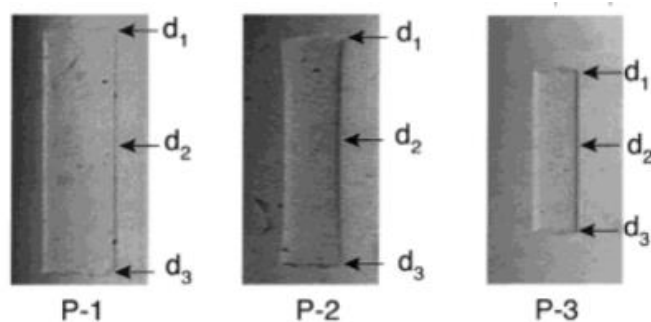


Figure 12. Schematic example of a responsive urease gel shrinking as a pH change consequence. Reproduced from ref. ⁶³ © 2002 American Chemical Society

In conclusion, responsive gels represent a significant breakthrough in material science and have the potential to revolutionize various fields. Their unique properties and capabilities, including chemo-mechanical response mechanisms and smart material capabilities, make them an exciting area of research and development.

1.2.4. Properties of enzyme biosensors

The fundamental principle behind biosensors is the detection of information and the production of a signal that can be interpreted by the user. Despite this commonality, each class of biosensor generates unique outputs based on its distinctive properties. The three primary categories of biosensors are electrochemical, magnetic, and optical, although this is not an exhaustive list. For a more comprehensive understanding of the various types, reference can be made to [Table 3]. The aim of this review is to provide an overview of the different properties, methods, and applications of these biosensors, highlighting their significance in various fields. It is important to note that biosensors play a critical role in a wide range of scientific and medical applications, and their continued development and refinement will undoubtedly result in even more innovative and impactful applications in the future.

Table 3. Biosensors' type of outputs. Reproduced from ref. ⁶⁴ © Taylor & Francis

Type	Principle	Advantage	Disadvantages
1. Optical a. Fiber optics	Evanescent wave based, allows measurement of binding at the fiber surface	Remote in-situ measurement, inherent sensitivity of optical approaches	Costly equipment and not portable,
b. Laser interferometry	Planar waveguides have evanescent field responsible to change in index of refraction	Highly sensitive, detect up to 1 cell	Susceptibility to turbidity interference
2. Electrochemical a. Conductometric b. Potentiometric c. Amperometric	Change in conductance Electric potential Oxidation/reduction	Fast, low cost	Highly buffered solution may interfere
3. Piezoelectric	Quartz crystals oscillation at defined frequency, binding of an analyte to it changes the mass of crystal hence oscillation frequency	High sensitive, fast	Sensitivity level up to 1 cell have not demonstrated
4. Colorimetric/Strip	Color development	Not required any instruments	Not quantitative
5. DNA biochip	Array based	Instrument required	Quantitative

The electrochemical biosensor is widely used. It can be differentiated into three other subgroups depending on the way the electrical output is produced: amperometric, potentiometric and piezoelectric. The support for this kind of biosensor may be carbon, in the form of nanotubes, as well as graphene, or nanoparticles. The limitation of using an electrochemical output in a biological environment is that it could be altered by electrochemical interference promoted by the chemicals present in the matrix.

The amperometric biosensor is based on oxidoreductase enzymes coupled with amperometric detection. The biocatalytic conversion of the analyte is related to a redox process, which results in electron transfer that consequently generates current, proportional to the analyte concentration, which is quantified using an electrochemical set-up. Potentiometric biosensors, conversely, are usually characterized by short lifespan, delayed response time and low sensitivity.

Piezoelectric biosensors take advantage of the compression of materials to create a localized charge, which gives a signal to be measured. Usually, to generate oscillations, acoustic waves are reproduced at a defined frequency and quartz crystal is the material chosen to allow high sensitivity. The piezoelectric method has emerged due to its simplicity, cost, sensitivity and real-time label-free detection⁶⁴.

Magnetic biosensors exploit magnetic or electromagnetic forces. One of the latest works uses nanoparticles for a "magnetic sensitive biosensor"⁶⁵. Magnetic nanoparticles (MNPs) have been shown to have wide application prospects in the field of biological detection due to their biocompatibility, stable physical and chemical properties and superparamagnetism. They can be magnetized by an oscillating magnetic field and by measuring the magnetic intensity, the number of magnetic particles can be detected. This type of labelled biosensor is sensitive to biomolecules with magnetic properties. It converts the magnetic signal into an available output signal for biomolecular detection. Compared with traditionally labelled biosensors, it has the advantages of easy operation, high sensitivity, quantitative accuracy, good reproducibility, specificity and interference-resistance. Applications are quite diverse and include the fields of biological detection, medicine and food hygiene inspection, the detection of various pathogenic bacteria, and as a tumour marker. As a result of its properties, it is becoming the most promising field detection tool, which can alter traditional biological detection methods⁶⁵.

An optical biosensor is a device using a signal as output which can be detected with the naked eye, as well as a microscope or related tools. These biosensors produce a colourimetric change, radiation, refraction, absorbance or fluorescence^{66,67}. The precise output depends mainly on the enzyme's properties: examples based on various enzymes are shown in [Table 4].

A variety of optical biosensors are available nowadays but possibly the simplest and easiest ones to use are the biosensors based on the colourimetric change and

fluorescence, called direct optical biosensors because of the absence of a transducer. This is because certain enzymatic reactions do not require optical transduction since optically detectable species are generated or consumed during the reaction. Optical biosensors are capable of giving changes in colour or luminescence at room temperature, at near-neutral pH, in a reasonably short time and in a reversible way. An indicator layer, usually sensitive to a species or pH, is spread over transparent inert support. An indicator dye is either directly dissolved in a polymer matrix or, alternatively, covalently immobilized or physically adsorbed on the surface of microbeads. The indicator layer is responsible for sensing either substrate consumed or products produced during the enzymatic reaction.⁶⁸ Optical sensors that exploit chemiluminescent and bioluminescent reactions are usually simpler because no indicator layer is required. Such sensors usually consist of a membrane that contains the immobilized enzyme. Chromogenic or fluorogenic substrates are added to the sample into which the sensor is submerged. Generally, the optical biosensor activity can be improved and amplified by coupling or using it in the form of nanoparticles⁶⁹, gold nanoparticles⁴, quantum dots⁴⁷ and liquid crystal⁷⁰.

Table 4. Examples of optical biosensors for various enzymes. Reproduced from ref.⁶⁸ © 2008 American Chemical Society

analyte	enzyme	transducer	analytical range	LOD	spectroscopy	indicator or substrate	ref
L-phenylalanine	L-phenylalanineDH		0.6–6 mM	?	LI.	PEG–NAD ⁺	223
phenylpyruvate	phenylpyruvateDH		0–0.7 mM	?	LI.	PEG–NAD ⁺	222
pyruvate	LOx + LDH		0–0.1 mM	8.4 μM	LI.	NAD ⁺ (coenzyme)	215
sorbitol	sorbitolDH + OR + b. luciferase		20 nM–10 μM	20 nM	BL		233
sulfite	sulfite oxidase	oxygen	0–100 ppm	?	LI.	perylene	151
sulfite	sulfite oxidase + HPOx	H ₂ O ₂	1–100 μM	0.5 μM	CL	luminol	163
superoxide radical	superoxide dismutase + HPOx	H ₂ O ₂	?	20 nM	LI.	Amplex Red	124
urea	urease	pH	0–40 mM	?	Abs.	BTB	172
urea	urease	pH	0–2 mM	?	Refl.	BTB	180
urea	urease	pH	40–250 μM	?	Refl.	phenol red	181
urea	urease	pH	?	?	LI.	FITC	182
urea	urease	pH	0–1 mM	20 μM	LI.	NBD-PE	186
urea	urease	pH	0–4 mM	?	Refl.	FITC	183
urea	urease	pH	0–100 mM	?	Abs.	PVP	187
urea	urease	pH	0.2–100 mM	0.1 mM	Abs.	Prussian Blue	185
urea	urease	pH	0.06–1 M	0.06 M	Abs.	polypyrrole	184
urea	urease	pH	2.0–12.0 mM	?	Abs.	Prussian Blue	97
urea	urease	pH	0.001–10 mM	2.5 μM	ratio of LI	FITC	39
urea	urease	pH	0–400 μM	?	ratio of LI	SNARF	34
urea	urease	NH ₃	0.05–2.5 mM	?	LI.	CF	188
urea	urease	NH ₃	0.25–8 mM	0.25 mM	Abs.	BTB	189
urea	urease	NH ₃	0.1–5 mM	?	LI.	HPTS	190
urea	urease	NH ₃	0.01–1 mM	0.03 mM	LI.	Nile Blue	191
urea	urease	NH ₃	0.1–100 mM	0.1 mM	Abs.	acridine orange	192
urea	urease	NH ₃	10 μM–100 mM	?	Abs.	ETH 5350	193
urea	urease	NH ₃	0.1–10 mM	?	Abs.	brilliant yellow	194, 195
urea	urease	NH ₃	0.1 mM–0.1 M	0.1 mM	LI.	octadecyl dichlorofluorescein	196

1.2.5. Applications

Biosensors have emerged as highly promising tools for a wide range of applications owing to their remarkable cost-effectiveness, ease of application, and exceptional versatility. They offer a plethora of benefits and have found their way into various fields such as biomedicine and industry (pharmaceutical and food), research, and diagnosis. There is tremendous potential for practical innovation with biosensors in the future. Their dynamic capabilities and adaptability make them an ideal choice for a diverse range of applications, and we can expect to see continued growth and development in this exciting field. Biomedical biosensors are exploited in different modes:

- As “offline” devices → samples are collected and measured using biosensor-based analytical equipment. For example, measuring blood glucose.
- As “in vivo” sensors → when they are implanted to detect extracellular changes. For instance, as drug delivery devices⁷¹

- As an “on-line” device → when integrated with a sampling device implanted in the body or biological material. For instance, microdialysis probes can be implanted and connected to a flow-through detector incorporating a biosensor element³.

Some of the first studies on biosensors were made for DNA detection and disease diagnosis⁶⁴. Later, uses of biosensors in the biomedical field concerned the detection of glucose⁴⁶ and hydrogen peroxide⁷², as well as urea/ammonia^{68,73,74}, tumours^{3,43}, lactate, glutamate and cholesterol²⁴ or coupled with antigens to build an immunoassay system (ELISA)^{14,41}.

Biosensors can also be applied in environmental applications. It is possible to detect pollutants, toxic intermediates and heavy metals from waste streams and to monitor weather conditions such as humidity. Nanomaterial-based sensing tools can be used to find the extent of damaging materials present in the environment as organic pollution, water treatment, and oil recovering^{47,75}. Biosensors have been used to monitor the abiotic conditions that are essential for the optimization of biological recovery from contamination^{26,44}. They have been developed for the detection of nitrates, inorganic phosphates, and biological oxygen demand⁵⁰.

In industry, it is possible to use biosensors to regulate the feeding of nutrient media and substrate mixtures in bioprocessing. On an industrial scale, many commercial preparations and separations can be improved with sensors. For instance, in metallurgical operations requiring the separation of impurities existing in a complexed form, nano-biosensors can be used to selectively separate the impurities by exploiting different configurations of the sensing enzymes²⁶.

A further application recently adopted in forensic analysis concerns biomarkers appearing in blood samples left at a crime scene by people of different ethnicities and gender³⁶. It combines the properties of biosensors with a Boolean logic gate and is discussed further below.

1.3. New directions in Enzyme biosensors

Biosensors have a high potential, great versatility and wide applications and scientists are trying to improve their properties and functionalities as well as couple them with more complex systems. The aim is to achieve a semi-automated device that is sensitive to a trace amount of substance (ultrasensitive), to control a cascade of reactions (e.g. in a feedback loop), to process biological information and give a clear and precise signal/answer (Boolean logic gates, noise-driven amplification).

1.3.1. Boolean logic gates

Recent advances in biochemical computing have made it possible to combine cascade enzymatic reactions and computing gates, such as AND, OR opening new biosensing opportunities⁷⁶⁻⁷⁷. The system is composed of an enzyme which will perform a biocatalytic reaction and it will be "the information processing system". It will then mimic computing networks where input/output signals will be represented by biochemical means. Supposing there are two enzymes present in the system, the possible answers are

- (1,1) → both present in the system
- (0,0) → both absent in the system
- (1,0) or (0,1) → just one of the two is present in the system.

When the AND gate is arranged to obtain the "yes" response from the system, both the enzymes have to present (1,1), if another configuration happens the response will be "no" [Figure 13]. when the OR gate is formulated, the configuration (0,0) will give a "no" whereas all the others will give a "yes" [Figure 14]. The enzyme-based logic gates are considered components of future biomolecular computing systems and their biosensing applications will be used in multiple fields.

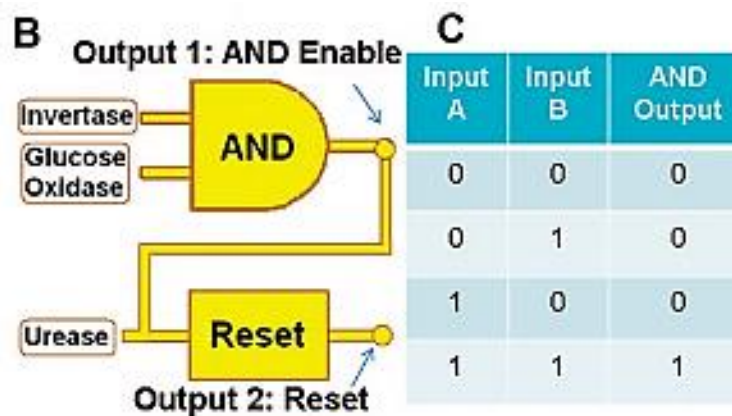


Figure 13. Schematic functioning of an AND gate. (B) Equivalent electronic circuit. (C) Results table. Reproduced from ref.⁷⁸ © 2016, Springer-Verlag

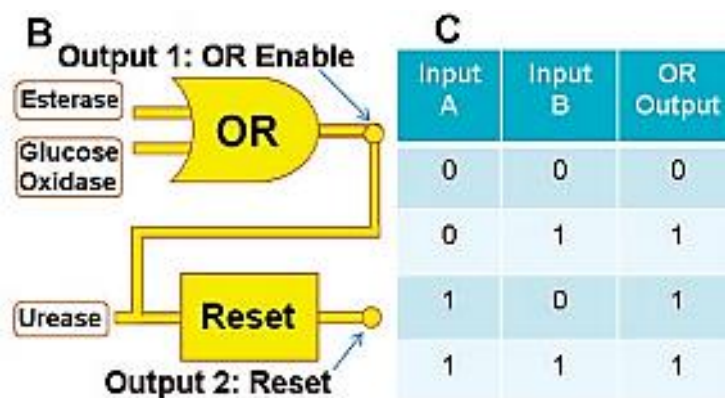


Figure 14. Schematic functioning of an OR gate. (B) Equivalent electronic circuit. (C) Results table. Reproduced from ref.⁷⁸ © 2016, Springer-Verlag

Significant progress in the design of enzyme logic systems has been achieved such as the formulation of various enzyme-based logic gates and highly sophisticated multi-input/multi-output logic systems. They are composed of many biocatalytic steps performing concatenated logic operations and elementary computing. The final main goal is to operate with biosensors to logically process multiple signals through Boolean logic gates composed of several biomolecular reactions, producing a final and clear output signal such as YES/NO responses⁷⁶⁻⁷⁸.

As an example, a biocatalytic cascade can mimic an AND gate and be activated by two enzymes which are present in different concentrations in the blood of Caucasian and African American groups. The difference between the response to 0,0 and 1,1

combinations (absence or presence of a particular enzyme), can distinguish the sample origin with high confidence. [Figure 15] shows the different absorbance changes originating from the natural distribution of the biomarker concentrations. A similar approach was applied for analysing blood samples to distinguish the difference between male and female samples⁷⁷.

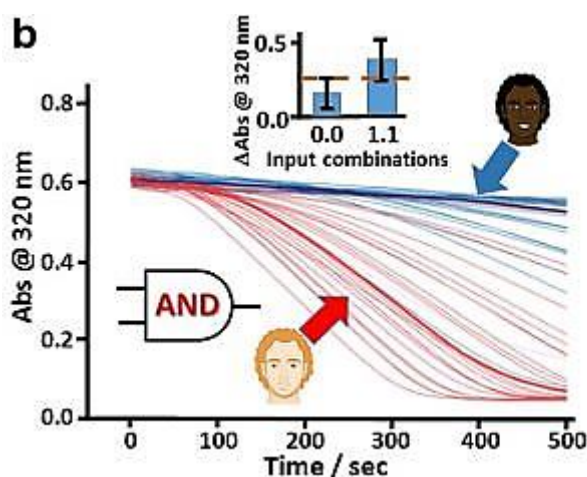


Figure 15. Example of sensor used in the forensic field. when it shows the red light, it means the sample belongs to a Caucasian group; when it is blue the sample belongs to an African American group. Reproduced from ref.⁷⁷ © 2016, Springer-Verlag

1.3.2. Ultrasensitivity

Ultrasensitivity is a phenomenon occurring when a biosensor is highly sensitive to a small variation of a stimulus so that its status changes e.g. in colour, pH, fluorescence and consequently undergoes a large amplitude response¹⁰⁻¹¹. The stimulus-response plot corresponding to this kind of behaviour is generally a sigmoid and the steeper the profile, the more the biosensor is ultrasensitive. When a system responds to a stimulus in a sigmoidal way, it is referred to as a switch [Figure 16] e.g. below a certain concentration of substrate (kinase) the biosensor is “off” and at a certain point the minimum increase of this concentration turns it “on”.

The terms ‘sensitive’ and ‘sensitivity’ usually refer to how much input is needed to achieve a particular level of output. A measure of this type of sensitivity is the EC₅₀,

which is the amount of input required to achieve a half-maximal output¹⁰. The lower the EC50, the higher the sensitivity. Alternatively, sensitivity can be calculated globally, through the EC90:EC10 ratio. For a Michaelian response in enzyme kinetics, the ratio is always 81 and therefore an ultrasensitive response is any response with an EC90:EC10 ratio smaller than 81. Often, the sigmoidal curve is well-approximated by the Hill equation, so the other way to quantify sensitivity is from the effective Hill exponent, n :

$$Output = \frac{Input^n}{K^n + Input^n} \quad (7)$$

where K is a fitted constant related to the process. The sensitivity is determined from the Hill exponent for a Hill curve that has the same EC90:EC10 ratio as the response curve in question. The Hill exponent is related to the EC90:EC10 ratio by the equation:

$$n = \frac{\text{Log}[81]}{\text{Log}[EC90:EC10]} \quad (8)$$

There are problems with this definition if the response is not well-approximated by the Hill equation.¹⁰

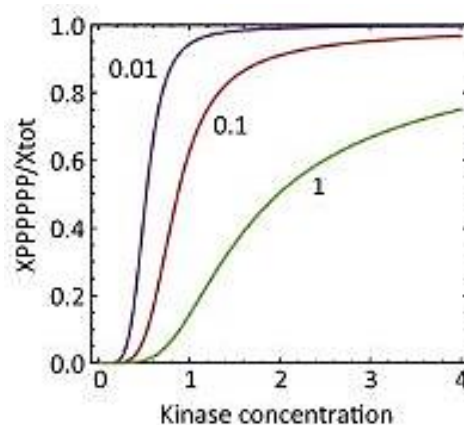


Figure 16. Example of sigmoidal/switch behaviour. Reproduced from ref. ⁷⁹ © 2014 Elsevier

Multiple mechanisms in enzyme-catalysed reactions lead to ultrasensitivity: including positive feedback or cooperativity (discussed in the next section). The

importance of ultrasensitivity lies in how it enables more complicated responses. A highly ultrasensitive response can approach a step function, or in systems with positive feedback loops, a switch can be bistable with hysteresis so that the response depends on the history of the process. Ultrasensitivity and bistable switches are important in biological systems and used in the engineering of synthetic biology circuits for smart devices¹¹.

1.3.3. Feedback

Feedback is a process present in different organisms which is capable of regulating the vital functions of a cell or the concentration levels of a certain substance⁸⁰⁻⁸¹. Nowadays, with increasing interest in complex reactions happening in biological organisms, scientists can recreate feedback loops in synthetic systems so that it is possible to build an autonomous self-regulating system in time: "Feedback-controlled molecular systems... will be able to sense, adapt, communicate, learn, evolve and replicate"⁸². There are several different types of feedback loop⁸²:

- Negative feedback → when a substance increases in the system, negative feedback reduces its production rate, making the signal level returning to its original value. The concept is demonstrated in [Figure 17A] where the negative regulator "b" is increased when "a" increases.
- Delayed negative feedback → To prevent the formation of an intermediate steady-state, the negative feedback must be delayed in time [Figure 17B].
- Positive feedback → when increasing a substance results in faster production of the substance. Usually, it happens with autocatalytic reactions, where the product catalyses the process [Figure 17C].

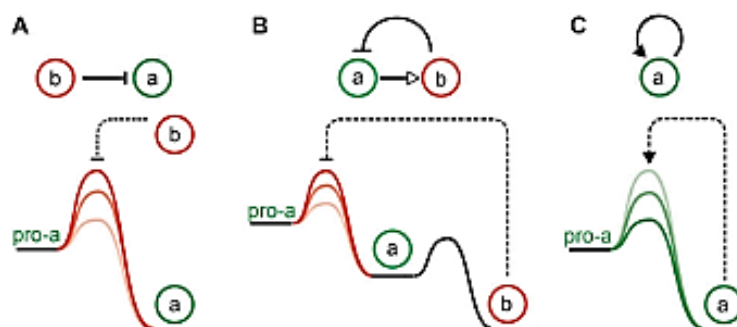


Figure 17. Different mechanisms of feedback loops. (A) regulation of “a” production by “b”, symbolized by an arrow with a flat head and the corresponding reaction profile. (B) Representation and reaction rate profile of delayed negative feedback, where the delay induced is represented by an arrow with an empty head. (C) Autocatalytic positive feedback for the formation of “a”, symbolized by an arrow with a filled head and the corresponding reaction profile. Reproduced from ref. ⁸² © The Royal Society of Chemistry 2017

Temporal control in living organisms is based on combinations of positive and negative feedback loops and delay mechanisms. [Figure 18] shows that these feedback loops produce complex responses such as signal amplification, bistable switches, memory, and rhythms. These networks are capable of adapting their control mechanisms according to variations in external parameters. Limitations of this technology are that most systems involve inorganic feedback-controlled loops, and rely on toxic reactants such as concentrated acids, halogen derivatives and transition metals. This makes it difficult to develop applications. Hence, attention has turned to the design of sustainable feedback-controlled reactions for user-friendly, environmentally benign and biocompatible devices. The feedback loops have potential applications in product selectivity, drug-delivery devices and active materials^{74,82,83,84}.

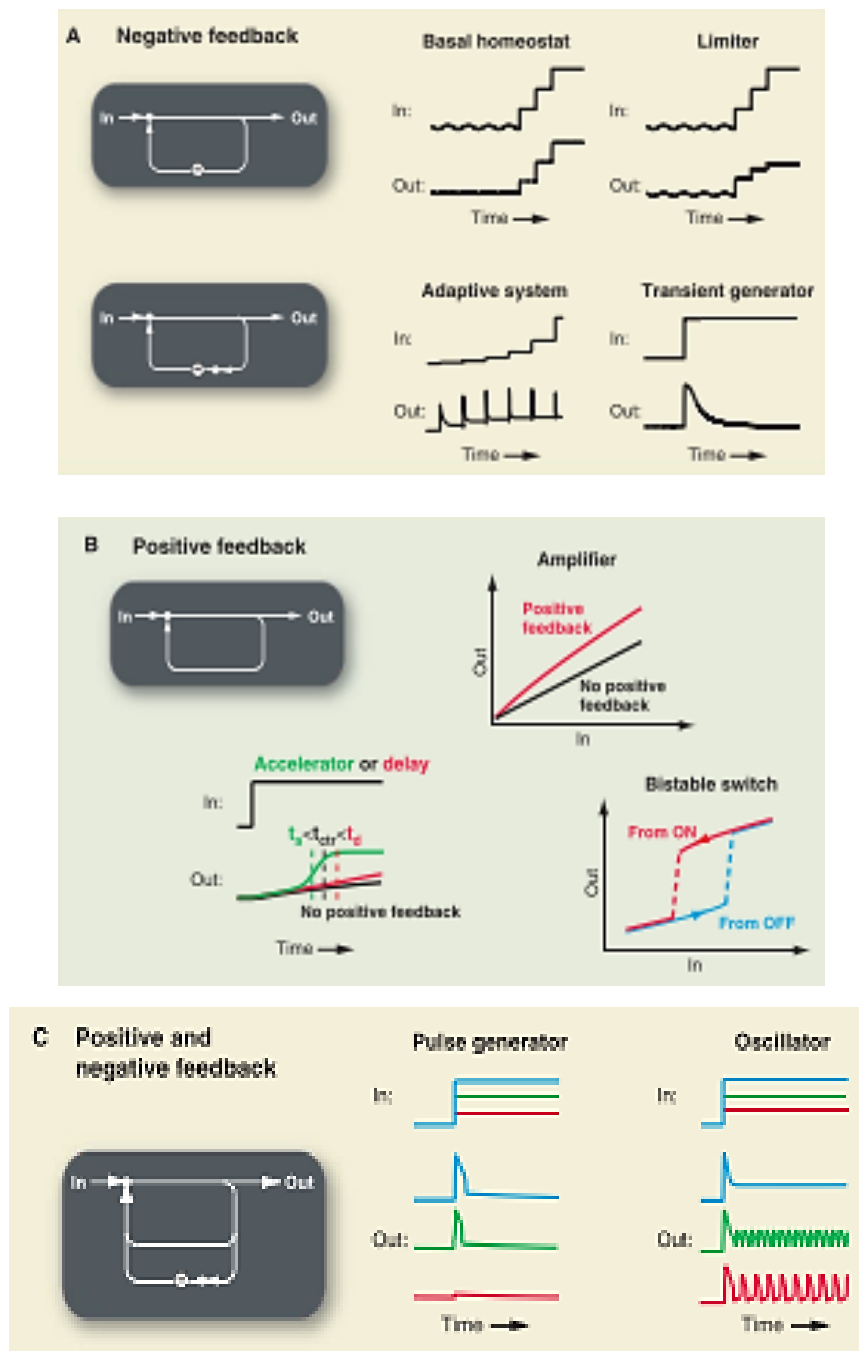


Figure 18. Examples of different feedback functions. (A) the negative feedback can stabilize, limit and create an adaptive response. (B) The positive feedback can amplify a signal, create a bistable switch, and alter the kinetics. (C) the combination can create pulses or oscillations. Reproduced from ref.⁸³ © 2008, The American Association for the Advancement of Science

In one paper, Semenov et al. combined ultrasensitivity, feedback loops, logic gates and reaction-diffusion processes to build a biosensor⁸⁵. They used controlled diffusion of enzymes from micropatterned agarose gels into hydrogels with modified fluorogenic substrates to quantitatively study reaction-diffusion

processes. Thanks to this system, a yes/no response is achieved through the introduction of a positive feedback loop and the autocatalytic activation of enzymatic activity. The combination of ultrasensitivity with a positive feedback loop (amplification) and a filtering layer containing a diffusible inhibitor makes it possible to digitally decode the spatial density of input signals. Previous computational work has shown that biochemical reaction-diffusion networks can be constructed to function as analog-to-digital converters.

These properties arise from the connectivity of the enzymatic reactions and the coupling between reactions and the diffusion of components. In their study, the authors have shown a network that can filter out certain aspects of a pattern and translate this information into a fluorescent signal. The next step in this area is to exploit future generations of "smart materials" to incorporate more complex versions of enzymatic reaction-diffusion pathways. Such materials might be able to sense, learn, adapt, and make autonomous decisions⁸⁵.

In another work, the authors realised a hydrogel system with distinct pre-programmable lag times and lifetimes in closed systems, combining two enzymes with an antagonistic pH- effect in a feedback-controlled biocatalytic reaction network (BRN) and coupling it to pH-responsive, advanced and autonomous hydrogel materials. The BRN enables temporal control of the "ON" and "OFF" switching times of the temporary gel state by modulation of programmable, nonlinear pH changes⁸⁶ **[Figure 19]**.

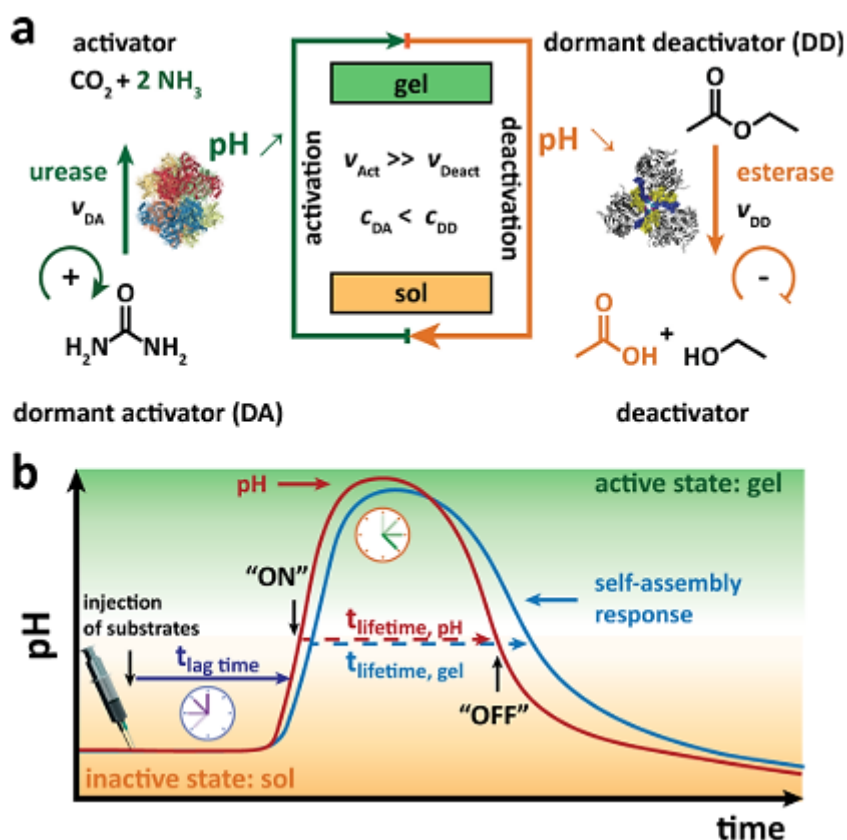


Figure 19. Illustration of temporal control of pH using antagonistic enzyme reactions. Reproduced from ref. ⁸⁶ © 2017 American Chemical Society

The last example concerns the development of a positive feedback loop reaction in an enzyme-catalysed reaction through the influence of the product on the rate. For instance, the urea-urease system is reported to show feedback through the pH. The urease is a pH-dependent enzyme, in particular, its activity increases with pH increasing up to a pH = 7 where there is the maximum and then decreases again. At the beginning of the reaction, if the pH is acid, the enzyme activity is very low, then with the ammonia production from the reaction, the pH increases and consequently the enzyme activity^{74,82}. So, building a reaction in which the product can influence the enzyme activity can result in ultrasensitivity, bistable switches and oscillators as shown in **[Figure 20]**:

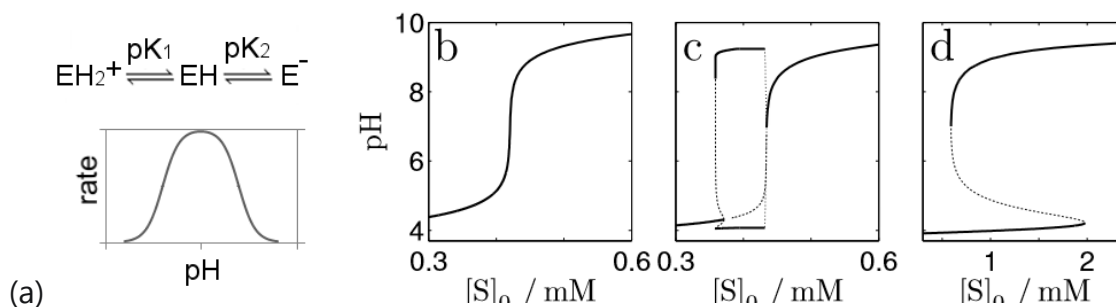


Figure 20. (a) Positive feedback loop amplification and pH vs urea in the urea-urease reaction with different enzyme concentrations showing (b) ultrasensitivity (c) oscillations (min/max shown) (d) bistable switch. Reproduced from ref. ⁷⁴ © 2010 American Chemical Society

1.3.4. Other Amplification mechanisms

Different methodologies for amplification have been demonstrated that depend on producing a chemical or physical output through some external/internal influence on the system. For example, the addition of noise can be used to increase the output signal strength. The noise can be added externally⁸⁷ or within⁸⁸ the system. In the first case, the addition of external noise, Stochastic Resonance noise (SR noise), can improve a weak signal [**Figure 21**]. SR noise is a non-linear phenomenon and in order to exhibit it, a system should have:

- "A nonlinearity in terms of threshold,
- A subthreshold signal with a small amplitude,
- A source of the additive noise."

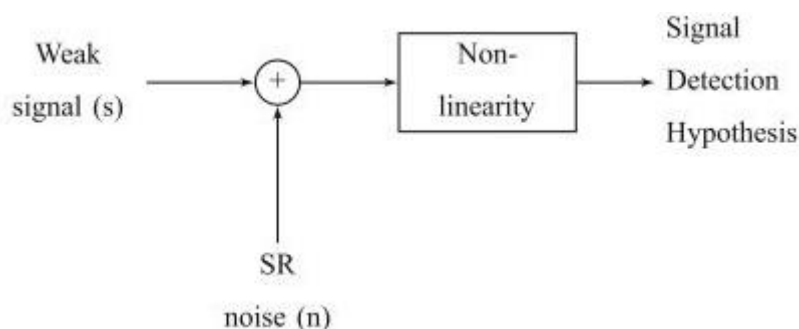


Figure 21. Addition of external noise scheme to amplify a signal. Reproduced from ref. ⁸⁷ © 2018, Springer Science

The second method to add noise is using a set of auxiliary chemical reactions, such as protein synthesis and degradation mechanisms⁸⁸.

Applying signals that can be modelled as an input of noise, it is possible to create an impact on the types of response that these systems can have. Stochastic noise-induced dynamics in regulatory networks can provide additional information such as topology, structure and kinetics. The noise input can create novel behaviour in the system, including the appearance of bistability. These features increase the amplification properties of the mechanism and allow it to function like a signal transducer (be able to filter noise or signals better than the corresponding deterministic system). Such “filtering” regulation might be used for control in and of biological systems. Furthermore, because the external driving noise is itself the output of yet another stochastic chemical or physical process, the form of its distribution is then determined by the nature of that mechanism. It has been shown analytically the difference of a system with and without the application of noise, by solving a Langevin stochastic differential equation model of a system governed by Michaelis-Menten MM kinetics. The equations come from the scheme in [Figure 22]⁸⁸.

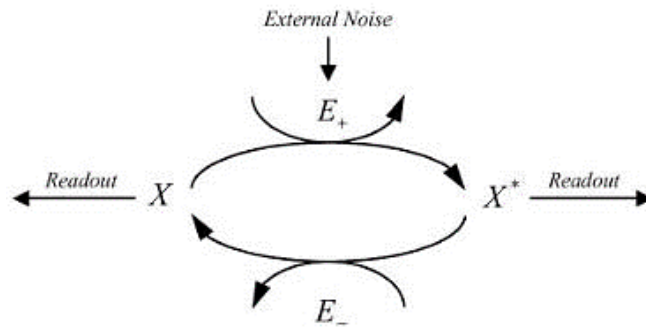


Figure 22. Enzymatic mechanism scheme referred to the equations written below (9-10). It can be easily noticed that the addition of noise generated a further term in the equation which affects the concentrations of the species present in the system. Reproduced from ref. ⁸⁸ © 2005, The National Academy of Sciences

$$R_0(X_{SS}, E_+, E_-) = E_+ - \frac{k_- (K_+ + X_{SS})(X_0 - X_{SS})}{k_+ (K_- + X_0 - X_{SS}) X_{SS}} E_- = 0 \quad (9)$$

$$R_{N(\sigma)}(X_{SS}, E_+, E_-) = E_+ - \frac{k_- E_- (X_0 - X_{SS})(K_+ + X_{SS})}{k_+ X_{SS} (K_- + X_0 - X_{SS})} + \frac{\sigma^2 k_+ K_+}{(K_+ + X_{SS})^2} = 0 \quad (10)$$

where x_0 is the total amount of x and x^* , X_{ss} is X at steady state, E^+ and E^- catalyse the forward and reverse reactions and K^+ and K^- are constants. It can easily be noticed that differently from the deterministic equation (9), in the stochastic equation (10) the effect of noise is immediately visible adding a corrective diffusive term to the classical result. Since in equation (10), the noise term is explicit at the stationary state, it does not affect only the behaviour of the system but also the quantities of the concentrations. In fact, in the stochastic case, the x_{ss}^* concentration is always bigger than the deterministic one responsible for signal amplification. The results are shown in **[Figure 23]** where p is the noise power⁸⁸:

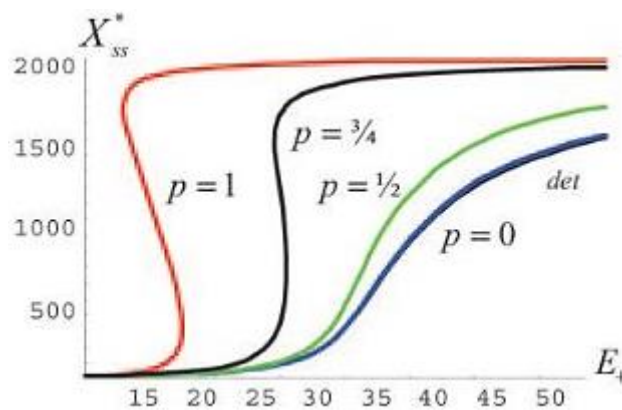


Figure 23. Product at the steady-state vs Enzyme using equations [1], [3] and the deterministic curve, in the function of p . Reproduced from ref.⁸⁸ © 2005, The National Academy of Sciences

In a different mechanism, D. L. Bates⁹ suggested that amplification can be achieved by coupling catalytically another enzyme to the primary one involved in the sensing. There are different methodologies to obtain the coupling; here we discuss the two most relevant. In **[Figure 24 (f)]** the primary enzyme (E) converts the primary substrate (S_0) to an active product (P) which can be cycled (between P_a and P_b) by the two enzymes. The product of the primary enzyme is an activator of the amplifier cycle which reacts to the concentration of the labelled enzyme. In **[Figure 24 (g)]** the amplification is achieved by an enzyme cascade⁸⁹. In this case, the primary

enzyme catalyses the first reaction producing the primary product which catalyses the second enzyme reaction which consequently catalyses the third enzyme etc.

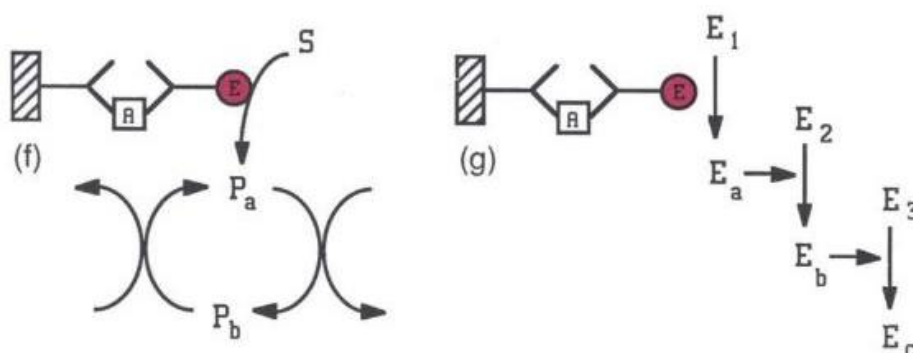


Figure 24. Enzyme amplification obtained with a secondary enzyme coupled in: a substrate cycle (f), and an enzyme cascade (g). Reproduced from ref. ⁸⁹ © 1987 Elsevier

Physical signal amplification has been obtained in a nanostructured signal-responsive thin hydrogel membrane coupled with an enzyme-based system⁷⁸. This system can produce an output consisting of the structural change of the membrane then resulting in the amplification of the biochemical signal. This method forms the basis of chemical information processing systems (CIPs) which will be responsible for collecting multiple external signals and processing the information, and these transformations will be responsible for the chemical/physical changes in the material's properties⁷⁸.

Alternatively, to traditional methods to obtain the signal amplification in biosensors, a new trend is to take advantage of the amplification present in the chain-growth process in radical polymerizations, making it adaptable to different conditions and detection methods. The authors obtain DNA detection from polymerization by Atom Transfer Radical Polymerization (ATRP) (normally obtained by electron transfer, fluorogenic, biocatalytic...)⁹⁰, Reversible addition–fragmentation chain transfer (RAFT) polymerization, Redox-initiated free radical polymerization, Photo-initiated free radical polymerization [Figure 25].

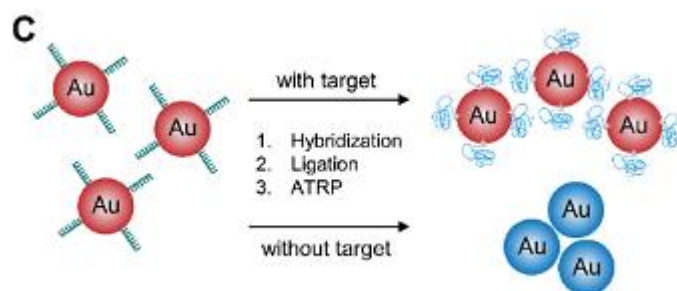


Figure 25. Colorimetric DNA detection coupled with normal ATRP. Reproduced from ref. ⁹⁰ © The Royal Society of Chemistry 2020

A plot of amplification time versus limit of detection is shown in [Figure 26] for the different polymerization detection methods and can be used to compare the approaches⁹⁰.

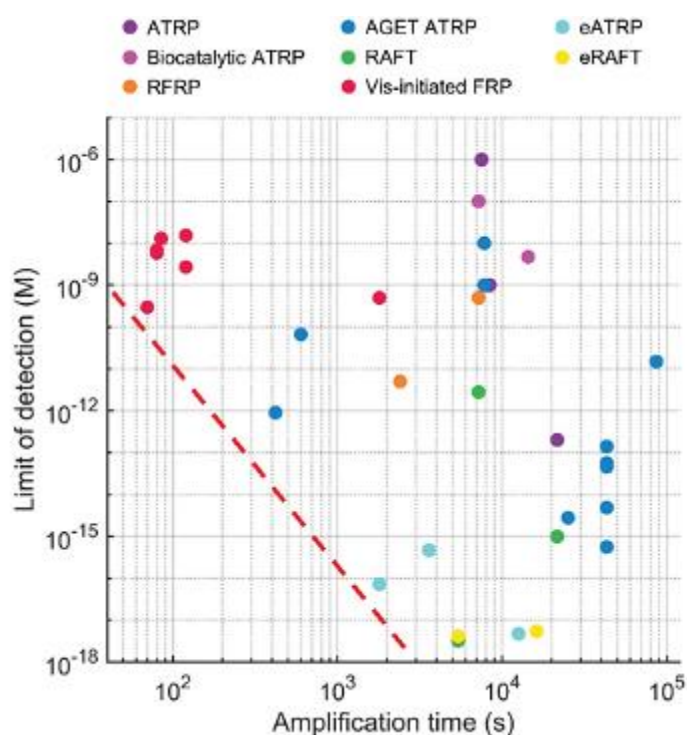


Figure 26. "Reported limit of detection (M) and amplification time (s) of polymerization-based bio-detection methods in the literature. Coloured dots represent different types of polymerization methods." Reproduced from ref. ⁹⁰ © The Royal Society of Chemistry 2020

1.3.5. Mass transport and enzyme biosensors

In the last few years, a lot of effort has been made to improve the performance of biosensors by considering mass transport. In one work, the authors show how it is

possible to improve the response of the system by improving the mass transport of the system. In particular, they use nanopillar electrodes varying their height and geometry. They show that sensing is enhanced when the reaction rate is low and when the mass transport is favoured so that the more the active surface area there is, the more the sensing increases. However, when the reaction rate is high only the top part of the nanopillar is used and the sensing capability decreases⁹¹.

Stein et al. investigated how to control an optical biosensor for the detection of glucose by adding externally to the particle a mass transport limiting nanofilm [Figure 27]. In fact, they are able to show how the sensitivity changes by adjusting the substrate transport properties with the thickness of the nanofilm and the conditions of assembly such as ionic strength. Moreover, they explored how the addition of salt can influence glucose diffusion, proving that the control of mass transport phenomena is essential in biosensor modelling and improvement⁹².

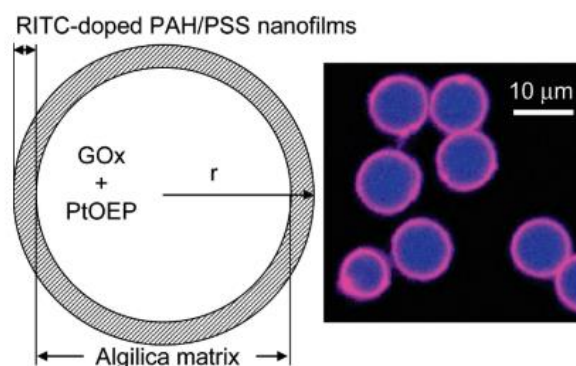


Figure 27. Optical biosensor equipped with a mass transport control nanofilm. Reproduced from ref.
⁹² © 2008 American Chemical Society

Enhancing mass transport can reduce response times or improve sensitivity. The latest studies have shown how employing nano or micropumps – enzyme catalytic particles using chemical fuel - can improve the mass transport limitations in highly sensitive systems. In particular, they are capable of transporting the analyte, containing fluid, to the sensor and since the micropump doesn't need an external

source of power, they can reach the sensors placed in a remote place in a dormant status, until it is triggered by the arrival of the analyte. Moreover, since the enzymes have a high degree of specificity they can be coupled with micropumps to create a chip which will enhance the signal amplification and incorporate logical operations⁹³. As discussed in ref. 93: "Synthetic nano- and microscale machines move autonomously in solution or drive fluid flows by converting sources of energy into mechanical work. Their sizes are comparable to analytes (sub-nano- to microscale), and they respond to signals from each other and their surroundings, leading to emergent collective behaviour"⁹³.

Some different materials and shapes can characterise a micro-motor or pump, they can be cylindrical rather than spherical, and they can be made of an organometallic or polymeric motor⁷⁵. Independently from each one of these characteristics, the principle of work doesn't change. This process can be actuated through an output signal generated by the biosensor itself, or when the chemical output signals are used for activation of "smart" chemical stimuli-responsive materials (bio-fuel cells, hydrogel membranes and pH-responsive nanoparticles), capable of producing an output readout changing their chemical or physical properties.

The motors can be used to move a certain type of analyte whenever it is detected in a magnetic field or by chemotaxis. They can also be programmed to move towards the analyte once it is formed⁹⁴ [**Figure 28**]. Micropumps, instead, have been used not only to detect the formation of the analyte but also to inject substances inside or outside the considered system²². For instance, in one work the author uses micropumps to detect glucose in the system which is consequently capable of releasing autonomously insulin and there are suggestions that multienzyme cascades may be used in the future for regulation of the response⁹³.

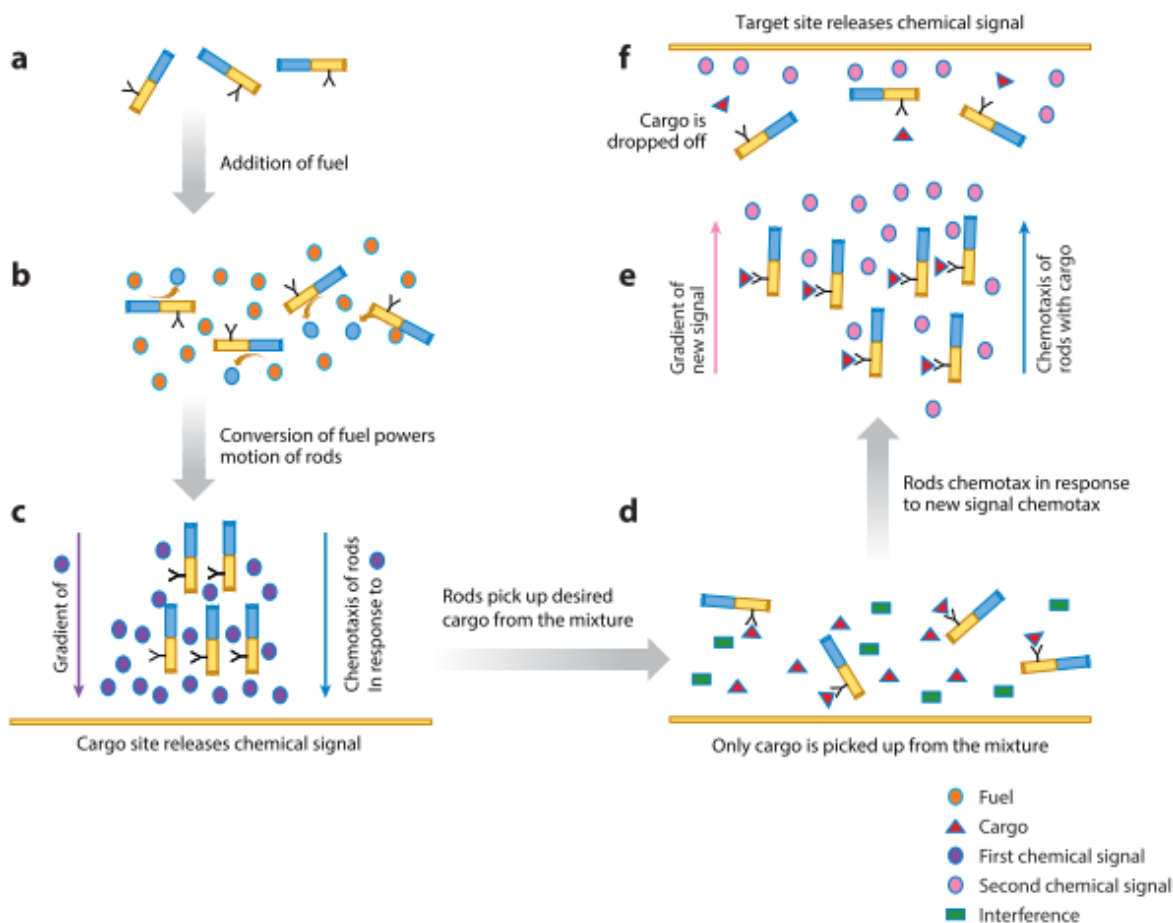


Figure 28. Schematic representation of micromotors producing a chemical signal. Reproduced from ref. ⁹³ © 2015 by Annual Reviews.

Mass transport was also used for the creation of a self-regulated “breathing microgel”⁹⁵. It takes advantage of two phenomena, the first one is the continuous supply of the substrate as fuel to keep it in a state of non-equilibrium. The second one is the use of urease as the enzyme, which has a rate dependent on the pH and makes it possible to achieve the switch-like behaviour of the system by a change in the size of the microgel [Figure 29]. In particular, when the microgel is first exposed to a solution of urea and acid, it swells. However, when the urease starts to catalyse the urea in ammonia and the pH continuously increases, the microgel contracts. The fluorescence switches “on” when the pH of the particle is high and switches “off” when it returns to low pH adding new acid to repeat the cycle [Figure 30].

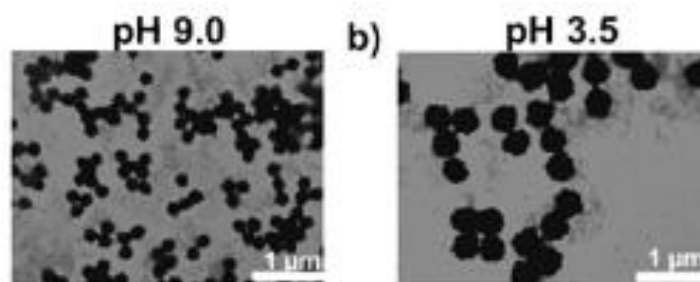


Figure 29. Microgel size changing with pH decreasing. Reproduced from ref. ⁹⁵ © 2017 The Authors. Published by Wiley-VCH

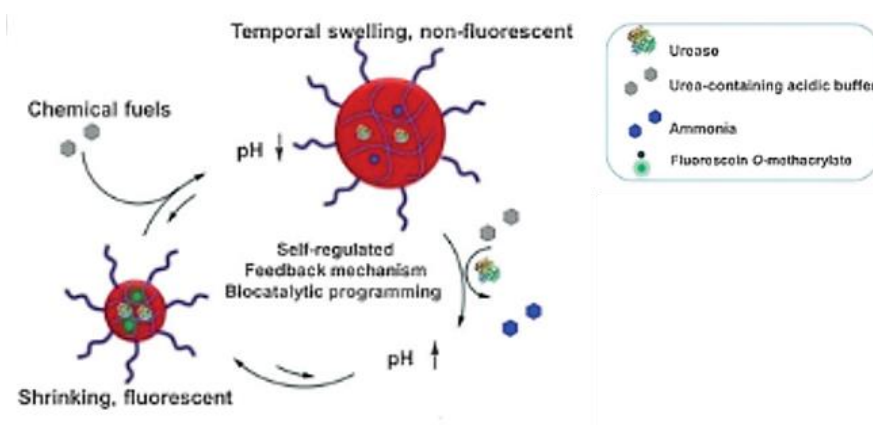


Figure 30. "Breathing" pH sensitive microgel which is able to shrink and swell cyclically according to pH changes. Reproduced from ref. ⁹⁵ © 2017 The Authors. Published by Wiley-VCH

Similar work was conducted by Che et al. who, rather than using a microgel, adopted as a material for their experiment a polymersome encapsulating urease and horseradish peroxidase (HRP). It is sensitive to pH. In this case, when the pH decreases, its permeability increases allowing the substrate for HRP in and, once the product is formed, the product diffuses out, so the polymersome is acting like a nano-reactor⁹⁶. Then the pH decreases and the reactor shrinks and the cycle can begin again. The scheme can be observed in [Figure 31].

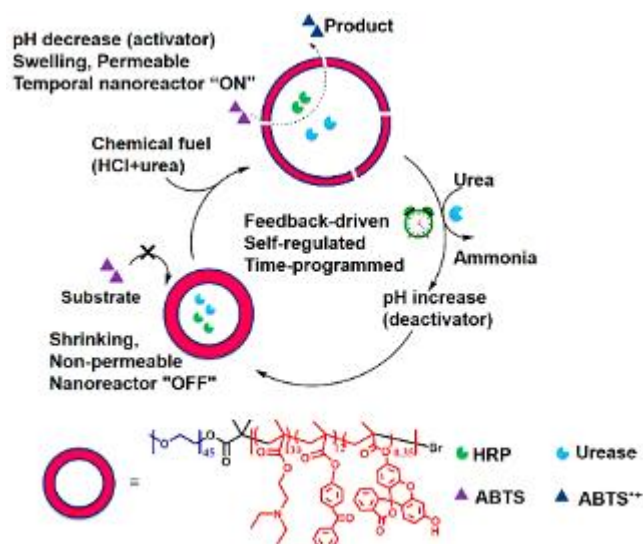


Figure 31. "Breathing polymersome" reaction scheme. Reproduced from ref. ⁹⁶ © 2018 American Chemical Society.

1.3.6. State of the art and new directions in urease-based biosensors

As seen in the previous sections, there is a wide variety of urease biosensors and devices currently employed by researchers. Enzymes are known for their durability, robustness, and versatility in terms of their applications. The achievements with urease have mainly been obtained taking advantage of the fact that the urea-urease reaction increases the pH via ammonia formation. The examples in the previous section demonstrated the recent progress in this area.

One of the aims of our work was to build a urease particle biosensor capable of detecting small amount of substances producing a response within minutes and generating an optical output signal visible by the naked eye. The work was based on the key studies conducted by Taylor, Pojman and collaborators regarding the kinetic characterisation and control of the urea-urease reaction^{74 97}. The fact that the system is capable of positive feedback was used for the formation of pH controlled polymerised hydrogels, where a gel was obtained via base catalysed polymerisation.^{98,99} Here we focussed on generating a urease gel-particle that displayed a threshold response, so that it could be used to determine whether a

substance is present or not. Additionally, optical biosensors have been selected here for their simplicity and cost-effectiveness. Although some optical biosensors may not be suitable for quantitative responses, they have been employed in this study to provide a qualitative and easily interpretable output for the threshold biosensor.

However, the cost of enzymes often poses a challenge. To address this limitation, a shift has been made towards utilizing more natural and unprocessed sources of enzymes, such as seeds. In terms of aiming for sustainable and cheap urease biosensors and materials, Pojman and Mai proposed the option of watermelon seeds as source of enzyme. Specifically, in his thesis Mai analysed the activity, stability and durability of watermelon seeds powder containing urease and proceeded to build a protocol for the powder preparation that has been used in this work¹⁰⁰.

The recent studies which combine urease enzyme with others such as peroxidase and esterase⁸⁶ usually require enzymes from multiple sources. After identifying the presence of multiple enzymes in watermelon seeds¹⁰⁰, the characterization and combination of select enzymes was undertaken here to determine whether simple chemical reaction networks can be established. We aimed to demonstrate the potential benefits of enzyme combinations from the same plant seed source to reduce cost and enhance enzyme compatibility for applications.

In the pioneering work of Ogawa et al^{57,101} pH-responsive gels were assessed for their chemo-mechanical response using urea-urease and glucose oxidase-glucose reactions to induce gel shrinkage and swelling, respectively. The outcomes of this investigation enabled the development of a protocol for fabricating filament gels that respond to pH changes from enzyme reaction networks.

1.4 Aims and objectives

In this project, we will investigate methods for improving the properties of biosensors using a combination of simulations and experiments. We will develop a system in which an enzyme-particle biosensor is capable of detecting a small amount of a substance producing an optical or mechanical output signal. Specifically, we will examine signal detection and amplification using experiments and kinetic simulations of enzyme catalytic reaction networks (CRNs) confined in micro- or nano- compartments.

The aims of the project are to improve the properties of enzyme-particle biosensors including response time, stability and sharpness, therefore the ultrasensitivity of the signal response curves typical of enzyme-catalysed chemical reaction networks with pH autocatalysis. We also aim to produce more complex and amplified responses using multiple enzymes in pH-sensitive polymers for applications such as periodic drug delivery.

In order to do so, several steps are needed:

1. to use pH feedback in urease enzyme to create threshold sensors for urea and reduce the response time in urease-particle biosensors: the field of biosensors has seen significant advancements in recent years, particularly in the development of pH-sensitive enzyme-based sensors. One approach that has gained considerable attention is the use of a urease enzyme as a threshold sensor for urea with pH feedback. In chapter 3, experiments are combined with simulations to determine the optimum conditions in terms of particle size and response time of these sensors. By modelling the response of this enzyme to changes in pH, we aim to create highly sensitive enzyme-particle biosensors that can detect small changes in their environment in the shortest time.

2. to improve the stability of enzymes for biosensors involving pH changes: one significant challenge in the development of pH-sensitive biosensors is the stability of the enzymes involved. In fact, in order to enhance its features in practical

applications, such as reusability, recovery and robustness, enzymes are required to be encapsulated on a solid support. One possibility is to use urease present in watermelon seeds (WMS). The recent advancements in enzyme utilisation directly from these natural sources which are protected by the protein microbodies shells, allow for the creation of more robust biosensors that can withstand a wider range of environmental conditions. In chapter 4, we compare the use of commercial urease powder and urease in watermelon seed powder in various hydrogels. The goal here, is to find an enzyme-hydrogel combination which will allow to maximise the enzyme threshold sensing characteristics and enhance features such as reusability and robustness.

3. to program more complex pH changes with enzyme reaction networks and use of WMS: to further enhance the capabilities of these sensors, our purpose consists in using enzyme reaction networks by incorporating multiple enzymes. Our objective is to combine diverse enzyme types like urease, catalase, glucose oxidase, and beta-glucosidase to program pH shifts. However, acquiring enzymes from different sources can prove costly and result in incompatible or unstable enzymes. In chapter 5, we characterise other enzymes present in WMS and show that by using some of these enzymes, we can achieve improved pH responses for applications.

4. to couple pH changes in enzyme cascade reactions with pH-sensitive polymers to control chemomechanical changes in time: another promising approach involves immobilising multiple enzymes in pH-sensitive polymers for applications such as self-oscillating gels. This innovative technique allows for the development of highly sensitive and selective sensors that can detect a wide range of analytes. Furthermore, the most intriguing aim here would be building a smart delivery device capable of detecting several substances, and generating a mechanical response by releasing the appropriate drug or chemical. Towards this aim, in chapter 6, we combine WMS and other enzymes in a pH-sensitive polymer and investigate the chemomechanical response of the polymer to analytes including urea and glucose.

We determine the reusability of these polymers and show enhanced response as a result of oxygen bubble formation with hydrogen peroxide and catalase.

Overall, the field of biosensors is rapidly evolving, and the development of pH-autocatalytic enzyme-based sensors is just one example of the exciting advancements being made in this area. Our results aim to improve understanding of such biosensors for future applications.

2. Materials and Methods

2.1. Materials

Polyethylene glycol diacrylate (PEGDA, MW = $700 \frac{g}{mol}$), polyvinyl alcohol (PVA, MW 61000 $\frac{g}{mol}$), hexane, mineral oil (light oil, M5904), urea, hydrochloric acid and urease powder type III (Jack beans) 25920 U/g were purchased from Sigma-Aldrich. The tri-thiol ethoxylated trimethyl propane tri (3-mercaptopropionate) (THIOCURE® ETTMP 1300) was acquired from Bruno Bock Chemicals., pyranine (Cat no. L11252.14) was purchased from Alfa Aesar. PVA was used from a stock solution prepared by mixing 5g in 50 ml of distilled deionised water. Solutions were prepared using deionized DIW Millipore water ($18.2 \text{ M}\Omega\cdot\text{cm}$). All other chemicals were used as received.

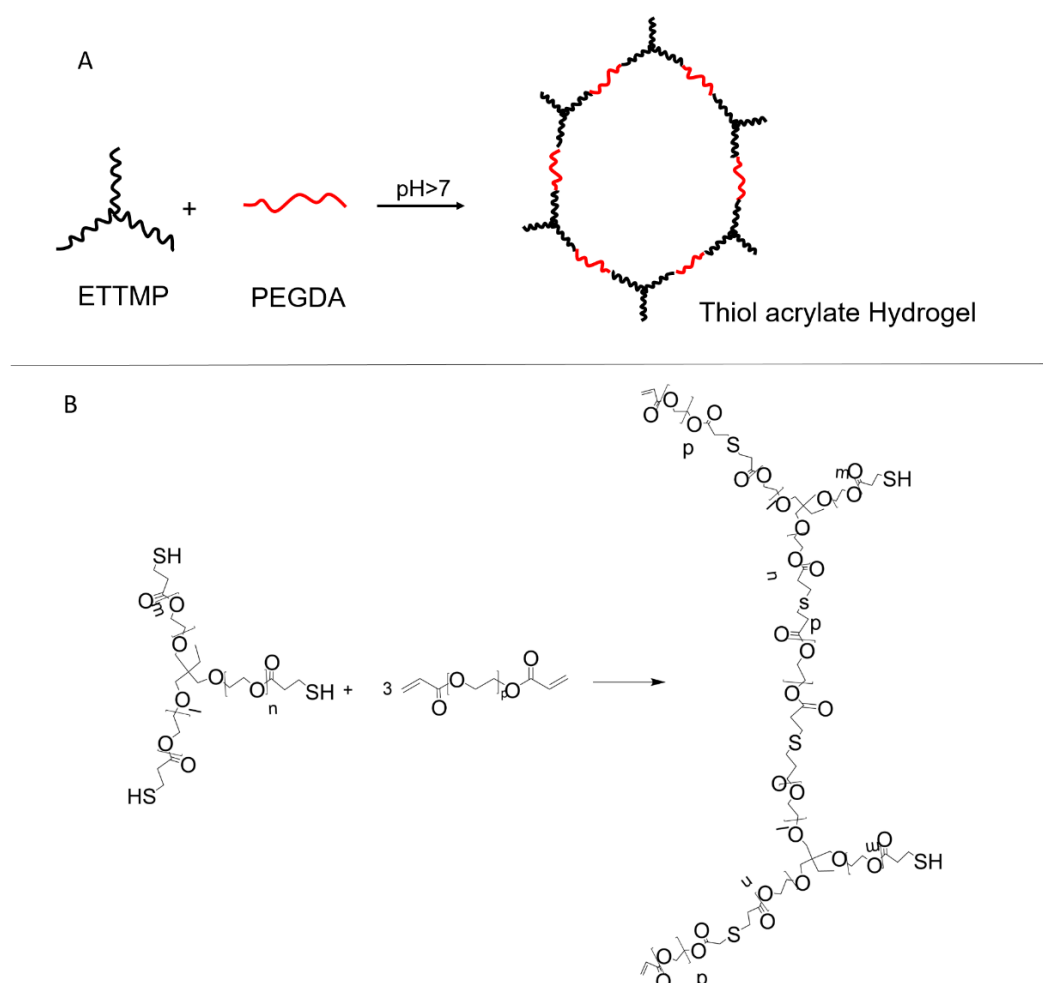
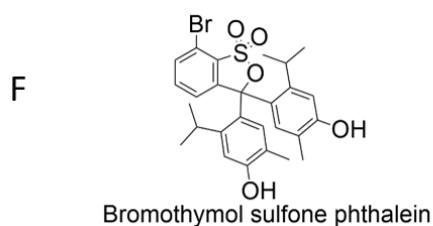
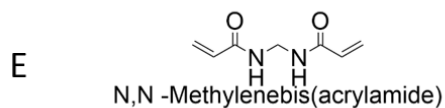
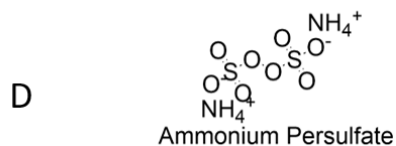
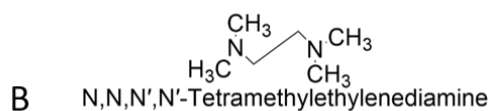
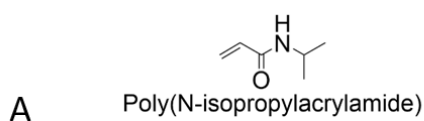


Figure 32. Thiol-acrylate polymer formation via ETTMP and PEGDA polymers. A) schematic representation and B) molecules structure.

Urea, 30 % hydrogen peroxide, glucose oxidase type X (GOX) 100000 U/g and urease powder type III (Jack beans) 25920 U/g were purchased from Sigma-Aldrich, cellobiose was purchased from Alfa Aesar, and all of them were used as received. Catalase, urease, and β -glucosidase (BGL) were used from watermelon seeds (WM) 2000 U/g. The watermelon-type 'sugar baby' seeds were purchased by Premium Seeds Direct and processed. Solutions were prepared using deionised DIW Millipore water (18.2 M Ω -cm). All experiments were performed at room temperature of 20 °C.



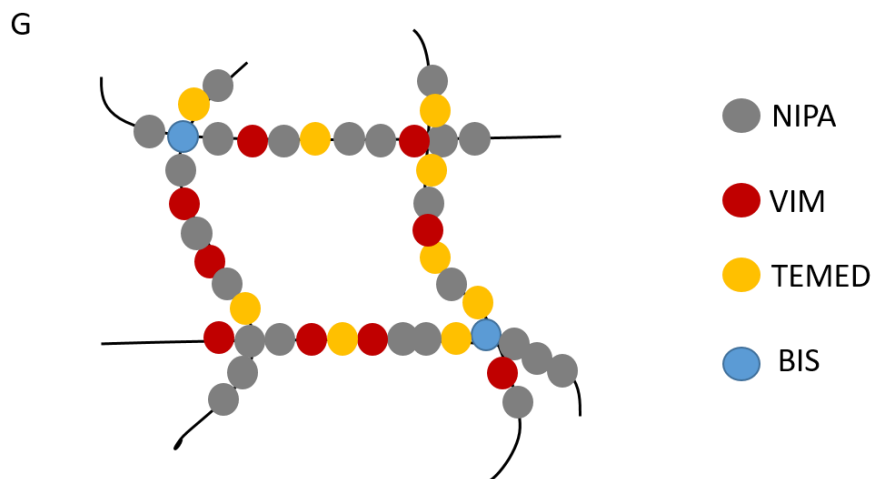


Figure 33. Molecular structure of: A) NIPA, B) TEMED, C) Vim, D) APS, E) Bis F) BTB G) Full structure¹⁰²

The 1-vinylimidazole (Vim), ammonium persulfate (APS), N,N,N',N'-tetramethylethylenediamine (TEMED) and N,N'-Methylenebisacrylamide (Bis), were purchased from Sigma-Aldrich. N-Isopropylacrylamide (NIPA) and sodium chloride (NaCl) were acquired from Thermofisher Scientific. The indicator bromothymol blue (also known as bromothymol sulfone phthalein and BTB) (pKa=7.1) from Alfa Aesar.

2.2. Methods for production and monitoring of urease particle biosensor

2.2.1. Particle formation in hexane

PEGDA and THIOCURE® in a $\frac{2}{3}$ molar ratio generate a polymer-based gel using the pH increase given by the urea-urease clock reaction.

For the formation of thiol-acrylate particles containing the enzyme urease [**Figure 32**], the emulsion polymerisation protocol was taken from a previous paper by Bubanja et al⁹⁷. The particles were obtained using the properties of the thiol-acrylate polymer to gel when the pH increases above 7. A solution containing 2 ml of PVA solution, 0.03 g of the enzyme urease, 1.15 ml of THIOCURE, 0.9 ml of PEGDA, 0.75 ml pyranine ([pyr] = 0.25mM) and 2.2 ml of 0.2 M urea was prepared with chemicals

added in that order. Theoretically, assuming all the enzyme used is encapsulated in the particles, with no losses to the hexane or mineral oil, the enzyme activity is $\frac{0.03g}{7ml} * 25920 \frac{u}{g} = 110 \frac{U}{ml}$ (particle). However, as will be noticed in the simulation section, we assumed that part of the enzyme is lost in hexane and therefore a reduced amount is trapped in the forming gel, therefore, a value of $80 \frac{U}{ml}$ has been chosen to better match the experimental results.

Following consistent mixing with a magnetic stirrer bar to make the solution homogeneous, the solution was then injected with a 1 ml syringe into 50 ml of hexane and stirred at 600 rpm on a magnetic stirrer hotplate (IKA) to create suspended particles. In order to generate a range of particle sizes, the solution was administered through a dual-injection approach. Initially, a portion of the solution was introduced in a single bolus, followed by the gradual injection of the remaining solution in the form of small droplets. This methodology allowed for the production of a diverse assortment of particle sizes, thereby enhancing the versatility and applicability of the solution. Once the urea-urease reaction has occurred, the thiol-acrylate particles polymerise and become fluorescent as pyranine is a pH-dependent indicator that fluoresces above pH 7. The demonstrated catalytic activity of the enzyme during the reaction-polymerization process is indicative of its enzymatic efficacy. The observed polymerization reaction is a clear indication of enzymatic activity, highlighting the enzyme's ability to accelerate the rate of the reaction and induce the formation of polymer chains. The particles were separated from the hexane by filtration, and stored in an acidic solution (HCl) at pH = 4 at 8°C to set them at low pH to be ready for the tests. They were also covered in foil to avoid exposure of pyranine to the light. The particles are immersed in an acidic solution to neutralize them to a low pH level, allowing the pyranine to revert back to a clear state. This procedure primes the particles for utilization in the urea urease reaction, which requires a shift from a low to high pH, prompting the indicator to fluoresce when the pH reaches 7.

2.2.2. Particle formation in mineral oil

The protocol was the same as described in the previous section to get a homogeneous solution. Then the solution was injected with a 1 ml syringe into 50 ml of mineral oil and stirred at between 300 and 600 rpm on a magnetic plate to create suspended particles throughout the emulsion. Once the reaction has occurred, the thiol-acrylate particles polymerise, and the pyranine fluoresces. The particles were separated from the mineral oil (by filtration), and stored in an acidic solution (HCl) at pH = 4 at 8°C covered in foil to avoid pyranine exposure to the light. Also in this case, the particles are stored in acidic solution to set them at a low pH and prepare them to be used in the experiments.

2.2.3. Urea-urease clock reaction

Experiments were performed several times using new particles to ensure reproducibility (the reusability of particles is explored further in the next chapter). In a typical experiment, 20 ml of urea solution at 0.3 mM and pH~4 (HCl) was pipetted into a small Petri dish (diameter = 5 cm) together with 0.5-1 ml of particles. Particles were sufficiently spaced far from each other (more than the particle radius) such that the diffusion of ammonia into the solution did not affect the reaction time on nearby particles. The epifluorescent microscope (LS560 Microscope, green fluorescence, and bright-field, green filter: excitation 457-493 nm; emission 508-552 nm, Etaluma) was used to follow the reaction through the pyranine fluorescence intensity. The settings for small and large particles were, respectively, gain = 7.750, illumination = 35.3 % and exposure = 30.5; gain = 3.875, illumination = 5.9% and exposure = 20.6, using 4x magnification. Pictures in the bright field and time-lapse images in the fluorescent field were acquired every 10 seconds with total times from 30 to 60 minutes and analysed via the software ImageJ.

2.2.3.1. Experimental Image Analysis

Pyranine is a fluorescent indicator commonly used to determine the pH of solutions. It shows visible fluorescence when the pH reaches the neutral value equal to 7^{103,104}.

Therefore, it was assumed that the urea urease reaction occurred once pH > 7 was achieved. The image analysis was performed using the software ImageJ to determine the average intensity in time in each particle and the sizes of the particles. The images were calibrated in ImageJ using the microscope image scale bar from the bright-field images. The relative intensity was determined as the intensity divided by the maximum intensity reached by a particle in the fluorescence images. The reaction time is defined here as the time needed to reach the maximum relative intensity. For the average reaction time, the data were collected from multiple particles of similar size.

2.3. Methods for immobilisation of protein microbodies and urease powder in hydrogel particles

2.3.1 Enzyme-loaded particles

To compare the two types of enzyme sources, different combinations of hydrogels and enzymes were tested. The advantages and disadvantages of these materials are listed in [Table 5].

Table 5. Scheme of hydrogels and enzyme sources used in the experiments

Hydrogel	Advantages/ disadvantages	Enzyme source	Advantages/disadvantages
Thiol- acrylate	Efficiently traps enzyme Reduced diffusion of acid	Urease powder (Sigma) (UP)	High activity/ g Expensive Small size (500 kDa)
Agarose (low EEO)	Natural polymer Low migration of species Potential loss of enzyme	Ground watermelon seeds (WM)	Low activity/ g Cheap Large-size particles (5 um) Contains multiple enzymes including urease
Agarose (high EEO)	Natural polymer Fast migration of species Potential loss of enzyme		

Specifically, thiol-acrylate particles have been shown to trap enzymes and indicators efficiently even for several weeks. However, the diffusion of acids through the particles is limited. The low and high EEO agarose differ from each other due to the species migration speed. EEO stands for electroendosmosis and represents the driving force of the liquid throughout the hydrogel. Both low and high EEO agarose are natural polymers; however, they revealed potential loss of enzymes and indicators from the particle. Regarding enzymes, the Sigma urease powder shows high activity at a high cost, while watermelon seed urease has been shown to be cost-effective and contains multiple enzymes, but relatively low activity¹⁰⁰.

Table 6. WM average activity and comparison between different varieties¹⁰⁰

Variety	Rate (mg NH ₃ / g WMSP/5 min)	Specific activity u g ⁻¹ WMSP
Crimson sweet	177 ± 20	2080 ± 233
Jubilee Improved	177 ± 17	2080 ± 204
Tendersweet orange	161 ± 2.6	1890 ± 31
Black Diamond Yellow Belly	179 ± 6.7	2097 ± 78

[**Table 6**] illustrates urease activity in different types of watermelon seeds. For all of them, the activity was comparable at approximately 2000 $\frac{u}{g}$. The peculiarity of watermelon seeds and the enzymes they contain reside in their physical structure. In fact, from the SEM images [**Figure 34**] small spherical entities called protein microbodies can be observed. These bodies are formed by a lipid layer that protects the enzyme from the outer environment.

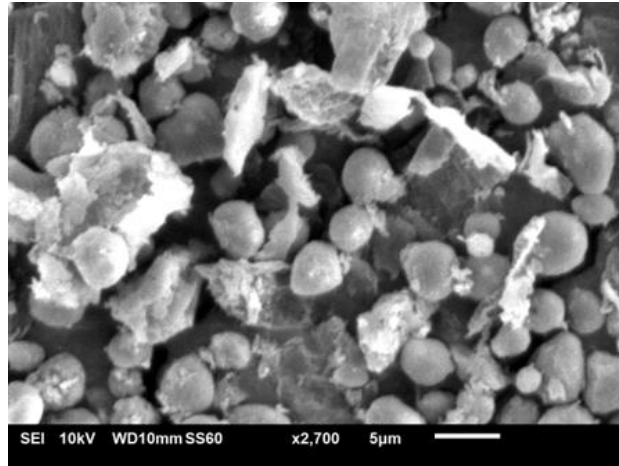


Figure 34. WM powder SEM picture showing protein microbodies

Watermelon seed powder preparation^{100,105}: 50g of seeds were weighed and ground in the IKA miller (model A10 basic) 15g per time for 45 seconds, twice. The process utilized for grinding the seeds into powder was executed with care not to overheat the sample. The intermittent mixing of the powder during the grinding intervals was used to guarantee homogeneity. The subsequent immersion of the powder in acetone in a ratio of 5:1 v/w (acetone: powder) and allowing it to settle for a duration of 20-30 minutes was employed for segregating the various particle sizes based on their respective weights. Of noteworthy mention is the identification of the shell as the inactive constituent, necessitating its separation from the remaining powder. Then, the upper layer of the mixture was filtered with a #1 Whatman filter (11µm, medium flow) using a vacuum pump to facilitate the filtration. The process was repeated three times. Lastly, the filtered powder was left to dry overnight.

Thiol-acrylate particles with Urease Powder (UP)⁹⁷ [Figure 35]: A solution was prepared by mixing 0.02 g urease ($112\frac{u}{ml}$) and 0.001g bromothymol blue with 2000 µl PVA; subsequently, 1150 µl THIOCURE® and 900 µl PEGDA were added to the solution. The mixture was a yellow colour as a result of the acidity caused by the THIOCURE® reacting with the indicator. After obtaining a homogeneous mixture with stirring, 2200 µl urea (0.05M) was injected. In the same beaker used to mix all

reactants, 20 ml of hexane was added. The beaker was placed on a cold stirrer-plate with a magnetic stirrer at 600 rpm for a couple of minutes to let the reactants blend. The beaker was removed from the magnetic stirrer and 15-30 minutes were allowed for the reaction to occur, the indicator change colour, and the gel polymerise. The next step was to separate the hexane from the gel which was placed on a Petri dish. In order to achieve uniform sized particles, sections were cut out with a 3 mm diameter cylindrical mould, obtaining circular particles. The particles were kept in an HCl solution (1×10^{-4} M) at 4°C, in order to reset them at a low pH. The BTB switched to yellow and the particles were ready to be used in the UU reaction. The final particle diameter, after overnight soaking in an acidic solution, was 6 mm.

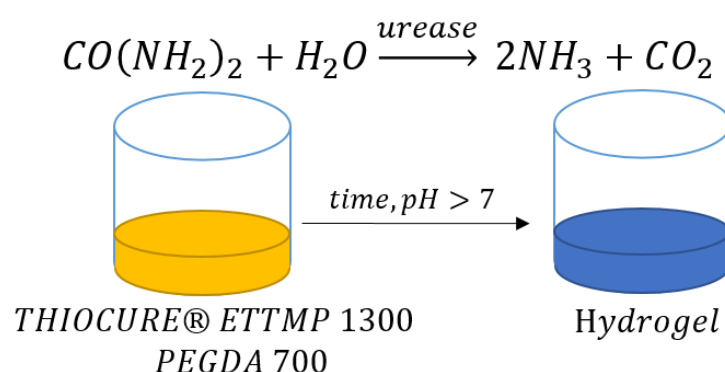


Figure 35. Polymerisation through the autocatalytic increase in pH of the urea-urease reaction

Thiol-acrylate particles with watermelon seeds urease (WM): A solution was prepared by mixing 0.35 g of watermelon seed urease powder* with the chemicals listed above in the same order. This time, the beaker was placed on a cold stirrer-hotplate with a magnetic stirrer at the minimum rpm for a couple of seconds to let all reactants mix. In this case, a fast stirring will generate bubble formation, which will cause the creation of a bilayer during the polymerization. The beaker was removed from the magnetic stirrer and approximately 30 minutes were allowed for the reaction. The continuing part of the protocol follows the one described above.

*the ratio between the urease activity of standard urease powder and watermelon seeds is:

$$UP = 34920 \frac{u}{g} \quad WM = 2000 \frac{u}{g} \quad \rightarrow \quad \frac{UP}{WM} = \frac{34920}{2000} = 17.5$$

Agarose particles with Urease Powder: A heat-resistant beaker was heated at 30 °C and 10 ml of DI water was added and stirred at 400 rpm for 15-20 minutes. When the temperature was reached, 1.5% agarose was added to the solution. Separately, a stock solution was prepared of enzyme and indicator so that the final concentrations were $2E-3 \frac{g}{ml}$ and $1E-3 \frac{g}{ml}$ respectively. (In this case, 0.024 g of the enzyme has been dissolved in 2 ml of DI water together with 0.002 g indicator.) After the solution had become transparent (the agarose was dissolved), the beaker was moved to a cold plate with the same stirring speed and let cool down gradually. Once it reached room temperature, the enzyme-indicator solution was added and mixed for a couple of seconds and the mixture was poured into a bigger beaker so that the polymer layer was not excessively thick. After 10-15 minutes, the polymer was ready to be placed in a Petri dish to be cut with a 6 mm mould (this time the mould used has a larger diameter since agarose particles don't swell in acidic solution). The particles obtained were kept in HCl solution of 1×10^{-4} M at 4°C.

Agarose particles with watermelon seed urease: The agarose solution and the gel production were obtained similarly as described above using a stock solution of WMS and indicator. The continuing part of the protocol follows the one described above.

2.3.2 Experimental setup

The enzyme (urease) and indicator (BTB) were physically encapsulated in hydrogel particles to perform two types of tests. The first was executed in an unstirred open reactor divided into compartments at room temperature. Here, 10 ml of increasing

urea concentration solutions at an initial pH \approx 4.5 were placed in each compartment together with a particle and BTB indicator [Figure 36]. Urea concentrations ranged from 5×10^{-5} M to 5×10^{-3} M. The reaction was followed and recorded through a Thorlab camera (Navitar objective F 1.4/8mm) that captured 360 frames every 10 seconds for a total of one hour of time-lapse. The goal was to evaluate and compare the particles-biosensor threshold and detection limit.

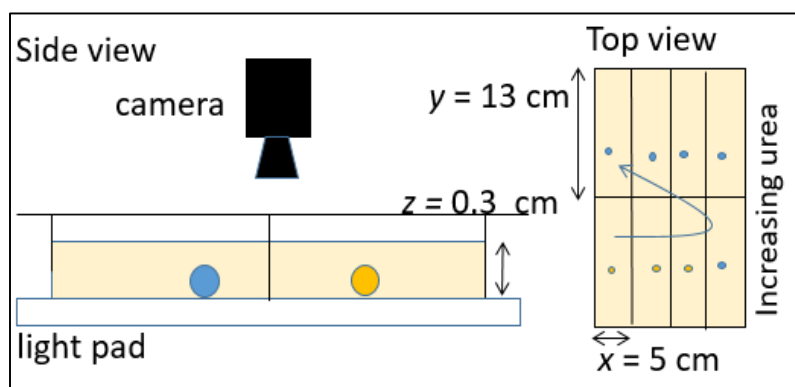


Figure 36. Reactivity limit tests experimental setup¹⁰⁶

The second test was conducted in a mixed open reactor at room temperature. In this case, 2 g of particles were placed in 60 ml of 5×10^{-3} M urea solution at an initial pH of 4 (the pH solution was adjusted using 1×10^{-4} M HCl solution). The beaker was placed on a magnetic plate, and the magnetic stirrer was set to 500 rpm. The reaction was followed by an increase in pH with a Mettler Toledo pH meter (InLab® Semi-Micro) [Figure 37]. The purpose of this test was to estimate the reusability and reproducibility of the particle biosensor. In particular, particles were left to react in urea and then re-set using an HCl solution. The particles were tested consecutively up to ten times and once per week over a month.

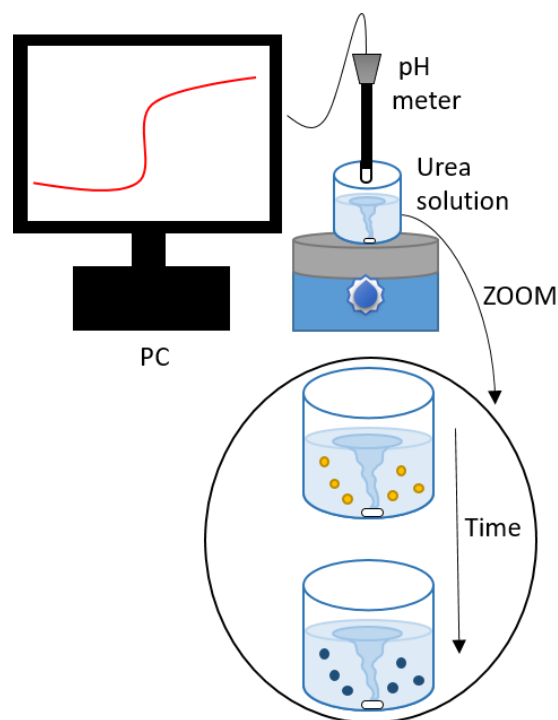


Figure 37. pH measurement for reusability and reproducibility setup

Data analysis for Test 1 was performed using the image analysis software ImageJ. The software generates an intensity value associated with a certain shade of colour. Therefore, a pH scale of 2 to 7 was prepared using an aqueous solution of BTB and the pH was adjusted using sodium hydroxide (NaOH) and hydrochloric acid (HCl). Subsequently, the intensity in Image J associated with that particular shade was recorded and associated with the colour (for further information, see Appendix 3). Once the colour/intensity scale was created, the pH of each compartment was determined. In Test 2, all runs were grouped into two plots (one consecutive and one weekly).

2.4 Methods for characterisation of activity of enzyme networks in watermelon seeds powder

2.4.1 Production of catalase- and urease-containing powder

50 g of watermelon seeds were divided into small groups and ground twice (IKA dry mill model A10 basic) for 45 seconds each time. In the intervals between grinding,

the powder was mixed with a small spatula to ensure a better homogeneity of the milling. When all the seeds were ground to powder, it was then placed in acetone in a 1:5 v/w ratio. The mixture was vigorously stirred with a spoon and left to settle for 20 minutes so that different particle sizes could settle according to their weight, forming distinct layers where the bottom layer is occupied by the heaviest part, the shell. Since the shell is identified as the inactive part, it needs to be separated from the rest of the powder. Therefore, the upper part of the mixture composed of acetone and active watermelon powder was separated through a Millipore filter (11.5 μm) and a vacuum pump. The bottom part of the settled powder was left in the decanter. The process was repeated three times to better recover as much active powder as possible. Once all the acetone had evaporated, the powder was stored in a closed container at 4°C, ready to be used.

2.4.2 Bubble counter

The bubble counter (Data Harvest Drop and Bubble Counter with EasySense software) was used to compare the different production rates of oxygen gas from catalase in watermelon seeds. A mass of 0.1, 0.01 and 0.001 g of catalase-containing watermelon seeds were added to 10 ml of increasing hydrogen peroxide concentrations from 0.5 to 3% in a glass test tube. The test tube was then closed with a cup perforated and equipped with a 1 mm capillary connected to a syringe filled with water. Finally, the syringe was placed in front of a bubble counter which detects bubbles through an infrared laser, the scheme can be seen in [**Figure 38**]. When the catalase started reacting with H_2O_2 forming oxygen, bubbles will flow through the capillary and consequently the syringe, where they are detected by the bubble counter. The tool is connected via USB cable to the computer where a software tracks the number of bubbles calculated.

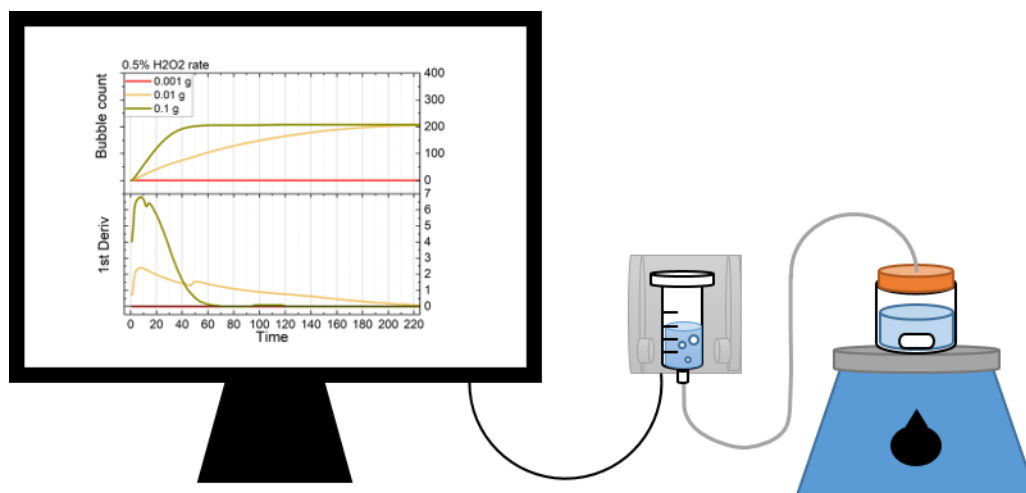


Figure 38. Representation of the bubble counter measurement set-up

2.4.3 Oxygen and pH meter

The oxygen meter test was performed to measure the oxygen content in the H_2O_2 -catalase, glucose-GOX-WM and cellobiose-GOX- β galactosidase solutions using a Hanna HI-2400 Dissolved Oxygen Meter HI76407 DO probe and Hanna Windows Software. The pH was measured with a DrDAQ pH logger and probe with the PicoLog software.

For the first system, we compared experiments with seeds already dispersed in solution or seeds added dry. 0.001 g of watermelon seeds containing catalase were combined with water (10 ml) and then added to 20 ml hydrogen peroxide solution 1% or dry to 30 ml of 1% hydrogen peroxide solution, beforehand deprived of oxygen by nitrogen bubbling for 5 minutes. The solution was then stirred at the minimum speed to avoid interfering with the oxygen probe.

For the glucose-GOX-WM reaction, 0.001 g of GOX in 10 ml of water and different amounts of WM in 10 ml of water were added to 10 ml of 30 mM glucose solution and mixed with a magnetic stirrer at around 600 rpm. The test was performed in the presence and absence of hydrogen peroxide (0.5 and 0.016%).

Lastly, for the cellobiose- β galactosidase-GOX measurement, 5 ml of GOX and WM or urease powder – having final concentrations of 200 for GOX and 112 u/ml for the urease from both sources, were added to 15 ml of cellobiose 0.15 M. The solution was mixed with a magnetic stirrer at around 600 rpm, in both the presence and absence of 0.5% H_2O_2 .

The oxygen and pH metre probes were added first to the hydrogen peroxide solution. The measurement was recorded through the appropriate software on the computer. The test scheme can be seen in [Figure 39].

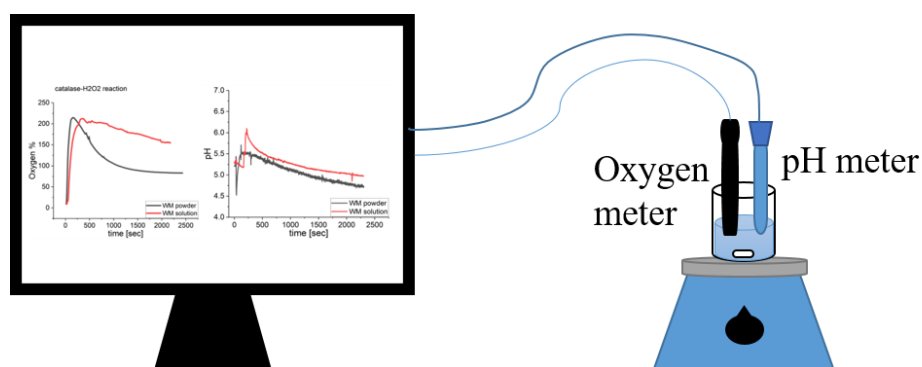


Figure 39. Oxygen measurement configuration scheme

2.4.4 Foam front propagation

The foam produced by the catalase reaction and the watermelon seeds was also monitored to compare the reactivity of the catalase under different conditions. Watermelon seeds containing catalase (0.001 - 0.3 g) were added to 10 ml of hydrogen peroxide (0.5, 1 and 3%) in a test tube placed on a magnetic plate and mixed with a magnetic stirrer at 900 rpm [Figure 40]. The stirred mixture of hydrogen peroxide and catalase solution produced a foam because of the oxygen formed and, most probably, the natural phospholipids contained in the seeds. The foam front propagation was recorded every 10 seconds in time-lapse by a Thorlab camera (Navitar objective F 1.4/8mm) that captured a total of 360 frames, later analysed.

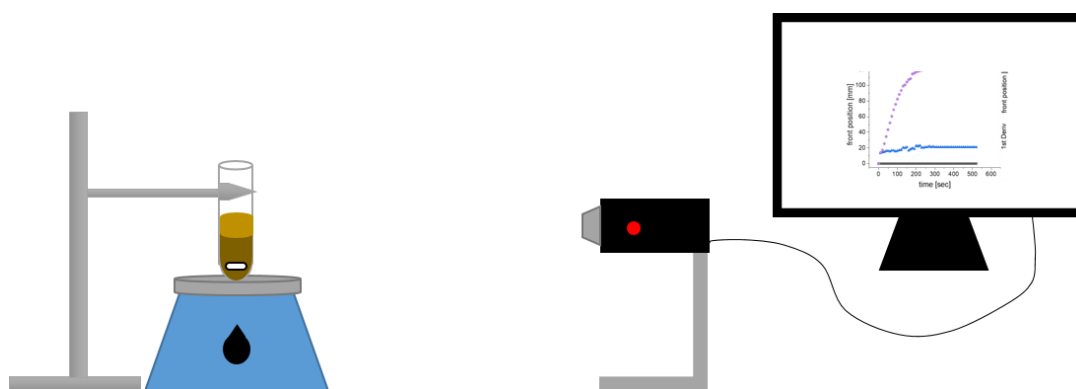


Figure 40. Foam front propagation configuration

2.4.4.1 Analysis

The foam front propagation data was captured in a video and then characterised via Matlab® (the full process is included in Appendix 4). The front was measured by setting the initial solution's height, using the change in intensity on the image at the air and water interface at time zero- before the foam formation, and at the final time expressed as the time when the maximum foam front expansion occurs. The code would then automatically measure the foam growth in time, from the change in intensity at the foam-air interface in each image, giving the final plot of position in time.

2.5 Methods for production and monitoring of enzyme-loaded chemomechanical gels

2.5.1 pH-responsive filaments production

We followed the work of Ogawa et al. for the synthesis of thin cylindrical polyelectrolyte gels with some minor modifications^{63,101} [Figure 33]. Twelve glass capillaries (wall thickness: >1mm; diameter: 1.0 mm) were placed in a Schlenk tube closed with a silicon septum and cooled to 10 ° C using an oil bath. 5.5 ml of DIO water were added to the test tube and mixed with 0.03 g UP and 0.015 g GOX or 0.5 g of WM plus 0.015 g GOX, according to the enzyme source that is used.

The ratio between the urease activity of standard urease powder and watermelon seeds is:

$$UP = 25920 \frac{u}{g} \quad WM = 2000 \frac{u}{g} \quad \rightarrow \quad \frac{UP}{WM} = \frac{34920}{2000} = 17$$

The glass test tube was deposited in the oil bath to refrigerate it at 10 ° C. Once the desired temperature has been reached, the remaining compounds were added in the following order: 1.13 g of NIPA, 0.66 ml of BIS, 0.63 ml of VIM, and 1.2 ml TEMED, mixing thoroughly until dissolution.

The APS solution was deoxygenated by bubbling nitrogen gas for 10 minutes. Then, the polymerisation reaction was initiated by injecting 0.9 ml APS solution. After thoroughly mixing for ~10 seconds, the pre-gel solution was immediately transferred to the Schlenk tube purging with nitrogen gas, then the septum was closed on the Schlenk. It is necessary to keep it immobile at ~10 °C for 1h. Lastly, the cooling was stopped and it was slowly warmed to room temperature. The capillaries were removed from the jellified mass with metal tweezers and put in a Petri dish half filled with tap water. Subsequently, they were placed in a large Petri dish with warm tap water and the gel filaments were pulled out from the glass capillary one by one with a smaller capillary tube. Lastly, the gel filaments were stored in a dilute NaCl solution (1 M) at 4 °C. The TEMED, Bis, and Vim solutions can be kept in a refrigerator for a few days. The APS solution should be prepared on the same day. An aqueous suspension of native urease, extracted from watermelon seeds, or a solution of the commercial enzyme, should be prepared freshly.

2.5.2 Experimental setup

The gel in the form of a filament is equipped with enzymes and an indicator (Bromothymol blue, BTB, pKa = 7.2) and placed in a 50 ml urea solution. For the reaction time test, the gels which were initially colourless, were placed in 5 mM urea solution (the pH was adjusted using 1E-4 M HCl solution) containing BTB, in an

unstirred open reactor, a 60 mm Petri dish, at room temperature and let to react for one hour. When the pH started increasing, both the filament and solution turned blue because of the indicator [**Figure 41**]. The whole process of detection and consequent output signalling works according to a reaction-diffusion mechanism.

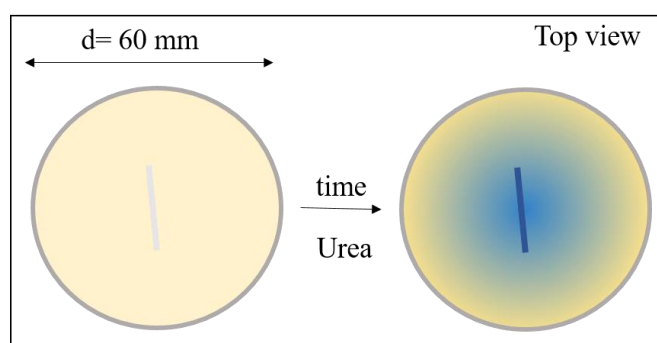


Figure 41. Schematic representation of the urea urease test 1 setup: gel filaments with enzymes in a solution of urea and acid.

Regarding the reusability test, the filament was placed alternately in 5 mM urea and 30 mM glucose solutions in order to reset the filament to low pH [**Figure 42**]. In this case, the filament was originally colourless and it turned blue after reacting with urea. The same filament was then placed in a glucose solution, which generated gluconic acid and the pH decreased. At this point, the filament reacted chemically, indicated by turning its colour yellow, and mechanically by swelling due to the acidic solution.

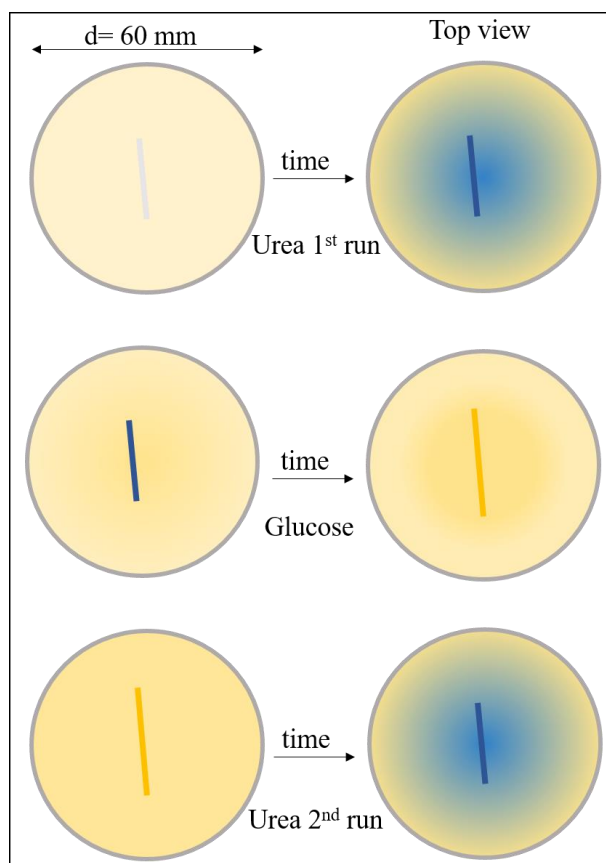


Figure 42. Schematic setup for Reusability test 2: gel filaments were placed alternately in urea/acid solution and glucose solution.

For the glucose reaction [Figure 43], the filament previously placed in urea to set it at high pH, was then used firstly with 30 mM glucose solution alone and then combined with 0.5% hydrogen peroxide to analyse and compare the reaction rate and area growth ratio. Hence, in this test, instead of using the optical indicator to determine the reaction characteristic, the filament area was taken into account.

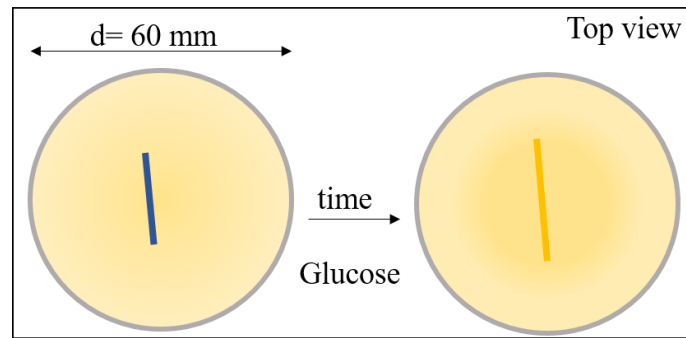


Figure 43. Glucose GOX test 3 representation setup: gel filaments were placed in glucose solution or glucose with hydrogen peroxide

Finally, to perform the oxygen production test [Figure 44], the filaments were placed in three different hydrogen peroxide concentrations (0.5, 1, 3%) to study the effect of the concentration on their expansion. Also, in this case, the chosen parameter to study the reaction effects was identified in the area of the filaments.

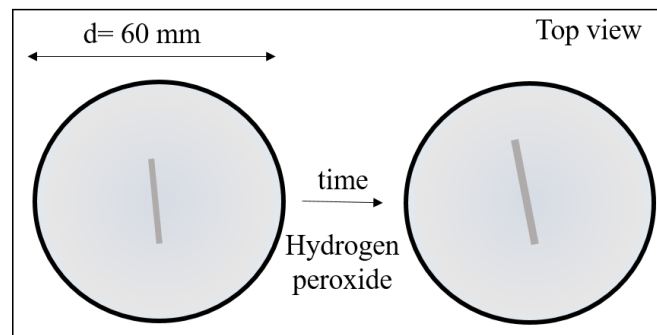


Figure 44. Hydrogen peroxide - catalase reaction test schematic representation to assess the filament as oxygen-responsive

The reactions were followed and recorded through a Thorlab camera (Navitar objective F 1.4/8mm) that captured a total of 360 frames every 10 seconds for a total of one hour of time-lapse [Figure 45]. The goal was to evaluate and compare the filaments' chemo-mechanical activity and robustness with simple enzyme reactions and chemical reaction networks.

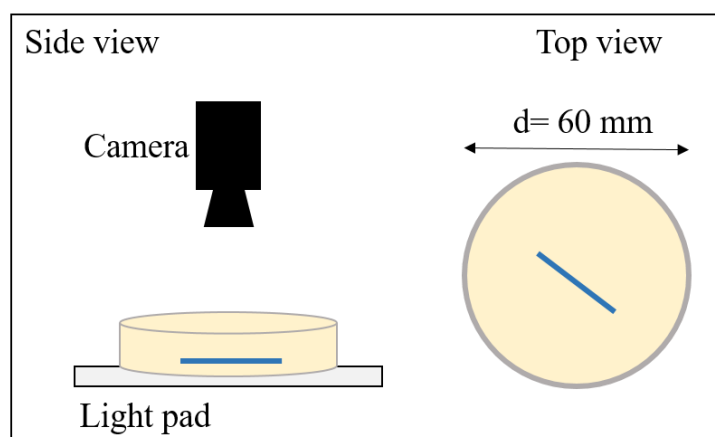


Figure 45. Experimental setup of all tests

2.5.3 Analysis

Analysis was performed according to the technique explained in the previous section [Immobilisation of protein microbodies in hydrogel particles for possible applications in threshold sensing]. In particular, the video analysis for Tests 1 and 2, was accomplished using the image analysis software ImageJ. The software creates an intensity value related to a certain shade of colour. Hence, a pH scale of 2 to 7 was arranged using an aqueous solution of BTB and the pH was adjusted using sodium hydroxide (NaOH) and hydrochloric acid (HCl).

The intensity in ImageJ associated with that particular shade was recorded and related with the colour observed. Once the colour/intensity scale was created, the pH of each test was determined. Therefore, when the pH-responsive filaments react by changing the colour from yellow (acidic environment) to blue (basic environment) or vice versa, the intensity was determined and associated with a pH. The absorbance was calculated from the intensity I using $\log(I/I_0)$, where I_0 is initial intensity.

Due to the swelling and shrinking nature of these gels, in addition to the pH study, an analysis of the apparent area occupied by the gel was performed. The work was carried out using the same image analysis software to determine the size of the filaments by a customised process. Specifically, the test involved time-lapse images

of the filaments in proximity to graph paper to calibrate the length scale. The software ImageJ was utilized to analyse the recorded data. The images were transformed into an 8-bit format, and the threshold option was employed to facilitate object recognition. Once the objects were detected, the circumference was traced, and the software provided the area of the detected object. The data were collected to obtain plots of the area versus time.

3. Particle biosensors: the influence of particle size on response times in enzyme reactions with feedback

3.1 Overview

Biosensors with immobilised enzymes are part of our daily lives. New technologies have been developed to make them smaller, more sensitive, durable and biocompatible. In this regard, it is important to study the parameters that influence the response of the sensors such as the support material, where the enzyme is trapped, the encapsulation technique, and the enzyme activity. When dealing with an autocatalytic reaction, the positive feedback mechanism can also be used to tune the sensor properties. In this paper, we investigate the optimisation of parameters in enzyme particle biosensors in order to decrease the response time. We use the autocatalytic urea-urease reaction and entrap the enzyme in thiol-acrylate polymer particles for the detection of urea. Particular attention has been paid to the particle size and both lab experiments and computational simulations were used with the aim of better understanding the behaviour. We have shown that there is an optimum radius that can be achieved to minimise the response time of the biosensor and that the diffusion of both the substrate urea and product ammonia from the particle plays an important role in the response time and signal stability.

3.2 Introduction

The immobilisation of biocatalysts in hydrogels is of great interest to better understand natural systems and also for industrial applications. In particular, biomolecules trapped in polymers can be used to replicate complex processes such as biofilm formation or as sensors and catalysts in bio-reactors¹⁰⁷. One of the most widely used biocatalysts due to its well-known kinetics and mechanism is the enzyme urease. Urease catalyses the hydrolysis of urea into ammonia and carbon dioxide and is of great importance for metabolic processes and cellular phenomena, as well as in urea biosensors¹⁹.

Many biocatalytic processes involve the presence of feedback^{28,74,97}. Feedback takes place when a product generated later in the reaction has an influence on the rate of its own production. In the case of urease, feedback occurs because the reaction produces ammonia and there is an optimal rate at pH = 7. If the reaction starts at a low pH, then the ammonia raises the pH and the rate increases⁷⁴.

Under defined conditions, autocatalytic reactions such as urease-catalysed hydrolysis of urea that show positive feedback mechanisms in their kinetics can exhibit clock behaviours¹⁰⁸. The characteristic of clock reactions is the increase in the concentration of one species after an initial delay time, and once this new regime is reached, the reaction reaches equilibrium in a closed system. For reactions such as the urea-urease reaction, it is also possible to observe ultrasensitivity^{79,11}. This is a phenomenon in which a small change in the input stimulus corresponds to a large variation in the output signal under conditions far from equilibrium. Unlike the clock reaction that is observed in time, ultrasensitivity is obtained by changing one parameter and generating a threshold variation in a second parameter, similar to an 'on-off' switch^{28,109}. Furthermore, ultrasensitivity is interesting since it is linked to more complex behaviour such as bistability, oscillations^{79,11} and applications in detection and sensing^{10,83,109}.

From this, it is clear that a better understanding of how to regulate and trigger these mechanisms is needed in enzyme biosensors. The number of parameters, narrow range of conditions for certain behaviours, and lack of reproducibility can make it difficult to find optimal behaviour in experiments. Therefore, in this work, we use a combination of simulations and laboratory experiments to evaluate the best conditions in which to operate. Our system involves a spherical hydrogel particle in which the enzyme and indicator are physically encapsulated. Subsequently, the particles were placed in urea solution. The particles were fabricated through an emulsion technique using pH-dependent thiol-acrylate polymerisation^{97,98}. Urease has been encapsulated in many different types of hydrogel¹¹⁰, however here we

decided to use the thiol-acrylate polymer because of its easy fabrication, improved stability to trap the enzyme and its biocompatibility and harmlessness⁹⁷. At the same time, a kinetic model of the urease-particle was developed and used to better identify the conditions leading to ultrasensitivity and fast response time.

Specifically, this work aimed to decrease the reaction time in order to get a faster output signal. Parameters affecting the sensor response time include e.g., enzyme concentration, mass transport coefficients, and especially particle size. Generally, for standard particle biosensors, the smaller the size, the faster the response⁸⁵. We found out that in contrast to standard sensors, a decrease in the urease particle size, or radius, results in a decrease and then an increase in response time. Previous studies with autocatalytic reactions on catalytic particles have shown that there is a correlation between the size of the particle and the period of oscillation or oscillation frequency. The studies also show that there is a minimum radius below which the reaction is not observed¹¹¹⁻¹¹². Here, we show that in autocatalytic biosensors, it is possible to tune the system to identify an optimum radius for minimum reaction time, to balance the diffusion in of substrate urea and the diffusion out of the product, in this case, ammonia.

Lastly, similar to previous studies, we have shown there is a radius below which no reaction is observed. In this work, we are going to refer to it as a cut-off point. This arises when the diffusion of ammonia out of the particle is faster than the rate of the autocatalytic reaction. We also include preliminary investigations in particles with mineral oil-gel shells designed to reduce the transport of species between the solution and particle.

3.3 Methods

The experimental methods are covered in chapter 2, section 2.2.

The simulations allow us to determine general trends and behaviours by changing the reaction parameters. The model represents a particle at low pH in which the enzyme (E) and indicator (I) are encapsulated. Subsequently, it was placed in urea

solution (S). Once urea diffuses inside the particle, it reacts with the enzyme and will produce ammonia (P). When enough ammonia is formed, the pH of the particle will change from 4 to 7 and above and the indicator will fluoresce (C), demonstrating that the reaction has occurred [Figure 46]. In this work, the model was developed considering the concentrations in the particle and the surrounding solution. We assumed that the particles are sufficiently small, such that the pH changes uniformly both on a particle and in the outer solution. For simplicity, an ordinary differential equation ODE model was used. Hence, this model is not expected to quantitatively reproduce the experiments. (For more information on the model approach, see Appendix 1).

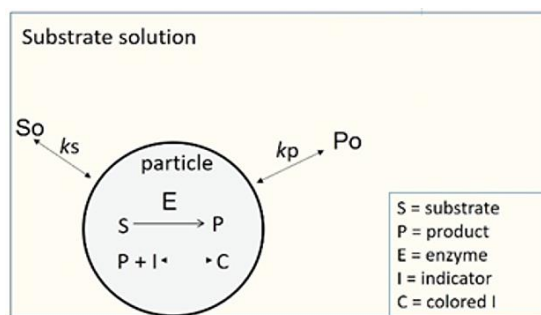
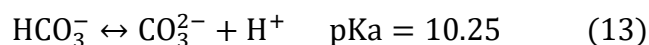
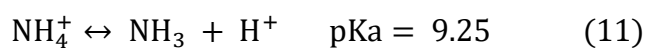
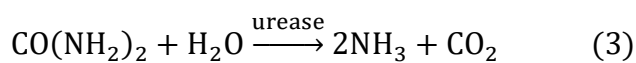


Figure 46. System Model representation

The reactions describing the system are taken from the previous work conducted by Hu et al.⁷⁴:



Equations 11-14 are used to determine pH. These equilibria result in 8 rate equations coupled with mass transport of species. The enzyme rate, v , follows the

Michaelis-Menten outline considering pH dependence, substrate and product inhibition:

$$v = \frac{v_{max}U}{\left(K_M + U\left(1 + \frac{U}{K_S}\right)\right)\left(1 + \frac{[NH_4^+]}{K_P}\right)\left(1 + \frac{K_{es2}}{[H^+]} + \frac{[H^+]}{K_{es1}}\right)} \quad (15)$$

$$v_{max} = k_E[E]_T \quad (16)$$

v_{max} is the maximum rate, $[E]_T$ is the total amount of enzyme and U is urea. K_M is the Micaelis-Menten constant, K_S and K_P are the equilibrium constants respectively for uncompetitive substrate and product inhibition. The relation between the rate equation (7) and the concentration of acid is given by:

$$\left(1 + \frac{K_{es2}}{[H^+]} + \frac{[H^+]}{K_{es1}}\right) \quad (17)$$

This is due to the rate dependence on the enzyme-substrate complex active protonated form (K_{es2}) and inactive protonated form (K_{es1}).

Two different models were used to simulate particles fabricated with hexane and the ones obtained by mineral oil.

The rate equations for all species in the particle are as follows:

$$\frac{d[CO(NH_2)_2]}{dt} = -R + \left(l * \frac{k_{sl}}{r}\right) ([CO(NH_2)_2]_o - [CO(NH_2)_2]) \quad (18)$$

$$\frac{d[NH_3]}{dt} = 2R + k_{2r}[NH_4^+] - k_2[NH_3][H^+] + \left(m * \frac{k_{sl}}{r}\right) [NH_{3o} - NH_3] \quad (19)$$

$$\frac{d[NH_4^+]}{dt} = k_2[NH_3][H^+] - k_{2r}[NH_4^+] + \left(\frac{k_{sl}}{r}\right) [NH_{4o}^+ - NH_4^+] \quad (20)$$

$$\frac{d[CO_2]}{dt} = R + k_3[H^+][HCO_3^-] - k_{3r}[CO_2] + \left(\frac{k_{sl}}{r}\right) [CO_{2o} - CO_2] \quad (21)$$

$$\begin{aligned} \frac{d[HCO_3^-]}{dt} = & k_{3r}[CO_2] - k_3[HCO_3^-][H^+] - k_{4r}[HCO_3^-] + k_4[CO_3^{2-}][H^+] \\ & + \left(\frac{k_{sl}}{r}\right) [HCO_{3o}^- - HCO_3^-] \end{aligned} \quad (22)$$

$$\frac{d[CO_3^{2-}]}{dt} = k_{4r}[HCO_3^-] - k_4[CO_3^{2-}][H^+] + \left(\frac{k_{sl}}{r}\right)[CO_{3o}^{2-} - CO_3^{2-}] \quad (23)$$

$$\begin{aligned} \frac{d[H^+]}{dt} = & k_{5r} - k_5[H^+][OH^-] + k_{4r}[HCO_3^-] - k_4[CO_3^{2-}][H^+] + k_{3r}[CO_2] - \\ & k_3[HCO_3^-][H^+] + k_{2r}[NH_4^+] - k_2[NH_3][H^+] + \left(o * \frac{k_{sl}}{r}\right) ([H^+]_o - [H^+]) \end{aligned} \quad (24)$$

$$\frac{d[OH^-]}{dt} = k_{5r} - k_5[H^+][OH^-] + \left(p * \frac{k_{sl}}{r}\right)[OH_o^- - OH^-] \quad (25)$$

The rate equations for all the species in the surrounding solutions, with subscript o, are:

$$\frac{d[CO(NH_2)_2]_o}{dt} = -l * k_{sl} * N * r * \frac{r}{V_o} ([CO(NH_2)_2]_o - [CO(NH_2)_2]) \quad (26)$$

$$\frac{d[NH_3]_o}{dt} = k_{2r} * NH_{4o} - k_2 * NH_{3o} * H_o - m * k_{sl} * N * r * \frac{r}{V_o} (NH_{3o} - NH_3) \quad (27)$$

$$\frac{d[NH_4^+]_o}{dt} = -k_{2r} * NH_{4o} + k_2 * NH_{3o} * H_o - k_{sl} * N * r * \frac{r}{V_o} * (NH_{4o} - NH_4) \quad (28)$$

$$\begin{aligned} \frac{d[CO_2]_o}{dt} = & -k - 3r * CO_{2o} + k_3 * H_o * HCO_{3o} - k_{sl} * N * r * \frac{r}{V_o} * (CO_{2o} \\ & - CO_2) \end{aligned} \quad (29)$$

$$\begin{aligned} \frac{d[HCO_3^-]_o}{dt} = & k_{3r} * CO_{2o} - k_3 * HCO_{3o} * H_o - k_{4r} * HCO_{3o} + k_4 * CO_{3o} * H_o - k_{sl} * N \\ & * r * \frac{r}{V_o} * (HCO_{3o} - HCO_3) \end{aligned} \quad (30)$$

$$\frac{d[CO_3^{2-}]_o}{dt} = k_{4r} * HCO_{3o} - k_4 * CO_{3o} * H_o - k_{sl} * N * r * \frac{r}{V_o} * (CO_{3o}^{2-} - CO_3^{2-}) \quad (31)$$

$$\begin{aligned} \frac{d[H^+]_o}{dt} = & k_{2r} * NH_{4o} - k_2 * NH_{3o} * H_o + k_{4r} * HCO_{3o} - k_4 * CO_{3o} * H_o + k_{5r} - k_5 \\ & * H_o * OH_o + k_{3r} * CO_{2o} - k_3 * HCO_{3o} * H_o - o * k_{sl} * N * r * \frac{r}{V_o} \\ & * (H_o - H) \end{aligned} \quad (32)$$

$$\frac{d[OH^-]_o}{dt} = k_{5r} - k_5 * H_o * OH_o - p * k_{sl} * N * r * \frac{r}{V_o} * (OH_o - OH) \quad (33)$$

Where R is the enzyme rate and k_{sl} is the mass transport coefficient of the substances contributing to the reaction. The transport coefficients are related to the radius of the particle r by the correlation:

$$k = \frac{k_{sl}}{r} \left[\frac{1}{S} \right] \quad (34)$$

The mass transfer coefficient has units $\frac{cm}{s}$ ^{113,114} and its value depends on the diffusion coefficient of the species. Therefore, an increase in the diffusion coefficient or k_{sl} , or a decrease in the radius of the particle, results in faster transport, and the rate of transport of substrate to a particle is given by:

$$\frac{d[S]}{dt} = k([S]_0 - [S]) \quad (35)$$

Where $[S]_0$ is the concentration of substrate in the solution.

The mass transport coefficient from solid particles to liquid k_{sl} , is in the range $10^{-4} - 10^{-1} \frac{cm}{s}$; for unstirred solutions, we took 10^{-3} from Pangarakar et al.¹¹⁵. The parameters l, m, o and p are included to account for the relative rate of diffusion of urea (l) compared to ammonia (m), protons H^+ (n) and OH^- (p) in different materials. The thiol-acrylate polymer exhibits a hydrophobic polymer surface, as illustrated in [Figure 48], which suggests that the diffusion of neutral species is expected to occur at a higher rate compared to charged species. In lipid bilayer membranes, the relative permeability of species follows the order *ammonia* \gg *urea* $>$ H^+ , and this sequence of transport rates was utilized for the particles synthesized in hexane¹¹⁶. In the case of shell-core particles, the oil layer acts like a barrier for charged species like H^+ and OH^- , whereas non-charged urea and ammonia diffuse faster through the hydrophobic oil layer. It also helps to trap the ammonia and ammonium formed by the reaction making the pH increase faster and be more stable in time. The transport rate of all species was reduced compared to the particles produced in hexane, and the transport rate of ammonia and urea was assumed to be faster than H^+ and OH^- . The values used were chosen to best match the experimental results.

For the solution, the change in chemical concentration in time depends on the rate of transfer $\left(\frac{k_{sl}}{r}\right)$ and also the dilution in volume from particle V , to solution V_0 :

$$\frac{d[S]_o}{dt} = \frac{kV}{V_o} ([S]_0 - [S]) = \frac{k_{sl}\left(\frac{4\pi r^3}{3}\right)}{rV_o} ([S]_0 - [S]) = \frac{k_{sl}Nr^2}{V_o} ([S]_0 - [S]) \quad (36)$$

The dilution factor is expressed as $\frac{V}{V_0}$ and assuming that the particles are spherical, their volume can be written as $V = \frac{4}{3}\pi r^3$. Setting the constant $N = \frac{4}{3}\pi \sim 4$, we arrive at the final formulation of the equation (26) already seen in the previously shown rate equations:

$$\frac{d[S]_o}{dt} = k_{sl} * N * r * \frac{r}{V_0} \quad (37)$$

The dilution factor is important to assert that not only the number of particles is not influencing the external solution pH when the reaction occurs, but also that the particles are sufficiently diluted that they do not even influence each other.

The initial values of the parameters used to simulate the process using hexane are as follows:

$$l = 2, m = 20, o = 1, p = 1, E = 80 \frac{\text{units}}{\text{ml}},$$

$$r = 1 \times 10^{-2} \text{ to } 0.1 \text{ cm} \quad k_{sl} = 3 \times 10^{-4} \frac{\text{cm}}{\text{s}}, \quad V_o = 20 \text{ ml}$$

The initial values of the parameters used to simulate the process using mineral oil are equal to the ones used for hexane, except:

$$l = 1, m = 1, o * k_{sl} = k_H = 9 \times 10^{-5} \text{ s}^{-1}, p * k_{sl} = k_{OH} = 4.5 \times 10^{-5} \text{ s}^{-1}$$

The enzyme concentration was taken lower than the theoretical value to take into account the possible loss of enzyme in the solution.

The rate constants and enzyme constants are⁷⁴:

k_2	$4.3 \times 10^{10} \text{ M}^{-1} \text{ s}^{-1}$	k_{2r}	24 s^{-1}
k_3	$7.9 \times 10^4 \text{ M}^{-1} \text{ s}^{-1}$	k_{3r}	0.037 s^{-1}
k_4	$5 \times 10^{10} \text{ M}^{-1} \text{ s}^{-1}$	k_{4r}	2.8 s^{-1}
k_5	$1 \times 10^{11} \text{ M}^{-1} \text{ s}^{-1}$	k_{5r}	$1 \times 10e^{-3} \text{ M s}^{-1}$
k_E	$8 \times 10^{-7} \text{ unit}^{-1} \text{ ml M s}^{-1}$	K_M	0.003 M
K_P	0.002	K_{ES1}	5×10^{-6}
K_{ES2}	2×10^{-9}		

The initial conditions in the particle and solution, unless otherwise stated, are imposed as:

S_0	$3 \times 10^{-4} \text{ M}$	S	0 M
P_0	0 M	P	0 M
H_0	$1 \times 10^{-4} \text{ M}$	H	$1 \times 10^{-4} \text{ M}$
OH_0	$1 \times 10^{-10} \text{ M}$	OH	$1 \times 10^{-10} \text{ M}$

The equations were solved using the XPPaut software package with the CVODE integration method⁷⁴⁻¹¹³. The model files are given in Appendix 2 and include all of the rate constants and parameters.

3.4 Results and Discussion

In the following sections, we compare the results obtained via experimental methods and simulations, respectively.

3.4.1 Experimental results

With the emulsion polymerisation in hexane, the urease-particles were obtained with a range of sizes from $\sim 100 \mu\text{m} - 2 \text{ mm}$ [**Figure 47**]:

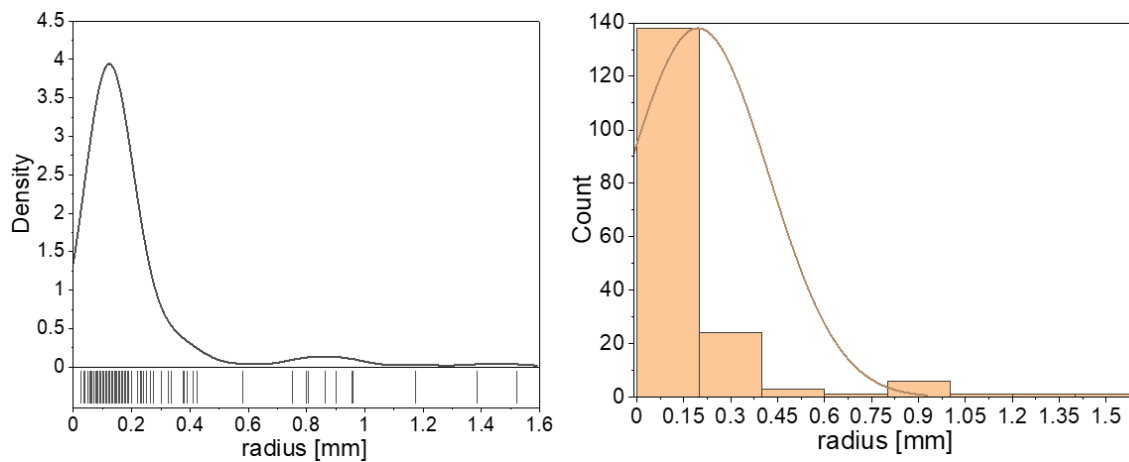


Figure 47. Distribution of particles sizes obtained through the emulsion polymerisation with hexane expressed via density vs radius and count of particles vs radius

A distribution of particles containing urease and pyranine was placed in 0.3 mM urea solution and the urea-urease reaction was observed using both bright-field and green fluorescence microscopy as shown in [Figure 48]. In particular, in [Figure 48 a)] there are three particles having radii between 0.25-0.30 mm. The first picture shows a bright-field image used to determine the size of the particles; the scale bar is set at 0.5 mm. The following three fluorescent images show the same particles at times of 2, 4 and 6 minutes since the beginning of the reaction. In [Figure 48 b)] a set of larger particles with a radius from 0.35 to 1.4 mm is shown, with the first picture taken in a bright-field. The subsequent fluorescent images show the particles reacting in time at 3, 8 and 13 minutes since the start of the reaction.

It can be observed that for this range of sizes from 0.25 to 1.4 mm, the particles with a smaller radius have a faster output response compared to those with a larger one. This is due to the urea diffusion within the particle and faster increase of urea in the smaller particle which reacts with enzyme to form ammonia, generating an increase in pH and the consequent pyranine fluorescing. It may be noticed that the very small particles in Figure 2(a) never react. This is attributable to the fast loss of ammonia from the particle, compared to the rate of reaction. Therefore, ammonia does not have time to accumulate inside the particle and the pH never increases.

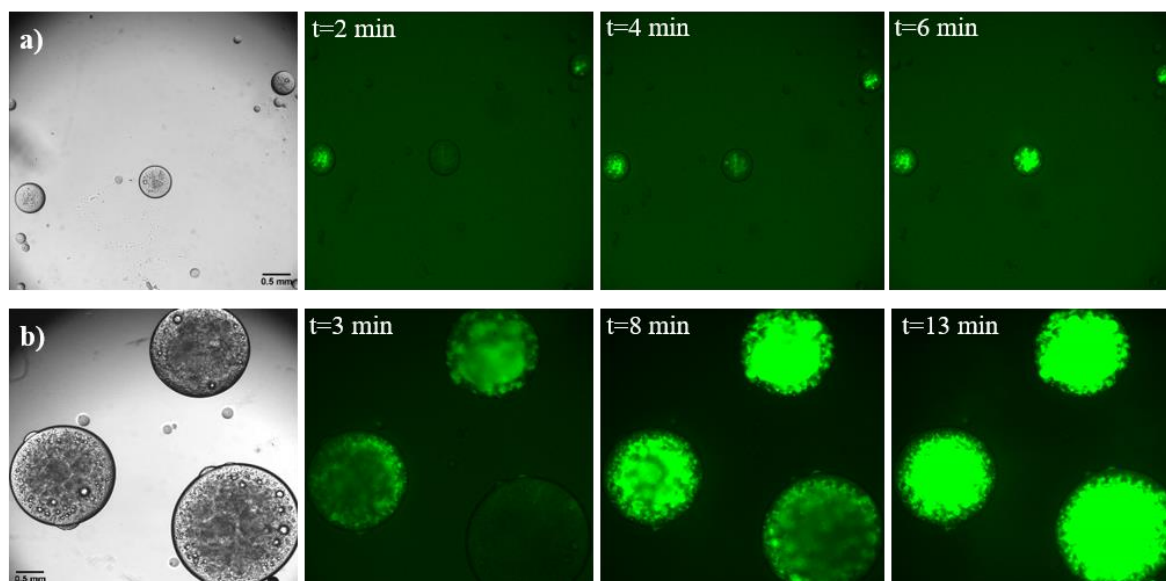


Figure 48. Thiol-acrylate a) small and b) large urease-particles in which urease powder and pyranine are encapsulated and placed in 0.3 mM urea solution at pH 4. The first image shows the particles in a bright field. The following pictures show the output response in time in terms of increasing fluorescence as a consequence of pH increase due to the urea hydrolysis reaction; scale bar 0.5 mm.

On sufficiently large particles, autocatalytic reactions may result in a front or a wave instead of the particle reacting uniformly^{98,117,100}. In **[Figure 49]** the spatial variation in intensity along the particle diameter is displayed for different size particles. Under the conditions used here, the particles appear structured internally, possibly as a result of some phase separation of the thiol-acrylate polymer. In the first two plots, the particle with radius $r = 0.22$ mm and $r = 0.80$ mm, the intensity increases uniformly across the particle as the reaction proceeds, meaning that there is no reaction-diffusion front. Regarding the third particle, where $r = 1.4$ mm, there is some evidence of a reaction-diffusion front starting to propagate. In this case, the reaction starts at the edges of the particles and consequently, it diffuses towards the centre. The uniform growth of the intensity in a small particle is an important assumption in the choice of ODEs in the computational model; it can be seen that this is likely valid up to a particle radius < 1.4 mm.

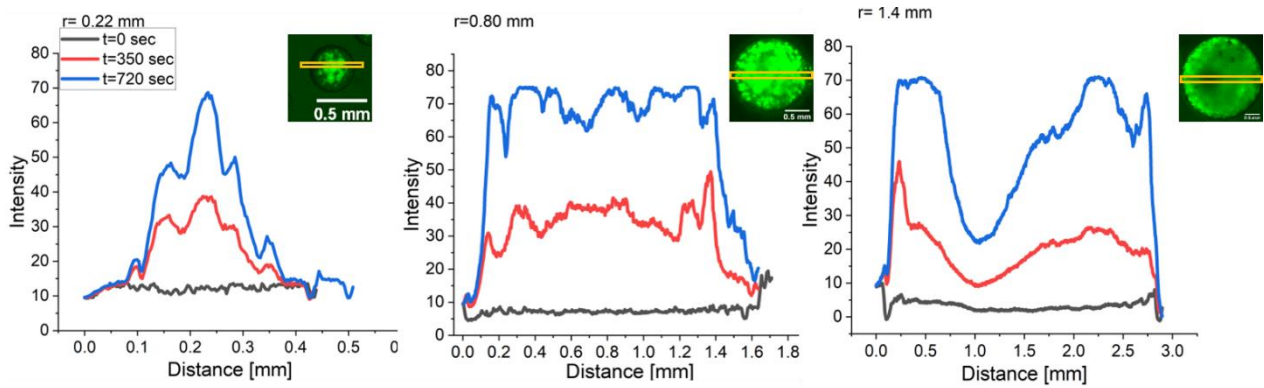


Figure 49. Intensity profile along the diameter of the urease-particles in 0.3 mM urea solution at pH 4. The sizes of the particles considered were $r = 0.22, 0.80, 1.4$ mm. For the first two, the intensity changes uniformly, whereas for the bigger particle, the effect of the reaction-diffusion waves starts showing and the reaction propagates from the edges towards the centre of the particle.

A comparison of the different particle biosensor reaction times is shown in [Figure 50]. The reaction time is defined as the time required to reach the maximum relative intensity. Here the fluorescence intensity is plotted in time for five different particles. Particles below $r = 0.1$ mm didn't show any fluorescence and therefore the intensity value is constant and equal to 10, which is similar to the background intensity. Particles with a radius < 0.30 mm start to react and exhibit an output response, but then the intensity gradually decreases. When the radius reaches values around 0.3 - 0.40 mm, the fastest response time is achieved without dampening. For particles larger than this, the maximum intensity value is slightly improved, however the reaction time is slower.

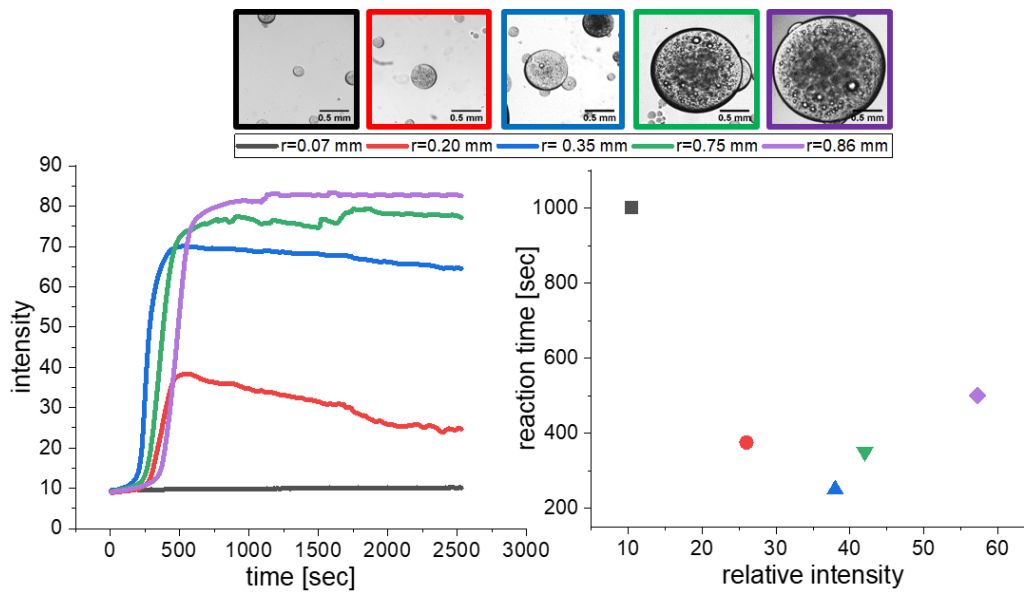


Figure 50. Intensity vs time for increasing urease-particle size in 0.3 mM urea solution at pH 4, and reaction time vs relative intensity for each particle size. Scale bar 0.5 mm

The data for all particles is summarised in **[Figure 51]**. Here, the average reaction time is plotted as a function of the particle size. It can be noticed that the optimum radius in terms of fastest reaction time is found to be ~ 0.3 mm. Above and below this value, the particles require longer to react and display the output response. In particular, for radii below 0.1 mm, no reaction has been observed, and therefore, this value has been identified as a cut-off point as the minimum particle radius capable of detecting urea and giving an output response signal. The large error at larger particle sizes > 1 mm is likely a result of the formation of reaction-diffusion fronts formed sometimes in these particles.

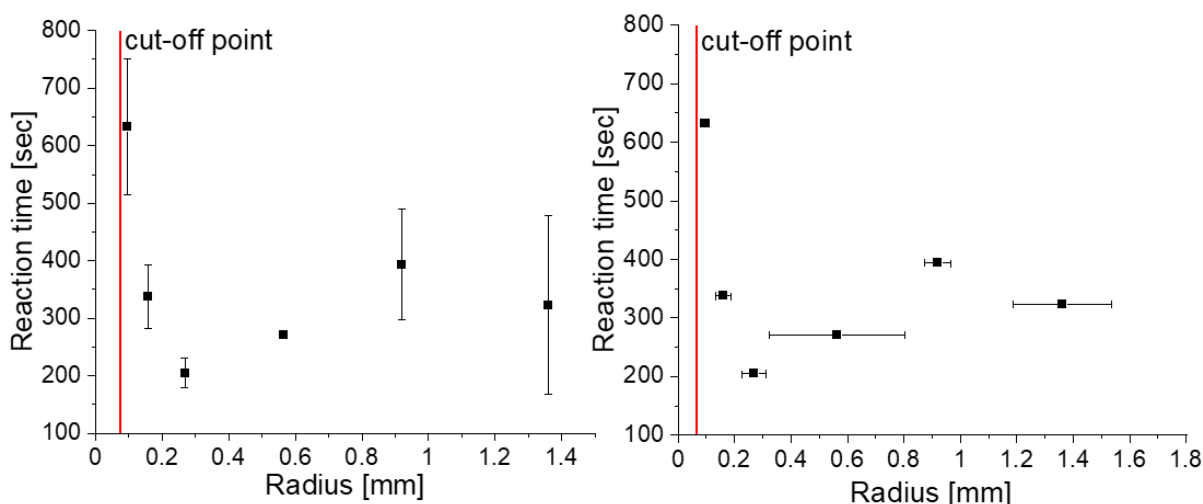


Figure 51. Average reaction time vs. particle radius for urease-particles showing the standard deviation for the average reaction time and radii respectively. Particles were placed in 0.3 mM urea solution at pH 4. Particles with a radius below the cut-off point do not display an increase in fluorescence.

Lastly, in order to further study the effect of the mass transport between the particle and solution on the intensity and consequently the reaction time, particles produced using an emulsion with mineral oil were studied and compared with ones prepared in hexane. The thiol acrylate polymerises in the mineral oil forming an oil-gel layer around the hydrogel core. This extra layer is expected to reduce the transport of species between the particle and solution; particularly the charged species such as protons.

In [Figure 52] there are two sets of particles having an internal water core containing pyranine and an outer oil layer, the 'shell', both in bright field and green fluorescence. To see the effect of the shell on the particle under different conditions, two sizes were chosen: 0.3 and 0.42 mm. The emulsion particles were placed in urea solution and the urea-urease reaction was observed. In this case, the fluorescence was observed only in the internal core due to pyranine's hydrophilic properties. It appears that, for both sizes, the oil layer delays the intensity increase compared to the particle having the absence of a shell because of the reduced transport rate of urea. However, for smaller particles, once the urea diffuses in the core and ammonia is formed, the intensity appears to be more stable with a shell compared to no shell.

This may be because the shell encapsulates and traps better the reaction product ammonia/ammonium inside the core, delaying their diffusion to the outer solution.

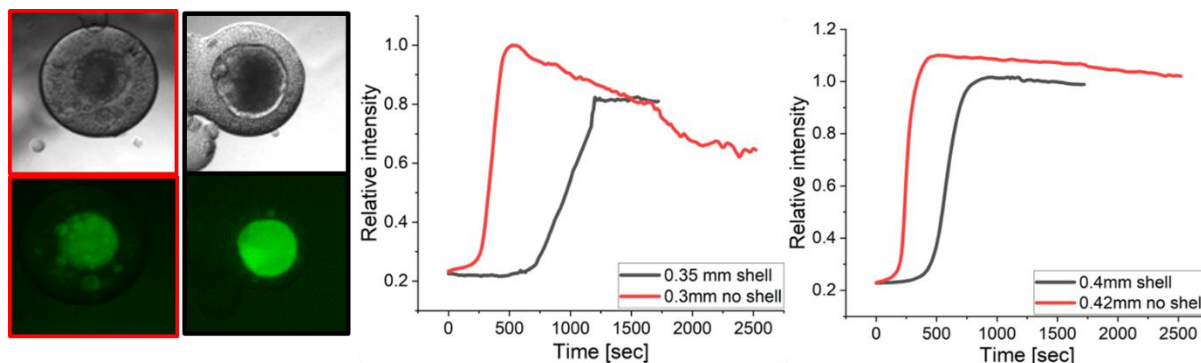


Figure 52. Relative intensity comparison between urease-particles made in hexane (no shell) and in mineral oil (shell) for particle radii of 0.35 and 0.4 mm

In summary, the general clock profile typical of autocatalytic systems is observed here^{97,108,118}. The clock time depends on the particle size as a result of the diffusion of urea and ammonia between the particle and solution. Below a radius equal to 0.1 mm, particles have shown no reaction due to the fast diffusion of species from the particle surface to the solution. When the size is around $r \sim 0.15$ mm, urea will diffuse quite rapidly; however, ammonia will leave the particle as rapidly, causing a delay in time for the pH to increase and consequently pyranine to show. In contrast, when the particle size is larger, urea will take longer to diffuse in and react with the enzyme. Thus, in a similar way, ammonia will accumulate inside the particle, and it will take longer for it to leave. We found that there is an optimum radius ($r \sim 0.35$ - 0.45 mm) for which particles have a fast response time. Usually, when working with sensors and general reactions, the smaller the radius, the faster the reaction⁸⁵. However, when autocatalytic reactions are used, this is not necessarily the case. We have shown that in order to get the best performance when working with autocatalytic reactions in particles, the radius is a key parameter to take into account. Therefore, in terms of sensors, in addition to the classical parameters on

which one usually operates, such as catalyst activity, supporting material, and encapsulation technique, here we demonstrate there is an optimum particle size for processes involving autocatalysis.

3.4.2 Simulations

Computational models help us to understand and optimise a system in order to save time and resources. Therefore, since the system presented in this paper is regulated by many parameters, a kinetic model was produced to predict and interpret its behaviour. The purpose here is to give a qualitative rather than quantitative description to compare with experiments. The model is based on earlier work^{113,100,106} and the files can be found in the Appendix. It is important to specify that the ODE computational model is valid only for particles up to $r \sim 1$ mm, this is due to the reaction-diffusion front that starts in the particles when the radius has bigger values.

The simulation results are shown for particles obtained through hexane and particles produced via mineral oil in two different sub-sections.

3.4.2.1 Particles in hexane

In **[Figure 53]** the profiles of pH, urea, and ammonia in the particle produced via hexane are plotted vs time. The pH profile can be correlated with the relative intensity previously seen in the experimental results section. As previously seen, there is an optimum radius for the fastest reaction time which is around 0.35 mm. For very small radii (0.1 mm), the pH doesn't increase due to the ammonia's fast effective diffusion, or high transport rate constant k : the particle surface area is large compared to the volume hence $k = \frac{k_{sl}}{r} = \frac{l}{r}$ is large. Then, as the radius increases, the pH increases after a delay associated with the time required for urea to build up in the particle and react with the enzyme, but also the time taken for ammonia to increase in the particle. For each pH profile, there is a maximum pH and after reaching the maximum value, the pH starts decreasing. This is due to the loss of

ammonia from the particles to the solution. Specifically, in small particles the ammonia produced will leave faster and therefore, the decrease in pH is more evident. In contrast, as the particle size increases, ammonia will take longer to diffuse out. The simulations show that for hexane particles after reaching a maximum pH the value decreases due to the diffusion out of ammonia.

The urea profile shows that for very small radii ($r \sim 0.1$ mm) the concentration of urea in the surrounding solution equals the one inside the particle as a result of the fast transport of urea in. Then, the process gets slower and the delay time is proportional to the particle size; for bigger radii urea needs a longer time to build up in the particle. It can be observed that for intermediate radii there is a plateau before a consequent decrease. For big particles, urea reaches a maximum and immediately decreases. This can be attributed to the competition between diffusion and reaction time. Intermediate particles are dominated by a reaction-limiting mechanism, whereas big particles are dominated by a diffusion-limiting mechanism. For simplicity, it can be said that in medium particles urea diffuses in quickly and then time is needed for the reaction to start. In big particles, diffusion takes long enough for the urea to be immediately converted into ammonia before reaching a plateau.

Lastly, the ammonia profile is qualitatively similar to the pH profile. The time required for ammonia to be produced and the consequent decrease depends on the particle size. For small particles, the reaction either does not occur or the rate has a very small value because the ammonia transport out of the particle is fast so the pH does not increase and for urease, the fastest rate occurs at pH = 7. For bigger particles, the ammonia reaches higher values as a result of a slower transport out of the particle. Again, it can be observed that there is an optimum radius around $r=0.35$ mm for the fastest response time.

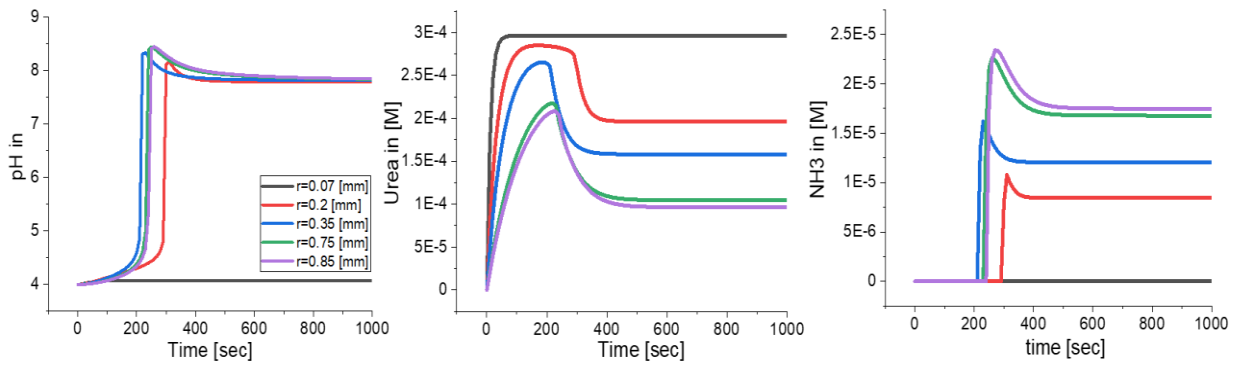


Figure 53. Simulated pH, urea and ammonia concentrations in the particle fabricated via hexane vs time for different particle radii (0.07 – 0.85 mm). The initial concentrations are: $[U]_0 = 0.3 \text{ mM}$, $pH_0 = 4$ in the surrounding solution and $pH = 4$, $E = 80 \text{ u/ml}$ in the particle.

In [Figure 54] the plots show pH, urea and ammonia profiles inside the particle fabricated with hexane vs time fixing the radius at $r = 0.35 \text{ mm}$ and changing the urea concentration. Regarding the pH, it can be observed that the more the initial concentration of urea is increased, the more the pH growth is fast and the final reached value is high. Urea also diffuses inside the particle faster, and the ultimate value reached is proportional to the initial urea concentration. Lastly, since ammonia is strictly dependent on urea, it is easy to predict that the higher the initial concentration of urea, the faster ammonia will be formed. In the same way, the more urea is in the particle, the more ammonia will be produced.

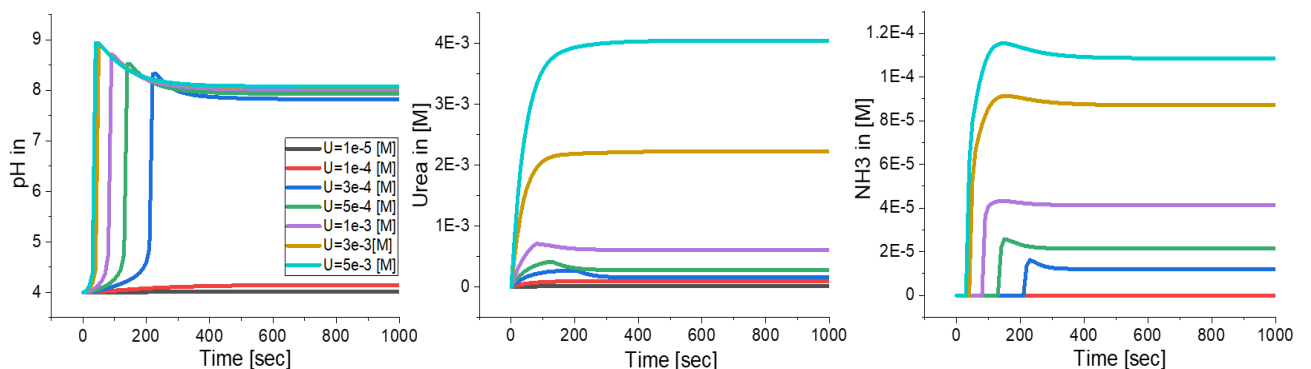


Figure 54. Simulated pH, urea, and ammonia profiles vs time in the urease-particle fabricated with hexane with radius $r = 0.35 \text{ mm}$ with varying urea concentration ($1e-5 - 5e-3 \text{ M}$). The initial concentrations are: $pH_0=4$ in the surrounding solution and $pH = 4$, $E = 80 \text{ u/ml}$ in the particle.

A summary of the behaviours previously explained is presented in [Figure 55]. It shows a plot of particle pH vs urea from the data in [Figure 54], which illustrates the ultrasensitivity seen in previous work with urease particles⁸⁵. There is a sharp increase in pH for a small increase in urea.

The reaction time is plotted by increasing the particle radius and is taken as the time to reach the maximum pH. In agreement with the experimental results, it can be seen that below the radius ~ 0.2 mm, no reaction is observed due to fast effective diffusion, or transport, of ammonia out of the particle. For bigger particles, the reaction time is slower because in this case the urea transport time inside the particle and its consequent production of ammonia are longer. However, there is an optimum particle radius for which the urea diffusion in is fast enough and the ammonia diffusion out is slow enough to allow the pH to increase with the fastest response time. The second plot on the left shows the radius versus the urea concentration representing the ultrasensitivity plot. In earlier works with urease particles, activity was observed in smaller particles of $100 \mu\text{m}$ but in this case the concentration of urea was much higher (75 mM) and the critical radius in autocatalytic reactions depends on the concentrations^{107,119}.

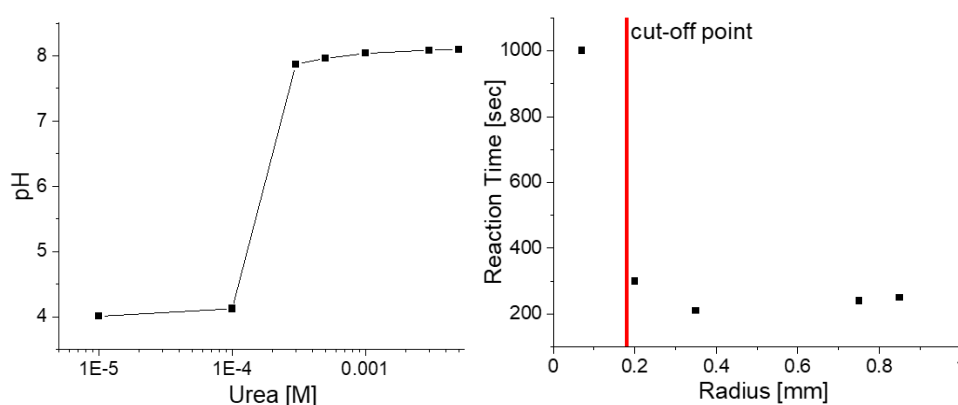


Figure 55. pH vs urea plot showing the ultrasensitivity obtained with the hexane particles system (left). Reaction time vs radius for simulations of particles made via hexane with initial concentrations: $[U]_0 = 0.3 \text{ mM}$, $pH_0 = 4$ in the surrounding solution and $pH = 4$, $E = 80 \text{ u/ml}$ in the particle (right).

3.4.2.2 Particles in mineral oil

Following, in [Figure 56] it can be observed the behaviour of particles produced with mineral oil. The plots represent pH, urea and ammonia vs time, respectively. Similarly, as previously seen for the hexane particles, an optimum radius can be identified with $r = 0.35$ mm. Below and above this radius value, the particles show a slower reaction time. This is a main difference compared to the hexane particles already reflected in the experiments. Specifically, it is that the mineral oil particles are slower than the hexane ones in terms of reaction time. However, once they react pH value is more stable in time. This is due to the oil layer surrounding the particle refrains ammonia from diffusing out and the species like protons and OH^- to diffuse inside the particle.

Equally, in the urea profile, the surrounding solution concentration of urea in a very small radius ($r \sim 0.07$ mm) is equal to the concentration of urea in the particle due to the rapid transport of urea. Then the process is slower, and the delay time is proportional to the size of the particles; for larger urea radii, it takes longer to accumulate. In the intermediate radii, there can be seen a plateau before a corresponding decrease. In the case of large particles, urea reaches its maximum and decreases immediately. Again, this is due to the competition between diffusion time and reaction time. The intermediate particle is dominated by the reaction limitation mechanism, and the large particle by the diffusion limitation mechanism. So, in medium-sized particles urea can be quickly distributed throughout the particle and then the reaction starts to consume urea. In larger particles, the diffusion takes long enough to convert more urea to ammonia before reaching a plateau.

Once more, the amount of ammonia produced dictates the pH behaviour and it is correlated with the particle radius. An optimum radius = 0.35 mm gives the fastest response time.

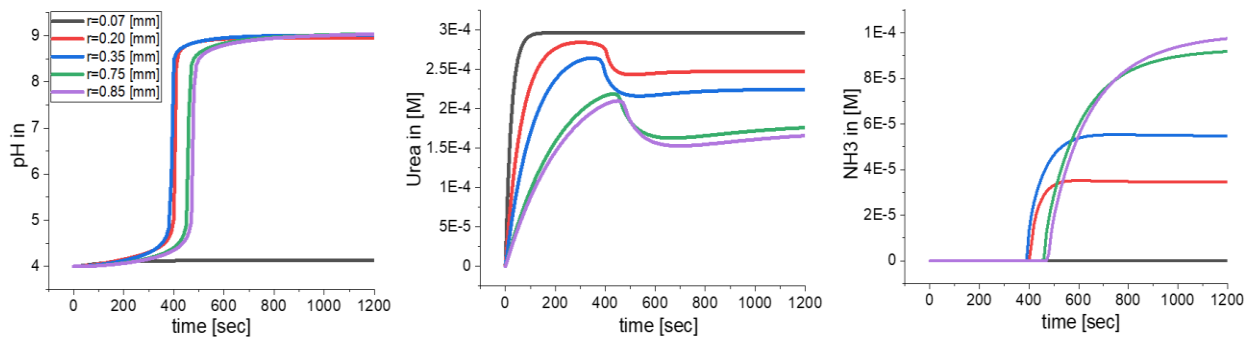


Figure 56. Simulated pH, urea and ammonia profiles in the particle fabricated via mineral oil vs time for different particle radii (0.07 – 0.85 mm). The initial concentrations are: $[U]_0 = 0.3 \text{ mM}$, $pH_0 = 4$ in the surrounding solution and $pH = 4$, $E = 80 \text{ u/ml}$ in the particle.

The graph in [Figure 57] shows the pH, urea, and ammonia profiles inside the particles manufactured with hexane, while the radius is determined at $r = 0.35 \text{ mm}$, thereby changing the concentration of urea. As far as pH is concerned, it can be observed that the higher the initial concentration of urea, the faster the growth of pH and the higher the final value. Urea is also faster to spread within the particles, and the final value reached is proportional to the initial urea concentration. Finally, since the concentration of ammonia is strictly dependent on initial urea, it is easy to predict that the higher the initial urea concentration, the faster ammonia will form. Similarly, the more urea there is in the particle, the more ammonia is produced. The main difference again is that, although mineral oil particles are slower showing the reaction time, once the reaction has happened the values of pH, urea and ammonia are more stable over time.

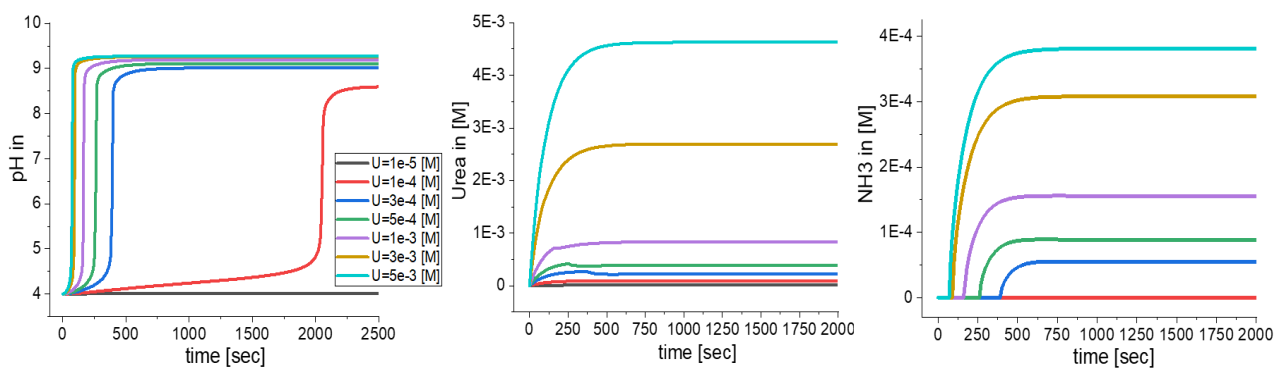


Figure 57. Simulated pH, urea, and ammonia profiles vs time in the urease-particle fabricated with hexane with radius $r = 0.35 \text{ mm}$ with varying urea concentration ($1E-5 - 5E-3 \text{ M}$). The initial concentrations are: $pH_0 = 4$ in the surrounding solution and $pH = 4$, $E = 80 \text{ u/ml}$.

Lastly, in [Figure 58] it is shown a plot of the ultrasensitivity trend on the left and the reaction time versus the radius on the right. The ultrasensitivity plot is not different from the hexane particle one. Correspondingly, the reaction time plot is qualitatively similar to the previous one, however as it was observed before, mineral oil particles require a longer time in order to react, therefore the reaction time here assumes a higher value.

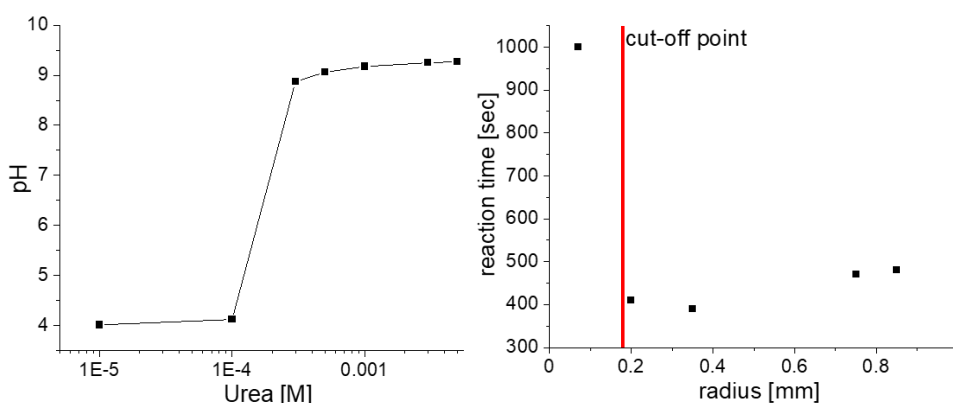


Figure 58. pH vs urea plot showing the ultrasensitivity obtained with the mineral oil particles system (left). Reaction time vs radius for simulations of particles made via mineral oil with initial concentrations: $[U]_0 = 0.3\text{mM}$, $pH_0 = 4$ in the surrounding solution and $pH = 4$, $E = 80\text{ u/ml}$ in the particle (right).

Thus the experimental results and simulation match qualitatively and have similarities on a quantitative level. For future applications, the model can be used to tune the system and set parameters to obtain optimal behaviour. It would also be possible for instance, to change the k_{sl} , with the aim of simulating other support materials or polymers to encapsulate the enzyme urease. It is expected that the general trends presented here for reaction time vs radius will not depend on the type of polymer used; however, this requires further investigation.

3.5 Conclusions

In this chapter, we have presented experiment and model results for optimising particle biosensor response in an enzyme reaction with feedback. In particular, in contrast to other reactions, when dealing with autocatalytic reactions apart from the standard parameters commonly used such as enzyme concentration, support material, entrapment technique etc... an important role is played by the particle size or radius, and the transport of both the substrate in and product out of the particle must be taken into account. The main goals here were to optimise both reaction time and the signal amplitude. These two features will determine the best biosensor output response for different applications. The approach involved a computational model in order to help understand the system and tune parameters in the future. The experiments and simulations have been compared qualitatively and found to be in good agreement.

The enzyme and indicator (pyranine) were encapsulated in a thiol-acrylate polymer particle via physical entrapment. A range of different particle sizes, or radii, was obtained through emulsion polymerisation using hexane. For both of them, it was shown that very small particles were unable to react as a result of the fast diffusion of ammonia out of the particles. On the other hand, large particles take a longer time to react due to the limiting effect of urea transport in the particle. However, in this case, the signal amplitude seemed more stable due to the long time for the product ammonia to diffuse out. For a particle of $r = 0.35$ μm , it was found that it was an optimum in terms of reaction time and signal amplitude. The particles in this range react faster than at lower or higher r showing that size plays a crucial role in the biosensor output response.

Lastly, to further investigate the transport effects, urease-particles made using thiol-acrylate emulsion polymerisation in mineral oil. In this case, the particles formed an internal core of hydrogel in which enzyme and indicator are trapped and an external oil-gel, or shell. The shell and non-shell particles (made with hexane) were compared

and it was found that although shell particles take longer to respond, the signal is more stable in time. The phenomenon is attributed to the oil layer which delays the diffusion of urea inside the core and in the same way traps the ammonia in it once is formed. Further investigations are required to confirm these results. The emulsion technique used here to obtain enzyme-particles was easy to perform; however, it is not suitable for producing precise particle sizes for reproducible particle biosensor properties.

4. Immobilisation of protein microbodies in hydrogel particles for improving stability of enzyme-particle biosensors

4.1. Overview

Effective techniques for enzyme immobilisation have been an important topic for the few past years. This is because one of the advantages is that it makes the reuse and recovery of enzymes easier, especially if the enzyme is expensive. Moreover, immobilising an enzyme enhances its stability in terms of pH and temperature, and ultimately, it gives the possibility of trapping and utilising multiple enzymes at a time. In terms of applications, it is well known that immobilised enzymes have changed the game in industrial production due to their reusability, easy separation and low mass transfer limitations, not to mention continuous process operation and heterogeneous use. Biosensors, industrial monitoring and transformation, and water inspection are just some of the possible applications of immobilised enzymes. However, the combination of enzyme and supportive material is not always straightforward and they might lack in accuracy, reusability and stability specifically because of the enzyme denaturation over time or storage conditions. In this work, we suggest a sustainable, process-free and robust enzyme source as an alternative to standard commercial enzymes for enzyme-particle biosensors. The enzymes contained in watermelon seeds are protected from the external environment by a lipid layer in 'protein microbodies'. Therefore, the enzyme has proven to be reusable, reproducible and able to be stored at room temperature for over a month in different hydrogel particles. The designed system was capable of reactivity that detects urea down to 0.4 mM in one hour.

4.2. Introduction

The immobilisation of enzymes has been a breakthrough in modern science. It has allowed for the improvement of enzymes' properties such as stability to pH and

temperature, robustness, heterogeneous use and low mass transfer limitations¹²⁰. Also in industrial applications, the possibility of reusing and easily recovering or separating the enzyme, especially if expensive, has had a great impact mainly in continuous process operations and multi-reaction systems^{17,121}. The importance and usage variety of immobilised biocatalysts has reached numerous fields: the food industry (β -galactosidase, Lipase), chemical industry (Lipase), pharmaceutical industry (Penicillin, Transaminase), medical devices (glucose, urea and lactose biosensors)¹⁷.

However, the biggest challenge faced is the immobilization of enzymes on solid supports³: it has to be a cost-effective method, reliable, reproducible and that will not affect the characteristics of the enzyme. Among the techniques to immobilise enzymes, we consider two major processes: chemical binding and physical encapsulation. Covalent binding is one of the most common techniques, but it is well known to decrease enzyme activity¹²². On the other hand, adsorption/encapsulation leaves unchanged the enzyme nature causing sometimes its diffusion throughout the support¹⁰⁸. Although several different solid supports have been tested e.g. silica^{40,123}, alginate¹²⁴, sol-gels¹²⁵, chitosan¹²⁶ and more¹²⁷, the challenge is that using urease, it will leak through the gel matrix. Therefore, what we suggest in this paper is to compare urease powder from Sigma (UP) with a more unprocessed, sustainable and inexpensive enzyme source: watermelon seeds (WM)^{107,105,128}. An important feature of enzymes contained in watermelon seeds is that they are contained in a lipid layer. The arrangement is called a protein microbody^{100,129} and it is typical of enzymes contained in natural sources, e.g., seeds, plants and generally fruits¹³⁰⁻¹³¹. These structures allow enzymes to be protected from the external environment and preserve their activity for longer.

In this paper, we have chosen to work with the urea-urease system since it is well-known and easy to reproduce. Urea is an organic compound highly soluble in water and non-toxic. It is the main nitrogen-containing substance in the urine of

mammals. The body uses it in many processes, especially nitrogen elimination. As a source of nitrogen, urea is widely used in fertilizers and is an essential raw material for the chemical industry¹³². Due to its wide use and application¹¹⁰, detection of urea is a current key task of researchers and scientists. Some applications focus on the pharmaceutical/biomedical approach, e.g., human sweat⁸, saliva¹³³ and blood¹³⁴. Some regard a more environmental and waste water treatment evaluation in rivers¹³⁵, effluent^{136,137} and seawater¹³⁸. Others focus on food freshness or quality¹³⁹.

The immobilized enzyme presented in this work is contained in a particle and is characterised by qualitative reactivity through the urea-urease 'on-off' threshold reaction⁹⁷. The particles were made by polymerization with the pH autocatalytic urease reaction with thiol-acrylate⁹⁸ and agarose gels¹²⁸. The two enzyme sources have been encapsulated in hydrogels and tested for activity, storage conditions and reusability. Watermelon seed urease has proven to be a robust, sustainable, and inexpensive alternative to standard processed enzymes. The WM biosensor is capable of reacting with urea down to 0.4 mM in one hour and can be stored for up to 1 month at room temperature, maintaining its reusability.

4.3. Methods

The methods are covered in chapter 2, section 2.3

4.4. Results and Discussion

To investigate the characteristics of urease powder and watermelon seed urease in terms of reactivity and stability, two types of tests were performed. For convenience, the results and discussion section was divided accordingly. The first part is dedicated to the activity and reaction time achieved by the particles: thiol-acrylate, low and high EEO agarose particles with UP [**Figure 59a**] with WM [**Figure 59b**]. In the

second part, the enzyme encapsulation reusability and reproducibility features are examined [**Figure 60 and Figure 61**].

4.4.1. pH profile and reaction time

The results of thiol-acrylate are in agreement with the findings of other studies, in which the enzyme is stable, well encapsulated, and able to perform the clock reaction^{97,107}. Thiol-acrylate particles generate an "on-off" signal that produces an optical output response with both enzyme sources, showing that with this type of hydrogel, UP and WM are stable, robust and able to produce a signal. The signal is represented in [**Figure 59 a) and b)**] by the absorbance recorded over time. Subsequently, it has been converted to pH according to the different concentrations of urea used to match the colour acquired by the indicator (Appendix 3). An additional parameter used to evaluate the particles' activity and stability was the reaction time. It was defined as the time required to reach a pH of 7, at which the BTB changes colour from yellow to blue. The response time increases when the urea concentration is decreased.

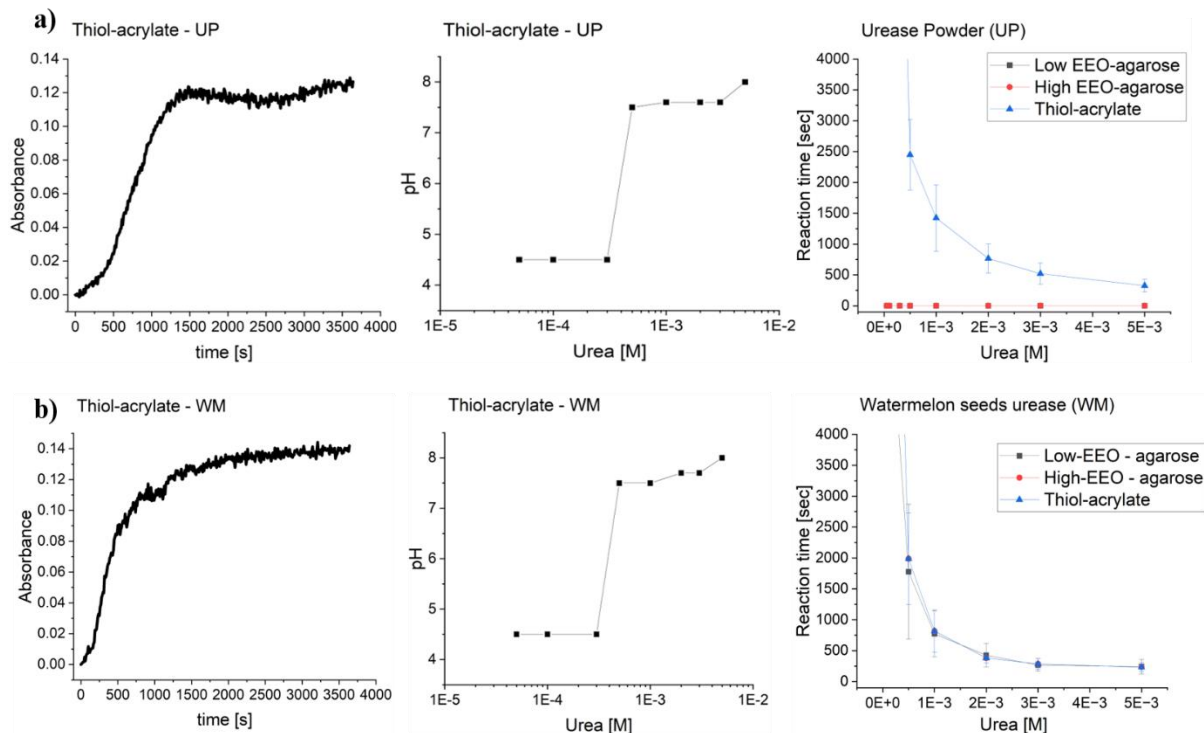


Figure 59. Absorbance vs time, pH vs. urea and response time vs urea of: a) thiol-acrylate particles with UP; b) thiol-acrylate particles with WM

Subsequently, both enzyme sources (UP and WM), were encapsulated in Low and High EEO agarose. In this case, the results show that the UP with the two types of agarose was unsuccessful; the combination of physical encapsulation of urease and the agarose matrix generates a leakage of enzyme from the particles. In fact, in [Figure 59a)], it can be observed that the set of particles was unable to react in the presence of increasing urea concentration for up to 1 hour.

However, when WM was used with agarose, the particle appeared to be robust and stable because of the larger size of the protein microbodies. From [Figure 59b)] it is evident that the particles were able to react to urea at a concentration of 0.4 mM, giving a change in pH and therefore an optical output. As previously seen for the thiol-acrylate particles, the reaction time depends on the urea concentration, and in particular, it decreases when the concentration is increased. In these tests, the time limit set was one hour.

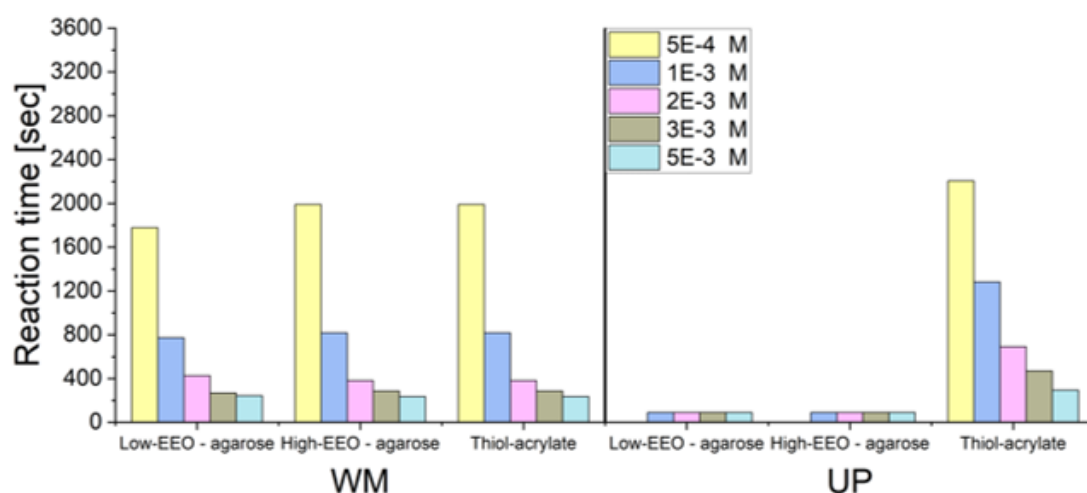


Figure 60. Summary of reaction times with by WM vs. UP particles for different urea concentrations

In summary, while UP has been shown to form a stable encapsulation only when it is trapped in thiol-acrylate particles, WM has proven to be adaptable to all hydrogels tested. In fact, for all of them, the detection limit was found to be 0.4 mM and the reaction time happened within one hour [Figure 60].

4.4.2. Reusability and reproducibility tests

Once the particles were tuned from the reactivity perspective, it was necessary to prove their stability in time. From an application-oriented perspective, two features were examined: reusability and reproducibility of the particles. The test was performed on two different timescales using the particles first consecutively [Figure 61] (10 times in succession) and then weekly over a month [Figure 63]. The reaction time is defined as time to pH 7.

In the consecutive test, a set of particles was left to react with urea, recording the pH over time; then, the same set was placed in an HCl solution until the indicator was restored to its original yellow colour. This procedure was repeated ten times.

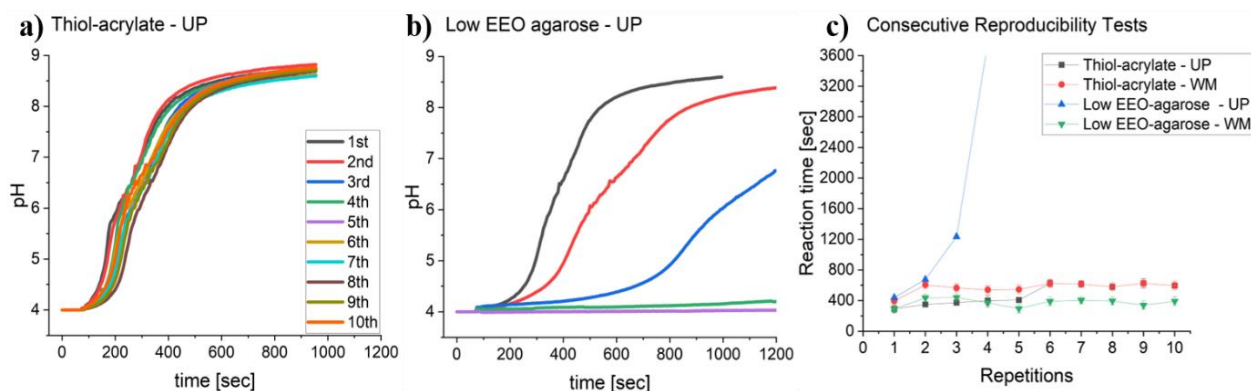


Figure 61. Reproducibility tests performed consecutively of: a) thiol-acrylate - UP, b) Low EEO agarose - UP, c) low EEO agarose - UP and d) low EEO agarose - WM

As shown in [Figure 61 c)], WM urease combined with both thiol-acrylate and low EEO agarose was able to reproduce the reaction signal and therefore be reusable, for all repetitions. However, when UP was tested, only the combination with thiol-acrylate lasted until the last run. In fact, when the enzyme from Sigma was combined with agarose, no response was observed after the third time. The reason for this could be the leakage of enzyme from the particle or its denaturation/deactivation.

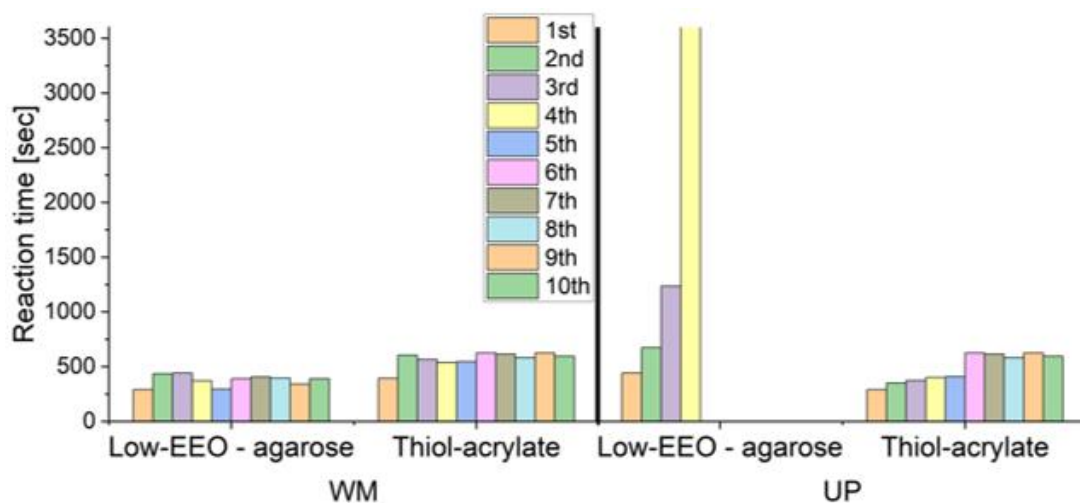


Figure 62. Summary of reaction times performed with WM vs. UP particles for consecutive reusability test

[Figure 62] shows a summary of the reaction times recorded using the particles ten times for watermelon seed urease and urease powder trapped in thiol-acrylate and agarose gels. Clearly, WM were more reusable and faster, whereas UP in agarose lost its activity after the fourth time.

For the weekly reusability tests, the particles were kept at room temperature and used with urea once one week for a month.

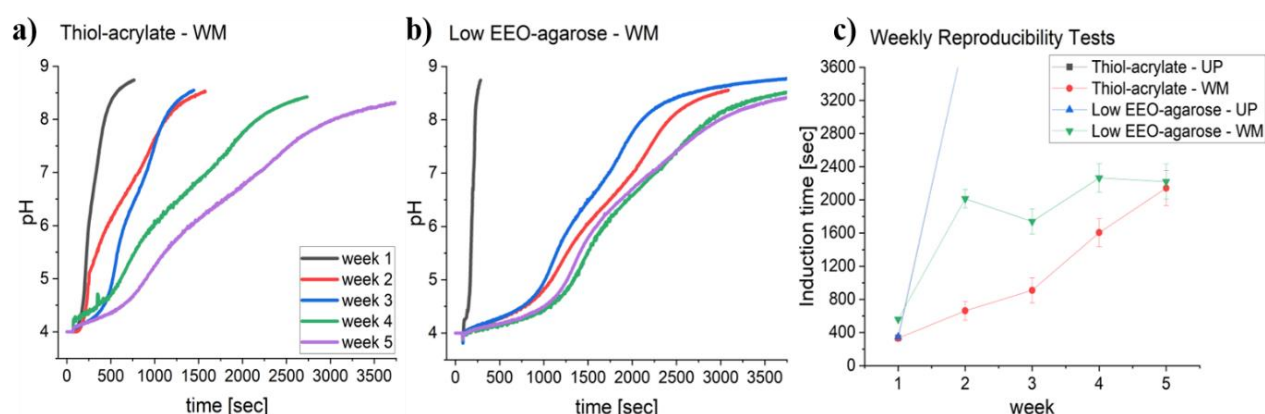


Figure 63. Reproducibility tests performed weekly over one month of a) thiol-acrylate - UP b) thiol-acrylate - WM, c) low EEO agarose - WM and d) low EEO agarose - WM

In this case, [Figure 63 c)] illustrates that the UP was unable to reproduce the signal and could not be reused whatsoever. On the contrary, WM, used with both thiol-acrylate and agarose, proved to make a robust combination capable of reproducibility even when stored at room temperature for five weeks.

One of the possible applications of immobilised biocatalysts, as previously mentioned, is using them as biosensors. [Table 7] highlights differences in terms of sensor type, response time and stability of different kinds of urea biosensors. As can be noticed, the enzyme/hydrogel combination proposed here in this paper has a longer response time that is longer than that of other systems. However, it shows comparable detection limit values and longer enzyme stability over time.

Table 7. The relative stability of different urea biosensors (adapted) ¹⁴⁰

Immobilization technique	Sensor type	Detected analyte	Response time [min]	Detection limit	Stability	Refs
urease entrapped in the polyion complex	amperometric	NH_4^+	0.03	50 μM	80% in 1 day	29
urease entrapment in the nanostructure	amperometric	NH_4^+	0.03	500 μM	80% in 7 days	29
urease entrapped in PVA-HMDI	Carbon-based electrode	Carbamic acid	1-2	500 μM	60% in 7 days	29
urease (UP) entrapped in thiol-acrylate particles	Optical, colorimetric	NH_4^+ through pH	<60	400 μM	0% in 7 days (room T)	Our study
urease (UP) entrapped in low EEO agarose particles	Optical, colorimetric	NH_4^+ through pH	<60	400 μM	0% in 7 days (room T)	Our study
urease (WM) entrapped in thiol-acrylate particles	Optical, colorimetric	NH_4^+ through pH	<60	400 μM	80% in 5 weeks (room T)	Our study
urease (WM) entrapped in low EEO particles	Optical, colorimetric	NH_4^+ through pH	<60	400 μM	80% in 5 weeks (room T)	Our study

Therefore, as a possible application of the urease from watermelon seeds, we propose a urea biosensor. The sensor will be capable of qualitative analysis working through a threshold value giving an optical output signal response.

4.5. Threshold sensing with WMS- thiol-acrylate particles

It is well-known that enzymes show selectivity to certain compounds^{14,141}, and they can be used as biosensors to detect even trace amounts of analyte due to their signal amplification capabilities¹⁴². Biosensors are gradually taking standard sensors' place in order to reduce pollution, be more cost-effective and bio-compatible^{4,5,8,143,144}. Moreover, according to the type of enzyme chosen, they can

be used in a multiplicity of fields (biomedical, pharmaceutical and food industry, wastewater management, forensic, etc...) ^{3,14,44,68,75,78}. In particular, optical biosensors are often chosen because they are easy to use, inexpensive, and have a fast response time ^{5,68,145}.

Enzyme biosensors have proven to be a robust, reliable, non-toxic, bio-compatible and degradable tool. They are capable of functioning continuously and catalysing at a very high level of specificity ⁵. Enzyme biosensors are known for their sensitivity, selectivity, and real-time monitoring. In addition, when coupled with indicators, they become optical biosensors capable of generating a colourimetric output signal. Optical biosensors are simple, affordable, and fast in detection ⁵: most of them do not need additional devices to read the response, and most materials are inexpensive and easy to dispose of.

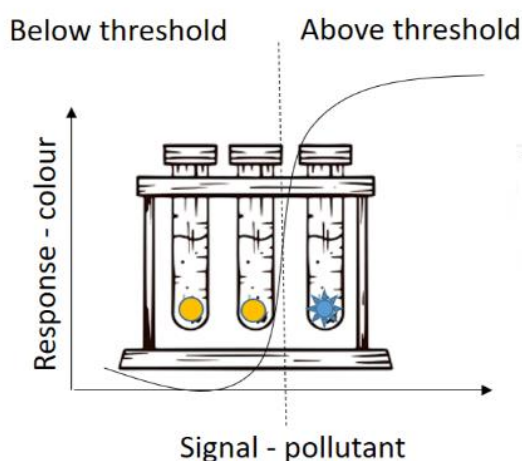


Figure 64. Representation of the urea-urease clock reaction. When enough pollutant is detected, it generates a switch in the colour of the particles that corresponds to an optical output signal.

A threshold sensor displays a signal above a threshold amount of a compound. The urea threshold biosensor could be a possible application for the WM-thiol-acrylate particles studied in this paper. The principle of the urea-urease clock is that as soon as sufficient ammonia is formed in the particle, the pH changes from 4.5 to above 7, changing the colour of the particle from yellow to blue. Therefore, the particles can be used as a biosensor in which the qualitative presence of the analyte is

determined through an optical output signal whenever it overcomes the threshold value [Figure 64].

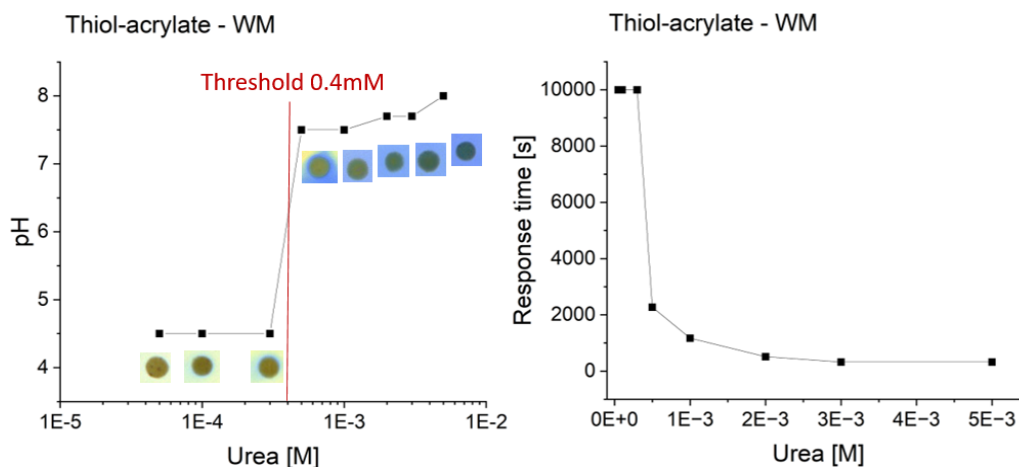


Figure 65. Threshold detection limit (pH vs urea) and response time plots vs. urea of thiol-acrylate particles with WM

The results of urease-thiol-acrylate particle experiments are in agreement with the findings of other studies, in which the clock reaction was observed in the urea-urease system^{97,107}. Thiol-acrylate particles generate an “on-off” signal that produces an optical output response with both enzyme sources. The response time is defined as the time required to reach a pH of 7, at which the BTB changes from yellow to blue. Response times increase with decreasing urea concentrations. The detection limit was established at 0.4 mM and the output signal was obtained in one hour in both cases [Figure 65].

4.6. Conclusions

In this work, we provided an overview of enzyme immobilisation methods, highlighting the importance of such combinations and defining the technical difficulties encountered. We demonstrated a possible alternative to commercial urease powder for maintaining enzyme stability. In fact, watermelon seed urease was shown to be sustainable, cost-effective and robust because the enzyme is

trapped in protein microbodies, which protects and maintains activity of the enzyme even at room temperature.

The two enzyme sources, urease powder and WMS powder, were encapsulated and tested in three different hydrogel particles of thiolacrylate, low EEO, and high EEO agarose. In order to characterise the particles, two tests were performed: one to evaluate the threshold detection limits and response time and the other to evaluate the reusability and reproducibility properties. In the first, particles of a specific hydrogel/enzyme source combination were placed in increasing urea concentration solutions from $5\text{E-}5$ to $5\text{E-}3$ M. The reaction development and reaction time were recorded through a camera and, consequently, analysed with image analysis software. In the second test, 2 g of particles were placed in 60 ml of $5\text{E-}3$ M urea and let react. Next, they were placed in $1\text{E-}4$ M HCl solution to be re-set. The steps were repeated ten times for the consecutive evaluation and then once a week for a month.

WMS urease was found to be suitable for an optical biosensor when immobilised in both thiol-acrylate and agarose particles. In both cases, the detection limit was 0.4 mM and the response time occurred within one hour. Moreover, WMS particles have been shown to produce an output signal and therefore be reusable consecutively (ten times) and over a month, even stored at room temperature. When UP urease was coupled with thiol-acrylate gel particles, the biosensors were robust in terms of the urea detection limit and response time, respectively, also 0.4 mM and 1 hour. However, when UP was paired with agarose, no output signal was observed. The enzyme was possibly able to diffuse out of the particle, making the biosensor inactive. Moreover, in the reusability tests, the only effective result was UP in thiol-acrylate in the consecutive repetitions. For all other experiments, no signal was achieved.

The robustness of watermelon seeds with different hydrogels could be exploited in several systems. One of them could be the observation of propagating reaction-

diffusion fronts¹⁴⁶. Additionally, an optical and chemomechanical biosensor could be used in the field of soft robotics¹⁴⁷. With the diverse spectrum of enzymes contained in WM, another option would be to combine different enzymes to have a single biosensor capable of detecting multiple analytes^{50,148,149}. Considering the reusability shown by WM, a biosensor built with this enzyme source would be a device applicable in a variety of fields such as pharmaceutical, biomedical but also waste water treatment.

5. Towards building chemical reaction networks for programming pH changes using watermelon seeds

5.1. Overview

Enzymes are a fundamental element needed to balance and equilibrate the difficult but delicate mechanisms regulating biological organisms. These systems are quite complicated due to the copious reactions taking place at the same time that are required for energy generation and chemical synthesis. Such a capacity has always fascinated scientists, who have tried to replicate it by artificially reproducing cascade reactions and chemical reaction networks. In fact, combining multiple enzymes has found various applications in many different fields e.g. industrial, biomedical and analytical to detect species, improve reaction rates and overcome product inhibition.

Networks of enzymes that change pH can be used for sensing in Boolean logic gates and chemo-mechanical processes such as pulsatile drug delivery. However, obtaining enzymes from different sources can require expensive extraction methods and also lead to incompatible or unstable enzymes that degrade over time. In this work, we aim to characterise and combine different varieties of enzymes that can be used for programming pH changes. The biocatalysts investigated here are urease, catalase, glucose oxidase, and beta-glucosidase. Glucose oxidase was used as received, whereas the others were all present in watermelon seeds. In particular, watermelon seeds have proved to be a fascinating source of many different enzymes, easy to obtain, and inexpensive, with improved stability of enzymes. The characterisation was performed via oxygen formation or consumption, pH changes and foam formation which was attributed to the phospholipids contained in the seeds.

We showed that the effects obtained by combining the enzymes and building reaction networks or cascade reactions could improve the reaction rate and give large amplitude pH changes, which would have been challenging otherwise.

However, in order to better understand such complicated systems and tune them to give autonomous and self-regulated pH signals, further investigations are required.

5.2. Introduction

Living organisms function through a delicate yet perfect mechanism that keeps all necessary reactions balanced. In order to do so, nature has equipped itself with natural catalysts which decrease the energetic barrier allowing substrates to be transformed into products¹¹³. The complex mechanisms behind biological organisms rely upon a multitude of different and balanced reactions that assure the perseverance of the species. In this regard, biocatalysts are known for their very high specificity and selectivity which regulates each and every reaction at a different rate and conditions. The biggest characteristic of enzymes is that they are capable of working even when separated from the original organism, besides their non-toxicity, biocompatibility and biodegradability^{13,14}.

Due to the large amounts of acids and bases contained in their structure, one of the most influencing parameters in enzyme activity is pH¹¹³. In fact, a characteristic of their active behaviour is a bell-shaped curve in which they show the maximum activity at a given pH. Another interesting peculiarity is that enzymes are able to be combined in order to produce a chemical reaction network which will follow defined rules to give a specific output in space and time⁹. Examples of chemical reaction networks are cascade reactions^{9,150,151} in which every generated product forms the next substrate; positive and negative feedback loops^{79,83,152} wherein the product enhances or inhibits a parameter linked to the reaction, or also Boolean logic gates in which according to the programmed response of the system, certain conditions need to be verified to achieve a response^{76,77}. Moreover, these complex mechanisms could bring to the possibility of building and programming pH changes from a network of enzymes.

Enzymes such as urease, catalase and glucose oxidase are really well studied nowadays, especially to build complex mechanisms as cascade reactions which are gaining increasing interest in order to replicate organisms' intricate stimuli-responsive behaviors. However, processed enzymes acquired from animals and plants are quite expensive due to the refining and stabilization practices they are exposed to. Hence, the possibility of having a cost-effective, multi-enzyme source such as the watermelon seeds provides a practical way to obtain a combination of biocatalysts. We aim to demonstrate that the watermelon seed powder can be used in place of commercial enzyme sources and most importantly, the enzymes naturally immobilized together may provide a more robust and stable platform for enzyme cascade reactions.

It is not surprising that enzymes have been studied, characterised, and utilised in many applications. Whether they are used as detectors^{30,46}, biosensors^{3,15,153} or nano/micro-reactors^{6,154}, nano-micro-motors⁷⁵, they can be applied in a variety of fields^{14,17} such as food¹⁵⁵ and pharmaceutical industry¹⁵⁶, biomedical analysis⁵, wastewater treatments¹⁵⁷ and environmental monitoring²⁶. Enzyme reactions that result in changes in pH are particularly useful, as they can be coupled to particle motion, material synthesis or chemo-mechanical responses, and self-oscillating gels such as pH oscillating chemo-mechanical devices which have been proposed to be used in drug delivery¹⁵⁸⁻¹⁵⁹.

In this regard, it is clear that biocatalysts combined in chemical reaction networks involving pH changes may be exploited in future applications. Therefore, there is a need to further investigate the possibility of building increasingly complex systems in order to improve their robustness^{85,86,160}. However, the number of parameters, different reaction rates and conditions make it a challenge to properly program the system and obtain an independent and self-regulated response, such as an oscillatory response to natural substrates like glucose and urea.

In this work, diverse enzymes found in watermelon seeds are combined along with others to build a chemical reaction network for programmable pH changes. The enzymes mainly used in this work are urease, catalase and glucose oxidase. Urease is a well-known enzyme that catalyses the hydrolysis of urea into ammonia and carbon dioxide, resulting in a pH rise. It is autocatalytic in the production of base. Urease's natural purpose is to regulate urea levels in the human body, but it can be found in other organisms like plants, bacteria, and fungi¹⁹. However, it has found many modern applications such as the removal of urea from aqueous solutions, analytical applications¹¹⁰, micro motors¹⁶¹ and pumps²², and biosensors^{7,145}. Catalase breaks down hydrogen peroxide into oxygen and water. It is present in almost all living organisms and its main purpose is to regulate H_2O_2 metabolism¹⁶². The main applications today see catalase used as micro pumps²² and motors¹⁶³, in bioremediation, food, medical fields¹⁶² and as a biomarker¹⁸. It is widely coupled with glucose oxidase in sensing applications. Lastly, glucose oxidase is naturally found in fungi, insects¹⁶⁴, citrus fruits, and bacteria¹⁶⁵. It catalyses the transformation of glucose in the presence of oxygen into gluconic acid and hydrogen peroxide and results in a pH drop. It is autocatalytic in acid. Industrial applications of glucose oxidase are food preservation¹⁶⁴, biosensors¹⁶⁵ and textile industry³². We also used β -glucosidase and cellobiose to construct more complex networks and pH changes. Urease, catalase and β -glucosidase were found together in ground watermelon seeds, whereas glucose oxidase was purchased and used as received. First, the enzyme activities were characterized singularly using parameters such as pH, oxygen, foam front propagation, and bubble formation. Then, they were combined together to achieve a more complex system of cascade reactions and to show the benefits of coordinating them to achieve a faster reaction and product formation. We proved that the arrangement of different biocatalysts not only impacts the reaction time and therefore the product generation but also that it is possible to build a cascade reaction in order to achieve a desired pH change that will be difficult to obtain via a simpler reaction.

However, to obtain a self-regulated mechanism for programming more complex pH changes such as oscillations, due to the large amounts of factors affecting the network, further studies are required.

5.3. Methods

The methods are covered in chapter 2, section 2.4.

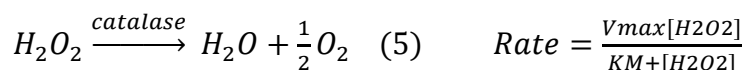
5.4. Results and Discussion

In this section, we present the characterisation of catalase, glucose oxidase and β -galactosidase in three different sub-sections, while the characterisation of urease in watermelon seeds was taken from previous works¹²⁹. Analysis is needed in order to understand the enzyme activity and, most importantly, the reaction time particularly using WM, which has not been previously examined. The reaction time here can be defined as the time needed by the system to generate a specific amount of product or pH change, according to the type of test performed. This information is crucial for the final purpose of combining multiple enzymes and building a chemical reaction network which can be used to program pH in time.

5.4.1. Catalase

Catalase is essential to neutralize harmful hydrogen peroxides in nature^{166,167} and various industries such as dairy, textiles and pharmaceuticals. At the same time, it also has some unusual features. It is a common enzyme found in almost all living organisms, it is also one of the first proteins to be isolated. However, this ancient enzyme has been captivating scientists, particularly with unusual phenomena such as the interconnection of subunits and remarkable thermal stability. It is also known for being destroyed by its own substrate^{18,162}.

The enzyme's most known function is the decomposition of hydrogen peroxide into oxygen and water according to the reaction. Below it is shown the rate equation of the reaction:



The rate is usually considered as Michaelis-Menten with Michaelis constant K_M , and V_{max} = maximum rate; the parameters depend on the source of the catalase¹⁶⁸. The standard unit is defined as the amount of catalase necessary to decompose 1.0 μM of H_2O_2 per minute at pH 7.0 at 25 °C. The optimal pH range for the enzyme catalytic operation is assumed to be between pH 6 and 8¹⁶⁹. Catalase activity can be measured through the consumption of H_2O_2 or generation of O_2 ¹⁷⁰. Conventional catalase tests involve colourimetric methods and components that may interfere with the watermelon seeds, therefore the first test we performed was via a bubble counter to determine the amount of oxygen in excess liberated via the gas phase. Then, in order to quantify the amount of oxygen produced in water, a test via an oxygen meter was performed. WM seeds have reportedly shown in a series of studies foaming capacity and foaming stability which is quite an important feature when used in the food industry^{171,172}. An alternative test was proposed which involved adding surfactant and measuring foam produced¹⁷³. In this test, catalase hydrogen peroxide and surfactant Triton X 100 were combined to study the enzyme activity. An interesting phenomenon during the experiments was noticed in which catalase from watermelon seeds placed in a higher hydrogen peroxide concentration was forming foam without added surfactant. The foam front speed was also taken as a parameter to quantify the reaction rate and compare under different conditions.

Some studies have proven that bubbling a solution containing protein/enzymes results in the formation of foam. This is because proteins and enzymes are surface-active compounds that are able to adsorb the gas/liquid interface¹⁷⁴. Furthermore, Sakai, Okada and Yamaguchi¹⁷⁵ have suggested that the foaming formation could

be due to the hydrogen peroxide expanding the ternary structure of protein and consequently exposure of some amino acid chains. In our case, this effect is possibly combined with the oxygen in the gas form generated by the catalase reaction.

5.4.1.1. Bubble counter

Watermelon seed powder (WM) containing catalase was added to different hydrogen peroxide concentration solutions and placed in a test tube. The number of bubbles was calculated using an infrared bubble counter, as can be seen in **[Figure 66]**. It is intuitive to assume that the higher the quantity of catalase added, the faster oxygen is produced (this can be appreciated in the first derivative plot). However, it was not predicted that there could be an optimum combination of catalase and hydrogen peroxide concentration which would give the largest amount of oxygen produced. In fact, it can be seen that for very low WM (0.001 g) no bubbles are produced, for very high concentrations (0.1 g) the formation is very fast, however, it remains constant after reaching a plateau, whereas the intermediate concentration (0.01 g) produces oxygen at a slower rate, but the amount produced overcomes the previous one. This could be because larger amounts of catalase produce oxygen so fast that a sufficiently large bubble for detection does not have time to form before leaving the solution.

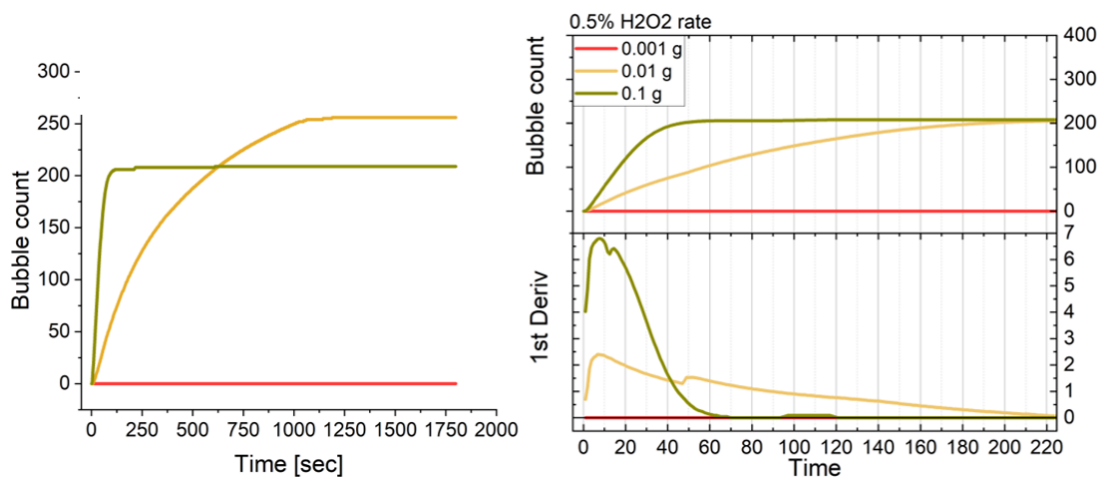


Figure 66. Bubble counts vs time (plot on left) and its first derivative (plot on right) in order to show the reaction rate, for 0.1, 0.01 and 0.001 g of watermelon seeds containing catalase

A better understanding of the maximum amount of bubbles that can be achieved via an optimal combination of catalase and hydrogen peroxide concentration, can be observed in [Figure 67]. Here the plot shows bubble count versus WM powder for different hydrogen peroxide concentrations. For $H_2O_2 = 0.5\%$ the optimum is between 0.01-0.05 g of WM seeds, for $H_2O_2 = 1\%$, the optimum is found at 0.05 g of watermelon seeds, and for $H_2O_2 = 3\%$ the value is precisely at 0.1 g. It is interesting to note that as the hydrogen peroxide concentration increases, the optimum value is shifted toward higher values of the WM powder concentration. Moreover, another peculiarity is that for lower H_2O_2 concentrations, there is a sharp change, or switch, in the bubble counter value as the WM powder is increased, then for higher H_2O_2 , the effect becomes less sharp and the bubble count value increases smoothly, before decreasing.

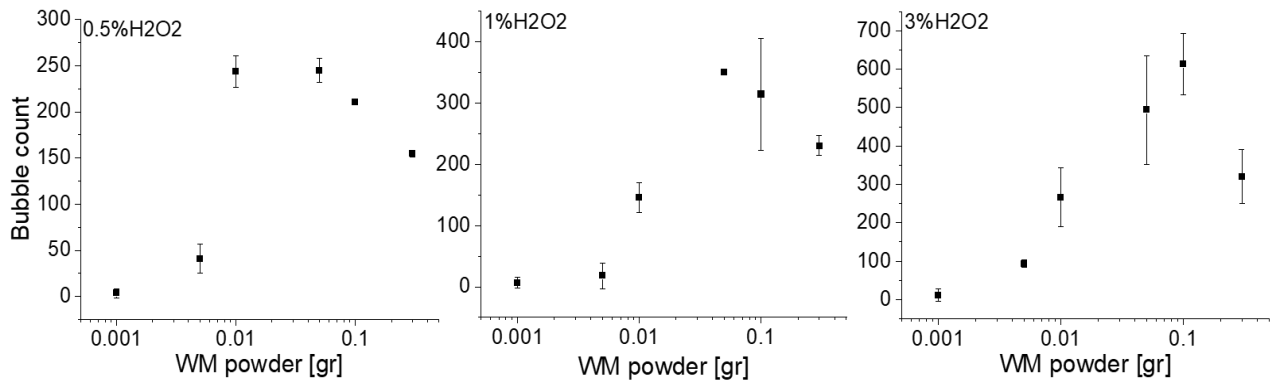


Figure 67. Bubble count vs WM powder concentrations (amount in 30 ml) for different hydrogen peroxide concentrations. Standard deviations were calculated from 3 runs.

What has been said previously regarding the optimum value reached in terms of bubble count can be analysed also in terms of bubble rate, as can be seen in [Figure 68]. Through the first plot, it is shown that for $H_2O_2 = 0.5 - 1\%$, an increase in WM powder concentration corresponds to a faster bubble rate, whereas for $H_2O_2 = 3\%$ when an abundant amount of WM powder is added, the bubble rate decreases, showing that the system is characterised by optimum conditions. The same conclusion is found by looking at the second plot where at 1% hydrogen peroxide concentration, a maximum can be appreciated. Lastly, the third plot shows a gradual increase meaning that although the process is quite sensitive to hydrogen peroxide/WM powder variations, it is not sensitive enough to be used as a threshold sensor to detect and classify H_2O_2 concentrations.

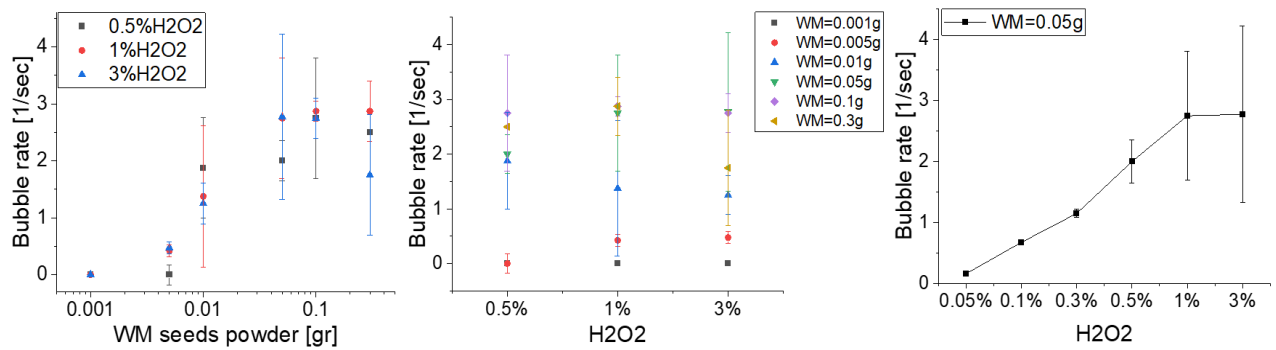


Figure 68. a) Bubble rate vs. WM powder, b) bubble rate vs. hydrogen peroxide for different WM seeds amounts, c) bubble rate vs. hydrogen peroxide for WM=0.05 g. Standard deviations were calculated from 3 runs.

5.4.1.2. Oxygen meter

In this test, catalase in the watermelon seeds was added to the hydrogen peroxide either in solution or as a dry powder. In both cases, through nitrogen bubbling, oxygen was removed from a solution containing 1% hydrogen peroxide and then placed on a stirring plate to mix the solution at the minimum speed. The oxygen and pH probes were set up in order to follow the reaction development. In [Figure 69] the oxygen and pH trends are shown versus time for dry and dispersed catalase.

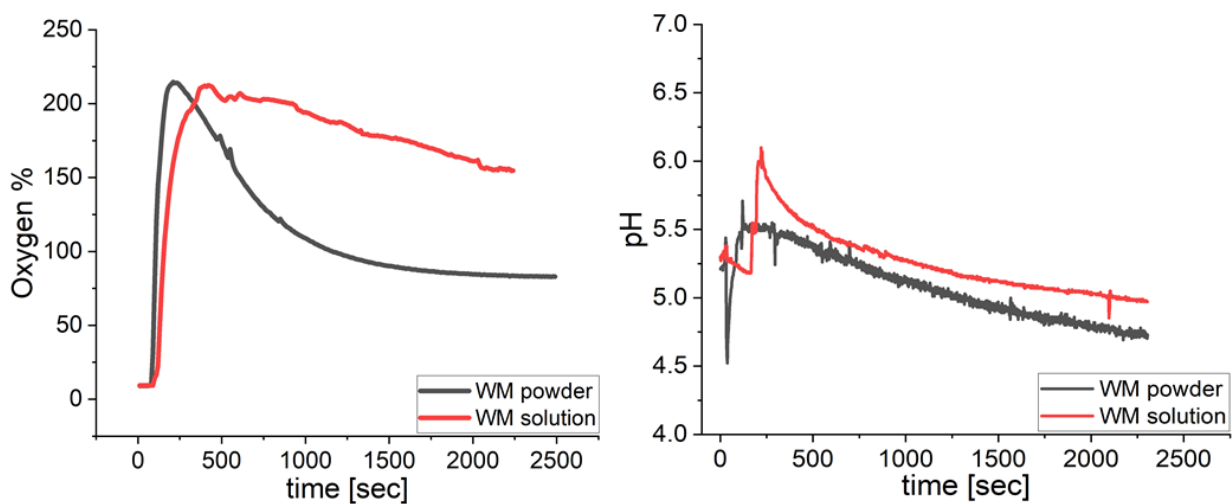


Figure 69. Trends of dissolved oxygen and pH vs time in the hydrogen peroxide-catalase reaction, tracked by oxygen and pH probes. WM was used both powder or dissolved in solution and then added to 1% hydrogen peroxide.

What can be perceived is that in both circumstances the amount of oxygen formed by the reaction is quite consistent with oxygen level reaching 200%. Although the free enzyme powder appears to react faster than the one in solution, it exhibits a maximum in oxygen production before decreasing its generation. On the other hand, the dispersed enzyme looks slower but it is more durable and active with time, keeping the oxygen level more stable. Regarding the pH in the two experiments, for the timescale considered the decrease in pH is not greatly significant, meaning that the reaction indirectly affects it. The oxygen produced may displace CO₂ which then diffuses back into solution. The noisy signal given by the free enzyme is possibly expected by the agglomerates created from the powder coming in contact with the probe.

5.4.1.3. Foam front propagation

In this test, H₂O₂ solution was combined with increasing watermelon seeds amounts to measure the quantity of foam formed by the reaction. The mixture was placed in a test tube on a stirred plate to ensure homogenous mixing. The phenomenon was recorded through a camera and then analysed. In **[Figure 70]** the propagation of the foam front is shown in mm versus time, when mixing 1% H₂O₂ with three different WM amounts.

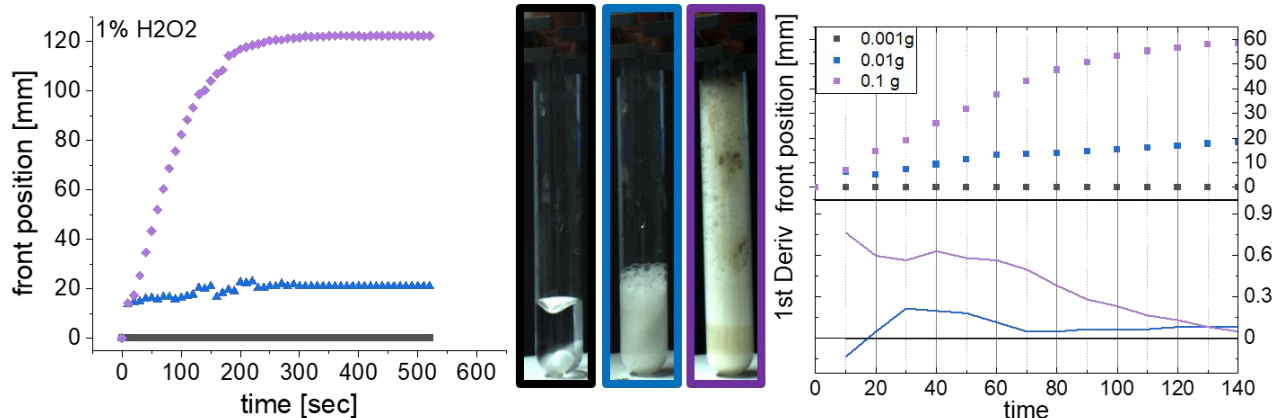


Figure 70. Foam front propagation versus time (inset shows the image of the front) and its first derivative for the hydrogen peroxide-catalase reaction

As could be anticipated, for a fixed concentration of hydrogen peroxide, increasing the amount of WM the foam front grows accordingly and the largest front obtained reaches 120 mm in height. Clearly, this is a combination of two phenomena. First, the larger production rate of oxygen and then the greater presence of phospholipids in solutions are the major sources for the foam formation. The second plot highlights the result, showing the growing foam front propagation rate according to the enzyme amount.

The concept may be better appreciated in [Figure 71], where the front rate versus WM quantity and the concentration of hydrogen peroxide are shown, respectively.

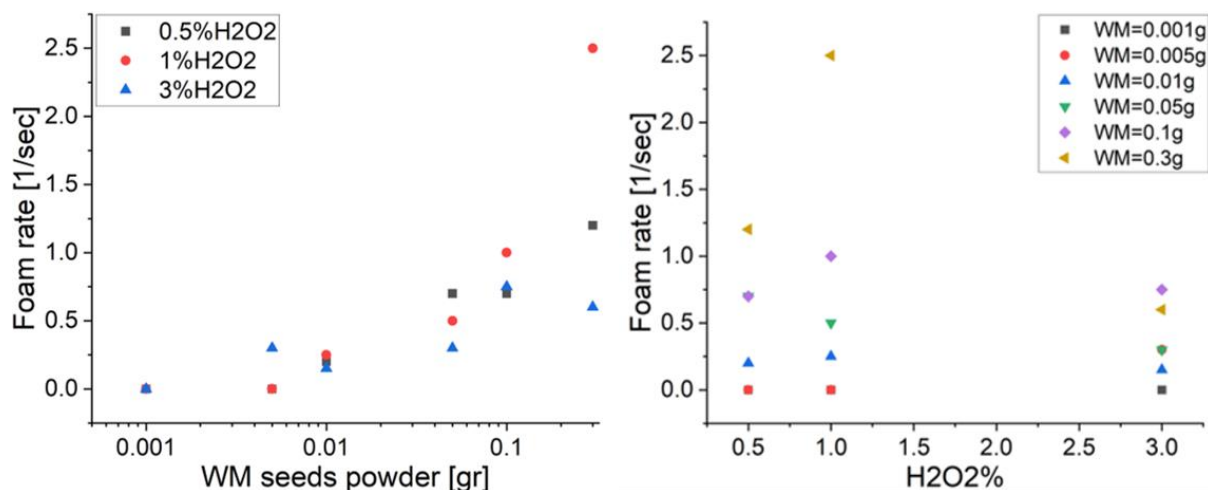


Figure 71. Foam front propagation rate versus watermelon seeds powder (WM) and hydrogen peroxide concentration

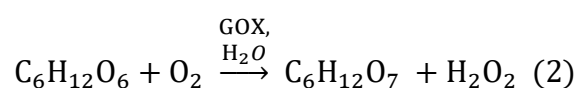
From the first plot it is clear that there is a trend of increasing foam production rate with WM powder added to the solution. The maximum speed is obtained with 0.3 g of watermelon seed powder used. However, from the second plot, it can be seen that there is an optimum concentration of hydrogen peroxide that needs to be used (equal to 1% H₂O₂) in order to get the highest rate. In fact, above this concentration, the rate decreases. This could be because the amount of foam formed in such cases is too dense and therefore reduces the speed.

Summarising, from the plots it can be observed that the best combination in terms of foam produced and foam front propagation speed is given by mixing 1% H₂O₂ with 0.3 g of watermelon seeds powder. Comparing the two tests, bubble production [Figure 68 b] and foam front [Figure 71 right], it can be seen that bubble production is a better measure of the concentration of hydrogen peroxide in a sample.

5.4.2. Glucose oxidase

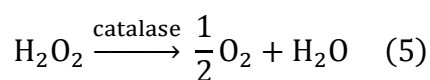
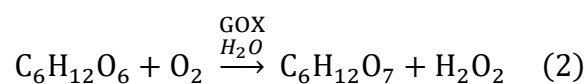
Glucose oxidase (GOX) has been suggested as one of the most ideal enzymes as a result of its specificity, stability and high turnover number¹⁶⁵. The GOX-catalysed

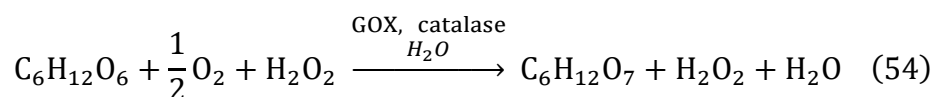
reaction removes oxygen and produces hydrogen peroxide, which is a function used in food preservation. GOX is also used in bakery, dry egg powder, wine, and gluconic acid production. Its electrochemical activity makes it an important component of glucose sensors and potential fuel cell applications³²⁻¹⁶⁴. The reaction can be expressed as:



Where the maximum activity is obtained at pH ~ 7.5¹⁶⁵. The pKa of the product gluconic acid is 3.86. In this work, the reaction is studied mainly through two different measurements –oxygen and pH. The oxygen is used mostly to show the reaction rate and highlight the effect of using a single enzyme compared to the building of a reaction network with the enzymes in the watermelon seed. The pH is used to follow the formation of gluconic acid and again to show that combining multiple enzymes could enhance product formation.

Glucose is widely coupled with catalase since the reaction needs oxygen to be sustained^{164,165}. Here, it will be shown that since all the oxygen in the solution is consumed in seconds, the reaction is inhibited by one of the two reactants' fast consumption. The watermelon seed powder is a natural extract which already contains catalase in order to regulate the amount of hydrogen peroxide in the plant, so it can be added to the system to react with the hydrogen peroxide formed, to produce more O₂. In this way, it will be possible to fuel the glucose reaction and push it towards the gluconic acid formation. However, to further shift the reaction towards the products, an initial addition of H₂O₂ was needed. In summary, the equations forming the network are:





We show that the two reactions can enhance each other to form a higher quantity of product faster, using the catalase present in the watermelon seed.

5.4.2.1. Oxygen meter

The test was performed both with dry enzyme and in solution. The first test was performed by adding 0.001 g of GOX and 0.001 g of WM powder already dispersed in 10 ml of water, to 20 ml of 30 mM glucose solution and mixed with a magnetic stirrer at 600 rpm. As can be observed from [Figure 72] it is evident that the reaction is taking place at a high rate due to the amount of oxygen consumed in a very short time. In fact, the oxygen level goes from 95% to around 0% in 100 seconds. As proof of gluconic acid formation, a pH meter was set up. However, in the second plot it is shown how in more than 1000 seconds, the pH does not decrease significantly. This could be due to the fast consumption of oxygen that does not allow the reaction produce sufficient gluconic acid for the pH to decrease. Therefore, tests were made where the watermelon seed powder concentration was increased. This improved the reaction rate, as can be seen in the third plot, where the slopes get more pronounced as the WM powder concentration grows. However, even in this case the change in pH is not sufficiently remarked or fast going from 5.5 to ~ 4. The sudden peaks present in the pH plot can be connected to the WM powder agglomerates breaking and dispersing into the system, perturbing the probe and unsettling the meter reading.

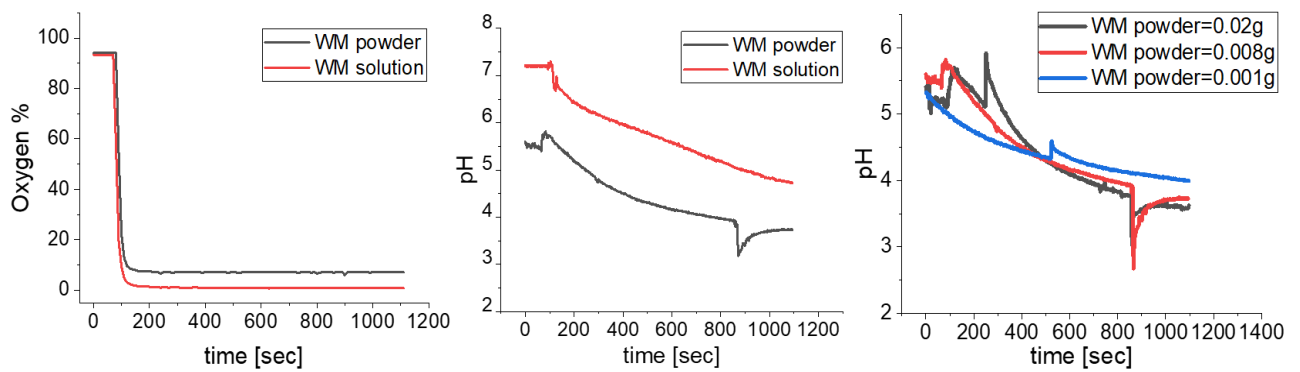


Figure 72. Dissolved oxygen percentage and pH vs time for the glucose-GOX-WM reaction, comparing the addition of WM in solution and dry WM to glucose-GOX solution. Glucose= 30 mM, GOX= 0.001 g and WM= 0.001, 0.008, 0.02 g in 30 ml solution.

Therefore, the test was repeated adding a consistent quantity of WM powder to try and provide the system with more oxygen. In this case, catalase in the form of WM powder was added separately with respect to glucose and GOX, as can be seen in [Figure 73]. Here the arrow marked with the number 1 corresponds to the glucose and GOX initiation, whereas point 2 is the catalase addition to the system.

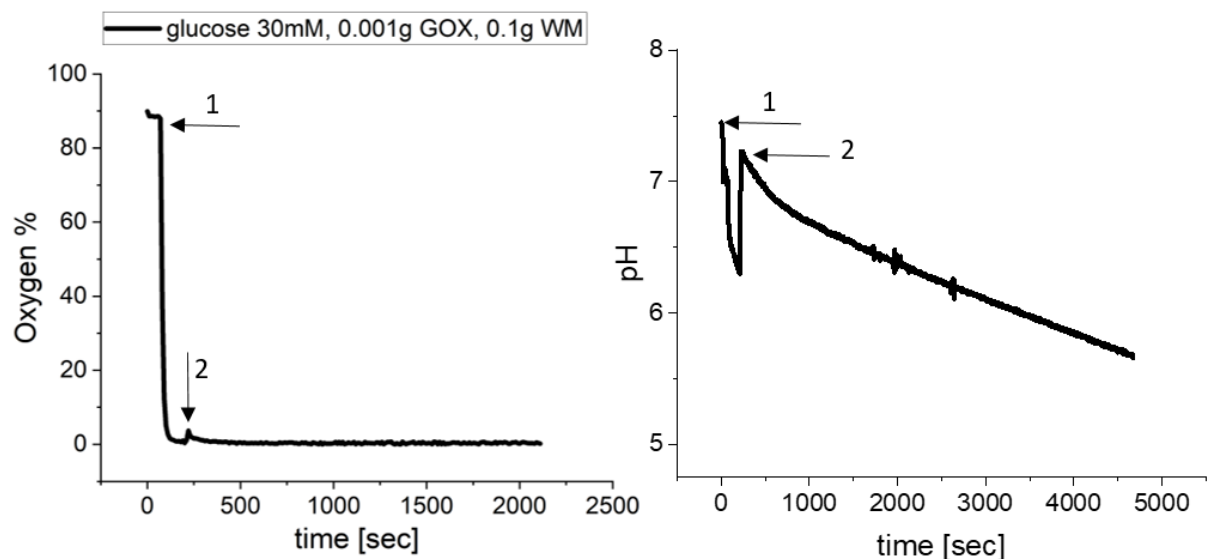


Figure 73. Dissolved oxygen percentage and pH vs time for the glucose-GOX-WM reaction. Glucose= 30 mM, GOX= 0.001 g, WM= 0.1 g in 30 ml solution. Number 2 corresponds to the addition of WM.

Although the system is attempting to produce oxygen, as can be seen below arrow number two it goes down straight away. The same behaviour is present in the second plot, where after an apparent sudden decrease, the pH settles and keeps decreasing at a slower rate. The reason why adding more WM powder seems not to work is that the hydrogen peroxide formed by the first reaction is not adequate to react with catalase in order to produce sufficient oxygen.

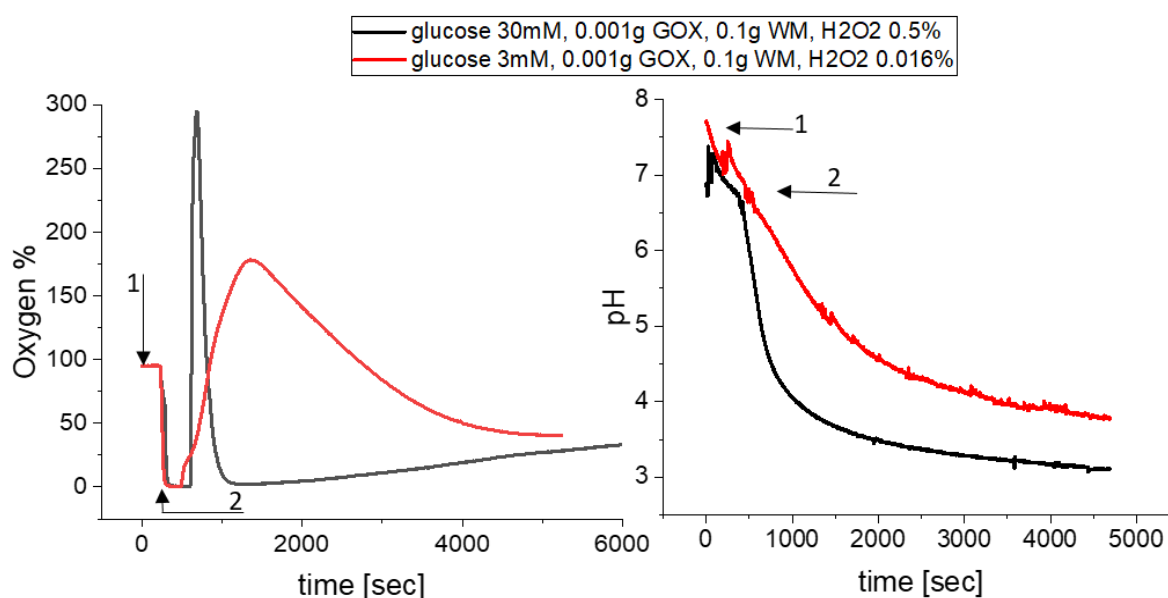


Figure 74. Dissolved oxygen percentage and pH vs time for the glucose-GOX-WM reaction. Glucose= 30 mM, GOX= 0.001 g, WM= 0.1 g, H₂O₂ = 0.5 and 0.016% in 30 ml solution. The number 2 corresponds to the addition of H₂O₂.

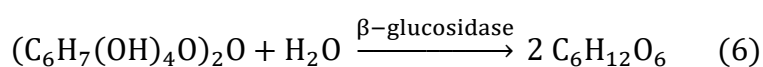
Hence, the last test was performed adding glucose, GOX and WM powder and consequently hydrogen peroxide to shift the reaction towards gluconic acid. In the first plot in [Figure 74], the arrow indicating number 1 corresponds to the measurement of the glucose-GOX-WM reaction where an immediate consumption of oxygen is witnessed. Where arrow number 2 is pointing, hydrogen peroxide was added and in fact, a sudden growth in oxygen is observed. Clearly the more H₂O₂ is added, the more oxygen is produced also reflecting the faster increasing rate. Following the peak, the glucose-GOX reaction continues, consuming the newly

available oxygen content. In the second plot displayed it can really be appreciated the different slope angles corresponding to the H_2O_2 addition to the system, indicating that more acid is being produced, compared to the first part where just glucose, GOX and WM were present. In this last case, the decrease in pH is clear and faster with respect to the previous cases, dropping from 7.5 to ~ 3.5 in 1000 seconds.

The cooperative effect of the different enzymes and the more complex system have made it possible for the reaction to generate a higher amount of product. This is due to the reactant having better access to oxygen, which is fundamental for this reaction to occur. This is the first evidence that building reaction networks with WM allows for improvement and speeds up reactions that would have difficulties to proceed otherwise.

5.4.3. B-glucosidase

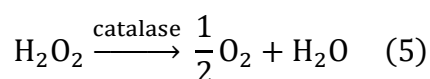
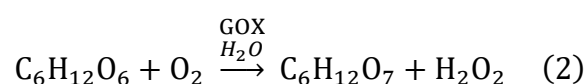
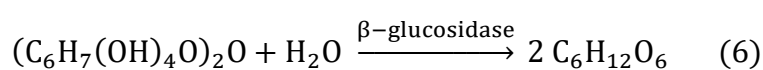
Biomass conversion is an innovative and equally fascinating recent topic in which generally raw materials such as cellulose or cellobiose are used as reactants to obtain liquid biofuels such as bioethanol²⁰. In this regard, β -glucosidase is the most used enzyme to convert lignocellulosic biomass into glucosyl derivatives¹⁷⁶⁻¹⁷⁷⁻¹⁷⁸ and for agriculture¹⁷⁹ applications. In particular, cellobiose is converted into two molecules of glucose according to the reaction:



which has the maximum activity at pH= 5-6.5¹⁷⁸.

The main challenge is the inhibition of the majority of β -glucosidases to the main product, glucose, which makes the enzymatic path rate-limiting for the effective degradation of cellulose¹⁷⁶⁻¹⁸⁰. For our reaction network involving pH changes, cellulose or cellobiose may provide an alternative substrate, producing gluconic acid. Hence, in this section, it is proposed a chemical reaction network to facilitate the conversion of cellobiose and also avoid enzyme inhibition. In particular, the

cellobiose-BGL reaction will be coupled with GOX in order to convert the glucose produced into gluconic acid. Furthermore, it is well known that it is difficult to convert these kinds of sugars into simpler molecules, especially due to the lack of oxygen needed to break glucose into gluconic acid. Therefore, having a multi-enzyme source such as WM seeds powder which not only contains BGL but also the enzyme catalase, will aid the reaction by providing additional oxygen to the system, all contained in one single source. The network can be schematised via the three equations and the scheme as follows:



A chemical reaction network consisting of this combination of different and multiple enzymes in watermelon seed powder could be used for other applications in the future.

5.4.3.1. Oxygen meter

Here the purpose was to verify the depletion of cellobiose by detecting the glucose-GOX consumption of oxygen, with glucose supplied only from cellobiose. In this test, the cellobiose-WM-GOX reaction was followed via oxygen and pH meters.

Initially, 5 ml solution containing WM and GOX (112 and 200 $\frac{\mu}{\text{ml}}$ respectively), were added to 15 ml of cellobiose 0.15 M mixing the compound on a stirring plate at 600 rpm as shown in [Figure 75]. It can be observed that the black curve decreases from 100 to 0 quite rapidly meaning that glucose was formed and it consumed all the available oxygen. Therefore, in the second trial, following the addition of cellobiose with WM and GOX (arrow 1), some hydrogen peroxide was added to the solution (arrow 2). The compound would trigger the catalase to produce more oxygen to sustain glucose oxidation. In test 2, the insertion of the largest amounts of hydrogen

peroxide into the solution increases the oxygen level and therefore, the cascade reactions can proceed.

Using the pH meter, it was possible to detect the formation of gluconic acid and therefore, assume that cellobiose was successfully converted into glucose. In the pH plot, it should be highlighted the difference using H_2O_2 compared to the standard conditions. In fact, test 1 starting from 7.5, reaches pH 5.5 quite slowly and in approximately 10 hours. Contrarily, although the measurement is not as long, it is evident that in test 2 (red curve) as a result of the addition of hydrogen peroxide there is an increase in the slope meaning that the production rate of gluconic acid is faster.

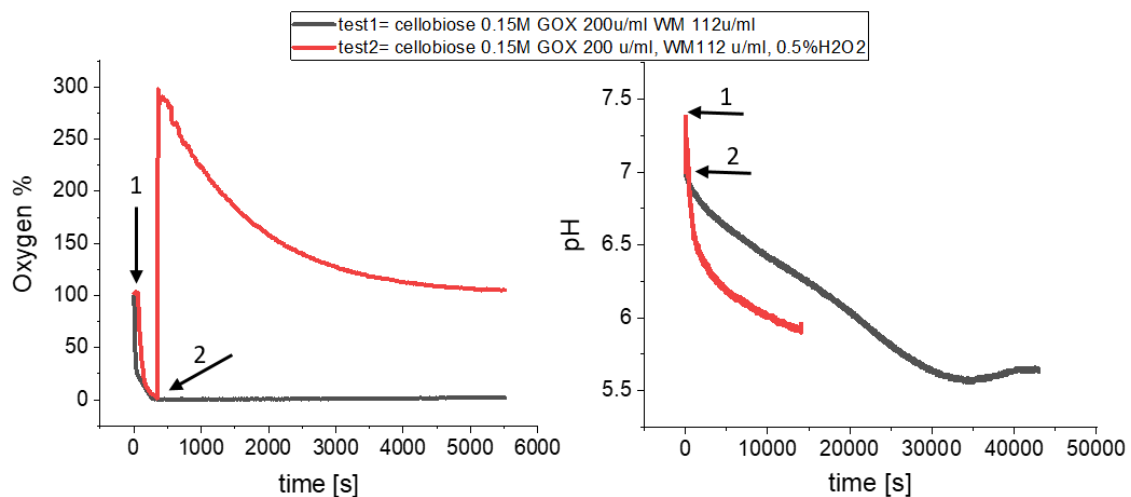


Figure 75. Dissolved oxygen percentage and pH versus time for the cellobiose-WM-GOX reaction (added where arrow 1 is pointing). Hydrogen peroxide was added where arrow 2 is showing. 0,15 M cellobiose 15 ml, 5 ml of WM and GOX having concentrations 112 and 200 u/ml, respectively.

[Figure 76] shows a quite difficult situation to achieve in which the system self-regulates to produce a temporal change in oxygen, without separate addition of substrates. Here the reaction network using cellobiose, glucose and hydrogen peroxide with the three enzymes BGL, GOX and catalase has been tuned in very specific conditions so that it can consume and form oxygen independently. In

particular, after cellobiose is converted into glucose and all the oxygen is consumed, the hydrogen peroxide formed reacts with catalase producing a fresh amount of oxygen that is following consumed again creating this pulse-like behaviour where oxygen levels go up and down according to the reaction having the fastest rate at that specific time.

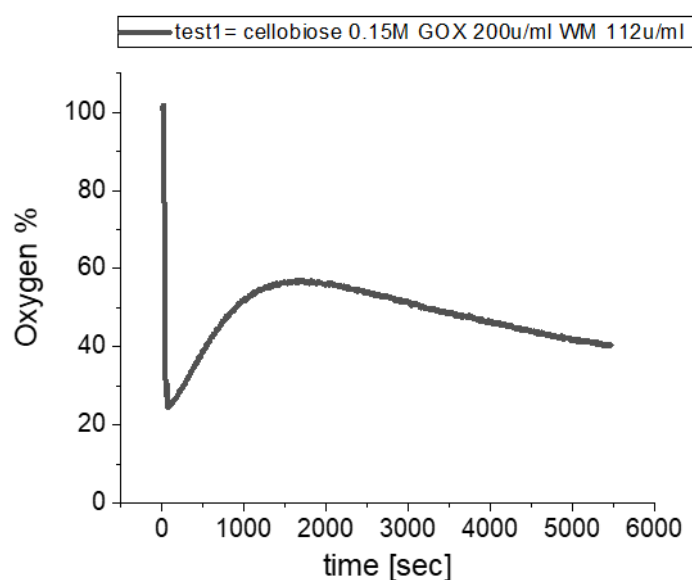


Figure 76. Dissolved oxygen level vs time representing cellobiose- WM and GOX reaction network functioning autonomously

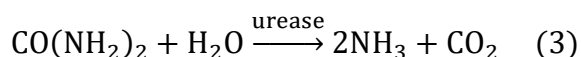
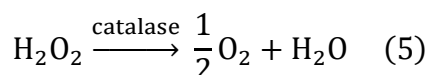
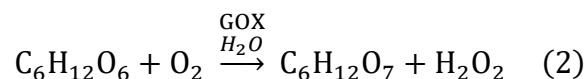
5.4.4. Catalase, glucose oxidase and urease coupling

The goal of this section is to tune and build a chemical reaction network that will show an output response through pH, in particular, to design a cascade reaction able to control the amount of acidic and basic compounds in time to produce a particular pH change in response to substrates. In this regard, at the beginning two reactions were chosen - glucose/GOX which produces gluconic acid and urea/urease which produces ammonia forcing the pH to rise again. Since both GOX and urease are autocatalytic in pH, it could be possible to obtain complex changes such as oscillations for chemo-mechanical devices.

Concerning the urease, tests were performed both with the urease used as purchased and the one from watermelon seeds. The results showed that urease

from WM is more suitable for this system due to the presence of catalase in the seeds that could contribute to the network by reacting with hydrogen peroxide producing oxygen that will subsequently sustain the glucose/GOX reaction.

Therefore, the system contained the three reactions that can be described as follows:



First, the substrates were added sequentially to understand the contribution of each reaction component. 10 ml of GOX and WM or urease powder solution (final concentration 200 for GOX and $112 \frac{\mu}{\text{ml}}$ for urease from both sources), were added to 10 ml of glucose 30 mM. The initial pH of each solution was set at 7 by the addition of NaOH. The reaction network was challenged by using 0.5% and 1% H_2O_2 to understand which concentration would be the optimum to speed up the system. Lastly, 10 ml of urea 0.5 mM was added to raise the pH. The system was observed via pH meter while being stirred in an open reactor by a magnetic bar at 600 rpm.

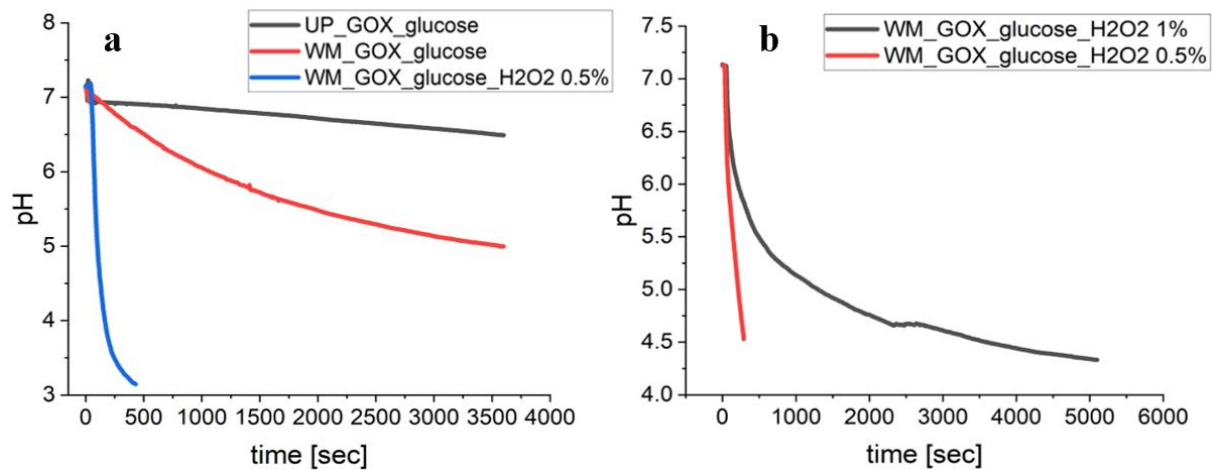


Figure 77. a) pH vs time using the reaction network composed of glucose/GOX, hydrogen peroxide/catalase and b) pH vs time using the reaction network composed of glucose/GOX and two different hydrogen peroxide concentrations (0.5 and 1%) with catalase. WM = watermelon seed powder glucose=30 mM, urea=0.5 mM, GOX=200 u/ml, urease=112u/ml; pH0 = 7.

The first plot of [Figure 77 a)], it is shown the pH response to the system formed by purchased urease (UP), WM and WM plus H₂O₂, combined with glucose. In this case, a solution formed by GOX- UP or GOX-WM combination was added to a glucose solution. It is evident how the first reaction is quite slow, probably because the production of gluconic acid is inhibited by the lack of oxygen flux into the solution. The rate increases a small amount when UP is substituted by WM due to the presence of catalase. However, in the end, it was possible to greatly speed up the reaction rate by adding 0.5% hydrogen peroxide to the system.

The [Figure 77 b)] shows the different reaction rates obtained using two different H₂O₂ concentrations. It can be seen that increasing the amount of hydrogen peroxide used does not correspond to a rate increase. This might be caused by two factors, first, the excessive oxygen production rate forming the gas phase making it inaccessible for the reaction, and the formation of foam which disturbs the main reaction. Therefore, for this test, it was chosen to use 0.5% hydrogen peroxide to build the network.

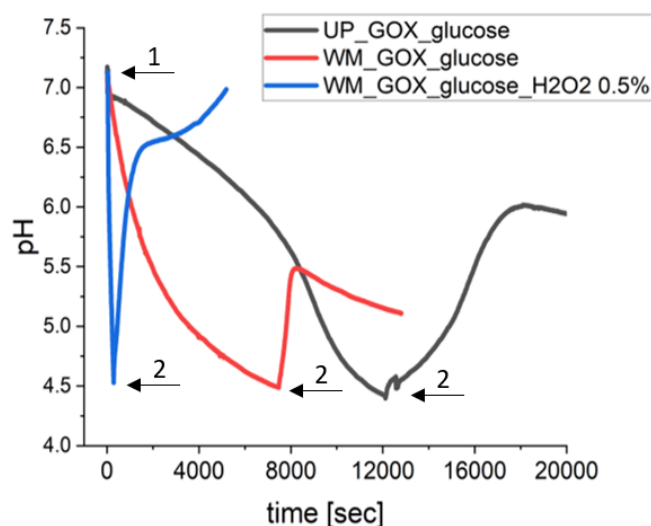


Figure 78. pH vs time using the reaction network composed of glucose/GOX, hydrogen peroxide/catalase added at point 1, and urea/urease added at point 2. UP = urease powder, WM = watermelon seed powder glucose=30 mM, urea=0.5 mM, GOX=200 u/ml, urease=112u/ml; $pH_0 = 7$.

Lastly, in [Figure 78], the combination of the three reactions are shown together. Arrow number one shows the point where the glucose reaction was initiated by adding the enzymes solution to the glucose one, whereas arrow number 2 indicates the point in time when urea was added to the system. The black curve represents the system formed by UP and GOX which in fact is the slowest taking more than 3 hours for the gluconic acid to be formed and consequently the pH to decrease. The red curve symbolises the reaction made by WM (urease and catalase) and GOX, here the gluconic acid formation rate gets faster and the pH decrease is more significant requiring around 2 hours. An interesting thing to notice in this case is that after the addition of urea and the pH increase, the curve starts decreasing again. This is because at $pH \sim 5.5$ both urease and GOX begin to be more active and therefore they compete with each other. The blue curve shows the combination of WM, GOX and H_2O_2 and as shown it has the fastest response in terms of pH decrease because of the combination of the three enzymes together requiring just hundreds of seconds for the pH to fall completely. In this case, the balance among the different enzymes and reactions is tuned so that the pH value at the end almost matches the initial pH.

Clearly, the pH is quite difficult to control due to the number of parameters and variables that affect the system. However, we showed that it is possible to build a chemical reaction network in which the combination of different biocatalysts in watermelon seed can be used together and they are also able to enhance each other's activity. Nevertheless, in order to build and tune a system able to self-regulate in terms of pH output responses, further studies are needed.

5.4.5. Additional enzymes contained in watermelon seeds

In addition to the results shown in this section, it is important to highlight that three out of the five enzymes used come from the same source identified in the watermelon seeds. This detail is important firstly because certain groups of enzymes can be quite expensive to acquire and finding them in an inexpensive source can reduce costs and also enhance the possibility of making them economically viable for industrial applications. Secondly, the concept of a natural source containing multiple enzymes can drastically reduce the effort in terms of compatibility studies and simplicity in building cascade reactions and reaction networks¹⁸¹. In particular, watermelon seeds were analysed using mass spectrometry (see acknowledgement section): LC-MS/MS was performed on watermelon proteins in ground seed powder, with guanidine hydrochloride to denature the enzymes. A database that has the watermelon genome: <http://cucurbitgenomics.org/> was used to identify proteins. They were ranked by an estimate of relative abundance (iBAQ), high to low and urease and catalase were identified. The sample was complex, many enzymes, including metabolic enzymes, structural proteins, seed proteins and oil-related proteins were found. In **[Table 8]**, a number of biocatalysts are shown which might have interesting applications.

Table 8. Table of other enzymes found in watermelon seeds via mass spectrometry

Protein identification	iBAQ - abundance	Applications	Majority protein IDs	MW [kDa]
β -galactosidase	138210	catalyses lactose decomposition to glucose and galactose	CICG02G000040.1	84.932
α -galactosidase	41388	can digest oligosaccharides like raffinose	CICG07G005010.1	107.76
Sarcosine oxidase	37212	catalyses the oxidative de-methylation of sarcosine to yield glycine and H ₂ O ₂	CICG02G010790.1	54.749
Aspartic proteinase	638460	cut proteins into smaller chains	CICG03G004590.1	55.335

β -galactosidase's natural function is lactose decomposition. It is of great importance in the food industry to produce dairy-manufactured goods accessible to lactose-intolerant people¹⁸². Similarly, α -galactosidase has enormous importance in the food industry for soya processing, biomedicine to aid the digestive progression of certain oligosaccharides, and biomass processing^{183,184}. The application of sarcosine oxidase is more directed toward the biomedical and analytical fields. The enzyme is able to detect creatinine which is used to determine renal function and is a significant component in muscle, brain, and blood¹⁸⁵ and sarcosine which is an important indicator of prostate cancer¹⁸⁶. Lastly, aspartic proteinase is known to perform many diverse functions such as protein processing and degradation, or viral polyprotein processing¹⁸⁷, therefore it is mostly used in laboratory analysis and biomedical applications.

Watermelon seeds have potential in many different fields with innovative and interesting applications. However, to possibly use the enzymes and build more complicated cascade mechanisms further investigations are needed.

5.5. Conclusions

In this work, the characterisation of three enzymes in order to build a chemical reaction network using watermelon seed powder was undertaken. Coupling catalysts in chemical reaction networks provide a mechanism to improve reaction rates and in certain cases useful tools to overcome product inhibition and reactions that would be difficult to perform otherwise. Complex output responses in pH have been used in sensing, information processing with Boolean logic and oscillating chemo-mechanical devices. We combined enzymes that can alter pH: glucose oxidase (GOX) and urease (UP) were used as purchased, whereas urease (WM), catalase and β -glucosidase (BGL) were obtained from watermelon seeds. The biocatalysts were characterised via oxygen formation, pH change and foam front propagation to explain what was happening during the process. First, the enzyme reactions were analysed individually and then they were combined to show the coupling effect on the system.

The first enzyme investigated was catalase used to decompose hydrogen peroxide into water and oxygen. Its activity was analysed via a bubble counter and oxygen meter to understand the best conditions in order to produce the largest amount of oxygen possible. Tests have shown that simply increasing the amount of hydrogen peroxide or the catalase concentration does not imply an improvement in oxygen production. In fact, the system is characterised by an optimum condition that initially was found to correspond to 0.3 g WM and 1% H_2O_2 . However, it was noticed that the system was producing something besides oxygen bubbles. More specifically it was producing a foam propagating according to the amount of WM present in the system. The side product is possibly due to the phospholipids contained in the seeds and it was observed to interfere with the main reaction. Therefore, to control the foam formation and still achieve a large amount of oxygen production, the optimal conditions were identified as 0.1 g WM and 1% H_2O_2 .

Then, glucose oxidase was investigated. It was used to catalyse glucose oxidation into gluconic acid and hydrogen peroxide from glucose. The process was analysed using the oxygen and pH meter so as to show that oxygen was being consumed and the acid was formed. Results show that due to the oxygen limiting influx to the solution, all the oxygen present at the beginning is consumed at a fast rate whereas the gluconic acid is not produced in appreciable quantities for the pH to decrease sufficiently. Therefore, catalase in watermelon seed and GOX were coupled in the system so that the two reactions could work together to enhance reaction rate and increase product formation. Nonetheless, the fastest reaction rate for gluconic acid production was obtained by adding to the initial system some hydrogen peroxide to further stimulate oxygen production from the catalase reaction.

β -glucosidase was the next enzyme to be studied. It is responsible for cellobiose hydrolysis into glucose. In this case, the enzyme activity was investigated using the product formed by the second step of the cascade reaction. In fact, following the glucose formation, GOX was used to oxidize it into gluconic acid and hydrogen peroxide. Therefore, GBL activity was presumed based on oxygen consumption and acid formation following glucose formation. The test was performed initially using only GOX and WM (containing catalase and BGL), however, the oxygen generation/consumption was not balanced and therefore, glucose was not produced in sufficient quantities in order for the pH to decrease appreciably. Hence, some hydrogen peroxide was added to the system. It was noted that the addition boosted the reaction rate and product formation.

Then, in order to generate controlled pH changes, urease in watermelon seed was added to the GOX-catalase. Urease and GOX are both autocatalytic in pH and could be used to make pH oscillations. It was demonstrated that a pH drop and rise could be achieved with a network of GOX-catalase-urease with sequential additions.

In addition, we point out that WM seeds are a natural source of multiple different enzymes already coexisting and cooperating according to complex biological

mechanisms. Some examples shown concern different types of glucosidase and galactosidase, sarcosine oxidase and aspartic proteinase. In this regard, they have the potential to become an inexpensive and accessible enzyme source for industrial, analytical and sensor applications in a variety of fields.

Although some of the mechanisms for programming pH changes shown in this work are quite challenging to achieve, it was shown that a combination of enzymes with the aim of building cascade reactions and chemical reaction networks using watermelon seeds is possible. Furthermore, having a combination of several different effects has improved product formation and in some cases, it made it possible to accelerate a reaction that would need a long time otherwise. Nevertheless, it is clear that to have a better understanding of the processes and tune them accordingly, further investigations are required.

6. Employing multiple enzymes in chemo-mechanical devices: towards smart biosensing and drug delivery systems

6.1. Overview

Nature has an outstanding ability to create complex mechanisms of response to external stimuli and adapt biomaterials to the environment. There are several examples of plants and animals changing colour or having the aptitude to grow and shrink their tissues to defend themselves from predators. One of the most fascinating abilities is the capacity to create chemo-mechanical response mechanisms. Scientists have been trying to reproduce such systems via the use of responsive hydrogels that can transform themselves by shrinking and swelling following an alteration in external conditions such as temperature, pH, pressure, and chemical species. Some of the hydrogels' most used applications include drug delivery, sensors and tissue regeneration.

In this work, we present a pH-responsive gel, prepared with N-isopropylacrylamide with N-vinylimidazole, capable of displaying complex chemo-mechanical responses. The gel was equipped with enzymes (urease, glucose oxidase, and catalase) and a colourimetric indicator (bromothymol blue), cut in the shape of a thin cylinder and we investigated the use of watermelon seed powder, as a source of multiple, stable enzymes. We showed that the filament is able to simultaneously produce a chemical and mechanical response when exposed to substrates urea and glucose, changing in size and colour. The gel was also studied for its swelling properties exhibited by the formation of oxygen bubbles from the reaction of catalase with hydrogen peroxide. Furthermore, it was investigated how coupling catalase and glucose oxidase to build a chemical reaction network, enhanced the response time and the swelling response level. The ultimate goal would be to use such a device as a sensor capable of regulating the release of a substance (such as a drug) in time, with a pulse or oscillatory responses, using a combination of chemicals found in the body.

However, we recognise that to achieve such a complex application, further researches are needed.

6.2. Introduction

Materials existing in nature present some fascinating characteristics such as adaptability, biocompatibility, biodegradability, and strength^{188,189}. Moreover, animals continuously and dynamically interact with the external environment in order to adjust and defend themselves from predators, and light^{190,191}, and control temperature and pH¹⁴¹. Sometimes, biological systems are also able to combine chemical and mechanical responses^{192,193} to external triggers, making it possible to change skin colour and grow muscles as needed¹⁹⁴. In this regard, modern science has been trying to understand and replicate both materials^{195,196} and response mechanisms¹⁸⁹ via a combination of polymers, especially hydrogels^{189,197}.

When this type of materials is applied in the medicine and pharmaceutical field they are called biomaterials, capable of adapting and, in some circumstances, replacing tissues and structures in the human body¹⁶. The most common materials used nowadays are polymers, hydrogels and combinations of them^{16,198,199}. Hydrogels are formed via polymer cross-linking in an aqueous environment and according to the combination of polymer used and the adopted technique, different and enhanced features can be achieved²⁰⁰. From mechanical strength, extreme elasticity, and elongation, dynamic temporal control to stimuli-responsive feedback, engineered hydrogels give wide-ranging and varied possibilities of applications. Just to mention a few, there is drug delivery, biomedical, industrial^{141,200,201}, soft robotics²⁰² and regenerative medicine²⁰¹.

One of the most interesting types of hydrogels currently being investigated are the stimuli-responsive ones. They can react to light, pH, temperature, and also chemical species^{141,192,193,203}. In particular, according to the type of stimulus, the response can be divided into three categories: physical (temperature), chemical (pH)⁵⁷, and biological (enzyme)¹⁵⁶. All of them act according to a feedback mechanism in which

an external parameter alters the initial condition, corresponding to a temperature, pH or enzyme modification. The mechanism involves a response from the hydrogel which is usually mechanical such as shrinking and swelling^{141,156,200}. In regard of the mechanism, polymer chemistry provides an increasing range of possible reactions, but at the same time the induced response is fundamentally a reaction-diffusion process with a built in feedback regulating the chemical molecules changes and mechanical properties¹⁹².

Due to these properties, they are usually used as drug-delivery devices²⁰¹. An example is the glucose-responsive polymer. In particular, when insulin is present in the hydrogel tissue, after a temperature or a pH change, the hydrogel reacts by swelling and releasing the drug¹⁵⁶. The process can be temporally controlled in the lab by altering glucose concentrations or left to react on demand in practical applications. In addition, there have been a few examples of self-oscillating gels, that swell and shrink periodically^{71,204}. These have been proposed for periodic drug release. However, an equally interesting application for smart hydrogels is as sensors^{203,205}. Both temperature and pH are parameters that express variations in the human body. Temperature is a common natural reaction triggered by the body trying to eradicate an infection or virus, while pH can be used as an indicator of cancer cells that have a pH < 6.5 compared to healthy cells that have a pH ~ 7.4¹⁴¹.

In this work, our purpose is to build a pH-responsive gel capable of detecting substances and generating a combined chemo-mechanical response. In previous work, urease and glucose oxidase were trapped in a polymer that displayed either shrinking or swelling in response to additions of urea and glucose²⁰⁶. Here, we attempted to generate more complex responses by combining multiple enzymes. The present study builds upon the previous research conducted by Ogawa et al.^{63,101} in the field of enzyme immobilization within responsive gels. Specifically, this study sought to expand upon the initial work by focusing on the immobilization of glucose oxidase and urease enzymes, with the aim of utilizing the pH switch

mechanism to create a responsive gel capable of expanding and contracting in response to changes in the surrounding environment's pH levels. The resultant gel demonstrates promising potential for various applications in the field of materials science and beyond.

Particularly, enzymes urease, catalase, and glucose oxidase were encapsulated together with the colourimetric indicator bromothymol blue in the smart-hydrogel matrix. We tested the use of watermelon seed, as a long-lived source of urease and catalase. The gel was cut into a thin cylindrical shape and placed first in urea and then in glucose. Urea diffused inside the gel reacting with urease and generating ammonia which is responsible for the pH increase. The filament then switches colour to blue and shrinks. Following the process, the same filament is placed in glucose which diffuses inside it, reacting with glucose oxidase and producing gluconic acid. The newly produced product will be responsible for the filament swelling and the indicator switching to a yellow colour. The filament was also used with hydrogen peroxide alone and we observed that the formation of oxygen resulted in a swelling response. A further investigation combined the glucose reaction with additional hydrogen peroxide to speed up gluconic acid production by building a chemical reaction network within the filament. The combination of these two mechanisms generates a chemo-mechanical response which enhances the filament output response being, in fact, able to react to both stimuli, pH and oxygen, by changing colour and enlarging its area.

We here present these types of hydrogels showing an enhanced output response by combining chemical and mechanical responses. They are reusable up to eight times and can be used for cyclical reactions. Furthermore, thanks to their properties and the wide range of enzymes contained in watermelon seeds, there are numerous possible applications, such as oxygen detection or chemical reaction network developments. However, a further step would be encapsulating a drug in it, in order to assemble a drug delivery device able to be spatially and temporally controlled

which will react by releasing the medication following the detection of pH changes or compound concentrations variations. Due to the numerous parameters and challenging chemistry behind this system, further investigations are needed in order to achieve such a system.

6.3. Methods

The methods are covered in chapter 2, section 2.4.

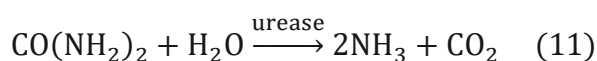
6.4. Results and Discussion

The pH-responsive filaments were built to generate both a chemical and a mechanical response, as a result of the encapsulation of enzymes. In particular, standard urease powder (UP) or urease from watermelon seeds (WM) conjugated with glucose oxidase (GOX) were used. Therefore, the filaments are characterised according to their reactivity and stability with the urea-urease reaction and then according to their area growth when in the presence of an acidic environment generated by the glucose-glucose oxidase reaction. The gels swell at low pH due to the formation of charged NH^+ groups and shrinks at high pH due to neutralisation of the $-NH^+$ groups on the poly-(N-vinylimidazole)⁶³. Furthermore, due to the presence of catalase in the WM seeds, the filaments were also combined with hydrogen peroxide to boost the reaction rate and generate a simple chemical reaction network. Lastly, they were also left to react with hydrogen peroxide alone in order to get a mechanical response from the production of oxygen.

Although different systems have been manipulated in this work, the basic common denominator of all of them is the reaction-diffusion mechanism. In fact, the system built here appears to be quite difficult to control due to the reaction or diffusion-limiting effect within the filaments.

6.4.1. pH profile, reaction time and reusability

In this section, we compare the two different sources of urease in the gels. Urease in the form of standard urease (UP) and urease from watermelon seeds (WM) was encapsulated in the gel filaments together with the indicator (BTB) to catalyse urea hydrolysis in relation to the reaction:



The results of the urease reaction in the filaments are consistent with those of other studies and show that the enzyme is stable, well encapsulated, and capable of performing the clock reaction^{97,100}. The responsive filaments generate an “on-off” signal that produces an optical output response (yellow to blue) from the two enzyme sources, indicating that UP and WM are stable, robust, and capable of producing a signal in response to urea (5 mM).

The signal is quantified by the absorption recorded over time in [**Figure 79 a) and b)**]. Subsequently, it was converted to pH to match the colour obtained by the indicator as explained in the analysis section. Another parameter that is used to evaluate the activity and stability of the particles is the reaction time. It is defined as the time it takes the system to reach pH 7, due to BTB changing colour from yellow to blue.

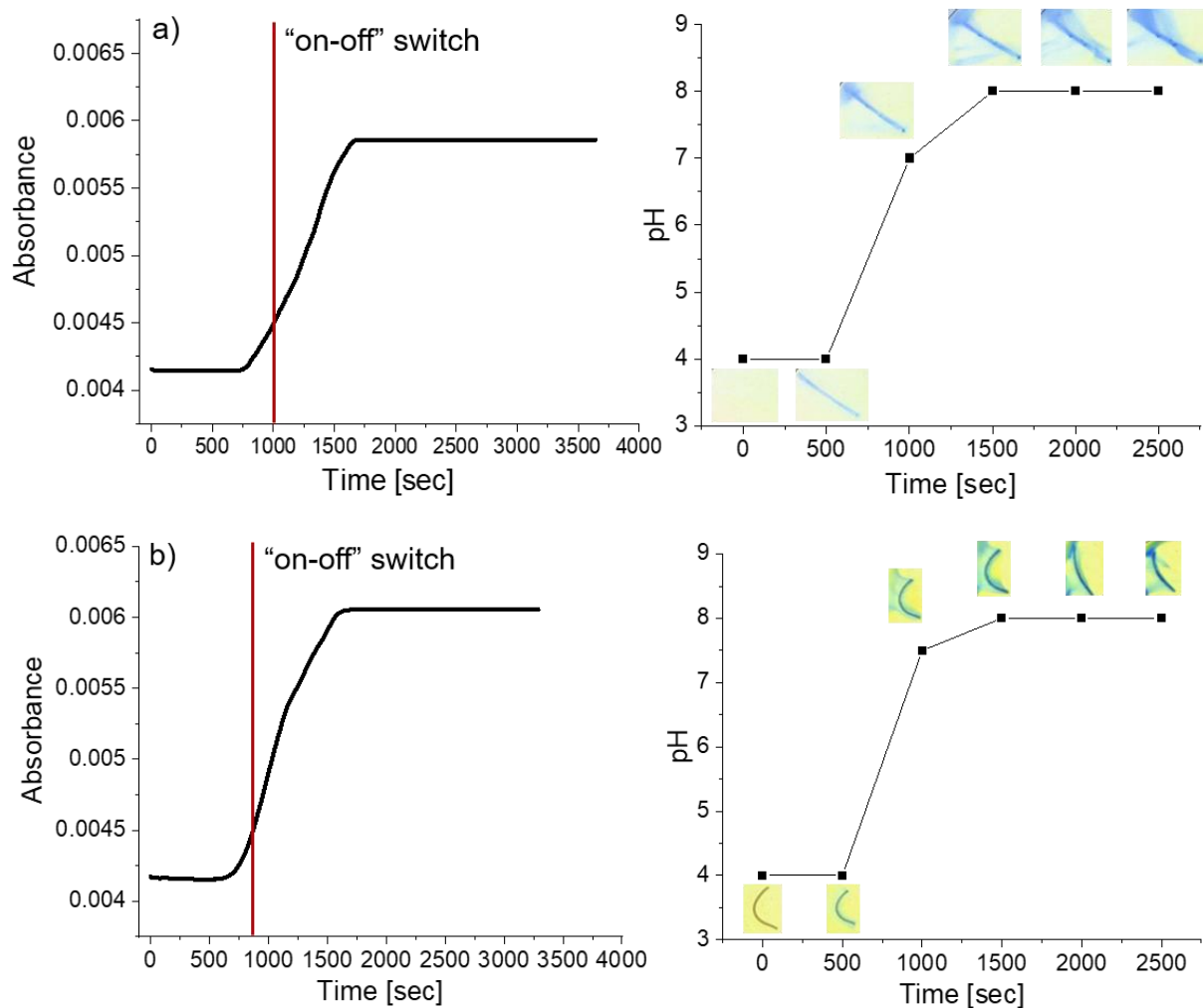


Figure 79. Urea urease reaction is shown through the absorbance vs. time plot (on the left) and pH vs. time (on the right) for a) UP and b) WM, encapsulated in gel filaments and placed in 5 mM urea at pH 4. The filaments are ~ 1 cm in length.

In the plots shown above it can be seen that for both enzyme sources, the sigmoidal curve typical of autocatalytic systems is achieved along with the pH switch from acidic to basic. In particular, the absorbance plots show a slight difference in terms of reaction time, where UP reaches pH 7 at around 1000 seconds, whereas WM realises the switch at around 800 seconds.

Although the two enzymes can be assumed reactive in the responsive filaments, WM filaments have shown a faster reaction time compared to the urease powder ones. This could be explained by taking into account the encapsulation. In fact, compared to standard urease powder, WM seeds' active enzyme is encapsulated in

protein microbodies consisting of a phospholipids bilayer shell which protects the enzyme from the outer environment²⁰⁷. Furthermore, the microbodies are bigger in size compared to the purchased enzymes, making it more difficult for them to diffuse or leak out of the gel.

Once the filaments were found to be reactive, they were investigated to determine if they were stable and robust. From an application-orientated point of view, two properties were examined: the reusability and reproducibility of the particles. The test was repeated in sequence over 8 successive times. The reaction time is defined as previously stated and taken into account here again. In continuous tests, the particles reacted with urea and images were recorded over time, then the same particles were placed in glucose solutions until the indicator re-emerged as yellow. This process was repeated eight times.

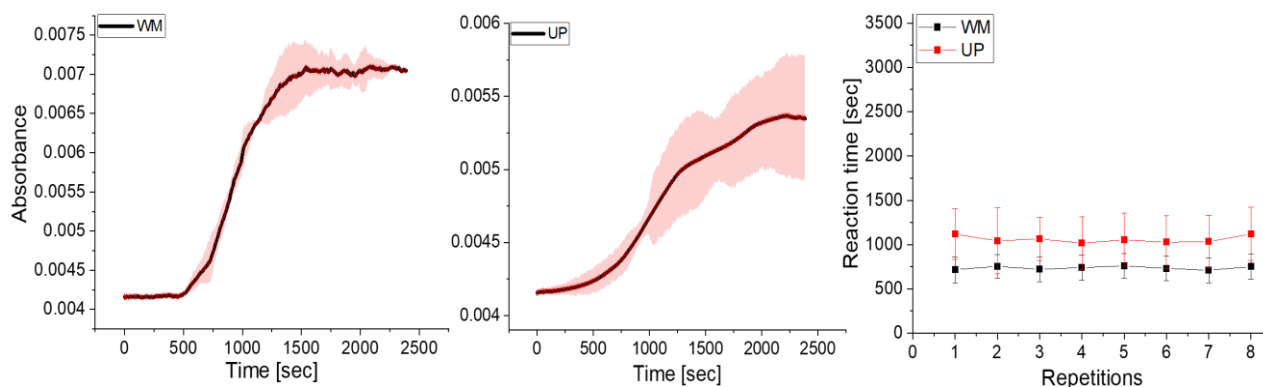


Figure 80. Reusability and reproducibility tests for urease from watermelon seeds (WM) and standard urease powder (UP) are shown in the absorbance versus time plot. on the right, reaction time vs. repetitions for WM and UP. Standard deviations were calculated from 8 measurements.

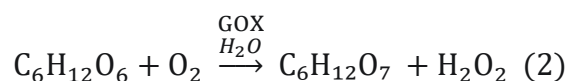
[Figure 80] shows the plots for reusability and reproducibility for WM and UP, where the pink area represents the standard deviation derived from the different repetitions. UP shows a more distributed standard deviation, showing it is less stable than WM. However, both enzyme sources were able to perform the urea urease reaction 8 times consecutively, showing the clock reaction. Once again, the physical encapsulation of the enzymes could be the reason for the greater stability and

reproducibility of WM seeds because of the microbodies constituting it, proving that the enzymes encapsulated in this type of gel are more durable and robust. As previously anticipated, the reaction time for the two different catalysts is slightly different. In fact, UP is capable of performing the switch at 1100 seconds, whereas WM reaches pH 7 more rapidly and precisely at 700 seconds. The values are calculated based on the repetition mean.

In summary, although both enzyme sources have shown to be able to perform the 'on-off' switch typical of autocatalytic reactions and to be reusable and reproducible up to 8 times, WM has been shown to generate an optical output earlier in time (around 700 seconds) and to be more stable and robust thanks to its physical conformation. This proves that enzymes taken directly from natural sources can represent an inexpensive, robust and reliable way to obtain pH changes other than purified enzymes.

6.4.2. Glucose

The pH-responsive filaments have the characteristic of shrinking at high pH and swelling at low pH. For filaments containing both urease and glucose oxidase enzymes, the area growth was used to determine the amount of acidic environment generated by gluconic acid production due to the glucose-glucose oxidase reaction as shown below.



The GOX-equipped filaments previously reacted with urea to set them at a high pH, were placed in glucose and left to react. In the glucose test, it can be observed the chemo-mechanical response. The filament, in fact, increased in terms of area but also switched colour to yellow as gluconic acid was formed [**Figure 81**].

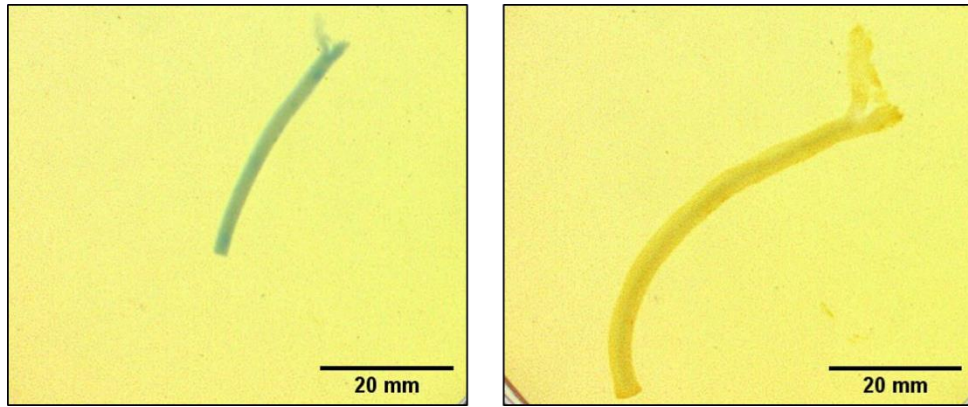


Figure 81. Filament containing GOX previously let react with urea 5 mM to set it at high pH, then placed in glucose solution 30mM, at time $t=0$ and $t=5000$ sec

During the reaction, the area was measured using the image analysis software Image J and plotted as can be observed in **[Figure 82]**.

The UP filament plot presents an initial more accentuated segment where the growth is quite pronounced as can also be seen in the respective right plot where we have the maximum slope at 400 seconds. On the other hand, the growth of the WM area is quite constant and homogeneous. However, UP achieves a larger area reaching 160 mm^2 at 5000 seconds, starting from 75 mm^2 , whereas WM starts from 80 mm^2 and reaches almost 200 mm^2 at the same point in time.

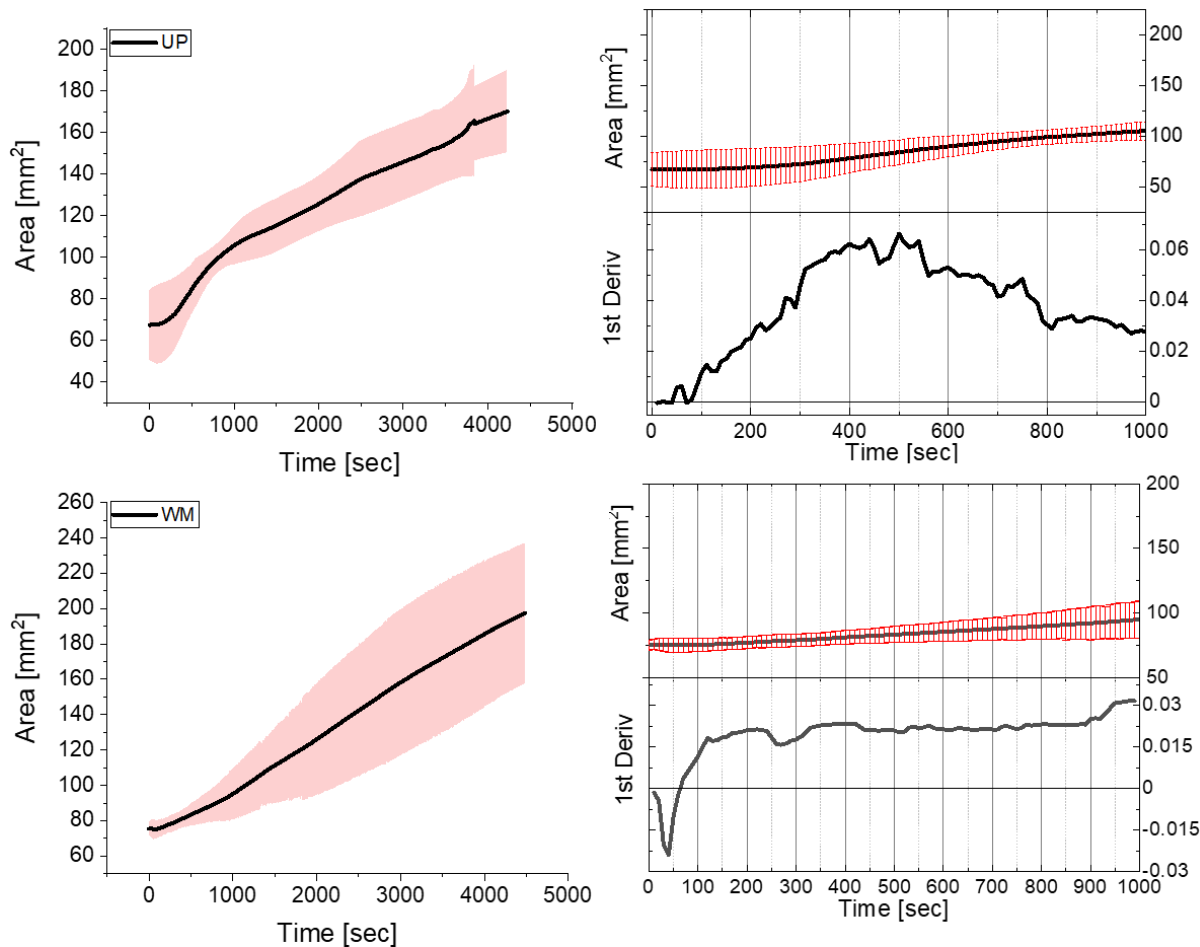


Figure 82. Area growth vs. time for UP and WM (on the left) GOX-filaments placed in glucose solution and their first derivative plot in time to show the growth rate

This means that, although UP filament has an initial faster growth when reacting with glucose, then it slows down and stops growing further. Instead, WM has a more constant growth and continues to increase with time. This behaviour could be attributed to the catalase present in the WM seeds powder, which reacts with the hydrogen peroxide produced by glucose and GOX, generating oxygen that consequently supports the first reaction. The longer the reaction, the greater the amount of gluconic acid formed and the decrease in pH, the larger the swelling of the filament.

6.4.3. Hydrogen peroxide

This test was performed in order to detect hydrogen peroxide and oxygen formation by using the filaments' area growth in time. In particular, a filament containing catalase in the form of WM seeds was placed in a 50 ml solution containing H_2O_2 at 0.5, 1 and 3% by volume to study whether its growth would be associated with the concentration. In particular, the filament expansion is given by the production of oxygen in the form of bubbles. Specifically, hydrogen peroxide diffused through the filaments and reacts with the catalase encapsulated in the WM seeds in the gel, as soon as oxygen is formed and bubbles are generated, they will physically stretch the filament, expanding it^{208,209}. The process can be better appreciated by observing [Figure 83] where it is shown a filament at time zero and then later in time, filled with bubbles.

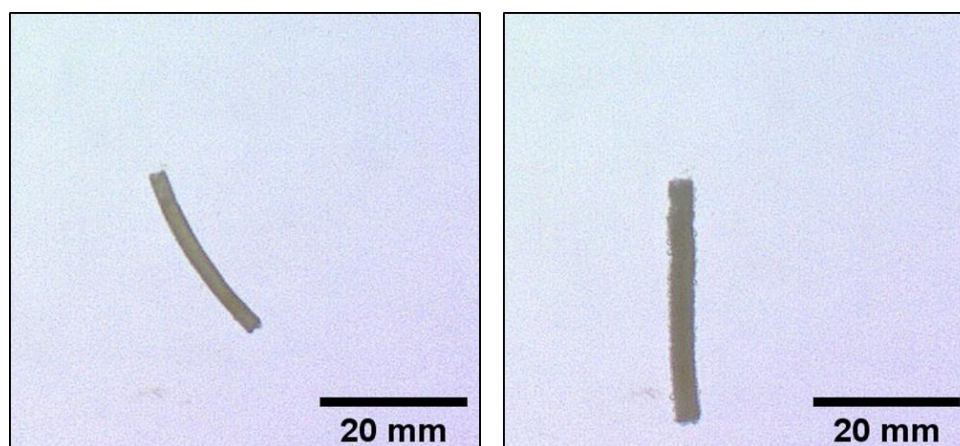


Figure 83. pH-responsive WM filament in hydrogen peroxide solution before and after bubble formation and consequent expansion

The concept expressed above can be well examined in [Figure 84] where filaments are placed into different concentrations of hydrogen peroxide solutions. On the left, the plot is presented showing the area growth in time for filaments placed in 0.5, 1 and 3% hydrogen peroxide. As could be expected, larger the amount of H_2O_2 is, more the filament will be expanded by the formed oxygen. In fact, the filament used with 3% hydrogen peroxide has reached 150 mm² starting from 50 mm², whereas

0.5 and 1% similarly start from 50 mm² and grow up to 130 mm². On the right plot, it is shown the first derivatives of the previously described curves in order to highlight the growth rate. In terms of speed, filaments placed in 1 and 3% H₂O₂ reach the maximum at around 12 seconds, meaning that the gel grows at the fastest rate in the first seconds of the reaction. On the other hand, the solution at 0.5% shows that the filament requires a longer time in order to grow. The phenomenon can easily be addressed to the limited amount of oxygen formed within the gel which causes a slower development of its own area.

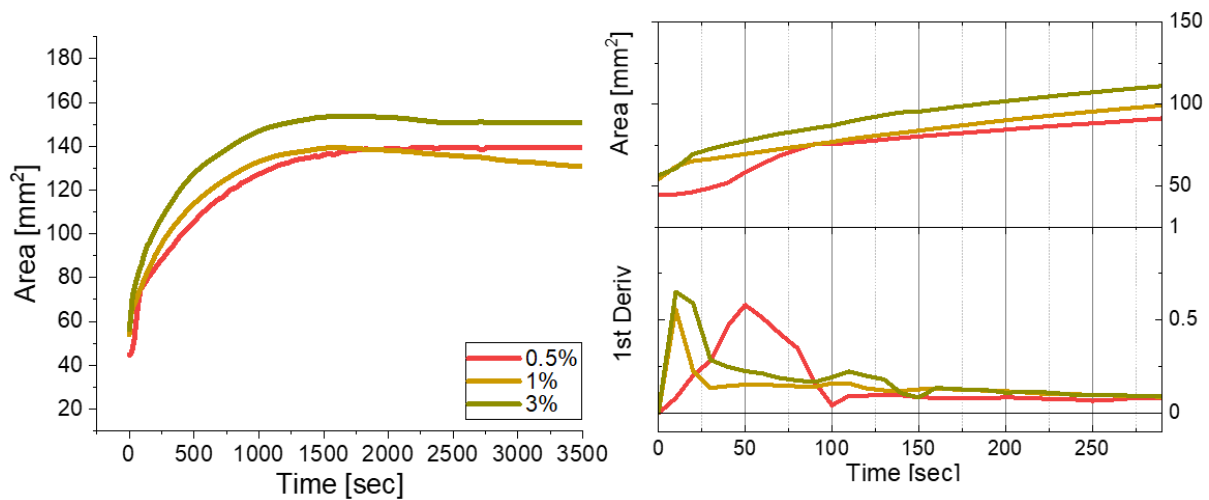


Figure 84. Area vs. time plot for different hydrogen peroxide concentrations in volume percentages and its derivative plot to show the area growth rate

The results shown in this section have been summarised in the bar plot presented in [Figure 85]. In fact, the plot displays the area growth ratio obtained from the maximum and minimum area expressed by the filaments. Similarly to what has already been observed, filaments placed in 0.5 and 1% show a comparable expansion ratio equal to 2.77 and 2.8 respectively. However, for gels used in solution with 3% hydrogen peroxide, the ratio grows to almost 3, showing that more oxygen was formed.

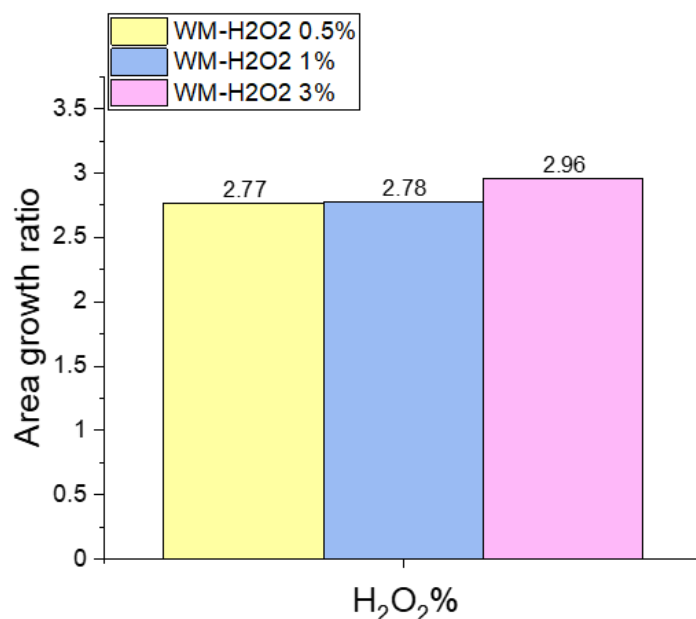
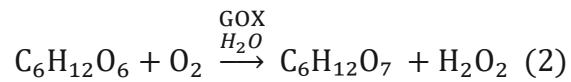


Figure 85. Bar plot showing the growth ratio between max/min area for filaments placed in hydrogen peroxide at 0.5, 1 and 3% concentration

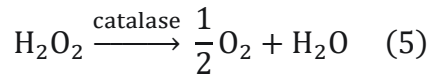
Recapitulating, the effect of hydrogen peroxide concentrations can be divided into two cases. According to the area growth, the larger the concentration, the bigger the filament's area expansion would be. Differently, according to the growth rate, 1 and 3% hydrogen peroxide solutions have been shown to be comparable and faster than the 0.5% one. This could signify that 1% might be taken as a detection cut-off point for a hydrogen peroxide biosensor. However, it is clear that in order to better tune the system further studies are required.

6.4.4. Glucose and hydrogen peroxide

As previously mentioned, the glucose-GOX reaction requires oxygen in order to produce gluconic acid. Therefore, a test using filaments containing GOX and catalase in the form of WM seeds was performed in a glucose solution with the addition of an initial concentration of hydrogen peroxide. In this way, a simple chemical reaction network was formed using two different enzymes encapsulated in the same gel according to the scheme presented below.



Plus



In doing this, the oxygen formed by reaction (5) helps reaction (2) to push towards the products and generate a further acidic external solution. The effect of the combined action can be seen in [**Figure 86**].

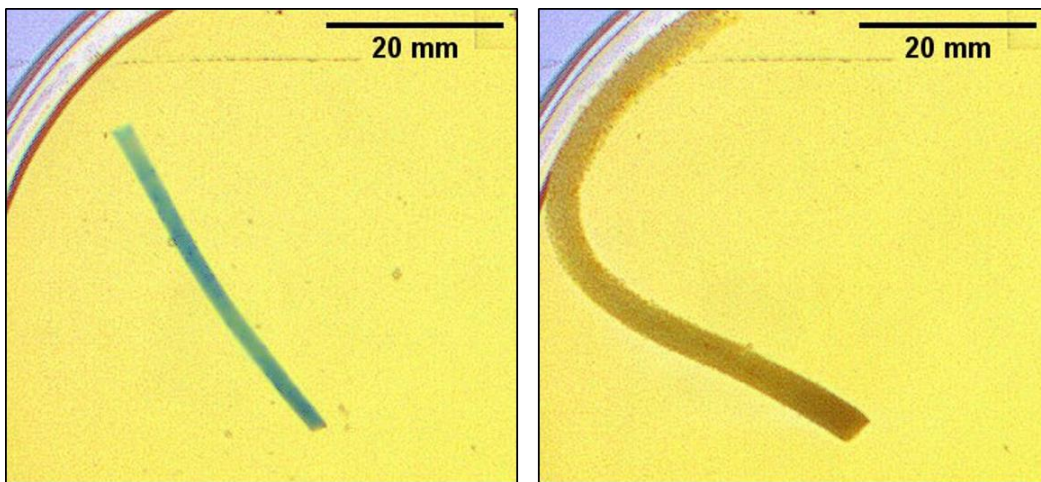


Figure 86. WM filament used with glucose 30mM and hydrogen peroxide 0.5% before and after the reaction occurred. The gel growth is given by the combined effect of gluconic acid and bubbles.

The filament containing WM seeds with catalase and GOX was placed in a solution containing 30 mM glucose and 0.5% H_2O_2 . In [**Figure 87**] it can be observed that the area grows in time going from 88 mm^2 to 277 mm^2 . Differently from before, the initial growth is quite rapid and has the fastest growth in the first 50 seconds of the reaction.

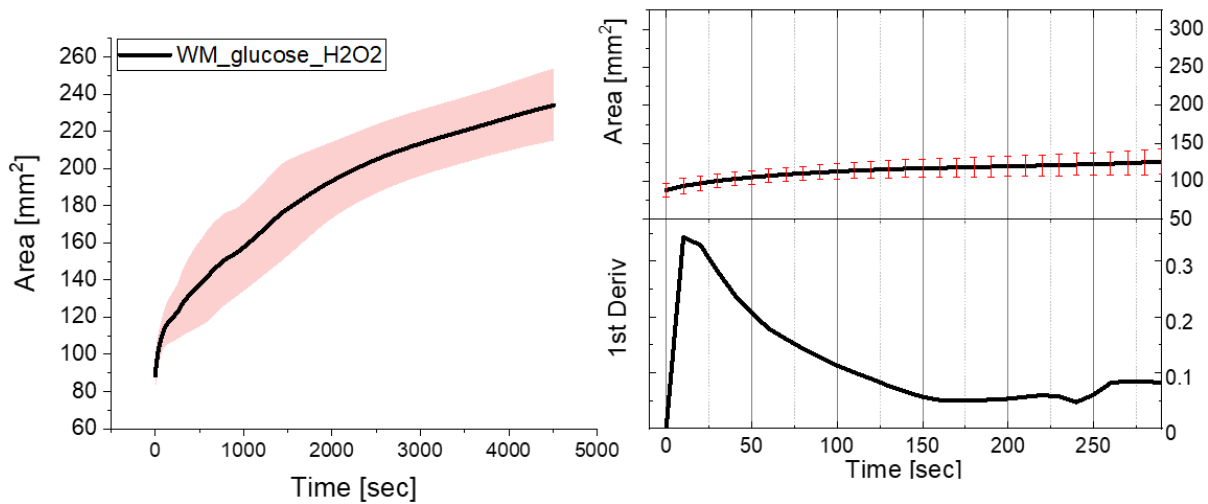


Figure 87. Area growth vs. time plot coupled with its first derivative curve to show the area growth rate for the WM seeds-glucose (30 mM) plus hydrogen peroxide (0.5%) reaction

A better comparison concerning the behaviour of filaments in glucose solutions with and without the addition of hydrogen peroxide can be appreciated in [Figure 88 a]. Here the area growth in time is plotted for UP and WM pH-responsive gels. As previously mentioned, UP filaments show an initial faster growth which then slows down, possibly due to the consumption of available oxygen in solution. On the other hand, WM filaments tend to persistently grow in the area as a result of the enzyme catalase present in the seeds, which sustains the reaction for longer, resulting in a final bigger gels' area growth. Finally, when an initial concentration of hydrogen peroxide (0.5%) is added to the glucose solution and a WM filament is used, the result in terms of area expansion is quite enhanced. The effect is possible mainly due to the double, combined action of two mechanisms. Firstly, oxygen production is faster and more consistent, increasing the area growth rate by sustaining the glucose-GOX reaction by producing a higher gluconic acid amount. Then the combination of bubble formation by the catalase-hydrogen peroxide reaction added to the acidic environment caused by the gluconic acid enhances the area growth ratio. This results in a faster and larger filament which produces a chemo-mechanical response to the different stimuli it is subjected to.

Additionally, in [Figure 88 b] it is illustrated the area growth ratio for the glucose investigation for the UP, WM and WM- H_2O_2 tests. It can be observed how using WM seeds in the filaments slightly increases the area ratio compared to UP going from 2.5 to 2.54. However, the real improvement is produced when WM filaments are used with glucose combined with hydrogen peroxide, where the ratio arrives at 2.7.

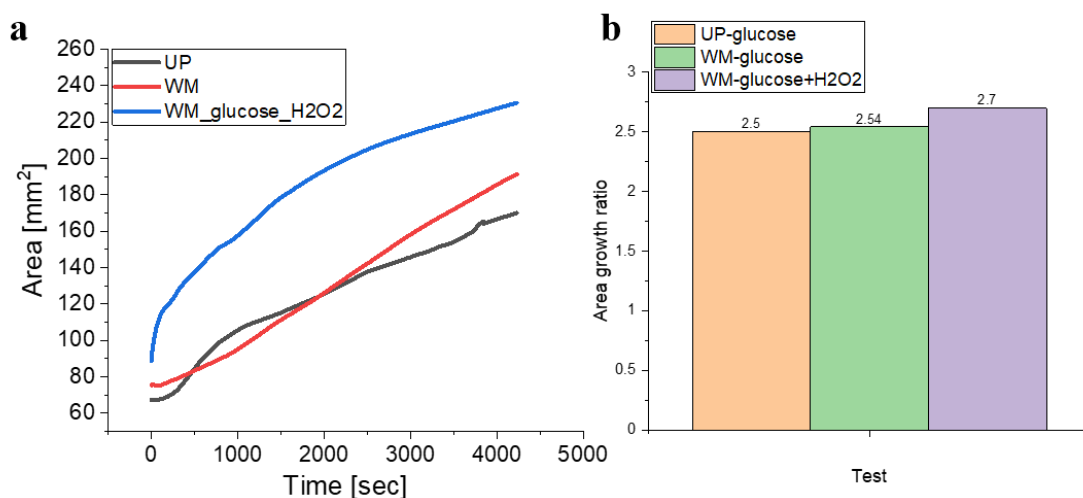


Figure 88. a) Area growth vs time for filaments made with UP, WM, and WM plus hydrogen peroxide (0.5%) in glucose solution. b) Bar plot showing the area growth ratio considering the end of the reaction over the initial stage for UP, WM, and WM plus hydrogen peroxide (0.5%), in glucose solution (30 mM).

This test has proved that adding hydrogen peroxide to the system has indeed increased the reaction into forming more gluconic acid which has consequently produced a faster and bigger growth in the filament area compared to the previous two studies. This means that building a chemical reaction network in combination with "smart" gels can bring to the formation of faster and clearer optical chemo-mechanical output responses.

6.5. Conclusions

The utilization of pH-responsive materials in drug delivery has been extensively researched, with notable success in the use of gels that swell or shrink with pH, particularly those containing urease/glucose oxidase. However, recent advancements in this field have introduced novel approaches to further enhance the efficacy of such materials. Notably, the incorporation of watermelon powder as a means of achieving long-lasting enzyme activity at room temperature has been investigated, with encouraging results demonstrating the feasibility of reusability for a cyclical process. Moreover, the application of multiple enzymes and substrates, including catalase, has been explored as a means of achieving more complex and enhanced responses. This innovative approach holds significant promise for the development of novel drug delivery systems with improved efficacy and functionality.

However, developing such a complex system carries some challenges and in order to deeply understand these enzyme-filament phenomena and channel this knowledge into a possible application, it is not sufficient to only look at the contribution of chemistry and mechanics individually. In fact, a deep focus on the interaction between them is needed. In any system, chemical and mechanical changes rarely occur on the same time scale, and develop through feedback loops, which provide the foundations for constructing complex adaptive responses^{192,193,205}. An adaptation of any property into smart gels or systems in general, can be a difficult task in coordinating precise molecular and structural adjustments, but the interaction between chemistry and mechanics does the work for us - they shape each other. This could be the first step in order to build smart materials capable of complex responses such as oscillations.

The NIPA gel containing imidazole and urease powder was proposed by Kokufuta and co-workers⁵⁷. Their experiments were performed at pH 4 and 35 °C in a flow of outer solutions. Shrinking of the gel was observed as a result of the formation of

the pH gradient. They also investigated a glucose responsive gel with glucose oxidase using NIPAAm-acrylic acid and this gel shrank as the pH decreased²¹⁰. It was demonstrated that a co-immobilised GOX system with gluconolactonase resulted in faster gel shrinkage than GOX alone; however, the process was still quite slow²¹¹. Only one other co-immobilised system was investigated – urease and glucose oxidase in NIPA-AAc and imidazole. This gel shrank then swelled again upon addition of urea, a single cycle, but the reaction was very slow¹⁰¹.

In this work, we have investigated the potential of combining chemical and mechanical responses by utilizing various enzymes that are enclosed in pH-responsive gels. The results have shown that the combination of enzymes has a positive impact on the final output response. This is a crucial step towards creating chemical reaction networks in self-regulating responsive gels, which can be used in various industries like drug delivery devices and sensors. Firstly, a comparison between standard urease powder and urease from watermelon seeds was conducted. The test was performed by placing a filament containing the enzyme sources and an indicator in a urea solution at 5 mM. although both of the enzymes have reproduced a sigmoidal shape of pH in time typical of autocatalytic systems, WM filaments have shown a faster response in time, possibly due to the structural nature of microbodies. Subsequently, the filaments were analysed to characterise their resistance and robustness. In this case, the filaments were equipped with two enzyme sources, urease and GOX and placed alternatively in 5mM urea solution and subsequently reset at low pH using 30 mM glucose solution. The gel was able to encapsulate both enzymes effectively and robustly since they were able to perform reproducibility and reusability tests up to eight times consequently. This means the system so built could be used several times before being deactivated. However, even in this case, WM have proven to have a smaller standard deviation and faster response time, meaning they are more stable and robust compared to UP filaments.

In the second study, the focus was put on the glucose reaction, adding filaments containing a mixture of UP-GOX and WM-GOX. The activity of the enzymes was calculated taking into account the swelling properties of the gel when placed in an acidic environment. In fact, glucose reacting with GOX would produce gluconic acid which will decrease the pH solution. Although with both enzyme sources, the filament would increase its area, it was noticed that the ones containing WM urease were growing considerably more. The behaviour was attributed to the enzyme catalase contained in WM which was reacting with the hydrogen peroxide formed by the glucose-GOX reaction, consequently producing more oxygen, that would help sustain the main reaction. This was the first simple example of chemical reaction network mechanisms in which two enzymes would cooperate together to enhance the final output response.

Along these lines, the third analysis was conducted. In fact, the filament containing WM and GOX was placed in a solution containing glucose and an initial concentration of hydrogen peroxide. The results showed that by increasing the availability of H_2O_2 in solution, the filament's area growth was quite faster, especially in the first 50 seconds. Again, the reaction rate boost was caused by the secondary reaction involving catalase which helped the primarily glucose reaction by producing oxygen and therefore, pushing towards the formation of gluconic acid, generating a more acidic environment.

The boosting effect was also proved via the area growth ratios, representing the final area over the initial area. The ratio will suggest that filaments containing WM-GOX in the presence of an initial concentration of hydrogen peroxide had a bigger ratio compared to the WM and UP filaments placed in glucose only. This effect could be attributed to the double effect of oxygen bubbles forming in the gels, which stretched the filaments, and the more acidic environment created by the increased production of gluconic acid facilitated by the enzyme catalase. The latter contributed to the sustainment of the glucose-GOX reaction by providing oxygen.

Lastly, the combination of WM filaments and hydrogen peroxide alone was tried. In this case, the chemo-mechanical response was given by the hydrogen peroxide-catalase reaction producing oxygen in bubbles form which were stretching the gel from within. In particular, three different concentrations of H_2O_2 were used in order to set a detection cut-off point to use the filament as an oxygen biosensor. In particular, the concentrations used were 0.5, 1 and 3% hydrogen peroxide and the results have shown that the more hydrogen peroxide is contained in the solution, the more oxygen is formed faster, and the more the area growth rate is sped up. In fact, the filaments placed in 3% H_2O_2 , increased their area more rapidly than the other two concentrations. Also, in this case, a bar plot showing the area ratios was built. It shows that for lower concentrations as 0.5 and 1%, the ratio is around 2.7, whereas when using 3% it almost reached 3, meaning the filament was growing triple compared to its initial area. To this extent, 1% hydrogen peroxide can be taken as a cut-off point after which the filaments cannot really differentiate among concentrations.

Concluding, we proved that building a system using chemo-mechanical responses in order to achieve a clearer output signal was possible. The gel was able to encapsulate successfully different types of enzymes remaining active even after using it eight times consecutively. The filaments were used with different substrates obtaining a robust output response with each one of them. Furthermore, simple chemical reaction networks using two types of enzymes were performed and the results show that the reaction rate was improved. However, the formation of bubbles will affect the system's growth to some extent. Such a system could be applied as a sensor which will shrink and swell according to the external pH, being able to regulate according to the external stimuli, as demonstrated by the glucose responsive gel²¹⁰. Finally, the gels were used to visualise the oxygen produced by the reaction. In this case, the filaments have proved to perform a clear and robust output signal but in order to tune it and make it more precise and usable, further investigations are required.

7. Conclusion of the thesis and future work

In this doctoral thesis, it has been demonstrated how enzyme-particle biosensors are versatile, easy to use with innovative properties. The purpose of our project is to try to fill the gap present in the literature by quantifying and better understanding the basic processes in enzyme-particle biosensors with pH autocatalysis in order to optimize and improve signal amplification and ultrasensitivity. One of the main goals was to set up an enzyme biosensor capable of detecting small changes in the amount of substances (ultrasensitivity), showing a clear and robust output signal which can also be appreciated by the naked eye (amplification) within seconds (response time). The characteristics should include small size, multiple uses and the possibility to connect it to a smart material (through e.g. the Boolean logic gates) to obtain a complex and autonomous system capable of sensing, reacting and transferring the signal in novel devices.

Firstly, an overview of enzyme biosensors was presented in Chapter 1. Initially, a historical excursion was presented to understand how the importance of the enzyme has developed over time. A great advancement occurred when enzymes were combined with different types of materials to produce biosensors. These biosensors differ from classical sensors as a result of the particular properties of enzymes as catalysts and also the wide applications of biocatalysts in different fields. Depending on the final application, the type of biosensor (nano/micro-particles, membrane, filaments...) is chosen to achieve different functionalities and also diverse properties depending on which type of output (optical, magnetic, electrical...) is desired or needed. In fact, enzyme-based biosensors usually involve a combination of mass transport phenomena and reactions, including substrate diffusion to the immobilised enzyme, enzyme-catalysed reaction, and the conversion of the product into an output signal. While experimental research on enzyme biosensors is extensive, modelling studies have been relatively scarce.

In Chapter 3, we have presented the outcomes of our experiments and model simulations aimed at optimizing the response of particle biosensors in an enzyme reaction with feedback. Specifically, we have shown that, unlike in other reactions, the particle size and transport of substrates and products play a crucial role in autocatalytic reactions. Our main objectives were to optimize the reaction time and the signal amplitude, which are key determinants of the biosensor output response for various applications. To achieve this, we employed a computational model to understand the system and tune parameters in the future. Our qualitative comparison of experiments and simulations showed good agreement. In our study, we encapsulated the enzyme and indicator (pyranine) in a thiol-acrylate polymer particle through physical entrapment and obtained a range of particle sizes via emulsion polymerization using hexane. We found that very small particles were unable to react due to the fast diffusion of ammonia out of the particles, while large particles took longer to react due to the limiting effect of urea transport in the particle. However, we observed that the signal amplitude was more stable in larger particles due to the longer time for the product ammonia to diffuse out. We discovered that a particle of $r = 0.35$ μm was optimal in terms of reaction time and signal amplitude. This finding underscores the critical role of particle size in the biosensor output response. Finally, we investigated the transport effects by comparing urease-particles made through thiol-acrylate emulsion polymerization in mineral oil with shell and non-shell particles made with hexane. We found that shell particles took longer to respond, but their signal was more stable over time. This phenomenon could be attributed to the oil layer, which delayed the diffusion of urea inside the core and trapped the ammonia once it was formed. Future studies are required to confirm these results. We note that while the emulsion technique we used to obtain enzyme-particles was easy to perform, it was not suitable for producing precise particle sizes for reproducible particle biosensor properties.

In Chapter 4, we provided an overview of the state of the art regarding enzyme immobilisation, highlighting the importance of such combination and defining the

technical difficulties encountered. The aim was to demonstrate a possible alternative to standard urease powder for enzyme-effective immobilisation regardless of the solid support. We found that watermelon seed urease has been shown to be sustainable, cost-effective and robust especially because the enzyme is trapped in protein microbodies, which protects them and makes them active also at room temperature. We tested the two enzyme sources encapsulated in three different hydrogel particles such as thiolacrylate, low EEO, and high EEO agarose. We performed two tests to characterize the particles from different perspectives. In the first test, we evaluated the threshold detection limits and response time, while in the second test, we evaluated the reusability and reproducibility properties. We found that WM urease was suitable for the formation of an optical biosensor in an equal way with thiol-acrylate and agarose particles. In both cases, the detection limit was set at 0.4 mM and the response time occurred within one hour. Moreover, WM particles have been shown to produce an output signal and therefore be reusable consecutively (ten times) and over a month, even at room temperature. When UP urease was coupled with thiol-acrylate gel particles, they showed a robust match in terms of the urea detection limit and response time, respectively, set at 0.4 mM and 1 hour.

However, when UP was paired with agarose, no output signal was observed. The enzyme was able to diffuse out of the particle, making the biosensor inactive. Moreover, in the reusability test regards, the only effective result was UP matched with thiol-acrylate in the consecutive repetitions. For all other experiments, no signal was achieved. The adaptability and robustness of watermelon seeds with different hydrogels could be exploited in several systems. One of them could be the mass transport phenomena in terms of propagating reaction-diffusion fronts. Additionally, an optical and chemomechanical biosensor could be used in the field of soft robotics. With the diverse spectrum of enzymes contained in WM, another option would be to combine different enzymes to have a single biosensor capable of detecting multiple analytes. Considering the reusability shown by WM, a

biosensor built with this enzyme source would be a device applicable in a variety of fields such as pharmaceutical, biomedical but also waste water treatment detection.

In Chapter 5, we looked at the characterization of three enzymes to build a chemical reaction network using watermelon seed powder. The use of coupling catalysts in chemical reaction networks has been proven to be an innovative yet challenging mechanism used to improve reaction rates and overcome product inhibition. We combined enzymes that can alter pH and characterized the biocatalysts through oxygen formation, pH change, and foam front propagation. We analysed each enzyme individually and then combined them to show the coupling effect on the system. The first enzyme investigated was catalase, which decomposes hydrogen peroxide into water and oxygen. We found that increasing the amount of hydrogen peroxide or the catalase concentration does not improve oxygen production. Instead, the system has an optimum condition that initially corresponded to 0.3 g WM and 1% concentration.

Nevertheless, it was found that the system was producing a foam propagating according to the amount of WM present in the system, which interfered with the main reaction. We identified optimal conditions as 0.1 g WM and 1% concentration to control the foam formation and achieve a large amount of oxygen production. Glucose oxidase was used to catalyze glucose oxidation into gluconic acid and hydrogen peroxide from glucose. We found that due to the oxygen limiting influx into the solution, all the oxygen present at the beginning is consumed at a fast rate whereas the gluconic acid is not produced in appreciable quantities for the pH to decrease sufficiently. Therefore, we coupled catalase in watermelon seed and GOX in the system so that the two reactions could work together to enhance each other's reaction rate and increase product formation. β -glucosidase was the next enzyme to be observed, responsible for cellobiose hydrolysis into glucose. The enzyme activity was investigated using the product formed by the second step of the

cascade reaction. We found that adding hydrogen peroxide to the system boosted the reaction rate speed and product formation.

Finally, urease in watermelon seed was added to the GOX-catalase to generate controlled pH changes. Urease and GOX are both autocatalytic in pH and could be used to make pH oscillations. It was demonstrated that a pH drop and rise could be achieved with a network of GOX-catalase-urease with sequential additions. Watermelon seeds are a natural source of multiple different enzymes already coexisting and cooperating according to complex biological mechanisms. They have potential to become an inexpensive and easy enzyme source for industrial, analytical, and sensor applications in a variety of fields. Further investigations are required to have a better understanding of the processes and tune them accordingly.

Lastly, in Chapter 6, the study investigated the potential of combining chemical and mechanical responses by utilizing various enzymes that are encapsulated in pH-responsive gels. The results demonstrated that the combination of enzymes has a positive impact on the final output response. This represents a crucial step towards creating chemical reaction networks in self-regulating responsive gels, which can be used in various applications such as drug delivery devices and sensors.

Firstly, a comparison between standard urease powder and urease from watermelon seeds was conducted. Although both of the enzymes have reproduced a sigmoidal shape of pH in time typical of autocatalytic systems, WM filaments have shown a faster response in time, possibly due to their structural nature of microbodies. Subsequently, the filaments were analyzed to characterize their resistance and robustness. The gel was able to encapsulate both enzymes effectively and robustly since they were able to perform reproducibility and reusability tests up to eight times consequently. However, WM have proven to have a smaller standard deviation and faster response time, meaning they are more stable and robust compared to UP filaments. In the second study, the focus was put on the glucose

reaction, adding filaments containing a mixture of UP-GOX and WM-GOX. Although with both enzyme sources, the filament would increase its area, it was noticed that the ones containing WM urease were growing considerably more. The behaviour was attributed to the enzyme catalase contained in WM, which was reacting with the hydrogen peroxide formed by the glucose-GOX reaction, consequently producing more oxygen, that would help sustain the main reaction. This was the first simple example of chemical reaction network mechanisms in which two enzymes would cooperate together to enhance the final output response. Along these lines, the third analysis was conducted. In fact, the filament containing WM and GOX was placed in a solution containing glucose and an initial concentration of hydrogen peroxide. The results showed that by increasing the availability of H_2O_2 in solution, the filament's area growth was quite faster, especially in the first 50 seconds. Again, the reaction rate boost was caused by the secondary reaction involving catalase, which helped the primary glucose reaction by producing oxygen and therefore, pushing towards the formation of gluconic acid, generating a more acidic environment.

Additionally, the boosting effect was further confirmed through the area growth ratios, which represent the final area over the initial area, by further investigating the enhancing impact of WM-GOX on the growth ratios of filament area in the presence of an initial concentration of hydrogen. The findings revealed that filaments incorporating WM-GOX- H_2O_2 displayed a significantly higher area growth ratio compared to the WM and UP filaments placed in glucose only. The observed effect could be explained by the dual mechanism of oxygen bubbles formation in the gels, which caused the stretching of the filaments, and the more acidic environment created by the enzyme catalase, which facilitated the increased production of gluconic acid. This resulted in the sustenance of the glucose-GOX reaction by providing oxygen. Hence, it can be inferred that filaments containing WM-GOX in the presence of an initial concentration of hydrogen peroxide had a larger ratio compared to filaments placed in glucose only.

Finally, the combination of WM filaments and hydrogen peroxide alone was tried. In this case, the chemo-mechanical response was given by the hydrogen peroxide-catalase reaction producing oxygen in bubbles form, which expands the gel from within. In particular, three different concentrations of H_2O_2 were used in order to set a detection cut-off point to use the filament as an oxygen biosensor. The results have shown that the more hydrogen peroxide is contained in the solution, the more oxygen is formed faster, and the more the area growth rate is sped up. To this extent, 1% hydrogen peroxide can be taken as a cut-off point after which the filaments cannot really differentiate among concentrations.

The results showed that the combination of enzymes has a positive impact on the final output response and represents a crucial step towards creating chemical reaction networks in self-regulating responsive gels, which can be used in various industries. The filaments were able to encapsulate successfully different types of enzymes and remained active even after using it eight times consecutively. Such a system could be applied as a drug delivery device that will shrink and swell according to the external pH, being able to regulate according to the external stimuli. Finally, the gels were used to visualize the oxygen produced by the reaction. In this case, the filaments have proved to perform a clear and robust output signal but in order to tune it and make it more precise and usable, further investigations are required.

The future work of this doctoral thesis exhibits potential for expansion on various levels, all of which contribute to the development of a robust, reusable, and cost-effective biosensor. Such a biosensor would possess the ability to detect analytes with utmost sensitivity and fast response time. Firstly, the investigation of WM seeds and their potential in enzyme applications is paramount. The presence of certain cooperative enzymes in this work has been observed, but the mass spectrometry analysis revealed many other enzymes that could be beneficial for current research and applications. Additionally, the microbodies protecting the biocatalysts in WM

seeds have the potential for enzyme applications in the synthesis of chemicals, as they are sustainable, robust, biocompatible, and easily stored even in solution at room temperature.

Secondly, the focus should be on multiple enzyme encapsulations on various solid supports for reproducible observation of the output signal. This thesis has focused on inexpensive and bio-compatible hydrogels such as thiol-acrylate and agarose, but the robust nature of WM seeds allows for the testing of different supports to examine durability, encapsulation, reusability, and reproducibility. Moreover, trapping several different enzymes that cooperate and self-regulate will create a system capable of detecting several analytes and reacting accordingly.

Finally, the ultimate step is to combine the multiple-detector biosensor with responsive materials, resulting in a system capable of detecting multiple substances and responding to them through a chemo-mechanical mechanism. This system can then be used to encapsulate drugs and create the ultimate drug delivery device that is capable of multi-analyte detection and personalised to the patient's needs and disease. This work holds potential in the field of biosensors and drug delivery systems, and further research can undoubtedly contribute to the advancement of these areas.

8. Appendices

8.1. Appendix 1. Modelling of enzyme-based sensors

Enzyme-based biosensors are known to involve a complex interplay of mass transport phenomena and reaction mechanisms, including substrate diffusion to the immobilised enzyme, enzyme-catalysed reaction, and transformation of the product into an output signal. Despite the critical role of modelling in understanding and optimizing biosensor performance, there has been limited theoretical investigation in comparison to experimental studies. As such, further exploration of the underlying mechanisms governing the response of enzyme-based biosensors is essential to unlock their full potential in a range of applications.

8.1.1. Models, reactions and kinetics

The kinetics of enzyme-catalysed reactions have been widely studied. By indicating the enzyme, substrate and product with E, S, and P respectively, the general mechanism of reaction such as $S \leftrightarrow P$ in the presence of a specific enzyme is:



- Enzyme-substrate interaction
- Enzyme substrate complex
- Transformation of the substrate in the product complex with the enzyme
- The liberation of the enzyme from the product

Different reaction models have been formulated but the most common is the classical Michaelis-Menten model, which offers the basis for most current research on the mechanism of enzyme action. It is based on the hypothesis that the first step of the reaction is a pseudo equilibrium. Thus, with simple mass balance equations the final reaction rate, V , can be calculated as:

$$V = \frac{k[E][S]}{K_M + [S]} \quad (\text{A } 2)$$

where k is the turnover number and $K_M = \frac{[E][S]}{[ES]}$ is the Michaelis constant. Several enzymes have a pH dependence which can influence the reaction rates. There are two main groups of acid-base catalysis by enzymes:

- Specific catalysis → the reaction rates fluctuate under the influence of changes in H^+ or H_3O^+ concentration but are independent of the concentrations of the other acids or bases present in the solution.
- General acid or general base catalysis → when reaction rates are very sensitive to all acids or bases present in the solution¹⁴

The dependence of rate on pH results in a bell-shaped curve where the maximum rate occurs at an optimum pH. This behaviour arises as a result of the binding of acid to the enzyme and can be modelled as:

$$rate = \frac{r_{max}S}{(K_M + S) \left(1 + \frac{K_2}{[H^+]} + \frac{[H^+]}{K_1} \right)} \quad (\text{A } 3)$$

Where $r_{max} = k[E]$, K_1 and K_2 represent the binding coefficient of acid to the enzyme.

8.1.2. Reaction-diffusion processes

Reaction-diffusion is a process in which the molecules included in the reaction are transported through space by the mechanism of diffusion. Diffusive transport is described by a flux that is proportional to the local concentration gradient. Consequently, the diffusive flux J is defined as the number of molecules passing through a unit section area per unit time and in one dimension is given by:

$$\vec{j}(x, t) = -D \frac{\partial C}{\partial x} \quad (\text{A } 4)$$

where D is the diffusion coefficient. When a reaction occurs, molecules are created or consumed according to specific reaction kinetics [Figure A 1]. Thus, the reaction-diffusion equation of the general form is like the one of the classic diffusion equation, plus a term for the reaction:

$$\frac{\partial C_i}{\partial t}(x, t) = D_i \nabla^2 C_i + R_i([C_j], t) \quad (A 5)$$

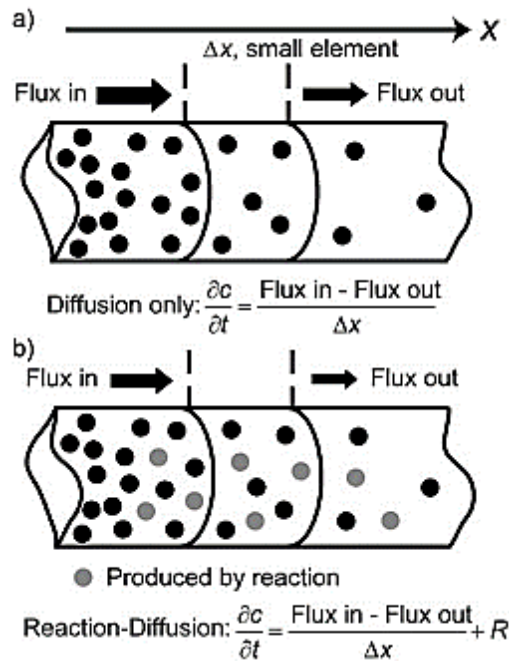


Figure A 1. Diffusion scheme: (A) without reaction and (B) with the reaction¹¹⁷

For enzymes encapsulated in a particle such as a nanoparticle or a vesicle a simplified model scheme can be developed to investigate the influence of mass transport on the chemical reaction. For example, in [Figure A 2], it is possible to observe the simplified two-variable scheme where the exchange of matter is incorporated as flow terms of urea-urease reaction taking place in a membrane or particle, considering:

- $R =$ enzyme catalysed rate
- H, S and $E =$ respectively the acid, substrate and enzyme concentration
- k_H and $k_S =$ transport coefficient

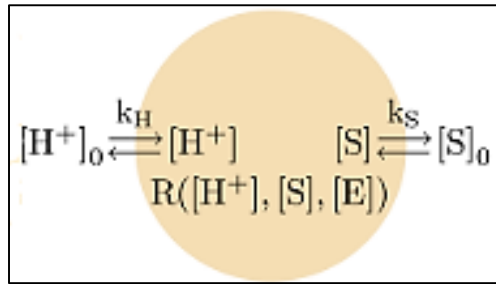


Figure A 2. Enzyme-particle scheme¹¹³

The last two, in particular, are very important since they govern the substrate and acid molecules exchange between the compartment and the reservoir. The passage from the reaction-diffusion model which uses the diffusion coefficient to the transport coefficient can be explained thanks to the film theory. Adjacent to the interface between the membrane (or particle) and the bulk solution, there is a thin, but still not calculable, film whose thickness is δ . The species concentration is uniform everywhere in the bulk solution apart in the film [Figure A 3].

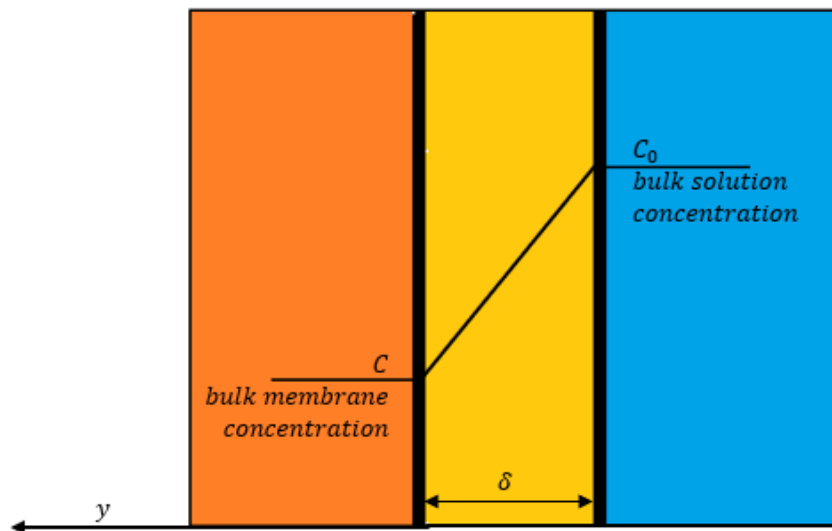


Figure A 3. Film theory representation

Due to the different concentrations between the outside and the inside of the membrane, the matter flux starts, and it is described as:

$$J = -D \frac{dC}{dy} \quad (\text{A } 6)$$

Simplifying the equation through the finite-difference it becomes:

$$J \left[\frac{M \text{ cm}}{s} \right] = -D \frac{\Delta C}{\Delta y} = -D \frac{C_0 - C}{\delta} \left[\frac{cm^2}{s} \frac{M}{cm} \right] \quad (A 7)$$

where:

$$\frac{D}{\delta} \left[\frac{cm^2}{s} \frac{1}{cm} \right] = k_{sl} \left[\frac{cm}{s} \right] \quad (A 8)$$

The ratio between the diffusion coefficient and the film thickness is equal to the transport coefficient. The ordinary differential equations (ODEs) representing this simplified scheme in [Errore. L'origine riferimento non è stata trovata.] are¹¹³:

$$\frac{d[S]}{dt} = k_s([S]_0 - [S]) - R \quad (A 9)$$

$$\frac{d[H^+]}{dt} = (k_H \left([H^+]_0 - \frac{K_w}{[H^+]_0} - [H^+] + \frac{K_w}{[H^+]} \right) - 2R) \left(1 + \frac{K_w}{[H^+]^2} \right)^{-1} \quad (A 10)$$

Where

$$R = \frac{k_E[E][S]}{(K_M + [S]) \left(1 + \frac{K_{ES2}}{[H^+]} + \frac{[H^+]}{K_{ES1}} \right)} \quad (A 11)$$

Where k_S and k_H are the transport coefficients $\sim \frac{k_{sl}}{r} [s^{-1}]$ and k_{sl} is the mass transfer coefficient for solids to liquids.

The value of the transport coefficients can have consequences on the behaviour of the enzyme-catalysed reaction¹¹³⁻¹¹⁴.

8.2. Appendix 2. XPP-ODE code for urea-urease reaction chapter 3

8.2.1. Hexane particle sensor

```
#particle

U'=-kE*E*U/((1+KE2/H+H/KE1)*(KME+U*(1+U/KS))*(1+NH4/Kp))+
(1*ksl/r)*(Uo-U)

NH3'=2*kE*E*U/((1+KE2/H+H/KE1)*(KME+U*(1+U/KS))*(1+NH4/Kp))+k2
r*NH4-k2*NH3*H+(m*ksl/r)*(NH3o-NH3)

NH4'=-k2r*NH4+k2*NH3*H+(ksl/r)*(NH4o-NH4)

CO2'=kE*E*U/((1+KE2/H+H/KE1)*(KME+U*(1+U/KS))*(1+NH4/Kp))-
k3r*CO2+k3*H*HCO3+(ksl/r)*(CO2o-CO2)

HCO3'=k3r*CO2-k3*HCO3*H-k4r*HCO3+k4*CO3*H+(ksl/r)*(HCO3o-HCO3)

CO3'=k4r*HCO3-k4*CO3*H+(ksl/r)*(CO3o-CO3)

H'=k2r*NH4-k2*NH3*H+k4r*HCO3-k4*CO3*H+k5r-k5*H*OH+k3r*CO2-
k3*HCO3*H+o*ksl/r*(Ho-H)

OH'=k5r-k5*H*OH+p*ksl/r*(OHo-OH)

#surrounding solution      Vo = volume of solution; N = constant
(number of particles*(4pi/3))

Uo'=-1*ksl*N*r*r/Vo*(Uo-U)

NH3o'=k2r*NH4o-k2*NH3o*Ho-m*ksl*N*r*r/Vo*(NH3o-NH3)

NH4o'=-k2r*NH4o+k2*NH3o*Ho-ksl*N*r*r/Vo*(NH4o-NH4)

CO2o'=-k3r*CO2o+k3*Ho*HCO3o-ksl*N*r*r/Vo*(CO2o-CO2)

HCO3o'=k3r*CO2o-k3*HCO3o*Ho-k4r*HCO3o+k4*CO3o*Ho-
ksl*N*r*r/Vo*(HCO3o-HCO3)

CO3o'=k4r*HCO3o-k4*CO3o*Ho-ksl*N*r*r/Vo*(CO3o-CO3)

Ho'=k2r*NH4o-k2*NH3o*Ho+k4r*HCO3o-k4*CO3o*Ho+k5r-
k5*Ho*OHo+k3r*CO2o-k3*HCO3o*Ho-o*ksl*N*r*r/Vo*(Ho-H)
```

```

OHO'=k5r-k5*Ho*OHO-p*ksl*N*r*r/Vo*(OHO-OH)

aux pH=-log(H)/log(10)

aux pHo = -log(Ho)/log(10)

#parameters

par l=2, m=20, o=1, p=1

par k2=4.3e10, k2r=24, k3=7.9e4, k3r=0.037

par k4=5e10, k4r=2.8, k5=1e11, k5r=1e-3

par kE=8e-7, E=80, KME=0.003, KS=3, KP=0.002, KE1=5e-6, KE2=2e-9

par ksl=3e-4, N=4, Vo=20, r=?

#initial conditions

init U=0.00, NH3=0, NH4=0, CO2=0, HCO3=0, CO3=0, H=1e-4, OH=1e-9

init          Uo=3e-4, NH3o=0, NH4o=0, CO2o=0, HCO3o=0, CO3o=0, Ho=1e-
4, OHO=1e-9

#numerical stuff

@ total=5000, dt=10, tol=1e-14, atol=1e-14, meth=cvode

@ xplot=t, yplot=pH, xhi=4000, ylo=1, yhi=14

done

#   $01   $0.007

#   $02   $0.02

#   $03   $0.035

#   $04   $0.075

#   $05   $0.085

```

8.2.2. Mineral oil particle sensor

#particle

$$U' = -k_E * E * U / ((1 + K_{E2}/H + H/K_{E1}) * (K_{ME} + U * (1 + U/K_S)) * (1 + NH_4/K_p)) + (k_{s1}/r) * (U_o - U)$$

$$NH_3' = 2 * k_E * E * U / ((1 + K_{E2}/H + H/K_{E1}) * (K_{ME} + U * (1 + U/K_S)) * (1 + NH_4/K_p)) + k_2 * r * NH_4 - k_2 * NH_3 * H + (k_{s1}/r) * (NH_{3o} - NH_3)$$

$$NH_4' = -k_2 * r * NH_4 + k_2 * NH_3 * H + (k_{s1}/r) * (NH_{4o} - NH_4)$$

$$CO_2' = k_E * E * U / ((1 + K_{E2}/H + H/K_{E1}) * (K_{ME} + U * (1 + U/K_S)) * (1 + NH_4/K_p)) - k_3 * r * CO_2 + k_3 * H * HCO_3 + (k_{s1}/r) * (CO_{2o} - CO_2)$$

$$HCO_3' = k_3 * r * CO_2 - k_3 * HCO_3 * H - k_4 * r * HCO_3 + k_4 * CO_3 * H + (k_{s1}/r) * (HCO_{3o} - HCO_3)$$

$$CO_3' = k_4 * r * HCO_3 - k_4 * CO_3 * H + (k_{s1}/r) * (CO_{3o} - CO_3)$$

$$H' = k_2 * r * NH_4 - k_2 * NH_3 * H + k_4 * r * HCO_3 - k_4 * CO_3 * H + k_5 * r - k_5 * H * OH + k_3 * r * CO_2 - k_3 * HCO_3 * H + k_H / r * (H_o - H)$$

$$OH' = k_5 * r - k_5 * H * OH + k_{OH} / r * (OH_o - OH)$$

#surrounding solution V_o = volume of solution; N = constant
(number of particles * $(4\pi/3)$)

$$U_o' = -k_{s1} * N * r * r / V_o * (U_o - U)$$

$$NH_{3o}' = k_2 * r * NH_{4o} - k_2 * NH_{3o} * H_o - k_{s1} * N * r * r / V_o * (NH_{3o} - NH_3)$$

$$NH_{4o}' = -k_2 * r * NH_{4o} + k_2 * NH_{3o} * H_o - k_{s1} * N * r * r / V_o * (NH_{4o} - NH_4)$$

$$CO_{2o}' = -k_3 * r * CO_{2o} + k_3 * H_o * HCO_{3o} - k_{s1} * N * r * r / V_o * (CO_{2o} - CO_2)$$

$$HCO_{3o}' = k_3 * r * CO_{2o} - k_3 * HCO_{3o} * H_o - k_4 * r * HCO_{3o} + k_4 * CO_{3o} * H_o - k_{s1} * N * r * r / V_o * (HCO_{3o} - HCO_3)$$

$$CO_{3o}' = k_4 * r * HCO_{3o} - k_4 * CO_{3o} * H_o - k_{s1} * N * r * r / V_o * (CO_{3o} - CO_3)$$

$$H_o' = k_2 * r * NH_{4o} - k_2 * NH_{3o} * H_o + k_4 * r * HCO_{3o} - k_4 * CO_{3o} * H_o + k_5 * r - k_5 * H_o * OH_o + k_3 * r * CO_{2o} - k_3 * HCO_{3o} * H_o - k_H * N * r * r / V_o * (H_o - H)$$

$$OH_o' = k_5 * r - k_5 * H_o * OH_o - k_{OH} * N * r * r / V_o * (OH_o - OH)$$

```

aux pH=-log(H)/log(10)
aux pHo = -log(Ho)/log(10)

#parameters
par k2=4.3e10, k2r=24, k3=7.9e4, k3r=0.037
par k4=5e10, k4r=2.8, k5=1e11, k5r=1e-3
par kE=3.7e-7, E=80, KME=0.003, KS=3, KP=0.002, KE1=5e-6, KE2=2e-9
par ksl=0.0003, kH=9e-5, kOH=4.5e-5, N=4, Vo=20, r=?

#initial conditions
init U=0.00, NH3=0, NH4=0, CO2=0, HCO3=0, CO3=0, H=1e-4, OH=1e-10
init          Uo=3e-4, NH3o=0, NH4o=0, CO2o=0, HCO3o=0, CO3o=0, Ho=1e-
4, OHo=1e-10

#numerical stuff
@ total=12000, dt=10, tol=1e-14, atol=1e-14, meth=cvode
@ xplot=t, yplot=pH, xhi=4000, ylo=1, yhi=14
done

#   $01   $0.007
#   $02   $0.02
#   $03   $0.035
#   $04   $0.075
#   $05   $0.085

```

8.3. Appendix 3. Image Analysis in Chapter 4

Since the biosensor proposed in this paper is built in order to give an optical output signal, there is the need to associate the colours to the corresponding pH. In order to do so, a pH scale from 2 to 9 was created [**Figure A 4**]. The scale was made using aqueous solution of bromothymol blue adjusting the aimed pH with NaOH 0.01M and HCl 0.1M. Once the scale was built, an image was taken with the Thorlab camera and analysed via the image analysis software ImageJ.

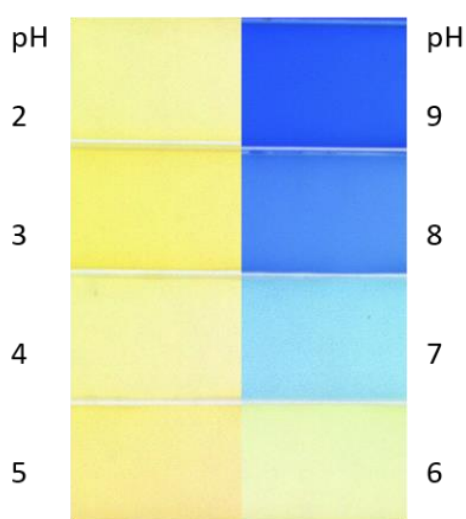


Figure A 4. pH scale representation

To give the most accurate shade possible, the image was manipulated in order to remove darks from the background and emphasise the different shades obtained. Following, through the option 'Plot Z-axis profile' intensity was associated with a colour shade [**Figure A 5**].

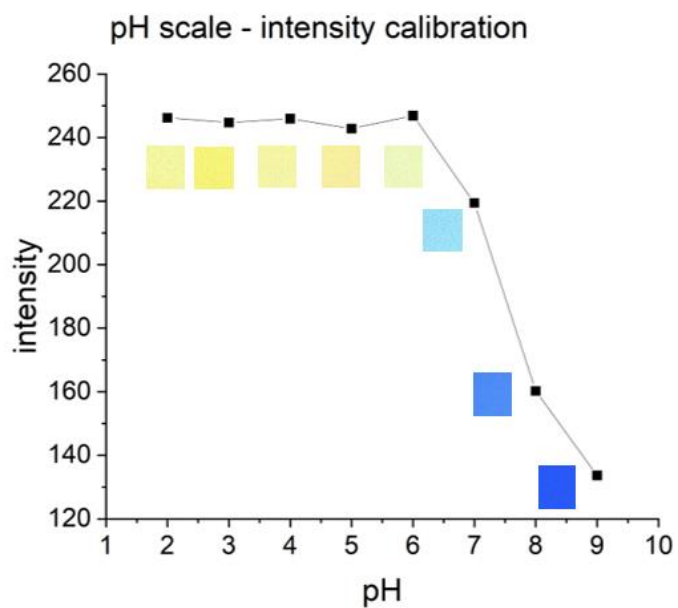


Figure A 5. Intensity vs pH

Thus, every time an image was analysed, once the intensity reached by the particle at that concentration was known, it could be switched to a pH value [Table A 1].

Table A 1. Intensity/ pH scale association

Intensity	pH	Intensity	pH
246	2	246	6
244	3	219	7
245	4	160	8
243	5	133	9

8.4. Appendix 4. Analysis and Simulations Chapter 5

8.4.1. Image Analysis

The foam front propagation images were taken every 10 seconds over 600 seconds. The images were acquired using a dark background to highlight the foam front development and graph paper adjacent to the test tube in order to use it as a reference.

The data were analysed via Matlab® which would display the first and last pictures from the selected folder. On the first data set picture, the initial point at time=0 sec and length=0 mm was set as can be seen in **[Figure A 6 a]**. Then, on the last data set picture at time=600 sec, the maximum foam front length was pointed by arrow number 2 as can be observed in **[Figure A 6 b]**. The software will then proceed to calculate the foam front length over time and create a data sheet which was then plotted.

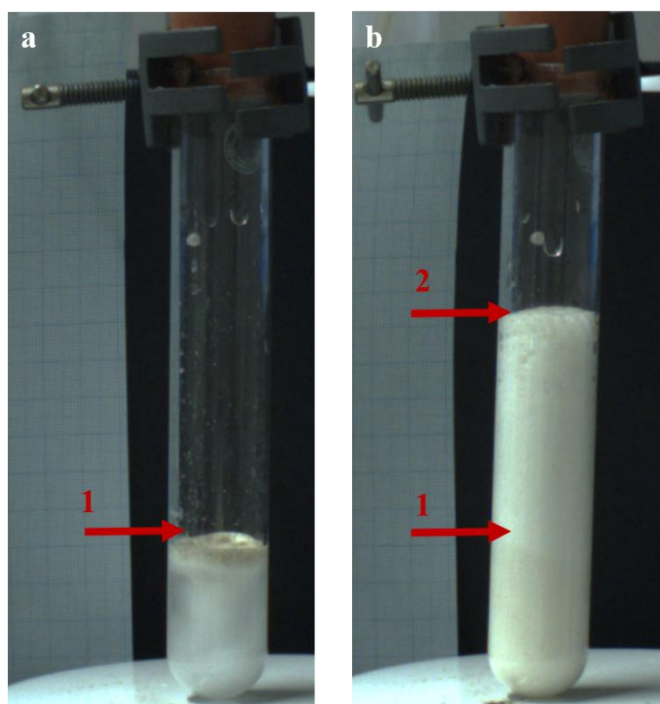


Figure A 6. Representation of the initial front point (arrow 1) and final front point (arrow 2) positions to determine the foam front propagation length

8.4.2. Code for analysis of foam fronts

```
close all
clear all
dir = 'C:\Users\';
rfn='2023.02.00'; % file name before number
rfn2='2023.02.0'
%=====PARAMETERS=====
===== rfn='Y:\CHM\Physical\AFT\MMW\ureapetri60\ureapetri60_';
% root of file names
%bg=28;      % background file
fi=28;      % first file
li=99;      % last file
mf=1;      % median filter radius
smf=10;     % smoothing factor for 1D cut
d=3;      % range of diff
sp_res=3; % pixel/mm
dt=10;     % time elapsed between consecutive frames (in
seconds)
s_time=5;  %time point to calculate slope
nc=1;     % number of cuts: 4,9,16 etc
ir=1;     % radius of the omitted area around origin
tr='0';
%=====
=====
t=fi*dt:dt:li*dt;
fc=sqrt(nc);
af=360/2/pi;
al=0;
ar=linspace(0,(360-360/nc),nc)/af;
%filename=[dir,rfn,num2str(bg),'.tif'];
%bg=imread(filename);
%bg2=medfilt2(bg(:,:,2), [mf mf]);
filename1=[dir,rfn,num2str(fi),'.tif'];
i=imread(filename1);
```

```

i_fi=i(:,:,2);
if li < 100
filename2=[dir,rfn,num2str(li),'.tif'];
else
    filename2=[dir,rfn2,num2str(li),'.tif'];
end
i=imread(filename2);
i_li=i(:,:,2);
i_si=uint8((double(i_fi)+double(i_li))/2);
imshow(i_si,'Border','tight');
text(1,10,[filename1,' + ',filename2],'BackgroundColor',[1 1
1]);
[xl,yl] = ginput(2);
length_of_cut=pdist([xl yl]);
xp=xl(2);
yp=yl(2);
xps=xl(1);
yps=yl(1);
xpt=round(xl(1)+cos(ar)*(length_of_cut+10));
ypt=round(yl(1)+sin(ar)*(length_of_cut+10));
cl=length(improfile(i,[xps(1) xp(1)],[yps(1) yp(1)])); %
length in pixels for length correction of oblique cuts
for p=1:nc
    line([xps(p) xp(p)],[yps(p)
yp(p)],'LineWidth',2,'Color',[0 0 0]);
    hold on
    quiver(xps(p),yps(p),(xp(p)-xps(p)),(yp(p)-
yps(p)),0.55,'MaxHeadSize',1/cl*100,'LineWidth',2,'Color',[0 0
0])

text(xpt(p),ypt(p),num2str(p),'HorizontalAlignment','Center','
Color',[1 1 1])
end
    hold off

```

```

for n=fi:li
    if n < 100
        st = [tr,num2str(n)];
    else
        st = num2str(n);
    end
    filename=[rfn2,num2str(st),'.tif'];
    i=imread(filename);
    i_f=medfilt2(i(:,:,2),[mf mf]);
    i_f=imadjust(i_f);
    %imshow(i_f,[1 1]);
    %ima(n-fi+1,(:,:,:))=double(i_f)-double(bg2);
    ima(n-fi+1,(:,:,:))=double(i_f);

end

figure
for ang=1:nc
    subplot(fc,fc,ang)
    for n=fi:li

        c=improfile(squeeze(ima(n-fi+1,(:,:,:))),[xps(ang)
xp(ang)],[yps(ang) yp(ang)],'nearest');
        csm=c;
        csm=smooth(c,smf);
        ds=round(d/2);
        for x=1:length(c)-d
            dcsm(x+ds)=csm(x+d)-csm(x);
        end
        dcsm=abs(dcsm);
        %plot(c,'-k')
        %hold on
        %plot(csm,'-r')
        %hold on
        %plot(dcsm,'-ob')
    end
end

```

```

        %hold on
        max_dcsm=max(dcsm);
        dcsm(dcsm < max_dcsm) = 0;
        fp=find(dcsm);
        frpo(n-fi+1)=mean(fp);
        dcsm_frpo(n-fi+1)=mean(dcsm(fp));
        plot(frpo(n-fi+1),dcsm_frpo(n-fi+1),'og')
    end

    lc=length(c);
    real_frpo=frpo/sp_res*c1/lc;
    maxheight=max(real_frpo)-min(real_frpo);
    fpifpf(ang,:)=[real_frpo(1) real_frpo(length(real_frpo))];
    plot(t,real_frpo,'ok')
    xlabel('Time (sec)')
    ylabel('Space (mm)')
    [fit_lin_par, stat] =
polyfit(t(1:s_time),real_frpo(1:s_time),1);
    lin = fit_lin_par(1).*t+fit_lin_par(2);
    slope(ang)=fit_lin_par(1)*60;
    hold on
    set(gcf,'Color','white')
    plot(t, lin,'-r','LineWidth',2);
    xtick=get(gca, 'XTick');
    ytick=get(gca, 'YTick');
    xtl=length(xtick);
    ytl=length(ytick);
    text_str=['\bf',num2str(ang),'\rm slope =
',num2str(fit_lin_par(1)*60)];
    text_str2=['\bf',num2str(ang),'\rm maxheight =
',num2str(maxheight)];
    text((xtick(1)+xtick(2))/2,(ytick(ytl)+ytick(ytl-
1))/2,text_str,'HorizontalAlignment','Left');

```

```

    text((xtick(1)+xtick(2))/2,(ytick(yt1)+ytick(yt1-
1))/2,text_str2,'HorizontalAlignment','Right');
    axis([xtick(1) xtick(xt1) ytick(1) ytick(yt1)]);

    % ===== MS Excel output (comment out if not needed)
=====

    data_matrix(1,1:3)={'time','front position','fitted front
position'};};
    for dat=1:li-fi+1
    data_matrix(dat+1,1:3)={t(dat),real_frpo(dat),lin(dat)};};
    end
    %
=====
=====

    filename_xls=[rfn,'rad_',num2str(ang),'.xls'];
    xlswrite(filename_xls, data_matrix);
    clear max_dcsm dcsm frpo dcsm_frpo fp c csm real_frpo
xtick ytick data_matrix
    hold off
end

```

9. Bibliography

1. Walker JM. *Biosensors and Biodetection*. Vol 504.; 2009.
<http://www.springerlink.com/index/10.1007/978-1-60327-569-9>
2. Castro KR, de Almeida SV, Fari RC, Crespilho FN. Fundamentals for Virus and Antigen Detection in Immunotechnologies. *Adv Bioelectrochemistry Vol 3 Biosensors, Wearable Devices Biomed Appl*. 2022;3:31-49. doi:10.1007/978-3-030-97921-8_2/COVER
3. Rocchitta G, Spanu A, Babudieri S, et al. Enzyme biosensors for biomedical applications: Strategies for safeguarding analytical performances in biological fluids. *Sensors (Switzerland)*. 2016;16(6). doi:10.3390/s16060780
4. Li Y, Schluesener HJ, Xu S. Gold nanoparticle-based biosensors. *Gold Bull* 43, 29–41 (2010). <https://doi.org/10.1007/BF03214964>
5. Ispas CR, Crivat G, Andreescu S. Review: Recent Developments in Enzyme-Based Biosensors for Biomedical Analysis. *Anal Lett*. 2012;45(2-3):168-186. doi:10.1080/00032719.2011.633188
6. Ansari SA, Husain Q. Potential applications of enzymes immobilized on/in nano materials: A review. *Biotechnol Adv*. 2012;30(3):512-523. doi:10.1016/j.biotechadv.2011.09.005
7. Kim J, Sung GY, Park M. Efficient portable urea biosensor based on urease immobilized membrane for monitoring of physiological fluids. *Biomedicines*. 2020;8(12):1-11. doi:10.3390/biomedicines8120596
8. Ye S, Feng S, Huang L, Bian S. Recent Progress in Wearable Biosensors: From Healthcare Monitoring to Sports Analytics. *Biosensors*. 2020;10(12):1-34. doi:10.3390/bios10120205
9. Küchler A, Yoshimoto M, Luginbühl S, Mavelli F, Walde P. Enzymatic reactions

- in confined environments. *Nat Nanotechnol.* 2016;11(5):409-420.
doi:10.1038/nnano.2016.54
10. Ferrell JE, Ha SH. Ultrasensitivity part I: Michaelian responses and zero-order ultrasensitivity. *Trends Biochem Sci.* 2014;39(10):496-503.
doi:10.1016/j.tibs.2014.08.003
 11. Ferrell JE, Ha SH. Ultrasensitivity part III: Cascades, bistable switches, and oscillators. *Trends Biochem Sci.* 2014;39(12):612-618.
doi:10.1016/j.tibs.2014.10.002
 12. Epstein IR, Xu B. Reaction-diffusion processes at the nano- and microscales. *Nat Nanotechnol.* 2016;11(4):312-319. doi:10.1038/nnano.2016.41
 13. Martínez Cuesta S, Rahman SA, Furnham N, Thornton JM. The Classification and Evolution of Enzyme Function. *Biophys J.* 2015;109(6):1082-1086.
doi:10.1016/j.bpj.2015.04.020
 14. Bhatia S, Bhatia S. Introduction to enzymes and their applications. *Introd to Pharm Biotechnol Vol 2.* 2018. doi:10.1088/978-0-7503-1302-5ch1
 15. Wilson GS, Hu Y. Enzyme-based biosensors for in vivo measurements. *Chem Rev.* 2000;100(7):2693-2704. doi:10.1021/cr990003y
 16. Biswal T, BadJena SK, Pradhan D. Sustainable biomaterials and their applications: A short review. In: *Materials Today: Proceedings.* Vol 30. ; 2020:274-282. doi:10.1016/j.matpr.2020.01.437
 17. Basso A, Serban S. Industrial applications of immobilized enzymes—A review. *Mol Catal.* 2019;479:110607. doi:10.1016/j.mcat.2019.110607
 18. Sepasi Tehrani H, Moosavi-Movahedi AA. Catalase and its mysteries. *Prog Biophys Mol Biol.* 2018;140:5-12. doi:10.1016/j.pbiomolbio.2018.03.001
 19. Krajewska B. Ureases I. Functional, catalytic and kinetic properties: A review. *J Mol Catal B Enzym.* 2009;59(1-3):9-21. doi:10.1016/j.molcatb.2009.01.003

20. Singhania RR, Patel AK, Sukumaran RK, Larroche C, Pandey A. Role and significance of beta-glucosidases in the hydrolysis of cellulose for bioethanol production. *Bioresour Technol.* 2013;127:500-507.
doi:10.1016/j.biortech.2012.09.012
21. Majore K, Ciprovica I. Bioconversion of Lactose into Glucose–Galactose Syrup by Two-Stage Enzymatic Hydrolysis. *Foods.* 2022;11(3).
doi:10.3390/foods11030400
22. Sengupta S, Patra D, Ortiz-Rivera I, et al. Self-powered enzyme micropumps. *Nat Chem.* 2014;6(5):415-422. doi:10.1038/nchem.1895
23. Ejaz U, Sohail M, Ghanemi A. Cellulases: From bioactivity to a variety of industrial applications. *Biomimetics.* 2021;6(3):44.
doi:10.3390/biomimetics6030044
24. Javaid M, Haleem A, Rab S, Pratap Singh R, Suman R. Sensors for daily life: A review. *Sensors Int.* 2021;2(July):100121. doi:10.1016/j.sintl.2021.100121
25. Brian R. Eggins, Chemical Sensors and Biosensors. 2002, John Wiley and Sons. ISBN: 978-0-471-89914-3
26. Malik P, Katyal V, Malik V, Asatkar A, Inwati G, Mukherjee TK. Nanobiosensors: Concepts and Variations. *ISRN Nanomater.* 2013;2013:1-9.
doi:10.1155/2013/327435
27. Grzelczak M, Liz-Marzán LM, Klajn R. Stimuli-responsive self-assembly of nanoparticles. *Chem Soc Rev.* 2019;48(5):1342-1361. doi:10.1039/c8cs00787j
28. Goldbeter A, Koshland DE. Sensitivity amplification in biochemical systems. *Q Rev Biophys.* 1982;15(3):555-591. doi:10.1017/S0033583500003449
29. Koshland DE, Goldbeter A, Stock JB. Amplification and adaptation in regulatory and sensory systems. *Science.* 1982;217(4556):220-225.
doi:10.1126/science.7089556

30. Saghatelian A, Guckian KM, Thayer DA, Ghadiri MR. DNA detection and signal amplification via an engineered allosteric enzyme. *J Am Chem Soc.* 2003;125(2):344-345. doi:10.1021/ja027885u
31. Newman JD, Setford SJ. Enzymatic biosensors. *Mol Biotechnol.* 2006;32(3):249-268. doi:10.1385/MB:32:3:249
32. Bankar SB, Bule M V., Singhal RS, Ananthanarayan L. Glucose oxidase - An overview. *Biotechnol Adv.* 2009;27(4):489-501. doi:10.1016/j.biotechadv.2009.04.003
33. Schlegel H-G, Kaltwasser H. Urease. *Methods Enzym Anal.* 1974:1081-1085. doi:10.1016/B978-0-12-091302-2.50106-7
34. Deisseroth A, Dounce AL. Catalase: Physical and chemical properties, mechanism of catalysis, and physiological role. *Physiol Rev.* 1970;50(3):319-375. doi:10.1152/physrev.1970.50.3.319
35. Esen A. β -Glucosidases Overview. *ACS Symposium Series*, 533: 1993. DOI: 10.1021/bk-1993-0533.ch001
36. Garcia-Galan C, Berenguer-Murcia Á, Fernandez-Lafuente R, Rodrigues RC. Potential of different enzyme immobilization strategies to improve enzyme performance. *Adv Synth Catal.* 2011;353(16):2885-2904. doi:10.1002/adsc.201100534
37. Homaei AA, Sariri R, Vianello F, Stevanato R. Enzyme immobilization: An update. *J Chem Biol.* 2013;6(4):185-205. doi:10.1007/s12154-013-0102-9
38. Imam HT, Marr PC, Marr AC. Enzyme entrapment, biocatalyst immobilization without covalent attachment. *Green Chem.* 2021;23(14):4980-5005. doi:10.1039/d1gc01852c
39. Sassolas A, Blum LJ, Leca-Bouvier BD. Immobilization strategies to develop enzymatic biosensors. *Biotechnol Adv.* 2012;30(3):489-511.

- doi:10.1016/j.biotechadv.2011.09.003
40. Yu A, Wang Y, Barlow E, Caruso F. Mesoporous silica particles as templates for preparing enzyme-loaded biocompatible microcapsules. *Adv Mater.* 2005;17(14):1737-1741. doi:10.1002/adma.200402045
 41. Lei C, Xu C, Nouwens A, Yu C. Ultrasensitive ELISA+ enhanced by dendritic mesoporous silica nanoparticles. *J Mater Chem B.* 2016;4(29):4975-4979. doi:10.1039/c6tb01023g
 42. Vandekerckhove J. *Methods in Molecular Biology, Vol. 32: Basic Protein and Peptide Protocols.* Vol 356.; 1994. doi:10.1016/s0014-5793(94)80079-0
 43. Zeng S, Yong KT, Roy I, Dinh XQ, Yu X, Luan F. A Review on Functionalized Gold Nanoparticles for Biosensing Applications. *Plasmonics.* 2011;6(3):491-506. doi:10.1007/s11468-011-9228-1
 44. Miranda OR, Li X, Garcia-Gonzalez L, et al. Colorimetric bacteria sensing using a supramolecular enzyme-nanoparticle biosensor. *J Am Chem Soc.* 2011;133(25):9650-9653. doi:10.1021/ja2021729
 45. Klajn R, Stoddart JF, Grzybowski BA. Nanoparticles functionalised with reversible molecular and supramolecular switches. *Chem Soc Rev.* 2010;39(6):2203-2237. doi:10.1039/b920377j
 46. Bhide A, Cheeran S, Muthukumar S, Prasad S. Enzymatic low volume passive sweat based assays for multi-biomarker detection. *Biosensors.* 2019;9(1):1-14. doi:10.3390/bios9010013
 47. Cui L, Li CC, Tang B, Zhang CY. Advances in the integration of quantum dots with various nanomaterials for biomedical and environmental applications. *Analyst.* 2018;143(11):2469-2478. doi:10.1039/c8an00222c
 48. Tan H, Yang S, Shen G, Yu R, Wu Z. Signal-enhanced liquid-crystal DNA biosensors based on enzymatic metal deposition. *Angew Chemie - Int Ed.*

- 2010;49(46):8608-8611. doi:10.1002/anie.201004272
49. Hussain A, Pina AS, Roque ACA. Bio-recognition and detection using liquid crystals. *Biosens Bioelectron.* 2009;25(1):1-8. doi:10.1016/j.bios.2009.04.038
 50. Martinez AW, Phillips ST, Butte MJ, Whitesides GM. Patterned paper as a platform for inexpensive, low-volume, portable bioassays. *Angew Chemie - Int Ed.* 2007;46(8):1318-1320. doi:10.1002/anie.200603817
 51. Akhtar MF, Hanif M, Ranjha NM. Methods of synthesis of hydrogels ... A review. *Saudi Pharm J.* 2016;24(5):554-559. doi:10.1016/j.jsps.2015.03.022
 52. Ullah F, Othman MBH, Javed F, Ahmad Z, Akil HM. Classification, processing and application of hydrogels: A review. *Mater Sci Eng C.* 2015;57:414-433. doi:10.1016/j.msec.2015.07.053
 53. Hoffman AS. Hydrogels for biomedical applications. *Adv Drug Deliv Rev.* 2012;64(SUPPL.):18-23. doi:10.1016/j.addr.2012.09.010
 54. Gehrke SH. Synthesis, equilibrium swelling, kinetics, permeability and applications of environmentally responsive gels. *Adv Polym Sci.* 1993;110:80-144. doi:10.1007/bfb0021130
 55. Díaz DD, Kühbeck D, Koopmans RJ. Stimuli-responsive gels as reaction vessels and reusable catalysts. *Chem Soc Rev.* 2011;40(1):427-448. doi:10.1039/c005401c
 56. Gupta P, Vermani K, Garg S. Hydrogels: From controlled release to pH-responsive drug delivery. *Drug Discov Today.* 2002;7(10):569-579. doi:10.1016/S1359-6446(02)02255-9
 57. Ogawa K, Kokufuta E. Enzymatic formation of pH gradients within polyelectrolyte gels with immobilized urease. *Langmuir.* 2002;18(15):5661-5667. doi:10.1021/la0115177
 58. Panja S, Panja A, Ghosh K. Supramolecular gels in cyanide sensing: A review.

- Mater Chem Front.* 2021;5(2):584-602. doi:10.1039/d0qm00551g
59. Tierney S, Volden S, Stokke BT. Glucose sensors based on a responsive gel incorporated as a Fabry-Perot cavity on a fiber-optic readout platform. *Biosens Bioelectron.* 2009;24(7):2034-2039. doi:10.1016/j.bios.2008.10.014
 60. Chatterjee S, Hui PCL. Review of applications and future prospects of stimuli-responsive hydrogel based on thermo-responsive biopolymers in drug delivery systems. *Polymers (Basel).* 2021;13(13):2086. doi:10.3390/polym13132086
 61. Xiao SH, Liu YY, Wei LH, Guo Y. [Advancement in researches of mast cell]. *Sheng Li Ke Xue Jin Zhan.* 2011;42(2):104-107.
 62. A. Isakova and K. Novakovic. Pulsatile release from a flat self-oscillating chitosan macrogel. *J Mater Chem B.* 2018;6(30):5003-5010. doi:10.1039/c8tb00781k
 63. Kokufuta O. Enzymatic Formation of pH Gradients within Polyelectrolyte Gels with immobilized Urease. *Langmuir* 2002, 18, 5661 <http://pubs.acs.org/doi/pdf/10.1021/ma011112t>
 64. Tombelli S, Marrazza G, Mascini M. Recent advances on DNA biosensors. *Int J Environ Anal Chem.* 2001;80(2):87-99. doi:10.1080/03067310108044375
 65. Mu XH, Liu HF, Tong ZY, et al. A new rapid detection method for ricin based on tunneling magnetoresistance biosensor. *Sensors Actuators, B Chem.* Published online 2019. doi:10.1016/j.snb.2018.12.127
 66. Ligler F, Taitt C. *Optical Biosensors.* Vol 10.; 2008. doi:10.1016/B978-0-444-53125-4.X5001-3
 67. Chen C, Wang J. Optical biosensors: An exhaustive and comprehensive review. *Analyst.* 2020;145(5):1605-1628. doi:10.1039/c9an01998g
 68. Borisov SM, Wolfbeis OS. Optical biosensors. *Chem Rev.* 2008;108(2):423-461. doi:10.1021/cr068105t

69. Lee YEK, Kopelman R. Optical nanoparticle sensors for quantitative intracellular imaging. *Wiley Interdiscip Rev Nanomedicine Nanobiotechnology*. 2009;1(1):98-110. doi:10.1002/wnan.2
70. Gupta VK, Skaife JJ, Dubrovsky TB, Abbott NL. Optical amplification of ligand-receptor binding using liquid crystals. *Science (80-)*. 1998;279(5359):2077-2080. doi:10.1126/science.279.5359.2077
71. Kumar MNVR. *J Pharm Pharmaceut Sci (Www.Ualberta.ca/~csps)* 3(2):234-258, 2000 234 *Nano and Microparticles as Controlled Drug Delivery Devices*; 2000. Accessed September 28, 2023. www.ualberta.ca/~csps
72. Aghbolaghy M, Karimi A. Simulation and optimization of enzymatic hydrogen peroxide production in a continuous stirred tank reactor using CFD-RSM combined method. *J Taiwan Inst Chem Eng*. 2014;45(1):101-107. doi:10.1016/j.jtice.2013.05.009
73. Kovács B, Nagy G, Dombi R, Tóth K. Optical biosensor for urea with improved response time. *Biosens Bioelectron*. 2002;18(2-3):111-118. doi:10.1016/S0956-5663(02)00164-1
74. Hu G, Pojman JA, Scott SK, Wrobel MM, Taylor AF. Base-Catalyzed Feedback in the Urea - Urease Reaction. *J. Phys. Chem. B* 2010, 114, 44, 14059-14063. doi.org/10.1021/jp106532d
75. Wong F, Dey KK, Sen A. Synthetic Micro/Nanomotors and Pumps: Fabrication and Applications. *Annu Rev Mater Res*. 2016;46(1):407-432. doi:10.1146/annurev-matsci-070115-032047
76. Katz E, Privman V, Wang J. Towards biosensing strategies based on biochemical logic systems. *4th Int Conf Quantum, Nano Micro Technol ICQNM 2010*. Published online 2010:1-9. doi:10.1109/ICQNM.2010.8
77. Katz E, Poghossian A, Schöning MJ. Enzyme-based logic gates and circuits—

- analytical applications and interfacing with electronics. *Anal Bioanal Chem.* 2017;409(1):81-94. doi:10.1007/s00216-016-0079-7
78. Tokarev I, Gopishetty V, Zhou J, et al. Stimuli-responsive hydrogel membranes coupled with biocatalytic processes. *ACS Appl Mater Interfaces.* 2009;1(3):532-536. doi:10.1021/am800251a
79. Ferrell JE, Ha SH. Ultrasensitivity part II: Multisite phosphorylation, stoichiometric inhibitors, and positive feedback. *Trends Biochem Sci.* 2014;39(11):556-569. doi:10.1016/j.tibs.2014.09.003
80. Brun Y, Di Marzo Serugendo G, Gacek C, et al. Engineering self-adaptive systems through feedback loops. In: *Lecture Notes in Computer Science (Including Subseries Lecture Notes in Artificial Intelligence and Lecture Notes in Bioinformatics)*. Vol 5525 LNCS. Springer, Berlin, Heidelberg; 2009:48-70. doi:10.1007/978-3-642-02161-9_3
81. Thomas R. Logical analysis of systems comprising feedback loops. *J Theor Biol.* 1978;73(4):631-656. doi:10.1016/0022-5193(78)90127-3
82. Merindol R, Walther A. Materials learning from life: Concepts for active, adaptive and autonomous molecular systems. *Chem Soc Rev.* 2017;46(18):5588-5619. doi:10.1039/c6cs00738d
83. Brandman O, Meyer T. Feedback loops shape cellular signals in space and time. *Science.* 2008;322(5900):390-395. doi:10.1126/science.1160617
84. Ferrell JE. Feedback regulation of opposing enzymes generates robust, all-or-none bistable responses. *Curr Biol.* 2008;18(6):244-245. doi:10.1016/j.cub.2008.02.035
85. Semenov SN, Markvoort AJ, De Greef TFA, Huck WTS. Threshold sensing through a synthetic enzymatic reaction-diffusion network. *Angew Chemie - Int Ed.* 2014;53(31):8066-8069. doi:10.1002/anie.201402327

86. Heinen L, Heuser T, Steinschulte A, Walther A. Antagonistic enzymes in a biocatalytic ph feedback system program autonomous DNA hydrogel life cycles. *Nano Lett.* 2017;17(8):4989-4995. doi:10.1021/acs.nanolett.7b02165
87. Kumar S, Jha RK. Noise-Induced Resonance and Particle Swarm Optimization-Based Weak Signal Detection. *Circuits, Syst Signal Process.* 2019;38(6):2677-2702. doi:10.1007/s00034-018-0987-1
88. Samoilov M, Plyasunov S, Arkin AP. Stochastic amplification and signaling in enzymatic futile cycles through noise-induced bistability with oscillations. *Proc Natl Acad Sci U S A.* 2005;102(7):2310-2315. doi:10.1073/pnas.0406841102
89. Bates DL. Enzyme amplification in diagnostics. *Trends Biotechnol.* 1987;5(7):204-209. doi:10.1016/S0167-7799(87)80009-4
90. Kim S, Sikes HD. Radical polymerization reactions for amplified biodetection signals. *Polymer Chemistry*, 2020, 11, 8, 1424-1444. doi:10.1039/c9py01801h
91. Anandan V, Yang X, Kim E, Rao YL, Zhang G. Role of reaction kinetics and mass transport in glucose sensing with nanopillar array electrodes. *J Biol Eng.* 2007;1:4-13. doi:10.1186/1754-1611-1-5
92. Stein EW, Singh S, McShane MJ. Microscale enzymatic optical biosensors using mass transport limiting nanofilms. 2. Response modulation by varying analyte transport properties. *Anal Chem.* 2008;80(5):1408-1417. doi:10.1021/ac701738e
93. Duan W, Wang W, Das S, Yadav V, Mallouk TE, Sen A. Synthetic Nano- and Micromachines in Analytical Chemistry: Sensing, Migration, Capture, Delivery, and Separation. *Annu. Rev. Anal. Chem.* 2015. 8:311-33. doi:10.1146/annurev-anchem-071114-040125
94. Kagan D, Calvo-Marzal P, Balasubramanian S, et al. Chemical sensing based on catalytic nanomotors: Motion-based detection of trace silver. *J Am Chem Soc.* 2009;131(34):12082-12083. doi:10.1021/ja905142q

95. Che H, Buddingh' BC, van Hest JCM. Self-Regulated and Temporal Control of a "Breathing" Microgel Mediated by Enzymatic Reaction. *Angew Chemie - Int Ed.* 2017;56(41):12581-12585. doi:10.1002/anie.201706716
96. Che H, Cao S, Van Hest JCM. Feedback-Induced temporal control of "breathing" polymersomes to create self-adaptive nanoreactors. *J Am Chem Soc.* 2018;140(16). doi:10.1021/jacs.8b02387
97. Bubanja IN, Bánsági T, Taylor AF. Kinetics of the urea–urease clock reaction with urease immobilized in hydrogel beads. *React Kinet Mech Catal.* 2018;123(1):177-185. doi:10.1007/s11144-017-1296-6
98. Jee E, Bánsági T, Taylor AF, Pojman JA. Temporal control of gelation and polymerization fronts driven by an autocatalytic enzyme reaction. *Angew Chemie - Int Ed.* 2016;55(6):2127-2131. doi:10.1002/anie.201510604
99. Wrobel MM, Bánsági T, Scott SK, et al. pH Wave-Front Propagation in the Urea-Urease Reaction. *Biophys J.* 2012 Aug 8; 103(3): 610–615. doi:10.1016/j.bpj.2012.06.020
100. Mai AQ, Bánsági T, Taylor AF, Pojman JA. Reaction-diffusion hydrogels from urease enzyme particles for patterned coatings. *Commun Chem.* 2021;4(1):1-7. doi:10.1038/s42004-021-00538-7
101. Ogawa Y, Ogawa K, Wang B, Kokufuta E. Biochemo-mechanical system consisting of polyampholyte gels with coimmobilized glucose oxidase and urease. *Langmuir.* 2001;17(9):2670-2674. doi:10.1021/la001577x
102. Ogawa Y, Ogawa K, Kokufuta E. Swelling - Shrinking Behavior of a Polyampholyte Gel Immobilized Polyanions. *Langmuir* 2004 Mar 30;20(7):2546-52 2003;(6):2546-2552. DOI: 10.1021/la0347408
103. Kano K, Fendler JH. Pyranine as a sensitive pH probe for liposome interiors and surfaces. pH gradients across phospholipid vesicles. *BBA - Biomembr.*

- 1978;509(2):289-299. doi:10.1016/0005-2736(78)90048-2
104. Avnir Y, Barenholz Y. pH determination by pyranine: Medium-related artifacts and their correction. *Anal Biochem.* 2005;347(1):34-41.
doi:10.1016/j.ab.2005.09.026
105. Mohamed TM, Mohamed MA, Mohamed SA, Fahmy AS. Purification of urease from water melon seeds for clinical diagnostic kits. *Bioresour Technol.* 1999;68(3):215-223. doi:10.1016/S0960-8524(99)00157-1
106. Markovic VM, Bánsági T, McKenzie D, Mai A, Pojman JA, Taylor AF. Influence of reaction-induced convection on quorum sensing in enzyme-loaded agarose beads. *Chaos.* 2019;29(3). doi:10.1063/1.5089295
107. Mai AQ, Bánsági T, Taylor AF, Pojman JA. Reaction-diffusion hydrogels from urease enzyme particles for patterned coatings. *Commun Chem.* 2021;4(1):1-7. doi:10.1038/s42004-021-00538-7
108. Yang D, Fan J, Cao F, Deng Z, Pojman JA, Ji L. Immobilization adjusted clock reaction in the urea-urease-H⁺ reaction system. *RSC Adv.* 2019;9(7):3514-3519. doi:10.1039/c8ra09244c
109. Ha SH, Ferrell JE. Thresholds and ultrasensitivity from negative cooperativity. *Science.* 2016;352(6288):990-993. doi:10.1126/science.aad5937
110. Krajewska B. Ureases. II. Properties and their customizing by enzyme immobilizations: A review. *J Mol Catal B Enzym.* 2009;59(1-3):22-40. doi:10.1016/j.molcatb.2009.01.004
111. Yoshikawa K, Aihara R, Agladze K. Size-dependent Belousov-Zhabotinsky oscillation in small beads. *J Phys Chem A.* 1998;102(39):7649-7652. doi:10.1021/jp982136d
112. Aihara R, Yoshikawa K. Size-dependent switching of the spatiotemporal structure between a traveling wave and global rhythm. *J Phys Chem A.*

- 2001;105(37):8445-8448. doi:10.1021/jp010908r
113. Bánsági T, Taylor AF. Role of differential transport in an oscillatory enzyme reaction. *J Phys Chem B*. 2014;118(23):6092-6097. doi:10.1021/jp5019795
114. Lovrak M, Hendriksen WE, Kreutzer MT, Van Steijn V, Eelkema R, Van Esch JH. Control over the formation of supramolecular material objects using reaction-diffusion. *Soft Matter*. 2019;15(21):4276-4283. doi:10.1039/c8sm02588f
115. Yawalkar AA, Heesink ABM, Versteeg GF, Pangarkar VG. Gas-liquid mass transfer coefficient in stirred tank reactors. *Can J Chem Eng*. 2002;80(5):840-848. doi:10.1002/cjce.5450800507
116. Hanneschlaeger C, Horner A, Pohl P. Intrinsic Membrane Permeability to Small Molecules. *Chem Rev*. 2019;119(9):5922-5953. doi:10.1021/ACS.CHEMREV.8B00560
117. Soh S, Byrska M, Kandere-Grzybowska K, Grzybowski BA. Reaction-diffusion systems in intracellular molecular transport and control. *Angew Chemie - Int Ed*. 2010;49(25):4170-4198. doi:10.1002/anie.200905513
118. Muzika F, Bánsági T, Schreiber I, Schreiberová L, Taylor AF. A bistable switch in pH in urease-loaded alginate beads. *Chem Commun*. 2014;50(76):11107-11109. doi:10.1039/c4cc03936j
119. Foerster P, Müller SC, Hess B. Critical size and curvature of wave formation in an excitable chemical medium. *Proc Natl Acad Sci*. 1989;86(18):6831-6834. doi:10.1073/pnas.86.18.6831
120. Tischer W, Wedekind F. Immobilized Enzymes: Methods and Applications. In: Springer, Berlin, Heidelberg; 1999:95-126. doi:10.1007/3-540-68116-7_4
121. Brady D, Jordaan J. Advances in enzyme immobilisation. *Biotechnol Lett*. 2009;31(11):1639-1650. doi:10.1007/s10529-009-0076-4
122. Sheldon RA. Enzyme immobilization: The quest for optimum performance. *Adv*

- Synth Catal.* 2007;349(8-9):1289-1307. doi:10.1002/adsc.200700082
123. Kucherenko IS, Soldatkin OO, Kasap BO, et al. Elaboration of Urease Adsorption on Silicalite for Biosensor Creation. *Electroanalysis.* 2012;24(6):1380-1385. doi:10.1002/elan.201200056
124. Fapyane D, Berillo D, Marty JL, Revsbech NP. Urea biosensor based on a CO₂ microsensor. *ACS Omega.* 2020;5(42):27582-27590. doi:10.1021/acsomega.0c04146
125. Tsai H chung, Doong R an. Preparation and characterization of urease-encapsulated biosensors in poly(vinyl alcohol)-modified silica sol-gel materials. *Biosens Bioelectron.* 2007;23(1):66-73. doi:10.1016/j.bios.2007.03.017
126. Krajewska B, Leszko M, Zaborska W. Urease immobilized on chitosan membrane: Preparation and properties. *J Chem Technol Biotechnol.* 1990;48(3):337-350. doi:10.1002/jctb.280480309
127. Datta S, Christena LR, Rajaram YRS. Enzyme immobilization: an overview on techniques and support materials. *3 Biotech.* 2013;3(1):1-9. doi:10.1007/s13205-012-0071-7
128. Prakash O, Puliga S, Upadhyay LSB. Immobilization of watermelon (citrullus vulgaris) urease in agarose gel for urea estimation. *Biotechnol Bioprocess Eng.* 2007;12(2):131-135. doi:10.1007/BF03028638
129. Mai A. Q. Q. Characterization, Immobilization, and Polymer Related Applications of Watermelon Seed Powder, a Practical Source of Urease Enzyme (2021). *LSU Doctoral Dissertations.* 5464. https://repository.lsu.edu/gradschool_dissertations/5464.
130. Trelease RN, Becker WM, Gruber PJ, Newcomb EH. Microbodies (Glyoxysomes and Peroxisomes) in Cucumber Cotyledons. *Plant Physiol.* 1971;48(4):461-475. doi:10.1104/pp.48.4.461

131. Feierabend J, Beevers H. Developmental Studies on Microbodies in Wheat Leaves. *Plant Physiol.* 1972;49(1):33-39. doi:10.1104/pp.49.1.33
132. Артюхин В. Introduction Urea. *Прикладная Информатика.* 2010;(4):376-389.
133. Bader R, Kora MA-A, El-Shalakany A, Mashal BAA-B. Clinical significance of saliva urea and creatinine levels in patients with chronic kidney disease. *Menoufia Med J.* 2015;28(2):406. doi:10.4103/1110-2098.163893
134. Eggenstein C, Borchardt M, Diekmann C, et al. A disposable biosensor for urea determination in blood based on an ammonium-sensitive transducer. *Biosens Bioelectron.* 1999;14(1):33-41. doi:10.1016/S0956-5663(98)00103-1
135. Evans WH, David EJ, Patterson SJ. Biodegradation of urea in river waters under controlled laboratory conditions. *Water Research* 1973, 7, 975–985. doi:10.1016/0043-1354(73)90179-6
136. Laghari AN, Siyal ZA, Soomro MA, Bangwar DK, Khokhar AJ, Soni HL. Quality Analysis of Urea Plant Wastewater and its Impact on Surface Water Bodies. *Eng Technol Appl Sci Res.* 2018;8(2):2699-2703. doi:10.48084/etasr.1767
137. George S, Chellapandian M, Sivasankar B, Jayaraman K. A new process for the treatment of fertilizer effluent using immobilized urease. *Bioprocess Eng.* 1997;16(2):83-85. doi:10.1007/s004490050292
138. Takeda N, Hashihama F, Kanda J. Automated colorimetric determination of nanomolar urea in seawater by gas-segmented continuous flow analysis using a liquid waveguide capillary cell. *Talanta.* 2020;208(August 2019):120371. doi:10.1016/j.talanta.2019.120371
139. Nikoleli GP, Nikolelis DP, Methenitis C. Construction of a simple optical sensor based on air stable lipid film with incorporated urease for the rapid detection of urea in milk. *Anal Chim Acta.* 2010;675(1):58-63. doi:10.1016/j.aca.2010.07.014

140. Fapyane D, Berillo D, Marty JL, Revsbech NP. Urea biosensor based on a CO₂ microsensor. *ACS Omega*. 2020;5(42):27582-27590.
doi:10.1021/acsomega.0c04146
141. Hu L, Zhang Q, Li X, Serpe MJ. Stimuli-responsive polymers for sensing and actuation. *Mater Horizons*. 2019;6(9):1774-1793. doi:10.1039/c9mh00490d
142. Scheller FW, Wollenberger U, Warsinke A, Lisdat F. Research and development in biosensors. *Curr Opin Biotechnol*. 2001;12(1):35-40. doi:10.1016/S0958-1669(00)00169-5
143. Kim J, Campbell AS, de Ávila BEF, Wang J. Wearable biosensors for healthcare monitoring. *Nat Biotechnol*. 2019;37(4):389-406. doi:10.1038/s41587-019-0045-y
144. Aikio S, Gronqvist S, Hakola L, et al. Bioactive Paper and Fibre Products: Patent and Literary Survey. *VTT Work Pap*. 2007;51.
<http://www.vtt.fi/publications/index.jsp%0Ahttp://govreports.library.gatech.edu/handle/123456789/7114>
145. He W, Luo L, Liu Q, Chen Z. Colorimetric Sensor Array for Discrimination of Heavy Metal Ions in Aqueous Solution Based on Three Kinds of Thiols as Receptors. *Anal Chem*. 2018;90(7):4770-4775.
doi:10.1021/acs.analchem.8b00076
146. Bottero I, Rgen Huck J, Kosikova T, Philp D. A Synthetic Replicator Drives a Propagating Reaction–Diffusion Front. *J. Am. Chem. Soc*. 2016, 138, 21, 6723–6726 doi:10.1021/jacs.6b03372
147. Korevaar PA, Kaplan CN, Grinthal A, Rust RM, Aizenberg J, Paulson JA. Non-equilibrium signal integration in hydrogels. *Nat Commun* **11**, 386 (2020). doi:10.1038/s41467-019-14114-0
148. Dungchai W, Chailapakul O, Henry CS. Use of multiple colorimetric indicators

- for paper-based microfluidic devices. *Anal Chim Acta*. 2010;674(2):227-233.
doi:10.1016/j.aca.2010.06.019
149. Reches M, Mirica KA, Dasgupta R, Dickey MD, Butte MJ, Whitesides GM. Thread as a Matrix for Biomedical Assays. *ACS Appl Mater Interfaces*. 2010;2(6):1722-1728. doi:10.1021/am1002266
150. Gruber P, Marques MPC, O'Sullivan B, Baganz F, Wohlgemuth R, Szita N. Conscious coupling: The challenges and opportunities of cascading enzymatic microreactors. *Biotechnol J*. 2017;12(7). doi:10.1002/biot.201700030
151. Aubert S, Bezagu M, Spivey AC, Arseniyadis S. Spatial and temporal control of chemical processes. *Nat Rev Chem*. 2019;3(12):706-722. doi:10.1038/s41570-019-0139-6
152. Ashkenasy G, Hermans TM, Otto S, Taylor AF. Systems chemistry. *Chem Soc Rev*. 2017;46(9):2543-2554. doi:10.1039/c7cs00117g
153. Malhotra BD, Srivastava S, Ali MA, Singh C. Nanomaterial-Based Biosensors for Food Toxin Detection. *Appl Biochem Biotechnol*. 2014;174(3):880-896.
doi:10.1007/s12010-014-0993-0
154. Caruso F, Schüler C. Enzyme multilayers on colloid particles: Assembly, stability, and enzymatic activity. *Langmuir*. 2000;16(24):9595-9603.
doi:10.1021/la000942h
155. Kuswandi B, Wicaksono Y, Jayus, Abdullah A, Heng LY, Ahmad M. Smart packaging: Sensors for monitoring of food quality and safety. *Sens Instrum Food Qual Saf*. 2011;5(3-4):137-146. doi:10.1007/s11694-011-9120-x
156. Almeida H, Amaral MH, Lobão P. Temperature and pH stimuli-responsive polymers and their applications in controlled and selfregulated drug delivery. *J Appl Pharm Sci*. 2012;2(6):01-10. doi:10.7324/JAPS.2012.2609
157. Krajewska B. Urease-aided calcium carbonate mineralization for engineering

- applications: A review. *J Adv Res.* 2018;13:59-67. doi:10.1016/j.jare.2017.10.009
158. Anna I, Katarina N. Pulsatile release from a flat self-oscillating chitosan macrogel. *J Mater Chem B.* 2018;6(30):5003-5010. doi:10.1039/c8tb00781k
159. Tamate R, Mizutani Akimoto A, Yoshida R. Recent Advances in Self-Oscillating Polymer Material Systems. *Chem Rec.* 2016;16(4):1852-1867. doi:10.1002/tcr.201600009
160. De Larica R, Fratila RM, Szarpak A, Huskens J, Velders AH. Multivalent nanoparticle networks as ultrasensitive enzyme sensors. *Angew Chemie - Int Ed.* 2011;50(25):5704-5707. doi:10.1002/anie.201008189
161. Choi H, Jeong SH, Kim TY, Yi J, Hahn SK. Bioinspired urease-powered micromotor as an active oral drug delivery carrier in stomach. *Bioact Mater.* 2021;(July):0-8. doi:10.1016/j.bioactmat.2021.08.004
162. Kaushal J, Mehandia S, Singh G, Raina A, Arya SK. Catalase enzyme: Application in bioremediation and food industry. *Biocatal Agric Biotechnol.* 2018;16(April):192-199. doi:10.1016/j.bcab.2018.07.035
163. Arqué X, Romero-Rivera A, Feixas F, Patiño T, Osuna S, Sánchez S. Intrinsic enzymatic properties modulate the self-propulsion of micromotors. *Nat Commun.* 2019;10(1):1-12. doi:10.1038/s41467-019-10726-8
164. Wong CM, Wong KH, Chen XD. Glucose oxidase: Natural occurrence, function, properties and industrial applications. *Appl Microbiol Biotechnol.* 2008;78(6):927-938. doi:10.1007/s00253-008-1407-4
165. Wilson R, Elizabeth Q. Glucose oxidase : An ideal enzyme. *Biosens t Biwleccronia.* 2016;5663(November):165-185.
166. Benmeziane F, Derradji. Composition, bioactive potential and food applications of watermelon (*citrullus lanatus*) seeds – a review. *J Food Meas Charact.* 2023;17(5):5045-5061. doi:10.1007/s11694-023-02012-5

167. Zia S, Khan MR, Shabbir MA, Aadil RM. An update on functional, nutraceutical and industrial applications of watermelon by-products: A comprehensive review. *Trends Food Sci Technol.* 2021;114(June):275-291.
doi:10.1016/j.tifs.2021.05.039
168. Chabot M, Morales E, Cummings J, Rios N, Giatpaiboon S, Mogul R. Simple kinetics, assay, and trends for soil microbial catalases. *Anal Biochem.* 2020;610:113901. doi:10.1016/j.ab.2020.113901
169. Espinoza-Vergara J, Molina P, Walter M, et al. Effect of pH on the Electrochemical Behavior of Hydrogen Peroxide in the Presence of *Pseudomonas aeruginosa*. *Front Bioeng Biotechnol.* 2021;9(December):1-11.
doi:10.3389/fbioe.2021.749057
170. Aebi H. Catalase. *Methods Enzym Anal.* 1974:673-684. doi:10.1016/B978-0-12-091302-2.50032-3
171. Behere M, Patil SS, Rathod VK. Rapid extraction of watermelon seed proteins using microwave and its functional properties. *Prep Biochem Biotechnol.* 2021;51(3):252-259. doi:10.1080/10826068.2020.1808792
172. Gadalkar SM, Rathod VK. Extraction of watermelon seed proteins with enhanced functional properties using ultrasound. *Prep Biochem Biotechnol.* 2020;50(2):133-140. doi:10.1080/10826068.2019.1679173
173. Iwase T, Tajima A, Sugimoto S, et al. A simple assay for measuring catalase activity: A visual approach. *Sci Rep.* 2013;3:3-6. doi:10.1038/srep03081
174. Linke D, Berger RG. Foaming of proteins: New prospects for enzyme purification processes. *J Biotechnol.* 2011;152(4):125-131.
doi:10.1016/j.jbiotec.2010.07.022
175. Sakai K, Okada M, Yamaguchi S. Decolorization and detoxication of plant-based proteins using hydrogen peroxide and catalase. *Sci Rep.* 2022;12(1):1-10.

- doi:10.1038/s41598-022-26883-8
176. Singhanian RR, Patel AK, Sukumaran RK, Larroche C, Pandey A. Role and significance of beta-glucosidases in the hydrolysis of cellulose for bioethanol production. *Bioresour Technol.* 2013;127:500-507.
doi:10.1016/j.biortech.2012.09.012
 177. Kuusk S, Väljamäe P. When substrate inhibits and inhibitor activates: Implications of β -glucosidases. *Biotechnol Biofuels.* 2017;10(1):1-15.
doi:10.1186/s13068-016-0690-z
 178. Singhanian RR, Patel AK, Pandey A, Ganansounou E. Genetic modification: A tool for enhancing beta-glucosidase production for biofuel application. *Bioresour Technol.* 2017;245:1352-1361. doi:10.1016/j.biortech.2017.05.126
 179. Pei J, Pang Q, Zhao L, Fan S, Shi H. Thermoanaerobacterium thermosaccharolyticum β -glucosidase: A glucose-tolerant enzyme with high specific activity for cellobiose. *Biotechnol Biofuels.* 2012;5(1):1-10.
doi:10.1186/1754-6834-5-31
 180. Cao LC, Wang ZJ, Ren GH, et al. Engineering a novel glucose-tolerant β -glucosidase as supplementation to enhance the hydrolysis of sugarcane bagasse at high glucose concentration. *Biotechnol Biofuels.* 2015;8(1):1-12.
doi:10.1186/s13068-015-0383-z
 181. Hwang ET, Lee S. Multienzymatic Cascade Reactions via Enzyme Complex by Immobilization. *ACS Catal.* 2019;9(5):4402-4425. doi:10.1021/acscatal.8b04921
 182. Xavier JR, Ramana KV, Sharma RK. β -galactosidase: Biotechnological applications in food processing. *J Food Biochem.* 2018;42(5).
doi:10.1111/jfbc.12564
 183. Kumar S, Sasi M, Bishi S, Sanyal R. Role of Probiotic α -galactosidases in the Reduction of Flatulence Causing Raffinose Oligosaccharides (RFOs). *Biotica*

- Research Today*. 4, 9 (2022), 640–642.
184. Bhatia S, Singh A, Batra N, Singh J. Microbial production and biotechnological applications of α -galactosidase. *Int J Biol Macromol*. 2020;150:1294-1313. doi:10.1016/j.ijbiomac.2019.10.140
 185. Suzuki H. Sarcosine oxidase: structure, function, and the application to creatinine determination. *Amino Acids*. 1994;7(1):27-43. doi:10.1007/BF00808444
 186. Rebelo TSCR, Pereira CM, Sales MGF, et al. Sarcosine oxidase composite screen-printed electrode for sarcosine determination in biological samples. *Anal Chim Acta*. 2014;850:26-32. doi:10.1016/j.aca.2014.08.005
 187. Simões I, Faro C. Structure and function of plant aspartic proteinases. *Eur J Biochem*. 2004;271(11):2067-2075. doi:10.1111/j.1432-1033.2004.04136.x
 188. Doppalapudi S, Katiyar S, Domb AJ, Khan W. Biodegradable Natural Polymers. *Adv Polym Med*. Published online 2015:33-66. doi:10.1007/978-3-319-12478-0_2
 189. Cui C, Fu Q, Meng L, Hao S, Dai R, Yang J. Recent Progress in Natural Biopolymers Conductive Hydrogels for Flexible Wearable Sensors and Energy Devices: Materials, Structures, and Performance. *ACS Appl Bio Mater*. 2021;4(1):85-121. doi:10.1021/acsabm.0c00807
 190. Monshausen GB, Haswell ES. A force of nature: molecular mechanisms of mechanoperception in plants. *Journal of Experimental Botany*, 64, 15, 2013, 4663–4680. doi.org/10.1093/jxb/ert204
 191. Fürstenberg-Hägg J, Zagrobelny M, Bak S. Plant defense against insect herbivores. *Int J Mol Sci*. 2013;14(5):10242-10297. doi:10.3390/ijms140510242
 192. Grinthal A, Aizenberg J. Adaptive all the way down: Building responsive materials from hierarchies of chemomechanical feedback. *Chem Soc Rev*.

- 2013;42(17):7072-7085. doi:10.1039/c3cs60045a
193. Zarzar LD, Aizenberg J. Stimuli-responsive chemomechanical actuation: A hybrid materials approach. *Acc Chem Res.* 2014;47(2):530-539. doi:10.1021/ar4001923
 194. Wang Q, Gossweiler GR, Craig SL, Zhao X. Cephalopod-inspired design of electro-mechano-chemically responsive elastomers for on-demand fluorescent patterning. *Nat Commun.* 2014;5(May):1-9. doi:10.1038/ncomms5899
 195. Gibson LJ, The mechanical properties of natural materials. II. Microstructures for mechanical efficiency. *Proc. R. Soc. Lond.* A450141-162doi.org/10.1098/rspa.1995.0076
 196. Langer R, Tirrell DA. Designing materials for biology and medicine. *Nature* 428, 487-492 (2004). <https://doi.org/10.1038/nature02388>
 197. Slaughter B V., Khurshid SS, Fisher OZ, Khademhosseini A, Peppas NA. Hydrogels in Regenerative Medicine. *Adv Mater.* 2009;21(32-33):3307-3329. doi:10.1002/ADMA.200802106
 198. Huebsch N, Mooney DJ. Inspiration and application in the evolution of biomaterials. *Nature.* 2009;462(7272):426-432. doi:10.1038/nature08601
 199. Lemons JE, Lucas LC. Properties of Biomaterials. *The Journal of Arthroplasty*, 1, 2, 1986, 143-147, doi.org/10.1016/S0883-5403(86)80053-5.
 200. Zhang YS, Khademhosseini A, Summary R. Advances in engineering hydrogels. *Science.* 2017;356(6337). doi:10.1126/science.aaf3627
 201. Taylor MJ, Tomlins P, Sahota TS. Thermoresponsive gels. *Gels.* 2017;3(1):60. doi:10.3390/gels3010004
 202. Paikar A, Novichkov AI, Hanopolskyi AI, et al. Spatiotemporal Regulation of Hydrogel Actuators by Autocatalytic Reaction Networks. *Adv Mater.* Published

- online 2022. doi:10.1002/adma.202106816
203. Zhao W, Quan M, Cao Z, et al. Visual multi-triggered sensor based on inverse opal hydrogel. *Colloids Surfaces A Physicochem Eng Asp.* 2018;554:93-99. doi:10.1016/j.colsurfa.2018.06.024
204. Tamate R, Mizutani Akimoto A, Yoshida R. Recent Advances in Self-Oscillating Polymer Material Systems. *Chem Rec.* 2016;16(4):1852-1867. doi:10.1002/tcr.201600009
205. Lin G, Chang S, Kuo CH, Magda J, Solzbacher F. Free swelling and confined smart hydrogels for applications in chemomechanical sensors for physiological monitoring. *Sensors Actuators, B Chem.* 2009;136(1):186-195. doi:10.1016/j.snb.2008.11.001
206. Misra GP, Siegel RA. Multipulse drug permeation across a membrane driven by a chemical pH-oscillator. *J Control Release.* 2002;79(1-3):293-297. doi:10.1016/S0168-3659(01)00523-5
207. Kagawa T, Beevers H. The Development of Microbodies (Glyoxysomes and Leaf Peroxisomes) in Cotyledons of Germinating Watermelon Seedlings. *Plant Physiol.* 1975;55(2):258-264. doi:10.1104/pp.55.2.258
208. Solomon Y, Natan B. Experimental investigation of the combustion of organic-gellant-based gel fuel droplets. *Combust Sci Technol.* 2006;178(6):1185-1199. doi:10.1080/00102200600620259
209. Zúñiga RN, Aguilera JM. Structure-fracture relationships in gas-filled gelatin gels. *Food Hydrocoll.* 2009;23(5):1351-1357. doi:10.1016/j.foodhyd.2008.11.012
210. Suzuki H, Kumagai A, Ogawa K, Kokufuta E. New type of glucose sensor based on enzymatic conversion of gel volume into liquid column length. *Biomacromolecules.* 2004;5(2):486-491. doi:10.1021/bm034331q
211. Ogawa K, Nakajima-Kambe T, Nakahara T, Kokufuta E. Coimmobilization of

gluconolactonase with glucose oxidase for improvement in kinetic property of enzymatically induced volume collapse in ionic gels. *Biomacromolecules*. 2002;3(3):625-631. doi:10.1021/bm025512f